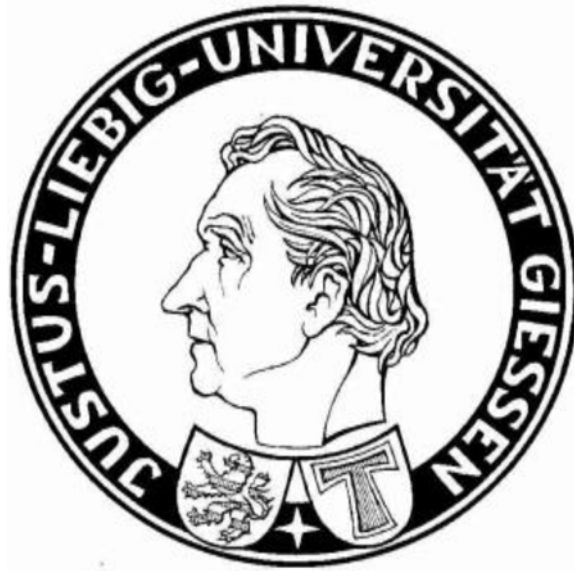


**MutL ATP-dependent conformational changes and the
interaction with MutH during DNA mismatch repair
processes**



Dissertation

zur Erlangung des Grades
Doktor der Naturwissenschaften
- Dr. rer. nat. -
des Fachbereiches Biologie und Chemie, FB08
der Justus-Liebig-Universität Gießen

von

M.Sc. Pingping Li
Gießen
September, 2018

Work Status:

The Ph.D. related work was carried out at the Institute of Biochemistry (FB08) of Justus-Liebig-University Gießen, from October 2012 to June 2017. The project was provided by Prof. Dr. Peter Friedhoff and obtained his guidance and support during the whole research process. The work was funded by CSC (The China Scholarship Council), the programs GRK 1384 (International Research Training Group) of the German Research Foundation. In addition, the work was supported by “Ph.D. Completion grant of Justus Liebig-Universität-Gießen” and the International Giessen Graduate Center for Life Sciences (GGL).

1. Reviewer / Gutachter

Prof. Dr. Peter Friedhoff

Institut für Biochemie, FB08

Justus-Liebig-Universität Gießen

Heinrich-Buff-Ring 58, 35392 Gießen

2. Reviewer / Gutachter

Prof. Dr. John Ziebuhr

Fachbereich Medizin, FB11

Justus-Liebig-Universität Gießen

Schubertstraße 81, 35392 Gießen

Submitted / Eingereicht: April 2018

Declaration:

I declare:

I prepared the present dissertation by myself and without unauthorized help from others. Every citation involved literally or adapted from the literature or oral communication has been marked appropriately. I have applied the principles of best scientific practice documented in the charter of the Justus Liebig University of Giessen in all investigations described in this thesis.

Erklärung

Ich erkläre: Ich habe die vorgelegte Dissertation selbständig und ohne unerlaubte fremde Hilfe und nur mit den Hilfen angefertigt, die ich in der Dissertation angegeben habe. Alle Textstellen, die wörtlich oder sinngemäß aus veröffentlichten Schriften entnommen sind, und alle Angaben, die auf mündlichen Auskünften beruhen, sind als solche kenntlich gemacht. Bei den von mir durchgeführten und in der Dissertation erwähnten Untersuchungen habe ich die Grundsätze guter wissenschaftlicher Praxis, wie sie in der „Satzung der Justus-Liebig-Universität Gießen zur Sicherung guter wissenschaftlicher Praxis“ niedergelegt sind, eingehalten.

(Pingping Li)

Giessen, August, 2018

Acknowledgments:

I sincerely express my gratitude to my supervisor Prof. Dr. Peter Friedhoff for the guidance and valuable suggestions in my Ph.D. period. Especially, he supports my independence and flexibility in my work through attending different conferences and talked with the various national scientists.

I sincerely express my heartfelt thanks to Prof. Dr. Katja Sträßer's friendly hospitality and enthusiasm for my science work at the Institute of Biochemistry.

Also, I would like to express my sincere gratitude to my second supervisor, Prof. Dr. John Ziebuhr's guidance at the beginning of my Ph.D. period, and all the professors who attended my Ph.D. training part in this university. They gave many instructions and valuable suggestions for my work which promoted my academic ability.

My heartfelt thanks express to Mrs. Heike Bungen, Dr. Anja Drescher, Dr. Wolfgang Wende, my pair worker Julia Gotthardt and all my excellent colleagues as well.

I acknowledged the CSC (The China Scholarship Council) funding support. The support from the programs GRK 1384 (International Research Training Group) of the German Research Foundation for academic communication and cooperation as an associated member from October of 2012 to October of 2015. "Ph.D. Completion grant of Justus Liebig-Universität-Gießen" for the last half year of my Ph.D.

Last but not least, I need to express my special thanks to my family—my original family, my family in law, and my own family (husband and my daughter). Their support and company motivate me to move on courageously. Thanks for their understanding when I cannot spend more time with them. I am pleased to be one family member of them.

List of publication:

1. Friedhoff P., Li P., Gotthardt J. (2015). "Protein-protein interactions in DNA mismatch repair."
DNA Repair (Amst) 38: 50-57

Contents

Work Status:	I
Declaration:	II
Acknowledgments:	III
List of publication:	IV
Contents	1
List of abbreviations	5
Summary	8
References	12
Chapter 1	14
Generation hetero-dimer of <i>Escherichia coli</i> MMR protein MutL from homodimer	14
Abstract	14
Introduction	14
Results	16
1, MutL CTD undergoes slow subunit exchange	17
2, Full-length (FL) MutL undergoes subunit exchange	18
3, Single-molecule (sm) FRET of MutL nucleotide-dependent conformational changes....	19
4, Closure of MutL-NTD by AMPPNP stabilizes the MutL dimer	22
Discussion	26
Method	27
Protein Expression and purification	27
Protein labeling and degree of labeling (DOL) determination	28
Analytical Ultracentrifugation (AUC)	28
DNA substrates	29
The smFRET	29
Thrombin cleavage assay	30
References	31
Chapter 2	34
Methods for monitoring MMR and protein-DNA interaction	34
Abstract	34
Introduction	35
Results	37

1, Associating SB on the different type of nucleic acids in different buffer	37
2, The kinetics of SB associating on ds/ssDNA assessed by Stopped-flow	41
3, Mg ²⁺ /K ⁺ dominating SB staining by changing the apparent K _{on} and K _{off}	42
4, Kinetics of MutS associating on SB stained DNA.....	44
Discussion	49
Material and methods	53
Protein Expression and purification	53
Protein labeling and degree of labeling (DOL) determination.....	53
Titration	53
Stopped-flow Fluorescence kinetics	54
MutL binding GT59DF DNA	54
MutS-MutL complex multiple loaded on nano-circular DNA	54
FRET correction.....	55
Calculating the 100 % binding of the dye	55
The fraction of bound state (θ) at different K⁺/Mg²⁺ conditions	55
References	57
Chapter 3.....	63
Multiple-loading combined conformational changes of MutL on mismatch-containing DNA, and the ionic strengthen effect to these processes	63
Abstract	63
Introduction	64
Results.....	66
1, Multi-loading combined conformational changes MutL on G: T mismatch-containing GT932 circular DNA	66
2. MutL conformational changes on mismatch-containing, end blocked GT59DF DNA, and buffer effect on MutL conformational changes	84
Discussion	96
Method.....	100
Steady-state Förster Resonance Energy Transfer (FRET).....	100
Stopped-flow Fluorescence kinetics	101
MutL binding GT59DF DNA	101
MutS-MutL complex multiple loaded on nano-circular DNA	101
Isothermal Titration	102

MutH activation assay	102
References	103
Chapter 4	106
Monitoring MutL binding nucleotides in real-time followed by conformational changes during MMR process in vitro	106
Abstract	106
Introduction	107
Results	108
1, Nucleotides effects on MutL subunit exchanges	108
2, Nucleotides effects on MutL conformational changes and its multiple loading on GT932 DNA	110
3, Nucleotides effects on MutL conformational changes in DNA	113
4, Effect of different nucleotides to At390 labeled MutL297	116
5, MutL conformational changes induced by wtMutS-GT59DF-ATP complexes	121
6, MutH mediating nucleotides effect on MutL297 changes	122
Discussion	122
Method	124
Isothermal Titration	124
Stopped-flow Fluorescence kinetics	124
Steady-state Förster Resonance Energy Transfer (FRET)	125
References	126
Chapter 5	128
Two <i>Escherichia coli</i> MMR key proteins: MutL and MutH interaction and maturation	128
Abstract	128
Introduction	129
Results	130
1, MutL and MutH interact independently of ATP, DNA, and MutS	130
2, MutH wreaking MutL inter-dimer interaction on GT932 circular DNA	132
3, Highly dynamic with lower affinity	136
4, Out-of-Step recruited MutL and MutH on DNA	137
Discussion	144
Method	147
Protein Expression and purification	147

MutH activation assay.....	148
Stopped-flow Fluorescence kinetics	148
Titration	148
References	149
Material	151
References	154
Appendix	159

List of abbreviations

% (v/v)	percentage in volume to volume
% (w/v)	percentage in weight to volume
aa	amino acid residues
app.	apparent
a.u.	arbitrary units
ADP	adenosine diphosphate
ATP	adenosine triphosphate
AMPPNP	Adenylyl-imidodiphosphate
ATP γ S	Adenosine-5'-(γ -thio)-triphosphate
mant-ATP	2'/3'-O-(N-Methyl-anthraniloyl)-adenosine-5'-triphosphate
AFM	atomic force microscope
AF488	Alexa Fluor 488 C5 Maleimide
AF594	Alexa Fluor 594 C5 Maleimide
At390	Atto390 Maleimide
AF647	Alexa Fluor 647 C5 Maleimide
bp	base pair
BR FRET	FRET between AF594 labeled proteins and SB stained DNA
BG FRET	FRET between AF488 labeled proteins and SB stained DNA
	FRET between AF488 labeled proteins and At390 labeled proteins
nt	nucleotide
BSA	bovine serum albumin
CF.	Correction factor
cc	closed circle
CTD	C-terminal domain
Da	Dalton
DNA	deoxyribonucleic acid
DOL	degree of labeling
dNTP	Deoxy-ribonucleotide triphosphate
ds	double-strand
DTT	dithiothreitol
EfA	FRET efficiency
e.g.	Exempli gratia (for example)
EDTA	ethylene diamine tetra acetic acid
Ex.	Excitation
Em.	Emission
FRET	Förster Resonance Energy Transfer
FL	Full-length
FI.	Fluorescence intensity
GR FRET	FRET between AF594 labeled protein and AF488 labeled proteins
HEPES	4-(2-Hydroxyethyl) piperazine-1-ethanesulfonic acid
HPLC	high performance liquid chromatography
HPNCC	Hereditary nonpolyposis colon cancer
H ₃ PO ₄	phosphoric acid
HCl	hydrochloric acid

List of abbreviation

IDLs	insertion-deletion loops
IPTG	Isopropyl β -D-1-thiogalactopyranoside
kb	kilo base pair
KCl	potassium chloride
KOH	potassium hydroxide
K ₂ HPO ₄	Dipotassium hydrogen-phosphate
KH ₂ PO ₄	Monopotassium phosphate
LB	Lysogeny broth
MMR	DNA mismatch repair
MgCl ₂	magnesium chloride
min	minute
mM	milli-molar
NTD	N-terminal domain
NaCl	sodium chloride
nM	nano-molar
obs.	observed
OD.	optical density
oc.	open circle
PAGE	polyacrylamide gel electrophoresis
PCR	polymerase chain reaction
pM	pico-molar
rpm	rounds per minute
RT	room temperature
smFRET	signal-molecule Förster Resonance Energy Transfer
sc	supercoiled
ss	single-strand
SB	SYTOX blue
SE	Subunit exchange
Tris	Tris (hydroxyl-methyl) amino-methane
Tol.	Total
U	units
UV	ultraviolet
MutS449	MutS_R449C
MutS449/D835R	MutS_R449C/D835R
MutL297	MutL_H297C
MutL452	MutL_452C
MutL4	MutL_Q4C
MutL118	MutL_Q118C
MutL218	MutL_T218C
MutL282	MutL_A282C
MutL297N33A	MutL_H297C/N33A
MutL297E29A	MutL_H297C/E29A
MutH156	MutH_E156C
MutH223	MutH_A223C
MutH77	MutH_C96S/S85C/E77A

List of abbreviation

GT932 DNA	single G: T mismatch and GATC site containing 932bp circular DNA
GT100D DNA	single G: T mismatch and GATC site containing 100bp oligo DNA with Dig at the end
GT100DF DNA	single G: T mismatch and GATC site containing 100bp oligo DNA with Dig at the end, and Fab-fragment attached to the Dig to bilock the DNA
GT59D DNA	single G: T mismatch and GATC site containing 59bp oligo DNA with Dig at the end
GT59DF DNA	single G: T mismatch and GATC site containing 59bp oligo DNA with Dig at the end, and Fab-fragment attached to the Dig to bilock the DNA

Summary

Robin Holliday first proposed mismatch repair (MMR) in Fungi (Holliday 1964, Modrich 2016), then Wagner and Meselson demonstrated that mismatch repair reaction exists in *E. coli* cell (Jones, Wagner, et al. 1987, Modrich 2016). Mismatch repair promotes genetic stability, inhibits recombination between non-identical DNA sequences and participating in responses to DNA damage (Harfe and Jinks-Robertson 2000). Deficiency of MMR in humans has been implicated in over 90 % of HPNCC (hereditary nonpolyposis colorectal cancers) (Peltomaki 2005). Lesion detection and removal are the two critical steps of MMR (Yang 2007), MutL bridges this mismatch recognition by MutS and generation a nick at GATC site by MutH endonuclease activity in *E. coli* MMR processes.

Both, bacterial homo-dimeric and eukaryotic hetero-dimeric MutL proteins belong to the GHKL ATPase/kinase superfamily and comprise an N-terminal ATPase domain and C-terminal dimerization regions. All GHKL proteins show substantial ATPase cycle-dependent conformational changes, including ATP binding coupled N-terminal domain dimerization. Interestingly, the ATPase domain of human PMS2 (a subunit of the MutL hetero-dimer) can bind and hydrolyze ATP without dimerization (Iino, Hikima, et al. 2015). The monomeric ATP-bound state of the domain has been thought to be characteristic of hetero-dimeric GHKL proteins (Iino, Hikima, et al. 2015). Hydrolysis of ATP by MutL has been shown to be relatively slow with a k_{cat} of 0.4 min^{-1} compared with rates between $0.6\text{-}6 \text{ min}^{-1}$ for most ATPase. The ATPase activity of LN40, an N-terminal fragment of MutL, with a k_{cat} of $<0.05 \text{ min}^{-1}$ is almost 10-fold slower than that of the intact MutL (Ban and Yang 1998, Ban, Junop, et al. 1999, Junop, Yang, et al. 2003).

Recent publications focused mainly on MutS conformational changes, the complex formation between MutS and MutL (Groothuizen, Winkler, et al. 2015, Qiu, Sakato, et al. 2015, Liu, Hanne, et al. 2016). In contrast, much less is known about conformational changes in MutL induced by ATP and its modulation by the interaction with MutS and G: T mismatch-containing DNA as well as the interaction between MutL and MutH. Studies using atomic force microscopy of the eukaryotic MutL homolog MutL α suggested that MutL adopts at least four distinct conformations called “extended”, “one-arm”, “semi-condensed” and “condensed”, and high ATP drives MutL α in to condensed state (Sacho, Kadyrov, et al. 2008). “Extended” and “condensed” structures in *E. coli* MutL ATPase cycle were observed as well about 20 years ago (Ban and Yang 1998, Ban and Yang 1999). To study conformational changes in MutL using Förster resonance energy transfer (FRET), a method for site-specific labeling of MutL and the formation of MutL hetero-dimers with a donor dye label in one domain and an acceptor dye label in the other domain was developed. Heterodimers were generated

Summary

by a so far unrecognized subunit exchange reaction of the MutL homodimers. Subunit exchanges could be followed in real-time between AF488 (G, donor) and AF594 (R, acceptor) labeled MutL-variants by FRET (GR FRET), e.g., MutL452G and MutL297R hetero-dimer formation in Chapter 1. Analytical ultra-centrifugation (AUC) and single-molecule (sm) FRET confirmed that MutL forms stable (down to 100 pM) yet dynamic ($k_{\text{exchange}} = 0.11 \text{ min}^{-1}$) dimers.

After generating the MutL donor/acceptor labeled hetero-dimers (NTD-NTD, NTD-CTD, and CTD-CTD), a method to simultaneously monitor mismatch-provoked recruitment of MutL to DNA by MutS and conformational changes in MutL during MMR processes was developed. In Chapter 2 the properties of nucleic acid staining fluorescent dye SYTOX blue (SB) with different types of DNA and the effect of K^+ , Mg^{2+} was investigated. FRET between SYTOX blue (B) stained DNA and AF594 (R) labeled MutL (BR FRET) allowed monitoring the G:T-mismatch and MutS dependent recruitment of MutL to DNA (59 bp end-blocked by Digoxigenin/Fab-fragments) in solution in real-time with an apparent KD of about 50 nM and fast bimolecular association rate constant of $10 \mu\text{M}^{-1}\text{s}^{-1}$.

On circular mismatched DNA substrates (932 bp) analysis of MutL recruitment to DNA and conformational changes became complicated due to multiple loading of MutS and MutL thereby making it difficult to separate FRET due to conformational changes with a MutL heterodimer from FRET between MutL hetero-dimers leading to much higher GR FRET on circular (932 bp) mismatched DNA compared to short, linear end-blocked (59 or 100 bp) mismatched DNA. Lifetime of MutL on circular DNA was 3-4 times longer on the circular DNA. Noteworthy, recruitment of MutL to these DNA substrates was observed already at low ATP (10 μM) whereas changes in GR FRET required binding of ATP to MutL (at higher ATP concentrations). At low ATP (10 μM) the FRET efficiency between SYTOX blue labeled DNA and MutL for proteins labeled at the NTD is in agreement with the postulated structure of the ternary complex between MutS, MutL and mismatched DNA (Groothuizen, 2015).

Stopped-flow kinetic analyses using short blocked end DNA and different labeled MutL variants monitoring either DNA binding (BR FRET between SYTOX blue and labeled MutL) or conformational change in MutL (GR FRET between MutL labeled with donor and acceptor dyes) lead to the following conclusions: MutL binding to DNA is fast when MutS-clamps are preformed (within 1-2 s), but the kinetics of MutL binding to DNA are multiphasic with at least three distinct phases, the slowest phase being dependent on ATP binding by MutL.

The effect of nucleotide binding to MutL was investigated in Chapter 4. Atto390 (At390) labeled MutL4 and MutL297 (but not MutL282) changed fluorescence intensity upon adenine nucleotides

Summary

binding and FRET experiments with At390 and AF488 labeled heterodimers resulted in MutL conformational changes after adenine nucleotide binding with apparent affinities between 50 -150 μ M similar as the reported K_m -values of 90 μ M for MutL ATPase (Ban, 1999).

MutL fails to active MutH endonuclease activity in the absence of ATP, but sufficient to active MutH with non-hydrolysable ATP analog AMPPNP (Joseph, Sawarkar et al. 2004). In Chapter 5 it is shown that both the ATP binding deficient mutant MutL297N33A and MutL297 with mant-ATP could bring MutH close to DNA, and generate the similar BR FRET intensity as wild-type MutL297 in the presence of ATP. That indicated that in the absence of ATP-binding by MutL, MutL can load MutH onto DNA (at least close to DNA), albeit at low apparent affinity. Moreover, MutH seemed to be able to bind to all states of MutL (open and closed on or off the DNA), while only clamped (ATP-bound) MutL can active MutH endonuclease activity which consistent with the literature (Liu, Hanne, et al. 2016). The kinetics of MutH and MutL interaction revealed very fast apparent association and dissociation rates, but rather low affinity (\sim 200 nM) in the absence or presence of wtMutS, ATP, and GT59DF DNA. The apparent affinity is even lower (\sim 500 nM) for MutL297N33A in the presence of wtMutS, ATP and GT59DF DNA. The non-specific DNA-binding activity of MutL is required for mismatch repair as mentioned in the literature (Junop, Yang, et al. 2003) which may due to increase the chance of MutH interact with DNA.

<p>MutL multiple loading and conformational changes</p>	<p>① MutL NTD stay less open at lower ionic strength while stay more open at higher ionic strength buffer (Fig 2.7 as well as Fig 2.4 and Fig. 2.5 chapter 3)</p> <p>② +ATP</p> <p>③ upon loading, MutL297 on DNA in FB75T buffer fast state more open and with $k_{off} \sim 24 \text{ mM}$ while $k_{on} \sim 50 \text{ mM}$ in FB150T buffer (Fig 2.3, Fig. 2.4 A-C and Fig 2.5 chapter 3; Fig 7 chapter 2)</p> <p>④ in FB75 buffer, both MutL297 and NTD-CTD could back to starting value after loading on DNA, and slightly higher than starting value in FB150T buffer (Fig. 2.4 A-C and Fig. 2.5 B chapter 3)</p> <p>⑤ 3-10 s GR FRET of MutL NTD-NTD and NTD-CTD no change, additionally, BR FRET of MutL452, GR CTD to DNA slightly decrease while BR FRET of MutL297, GR NTD to DNA stay no change and MutL452, GMutL297, R to DNA increased (Fig. 2.5 and Fig. 1.9 chapter 3)</p> <p>⑥ after 10 s, GR FRET of MutL NTD-NTD, NTD-CTD and CTD-CTD continuously increased even smFRET shown that MutL452 CTD-CTD without wMutS, DNA and ATP. FRET efficiency is ~ 0.9 (Fig. 1.8, Fig. 1.9 and Fig. 2.5 chapter 3, Fig 4 J chapter 1)</p> <p>⑦ the fast phase of MutL dissociation after adding competitor is the same for GT59DF DNA, GT100DF and GT932 DNA (Fig. 1.6 and Appendix 3.1 chapter 3 and as MutL297_R and MutS449/D835R_G decreased to (Fig. 1.1-1.11 and Appendix 3.1 chapter 3, Fig 8 chapter 2)</p> <p>⑧ same as described as ⑦; otherwise, after adding 2 mM ATP BR, FRET of MutL297_R and DNA only decreased 1/3 while GR FRET between MutL297_R and MutS449/D835R_G decreased to (Fig. 1.1-1.11 and Appendix 3.1 chapter 3, Fig 8 chapter 2)</p>		<p>① two steps with $k_{obs} \sim 0.1 \text{ s}^{-1}$ (Fig 2, Fig. 5A-B and Figure 6A-B chapter 5)</p> <p>② $k_{obs} \sim 20 \text{ s}^{-1}$ and $k_{off} \sim 200 \text{ nM}$ for both MutL297 and MutL297N33A with ATP, as well as supported by presence of mant-ATP (Fig. 5B and Figure 6B chapter 5)</p> <p>③ upon loading MutL on GT59DF/GT932 DNA, MutL and MutH complexes transiently separate (Fig. 6F and Fig. 8 chapter 5)</p> <p>④ After forming MutL-wMutS-DNA-ATP complexes, MutH rapidly associating on DNA with $k_{off} \sim 500 \text{ nM}$, supported by MutH and MutL297N33A interaction with presence of wMutS-DNA ATP (Fig. 6C and Fig. 8 A, B chapter 5)</p> <p>⑤ supported by with low ATP (0.01 mM) FRET between MutH156, AF594 and MutL297, AF488 decreased, while FRET between MutH156, AF594 and MutL452, AF488 increased after transient decrease at beginning with GT59DF DNA wMutS (Fig. 6C and Fig. 8 CD chapter 5)</p> <p>⑥ $k_{off} \sim 200 \text{ nM}$ as well supported by MutH and MutL297 interaction with presence of wMutS-DNA-ATP (1 mM ATP) (Fig. 5C and Fig. 8A-B chapter 5)</p> <p>⑦ multiple MutS and MutL loaded multiple MutH on GT932 circular DNA while cannot prevent a DNA loop formation which allows even NTD of MutL, not dimerized MutH still could interact with the other part of DNA through forming loops (Fig. 7AB Fig 9 and Fig. 10G chapter 5)</p>
<p>MutL and MutH in absence/presence of ATP, wMutS and GT59DF/GT932 DNA</p>	<p>① MutL NTD stay less open at lower ionic strength while stay more open at higher ionic strength buffer (Fig 2.7 as well as Fig 2.4 and Fig. 2.5 chapter 3)</p> <p>② +ATP</p> <p>③ upon loading, MutL297 on DNA in FB75T buffer fast state more open and with $k_{off} \sim 24 \text{ mM}$ while $k_{on} \sim 50 \text{ mM}$ in FB150T buffer (Fig 2.3, Fig. 2.4 A-C and Fig 2.5 chapter 3; Fig 7 chapter 2)</p> <p>④ in FB75 buffer, both MutL297 and NTD-CTD could back to starting value after loading on DNA, and slightly higher than starting value in FB150T buffer (Fig. 2.4 A-C and Fig. 2.5 B chapter 3)</p> <p>⑤ 3-10 s GR FRET of MutL NTD-NTD and NTD-CTD no change, additionally, BR FRET of MutL452, GR CTD to DNA slightly decrease while BR FRET of MutL297, GR NTD to DNA stay no change and MutL452, GMutL297, R to DNA increased (Fig. 2.5 and Fig. 1.9 chapter 3)</p> <p>⑥ after 10 s, GR FRET of MutL NTD-NTD, NTD-CTD and CTD-CTD continuously increased even smFRET shown that MutL452 CTD-CTD without wMutS, DNA and ATP. FRET efficiency is ~ 0.9 (Fig. 1.8, Fig. 1.9 and Fig. 2.5 chapter 3, Fig 4 J chapter 1)</p> <p>⑦ the fast phase of MutL dissociation after adding competitor is the same for GT59DF DNA, GT100DF and GT932 DNA (Fig. 1.6 and Appendix 3.1 chapter 3 and as MutL297_R and MutS449/D835R_G decreased to (Fig. 1.1-1.11 and Appendix 3.1 chapter 3, Fig 8 chapter 2)</p> <p>⑧ same as described as ⑦; otherwise, after adding 2 mM ATP BR, FRET of MutL297_R and DNA only decreased 1/3 while GR FRET between MutL297_R and MutS449/D835R_G decreased to (Fig. 1.1-1.11 and Appendix 3.1 chapter 3, Fig 8 chapter 2)</p> <p>① two steps with $k_{obs} \sim 0.1 \text{ s}^{-1}$ (Fig 2, Fig. 5A-B and Figure 6A-B chapter 5)</p> <p>② $k_{obs} \sim 20 \text{ s}^{-1}$ and $k_{off} \sim 200 \text{ nM}$ for both MutL297 and MutL297N33A with ATP, as well as supported by presence of mant-ATP (Fig. 5B and Figure 6B chapter 5)</p> <p>③ upon loading MutL on GT59DF/GT932 DNA, MutL and MutH complexes transiently separate (Fig. 6F and Fig. 8 chapter 5)</p> <p>④ After forming MutL-wMutS-DNA-ATP complexes, MutH rapidly associating on DNA with $k_{off} \sim 500 \text{ nM}$, supported by MutH and MutL297N33A interaction with presence of wMutS-DNA ATP (Fig. 6C and Fig. 8 A, B chapter 5)</p> <p>⑤ supported by with low ATP (0.01 mM) FRET between MutH156, AF594 and MutL297, AF488 decreased, while FRET between MutH156, AF594 and MutL452, AF488 increased after transient decrease at beginning with GT59DF DNA wMutS (Fig. 6C and Fig. 8 CD chapter 5)</p> <p>⑥ $k_{off} \sim 200 \text{ nM}$ as well supported by MutH and MutL297 interaction with presence of wMutS-DNA-ATP (1 mM ATP) (Fig. 5C and Fig. 8A-B chapter 5)</p> <p>⑦ multiple MutS and MutL loaded multiple MutH on GT932 circular DNA while cannot prevent a DNA loop formation which allows even NTD of MutL, not dimerized MutH still could interact with the other part of DNA through forming loops (Fig. 7AB Fig 9 and Fig. 10G chapter 5)</p>		

Table 1. MutL conformational changes and interaction with MutH derived from the 5 chapters

References

- Ahrends, R., J. Kosinski, D. Kirsch, L. Manelyte, L. Giron-Monzon, L. Hummerich, O. Schulz, B. Spengler and P. Friedhoff (2006). "Identifying an interaction site between MutH and the C-terminal domain of MutL by crosslinking, affinity purification, chemical coding and mass spectrometry." *Nucleic Acids Res* 34(10): 3169-3180.
- Ban, C., M. Junop and W. Yang (1999). "Transformation of MutL by ATP binding and hydrolysis: a switch in DNA mismatch repair." *Cell* 97(1): 85-97.
- Ban, C. and W. Yang (1998). "Crystal structure and ATPase activity of MutL: implications for DNA repair and mutagenesis." *Cell* 95(4): 541-552.
- Ban, C. and W. Yang (1998). "Structural basis for MutH activation in *E. coli* mismatch repair and relationship of MutH to restriction endonucleases." *EMBO J.* 17(5): 1526-1534.
- Cho, W. K., C. Jeong, D. Kim, M. Chang, K. M. Song, J. Hanne, C. Ban, R. Fishel and J. B. Lee (2012). "ATP Alters the Diffusion Mechanics of MutS on Mismatched DNA." *Structure*.
- Giron-Monzon, L., L. Manelyte, R. Ahrends, D. Kirsch, B. Spengler and P. Friedhoff (2004). "Mapping protein-protein interactions between MutL and MutH by cross-linking." *J Biol Chem* 279(47): 49338-49345.
- Groothuizen, F. S., I. Winkler, M. Cristovao, A. Fish, H. H. Winterwerp, A. Reumer, A. D. Marx, N. Hermans, R. A. Nicholls, G. N. Murshudov, J. H. Lebbink, P. Friedhoff and T. K. Sixma (2015). "MutS/MutL crystal structure reveals that the MutS sliding clamp loads MutL onto DNA." *Elife* 4: e06744.
- Hermans, N. (2014). On the mechanism of DNA mismatch repair, Erasmus Universiteit Rotterdam.
- Hermans, N., C. Laffeber, M. Cristovao, M. Artola-Boran, Y. Mardenborough, P. Ikpa, A. Jaddoe, H. H. Winterwerp, C. Wyman, J. Jiricny, R. Kanaar, P. Friedhoff and J. H. Lebbink (2016). "Dual daughter strand incision is processive and increases the efficiency of DNA mismatch repair." *Nucleic Acids Res* 44(14): 6770-6786.
- Holliday, R. A. (1964). "A mechanism for gene conversion in fungi." *Genet. Res.* 5: 282-304.
- Iino, H., T. Hikima, Y. Nishida, M. Yamamoto, S. Kuramitsu and K. Fukui (2015). "Small-angle X-ray scattering analysis reveals the ATP-bound monomeric state of the ATPase domain from the homodimeric MutL endonuclease, a GHKL phosphotransferase superfamily protein." *Extremophiles* 19(3): 643-656.

Summary

Jeong, C., W. K. Cho, K. M. Song, C. Cook, T. Y. Yoon, C. Ban, R. Fishel and J. B. Lee (2011). "MutS switches between two fundamentally distinct clamps during mismatch repair." *Nat. Struct. Mol. Biol.* 18(3): 379-385.

Jones, M., R. Wagner and M. Radman (1987). "REPAIR OF A MISMATCH IS INFLUENCED BY THE BASE COMPOSITION OF THE SURROUNDING NUCLEOTIDE-SEQUENCE." *Genetics* 115(4): 605-610.

Joseph, N., R. Sawarkar and D. N. Rao (2004). "DNA mismatch correction in *Haemophilus influenzae*: characterization of MutL, MutH and their interaction." *DNA Repair (Amst)* 3(12): 1561-1577.

Junop, M. S., W. Yang, P. Funchain, W. Clendenin and J. H. Miller (2003). "In vitro and in vivo studies of MutS, MutL and MutH mutants: correlation of mismatch repair and DNA recombination." *DNA Repair (Amst)* 2(4): 387-405.

Liu, J., J. Hanne, B. M. Britton, J. Bennett, D. Kim, J. B. Lee and R. Fishel (2016). "Cascading MutS and MutL sliding clamps control DNA diffusion to activate mismatch repair." *Nature* 539(7630): 583-587.

Modrich, P. (2016). "Mechanisms in *E. coli* and Human Mismatch Repair (Nobel Lecture)." *Angew Chem Int Ed Engl* 55(30): 8490-8501.

Peltomaki, P. (2005). "Lynch syndrome genes." *Fam Cancer* 4(3): 227-232.

Qiu, R., M. Sakato, E. J. Sacho, H. Wilkins, X. Zhang, P. Modrich, M. M. Hingorani, D. A. Erie and K. R. Weninger (2015). "MutL traps MutS at a DNA mismatch." *Proc Natl Acad Sci U S A* 112(35): 10914-10919.

Sacho, E. J., F. A. Kadyrov, P. Modrich, T. A. Kunkel and D. A. Erie (2008). "Direct visualization of asymmetric adenine-nucleotide-induced conformational changes in MutL alpha." *Mol Cell* 29(1): 112-121

Toedt, G. H., R. Krishnan and P. Friedhoff (2003). "Site-specific protein modification to identify the MutL interface of MutH." *Nucleic Acids Res* 31(3): 819-825.

Yang, W. (2007). "Human MutLalpha: the jack of all trades in MMR is also an endonuclease." *DNA Repair (Amst)* 6(1): 135-139.

Chapter 1

Generation hetero-dimer of *Escherichia coli* MMR protein MutL from homodimer

Abstract

The *Escherichia coli* DNA mismatch repair (MMR) processes require the recognition of the mismatch by MutS, ATP-dependent recruitment of MutL, and activation of the strand discrimination endonuclease MutH which marks the erroneous strand for removal. However, MutL, which C-terminal domain (CTD) stably dimerized, belongs to GHKL ATPase family and progresses ATP dependent conformational changes. MutL is a stable homo-dimer as shown by analytical ultracentrifugation (AUC) and single molecule Förster resonance energy transfer (smFRET) experiments. The C-terminal domain of MutL stably dimerized even down to sub-nanomolar level, that did not block two subunits within a MutL dimer dynamically exchange. In this chapter, we observed that MutL undergoes slow subunit exchange to generate hetero-dimers with the apparent constant rate of $k_{obs.} = 0.11 \pm 0.026 \text{ min}^{-1}$ (MutL CTD only $0.16 \pm 0.01 \text{ min}^{-1}$). Kinetics of MutL subunit exchange are only blocked by non-hydrolysable ATP analogue AMPPNP. Beyond that thrombin induced separation of NTD and CTD fragments lead to the dissociation of the N-terminal dimer (NTD) fragments but not the CTD dimer. And this dissociation of the NTD dimer could be blocked by the AMPPNP as well. Besides, both the NTD-NTD (N-terminal domain) and NTD-CTD of MutL are rather mobile which derived from the broad distribution of smFRET efficiency. This hetero-dimer generation process is providing the possibility to investigate MutL conformational changes, especially for NTD-CTD interaction within the hetero-dimeric MutL.

Keywords: MutL, MMR, FRET, subunit exchange, AMPPNP, NTD-CTD interaction

Introduction

MutL together with Gyrase, Hsp90, and histidine-kinase belong to the GHKL-family due to N-terminal ATPase binding and hydrolysis domain (Ban and Yang 1998, Ban, Junop et al. 1999, Dutta and Inouye 2000). GHKL-ATPase are dimeric proteins, and shows significant conformational changes upon ATP binding which are involve in dimerization of the ATPase domain at N-terminal regions (Ban, Junop et al. 1999, Dutta and Inouye 2000, Dong and Berger 2007, Li and

Buchner 2013). Bacterial MutL protein is homo-dimeric protein, while it is hetero-dimeric in eukaryotic systems (Hackman, Tannergard, et al. 1997, Ban and Yang 1998).

Similar to Hsp90 and DNA Gyrase B which are dimerized via their C-terminal domain (CTD) (Minami, Kimura et al. 1994, Brino, Urzhumtsev et al. 2000), the C-terminal domain of MutL mediate the dimerization of MutL (Ban and Yang 1998, Drotschmann, Aronshtam, et al. 1998, Guarne, Ramon-Maiques, et al. 2004, Kosinski, Steindorf, et al. 2005) as well as its eukaryotic homologues (Pang, Prolla, et al. 1997). 70 KDa *E.coli* MutL could be cleaved at residue 349 by thrombin to a 40 KDa N-terminal fragment and a 30 KDa C-terminal fragment (Ban and Yang 1998). Size exclusion chromatography and equilibrium ultracentrifugation indicated that LN40 state in monomer even in the presence of ADP, while it is still capable of ATP binding and hydrolysis with tenfold slower ($< 0.05 \text{ min}^{-1}$) (Ban and Yang 1998, Ban, Junop, et al. 1999). However, about stability of the full-length MutL dimer and thrombin chopped MutL CTD dimer is still elusive. Thus, in this chapter, we tested full-length MutL dimer and MutL CTD dimer stability with analytical ultracentrifugation (AUC) and signaled molecular Förster resonance energy transfer (smFRET).

As we know from literature, aggregation can cause FRET increase as well due to the energy transfer from donor to acceptor (Taisheng Wang 2018). Moreover, we monitor MutL aggregate in FB125T buffer only at lower concentration (16 nM) depending on AUC ($\leq 16 \text{ nM}$) and smFRET (around 1 nM) experiments (data not shown). Therefore, we used buffer M (with 5 mM Mg^{2+}) in which MutL exist in dimer only (Niedziela-Majka, Maluf, et al. 2011) instead of FB buffer.

A crosslinking and hydrogen/deuterium exchange mass spectrometry study on *Aquifex aeolicus* MutL revealed that the interactions between NTD and CTD within the same MutL dimer (Yamamoto, Iino, et al. 2011). Moreover, AFM (Atomic Force Microscopy) study of eukaryotic MutL homolog MutL α showed that "extended," "one-arm", "semi-condensed" and "condensed" four conformations, and high ATP driven condensed MutL α ratio (Sacho, Kadyrov, et al. 2008). Therefore, after binding ATP except for the dimerization at NTD ATPase domain, MutL NTD and CTD interaction exist as well (Ban, Junop, et al. 1999). Besides, about *E. coli* MutL NTD and CTD interaction are still unclear, and MutL exist in stable dimer at physiological concentration. Thus, the method could form the hetero-dimer from the homo-dimer was needed to study the interaction between NTD and CTD within a MutL dimer which cannot achieve through double labeling. Labeled at the site-specific position on MutL with different color fluorophores allow us to monitor MutL NTD and CTD interaction. Moreover, in this chapter, we investigate *E. coli* MutL dimer

stability and hetero-dimer generation process.

Results

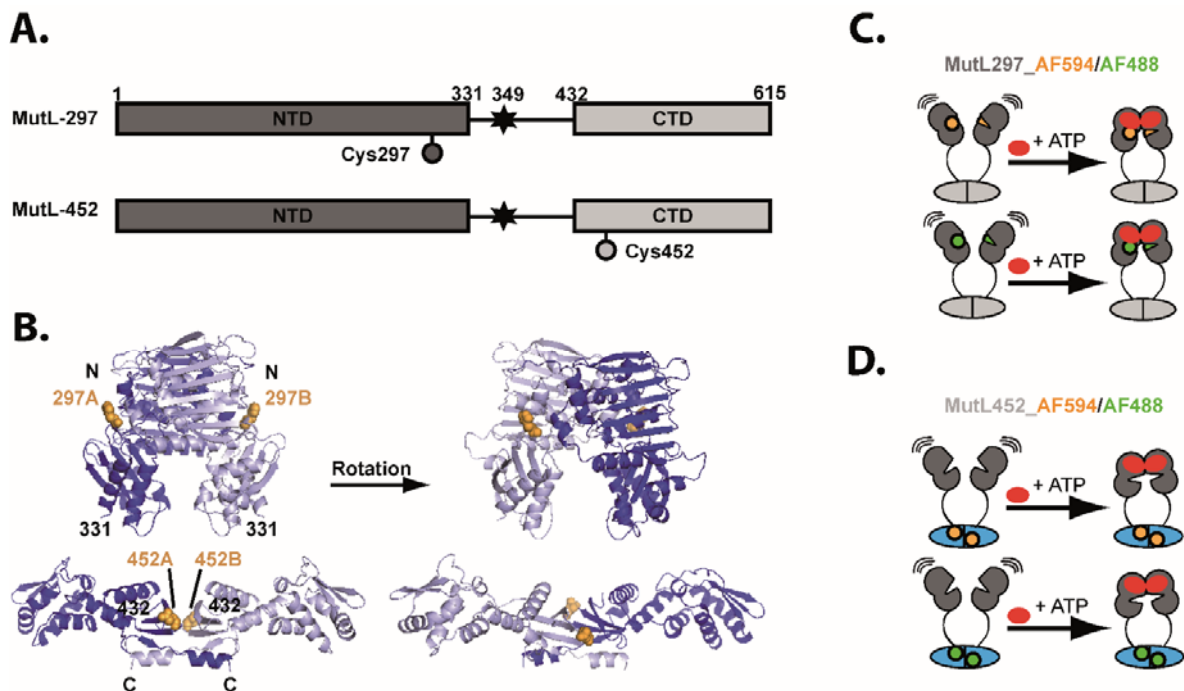


Figure 1. Single-cysteine variants of MutL, and NTD ATPase domain dimerized by ATP. (A) Schematic representation of the single-cysteine variants, the N-terminal domain (NTD) is depicted in dark gray which harbors the ATP-binding sites, and the C-terminal dimerization domain shown in light gray. The position of the internal thrombin cleavage site at position 349 shown as an asterisk. Positions of the cysteine residues indicated; (B) Structure of the closed NTD (PDB code: 1b63) bound to AMPNP (top) and the CTD (residues 432-615, PDB code: 1x9z, bottom); (C-D) Cartoons are drawing of MutL labeled at NTD or CTD with Alexa Fluor 488 (AF488, donor, G) or Alexa Fluor 594 (AF594, acceptor, R). A/B-atom of residue 452 is depicted as a sphere and proposed closure of MutL upon nucleotide binding (Ban, Junop, et al. 1999). Distance with AMPNP 297-297 (in NTD alone) is 4.5 nm and for 452-452 (in CTD alone) is 2.8 nm.

Either nucleotide or DNA binding could induce conformational changes in MutL. These changes have observed mainly through "static" methods, i.e. size-exclusion chromatography and chemical crosslinking (Heinze, Sekerina et al. 2012, Miguel, Correa et al. 2013), crystal structures (Ban and Yang 1998, Anbazhagan, Fujii et al. 1999, Guarne, Ramon-Maiques et al. 2004), dynamic light scattering (Duppatla, Bodda et al. 2009, Niedziela-Majka, Maluf et al. 2011, Pillon, Babu et al. 2015), or atomic force microscopy (Sacho, Kadyrov et al. 2008). Comparison with other members of the GHKL-ATPase family, e.g., Hsp90 and DNA gyrase B, suggesting that the dimeric form of the MutL protein is rather dynamic at its NTD and existing subunit exchange as well, even though reported as a stable dimer. Slow subunit exchange has been documented for Hsp90, and successfully used to generate hetero-dimeric proteins for the FRET studies (Fass, Bogden et al. 1999, Richter, Muschler, et al. 2001, Gubaev, Hilbert, et al. 2009). Consequently, we questioned

whether MutL could undergo subunit exchange as well. However, hard to find literature related MutL subunit exchange and conformational change based on FRET methods in real-time. Here, we established a FRET-based method to study MutL subunit exchange, and MutL nucleotide-induced the conformational change, especially between the NTD and CTD of MutL dimer in real-time. In the end, we use fully active single-cysteine variants of MutL, e.g. a single cysteine residue mutant either in the NTD (position 297, hereafter named MutL297) (Giron-Monzon, Manelyte et al. 2004) or the CTD (position 452, MutL452, Figure 1) (Kosinski, Steindorf et al. 2005).

1, MutL CTD undergoes slow subunit exchange

We treated MutL variants with thrombin to generate a 40 KDa N-terminal fragment (LN40, residues 1-349; MutL-NTD) and a 30 KDa C-terminal fragment (LC30, residues 350-615; MutL-CTD) (Ban and Yang 1998) to separate the N-terminal domain (NTD) and C-terminal domain (CTD) of MutL by size-exclusion chromatography. The concentration dependence of the quaternary structure (Figure 1 B) for the C-terminal domain (CTD) of MutL down to low nM concentrations. MutL452-CTD was labeled with AF488, then analyzed by sedimentation velocity analytical ultracentrifugation with fluorescence detection (Figure 2B) from 100 nM down to 2 nM. Analysis of the sedimentation coefficient distribution yielded an $S_{20,\omega}$ around 2.9 s in agreement with the dimeric form of MutL CTD which did not change over the investigated concentration range. That is in agreement with literature, MutL exists in solution as a dimer (hetero-dimer for eukaryotic MutL proteins) which is predominantly mediated by the CTD (Guarne, Ramon-Maiques, et al. 2004, Gueneau, Dherin, et al. 2013). Therefore, we used smFRET method monitor AF488 (donor, G) and AF594 (acceptor, R) labeled MutL452-CTD (200 pM) hetero-dimers (Figure 2 C) FRET efficiency and observed mainly a species with high apparent FRET efficiency (Figure 2 C). The FRET efficiency (E_{app}) between 0.85 and 0.95 which consistent with the short distance (~2.8 nm) between these two residuals within the same dimer, a small ‘donor-only’ peak ($E_{app} < 0$) due to the correction procedure (Lanz and Klostermeier 2011, Andreou and Klostermeier 2012) which was expected to form the statistical distribution after subunit exchange (Figure 2 C). It suggests that even under single-molecule condition at sub-nanomolar concentration level, the MutL CTD exists as a dimer in solution. Then we monitored the MutL452-CTD_AF488 and MutL452-CTD_AF594 subunit exchange at the ensemble level (Figure 2 D). We observed that a time-dependent slow decrease in the donor fluorescence channel and concomitant increase in the FRET-sensitized acceptor fluorescence channel both fit the single exponential function ($k_{obs} = 0.16 \text{ min}^{-1}$ at 25 °C) (Figure 2 D). Thrombin cleavages between positions 349/350 did not affect MutL

C-terminal domain (CTD) hetero-dimerization (Figure 7 I - L). MutL-CTD is pre-dominantly dimeric without any detectable formation of the monomeric form, and this high FRET between MutL-CTD is not due to aggregation.

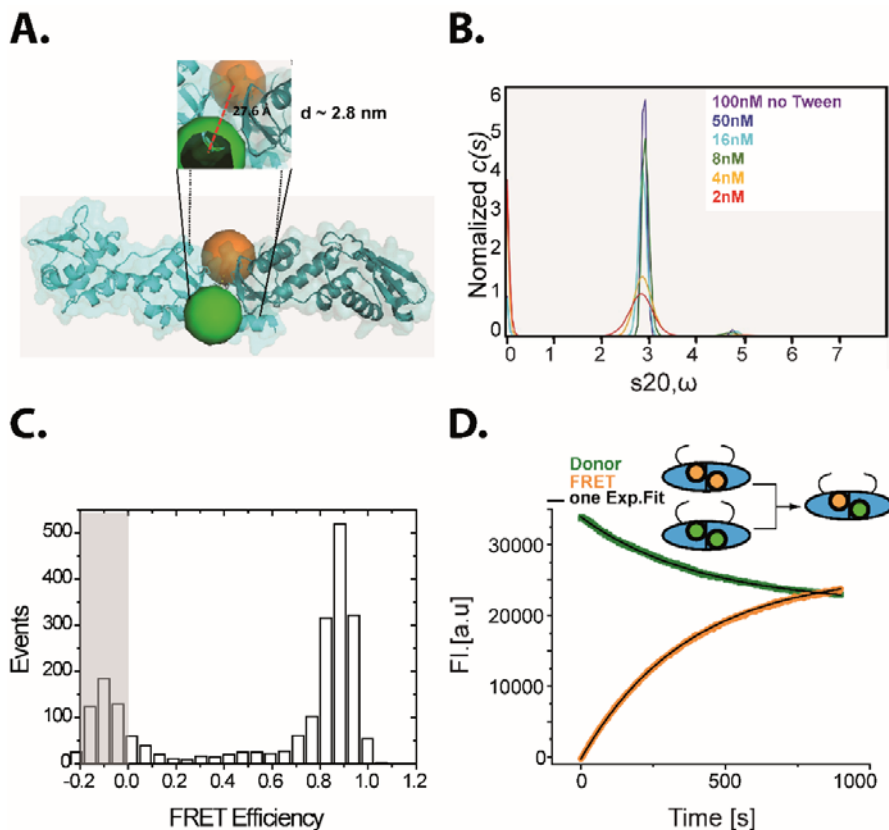


Figure 2. Subunit exchange of AF488/AF594 labeled stably dimerized MutL452-CTD. (A) Structure of the dimeric MutL CTD (residues 432-615, PDB code 1x9z); (B) Sedimentation velocity analysis of AF488 labeled MutL452-CTD at different concentrations between 2-100 nM. Sedimentation constant distribution analysis; (C) smFRET analysis of MutL452-CTD statistically labeled with Alexa Fluor 488 (AF488, light green point, Donor, G) and Alexa Fluor 594 (AF594, orange point, Acceptor, R); (D) Subunit exchange of MutL452-CTD_AF488 and MutL452-CTD_AF594 with apparent rate constants of around $0.16 \pm 0.01 \text{ min}^{-1}$, the kinetics were averaged from three independent experiments.

2, Full-length (FL) MutL undergoes subunit exchange

MutL-CTD exists as dynamic dimer, even down to sub-nanomolar concentration. However, FL MutL with a 40 KDa NTD fragment, this 40KDa NTD will and how to affect subunit exchange are still unclear. Here, donor-labeled FL MutL452 mixed with acceptor labeled FL MutL452 together, and similar results were observed (Figure 3A) with an apparent rate constant of $k_{obs} = 0.11 \pm 0.026 \text{ min}^{-1}$ at 25 °C. After that, the influence of the labeling position was tested by mixing FL MutL297 labeled with donor or acceptor fluorophores together and obtained a similar rate for the donor and FRET fluorescence of $k_{obs} = 0.11 \pm 0.026 \text{ min}^{-1}$ at 25 °C (Figure 3 B). Finally, we mixed donor labeled FL MutL452 with acceptor labeled FL MutL297 together, the observed subunit exchange

rate consistent with full-length MutL NTD-NTD/CTD-CTD subunit exchange rate (Figure 3 C). Taken together all these results suggest that full-length MutL can undergo slow subunit exchange similar as observed for other members of the GHKL-ATPase family. Owing to no full-length MutL crystallized, hence no quaternary structure of the full-length MutL is available from the literature. The MutL hetero-dimer generated from the subunit exchange offer us the chance to investigate the MutL NTD-CTD interaction during ATPase cycle, which will not fulfill through the double labeling process.

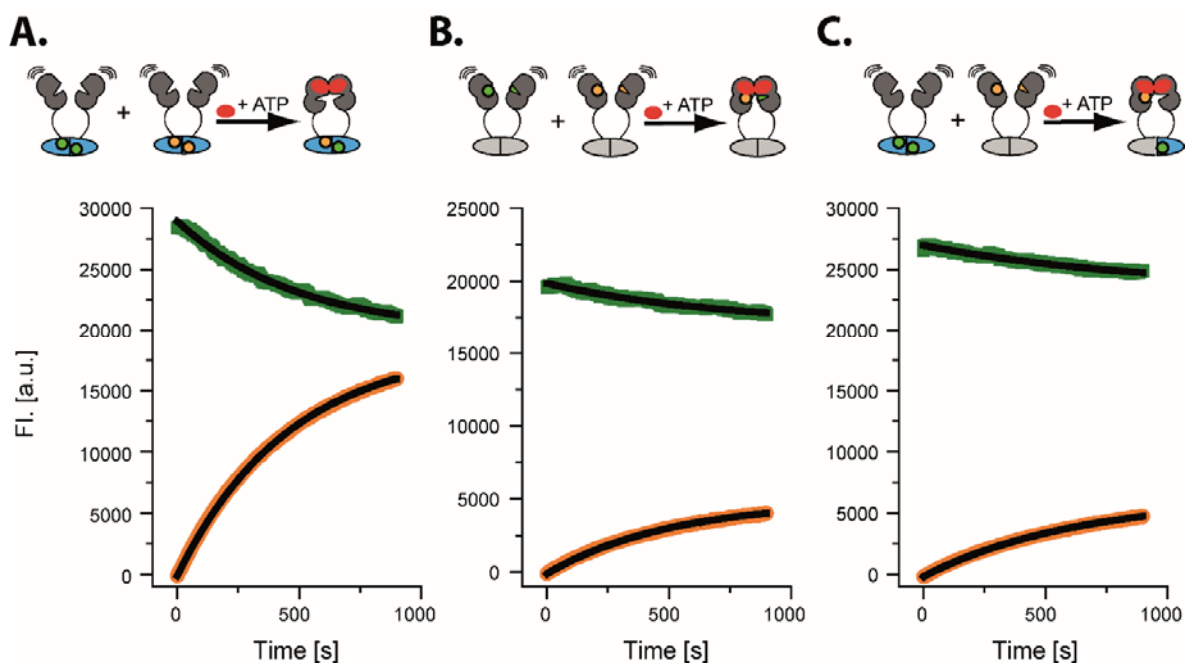


Figure 3 Subunit exchange of Full-length MutL monitored by ensemble FRET. Full-length MutL labeled with AF488 (donor) or AF594 (acceptor) mixed together: (A) MutL452_Af488 and MutL452_Af594 mixed together; (B) Mixed MutL297_Af488 with MutL297_Af594 together; (C) Mixed MutL297_Af594 with MutL452_Af488 together. The change in green signal intensity I_G^0 (green; donor) and orange signal intensity I_{GRF}^0 (orange; FRET channel) monitored. Data could fit with a single exponential fit (black line) for both channels. The apparent rate constants around $k_{obs.} = 0.11 \pm 0.026 \text{ min}^{-1}$ for the full-length MutL.

3, Single-molecule (sm) FRET of MutL nucleotide-dependent conformational changes

The conformational states of full-length MutL were studied using Förster resonance energy transfer (FRET) within hetero-dimers containing fluorophores in either the NTD (MutL297) and CTD (MutL452), or both NTD (MutL297) and CTD (MutL452) (Figure 4). For the FL MutL297_Af488Af594 hetero-dimer, in the absence of nucleotide the FRET efficiency distribution is rather broad distributed and there is no prominent peak (Figure 4 B), and the distribution did not change upon the addition of ATP (Figure 4 C). Even though, it did not change

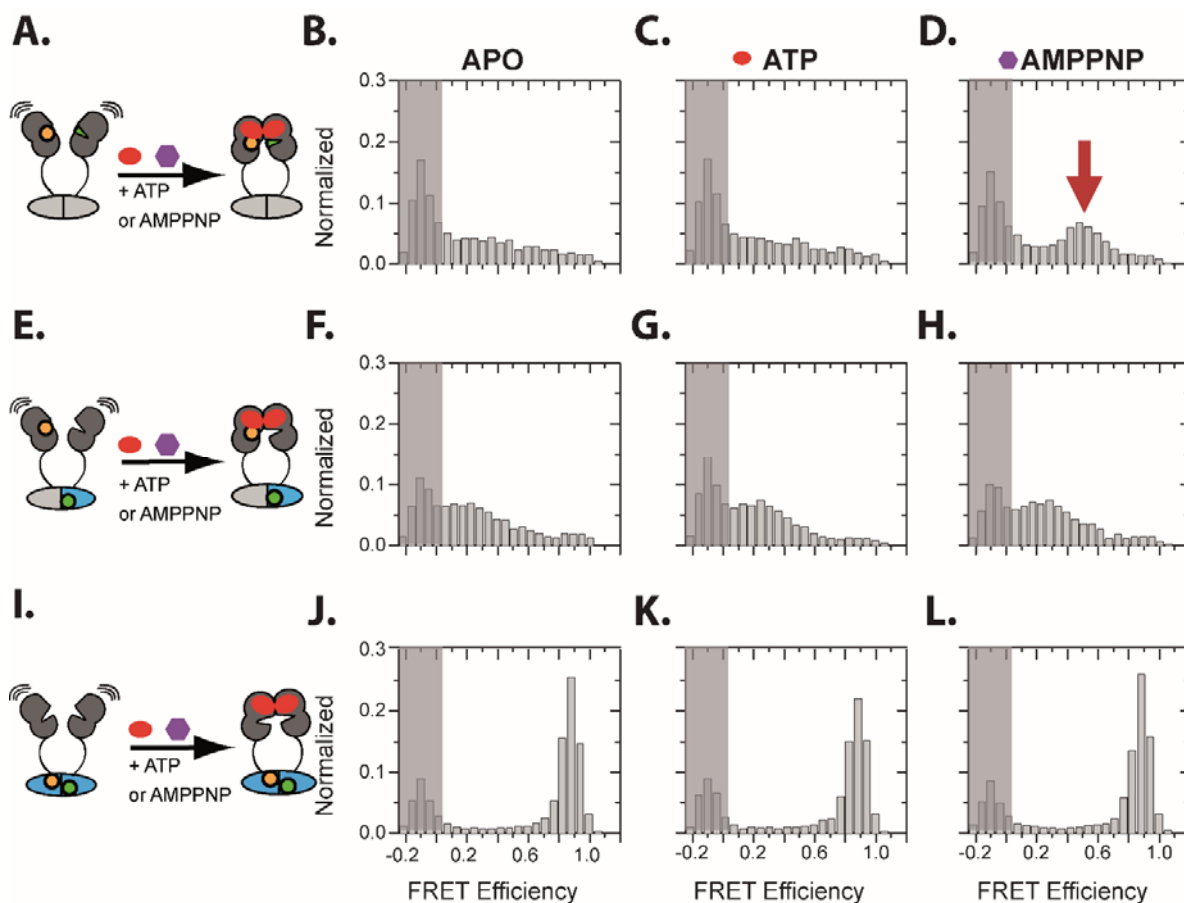


Figure 4. smFRET of Full-length MutL subunit exchange and conformational change. (A, E, I) Cartoons depicting subunit exchange and conformational change of MutL dimer containing cysteine residues at the NTD (297) and/or CTD (452) for fluorescence labeling; (B – D) smFRET histograms for MutL NTD labelled with donor and acceptor dyes without nucleotide (B), with ATP (C), or with AMPPNP (D); (F – H) smFRET histograms for MutL labelled with donor dye at CTD and acceptor dye at the NTD, without nucleotide (F), with ATP (G) or with AMPPNP (H); (J – L) smFRET histograms for MutL labelled with donor and acceptor dyes at the CTD without nucleotide (J), with ATP (K.), or with AMPPNP (L). The ‘donor-only’ peak shaded in light gray.

the FRET efficiency distribution of MutL NTD (NTD/NTD) at sub-nanomolar level (100 pM) with addition of ATP. While the changes could be monitored by fluorescence emission spectra (Figure 7 B. and 7 C) at steady state. Upon adding certain amounts of thrombin resulted the separation of NTD-NTD (Figure 7 D). However, the addition of AMPPNP resulted in the formation of a small peak of NTD-NTD interaction, which FRET efficiency between 0.45 and 0.55 (Figure 4 D). For the FL MutL₂₉₇_AF594/FLMutL₄₅₂_AF488 hetero-dimer, without nucleotide the FRET efficiency distribute rather broad as well, and with a small peak of FRET of NTD-CTD is around 0.25 and slightly higher Eavg. of 0.22 compared to that observed with NTD-NTD (Figure 7F). Similar as for NTD-NTD, the distribution did not change upon ATP binding (Figure 7G). In contrast to NTD-NTD, NTD-CTD FRET did not change upon addition of AMPPNP (Figure 4 H). Even though the quench at donor signal as well as the FRET signal stayed the same after adding the same

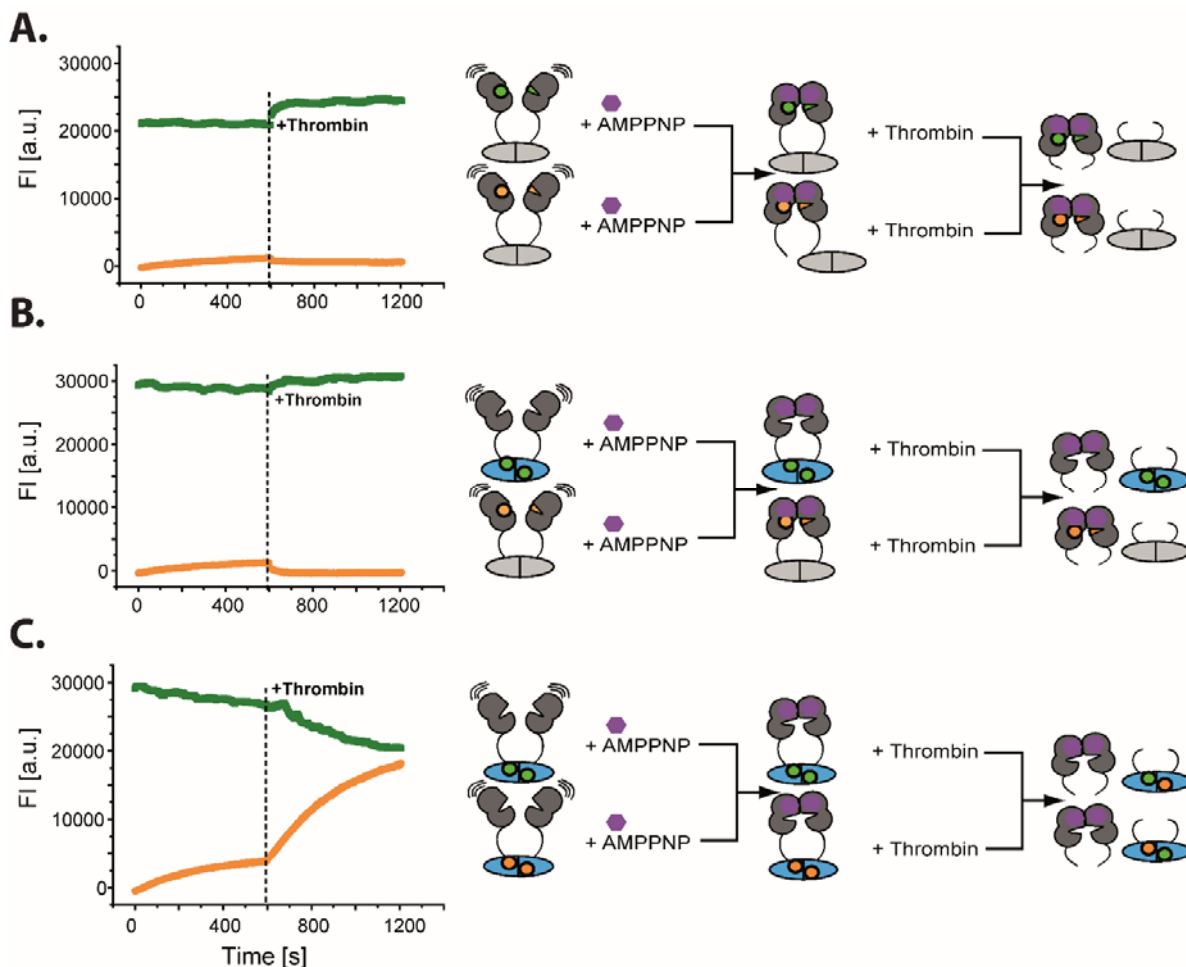


Figure 5. AMPPNP prevents full-length MutL subunit exchange. The subunit exchange kinetics of full-length MutL297 or MutL452 single-cysteine mutant labeled with AF488 or AF594 pre-incubated with AMPPNP for 20 h at 4 °C . (A) Mixed MutL297_AF488-AMPPNP with MutL297_AF594-AMPPNP together and later cleavage with thrombin (T); (B) MutL297_AF594-AMPPNP with MutL452_AF488-AMPPNP and added Thrombin later; (C) MutL452_AF488-AMPPNP and MutL452_AF594-AMPPNP mixed together and the apparent first-order rate constant (k_{obs} around 0.12 min⁻¹) after thrombin cleavage at 25 °C.

amount of ATP (Figure 7 F and 3G), the NTD-CTD interaction is weakened by thrombin (Figure 7 H). For the FL MutL452_AF488AF594 hetero-dimers, the FRET efficiency distribution of MutL labeled with donor and acceptor both in the CTD (452) showed a peak at high FRET efficiency (0.85-0.95) (Figure 4 J) in the absence of nucleotide, which will not change after adding of ATP (Figure 4 K), or AMPPNP (Figure 4 L). The bulk FRET emission spectra showed ascending at FRET signal when the donor quenched (Figure 7 J). After adding ATP (Figure 7 K) and thrombin (Figure 7 L), the donor channel not change while the FRET channel decreased due to the acceptor quenched as well.

4, Closure of MutL-NTD by AMPPNP stabilizes the MutL dimer

Since the N-terminal domain has been shown exist in a monomer/dimer equilibrium, and that can be shifted by binding the non-hydrolysable ATP analog AMPPNP to the dimeric form (Ban, Junop, et al. 1999, Guarne, Ramon-Maiques, et al. 2004, Aksentijevich. C, et al. 2007). We investigated the effect of AMPPNP on the subunit exchange rate using the FRET-based assay described above.

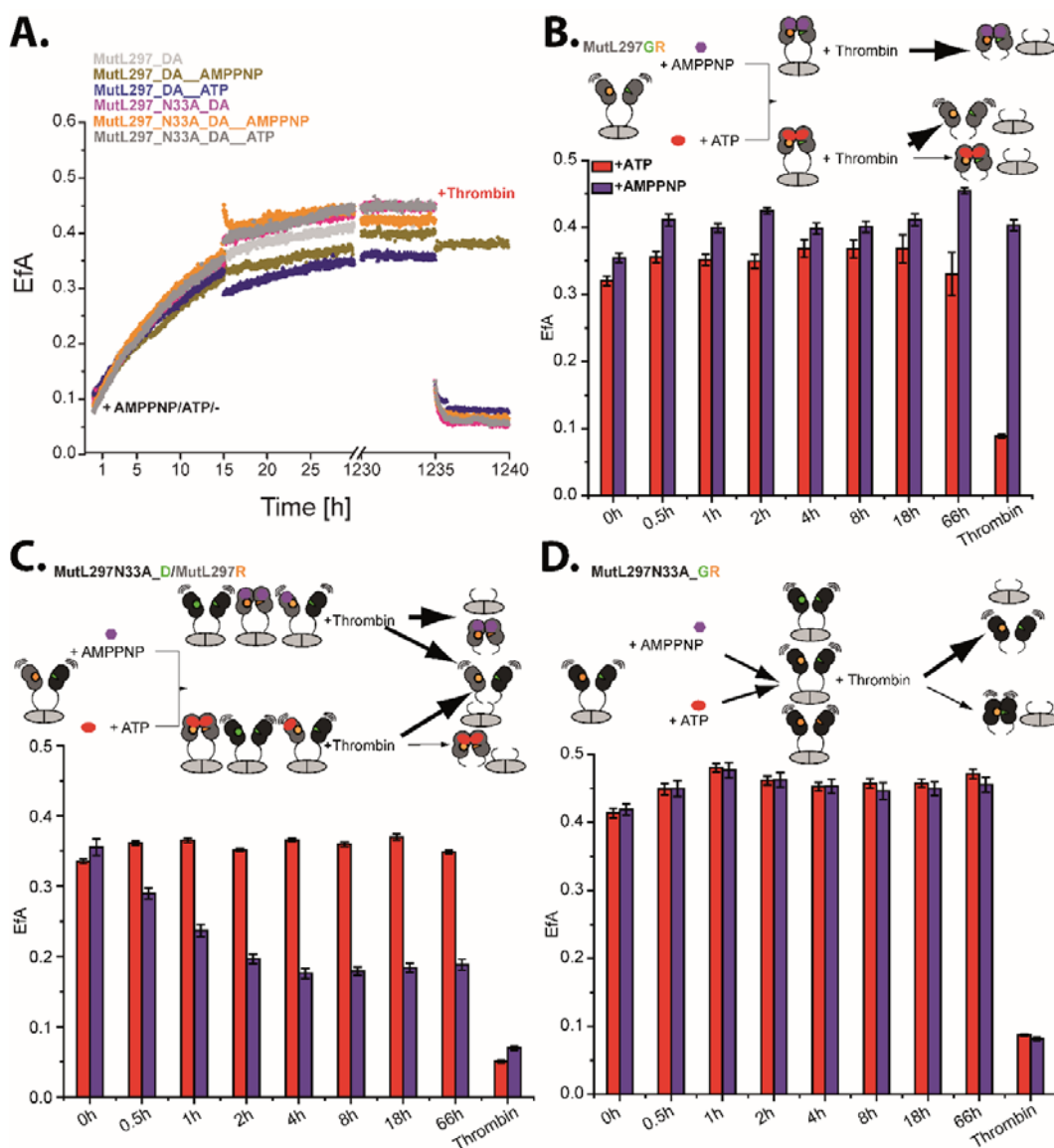


Figure 6. MutL297 (dark grey) and MutL297_N33A (black-grey) hetero-dimer dimer stabilized by AMPPNP. (A) the kinetics of all the measurements for A, B, and C.; (B) Pre-incubated MutL297_AF488 and MutL297_AF594 at 25 °C for 25 min then added 1 mM AMPPNP to monitor the FRET efficiency (Efa) at the different time, at last, added Thrombin (T) after 66 h; (C) Pre-incubated MutL297_AF488 and MutL297N33A_AF594 at 25 °C for 25 min then added 1mM AMPPNP to monitor the FRET efficiency (Efa) at the different time then added Thrombin (T) after 66 h; (D) Pre-incubated MutL297N33A_AF488 and MutL297N33A_AF594 at 25 °C for 25 min then added 1 mM AMPPNP monitor the FRET efficiency (Efa) at the different time then added Thrombin (T) after 66 h.

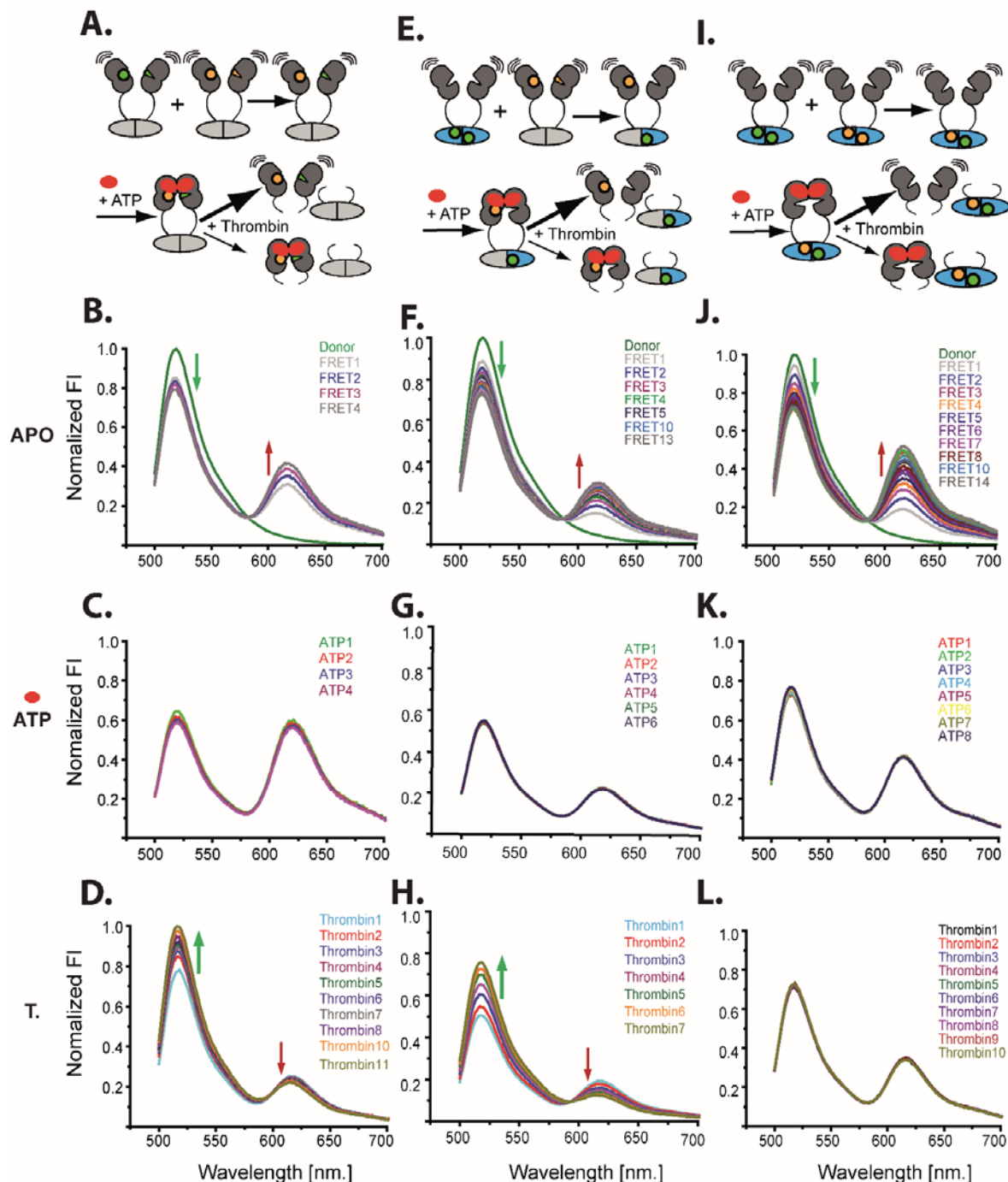


Figure 7. Fluorescence emission spectra in the absence and presence of ATP and ATP plus thrombin. (A, E, I) Cartoon depicting MutL dimer containing cysteine residues at the NTD and/or CTD for fluorescence labeling. (B– D) Fluorescence emission spectra of MutL297 labeled with a donor (AF488), and acceptor (AF594) dyes at the NTD without nucleotide (B), with ATP (C) and with ATP plus thrombin (D); (F – H) Fluorescence emission spectra of MutL labeled with acceptor at the NTD (MutL297) and donor at CTD (MutL452), without nucleotide (F), with ATP (G) or and with ATP and thrombin (H); (J – L) Fluorescence emission spectra of MutL452 labeled with AF488 or AF594 without nucleotide (J), with ATP (K) or with AMPPNP (L). T. stands for thrombin.

Pre-incubation of MutL (labeled with donor or acceptor at position 297 of the NTD, or position

452 of the CTD) with 2 mM AMPPNP for 20 h at 4 °C before mixing, that result the impaired subunit exchange (Figure 5 A-C). Upon cleavage of MutL with thrombin, which cleaves between position 349/350 in the non-conserved linker region between the NTD and the CTD (Figure 1 A) (Ban and Yang 1998), the subunit exchange could be observed only happens for MutL452-CTD but not for MutL297-NTD (Figure 5 and Appendix Figure 1.1). The fluorescence emission spectra in Figure 7 B, F and J indicated as mixed FL MutL297_AF488 and FL MutL297_AF594, FL MutL452_AF488 and FL MutL297_AF594, FL MutL452_AF488 and FL MutL452_AF594 as the donor signal decreased (around 525nm, as pointed by green arrow), while the FRET signal increased (close to 617nm, indicated by the red arrow). After adding ATP, the FRET signal stay no change while the donor signal of MutL297 rather than MutL452 decreased (Figure 7 C, G, and K). Addition of thrombin induce the FRET signal decreased (pointed with the red arrow) while the donor signal increased (indicated with the green arrow) for both the NTD- NTD and NTD-CTD interaction (Figure 7 D and H). However, both the donor and FRET channels are not changed by thrombin (Figure 7 L) with consistent with the result of Figure 5.

Except that, 2mM AMPPNP added to the pre-generated MutL297_GR (FL MutL297_AF488 and FL MutL297_AF594), MutL297N33A_AF488/MutL297_AF594 (FL MutL297N33A_AF488 and FL MutL297_AF594), and MutL297N33A_AF488AF594 (FL MutL297N33A_AF488 and FL MutL297N33A_AF594) hetero-dimers and incubated at room temperature and measured from 0-66 hours, then added thrombin (Figure 6). As indicated in Figure 6, MutL is rather stable in buffer FB150T no matter in the absence of nucleotide or the presence of ATP or AMPPNP. After adding thrombin, only MutL297_DA-AMPPNP dimer stays at high FRET efficiency (Figure 6 A and B) state which is consistent with Figure 3 and Figure 5. All other species FRET efficiency value dramatically decreased, but it is not drop back to zero (Figure 6 A, C, D) which means that the NTD of MutL are rather mobile and some species are getting entangled together. However, adding AMPPNP to MutL297N33A_AF488/MutL297_AF594 hetero-dimers seems driven MutL297_AF594-AMPPNP/MutL297_AF594-AMPPNP homo-dimers (Figure 6 C, red) and MutL297-N33A_AF488/MutL297N33A_AF488 homo-dimers formation (Figure 6 C, purple). All these results suggest that the binding of AMPPNP stabilizes the NTD in their dimeric state, hence the full-length MutL-protein prevented or impaired subunit exchange not only for the NTD but also for the CTD for the full-length proteins. Data indicated that AMPPNP could stabilize hetero-dimeric of FL MutL NTD. However, dissociation of NTD-NTD appears after thrombin cleavage MutL at the linker region and separating NTD from CTD (Figure 8 A and B).

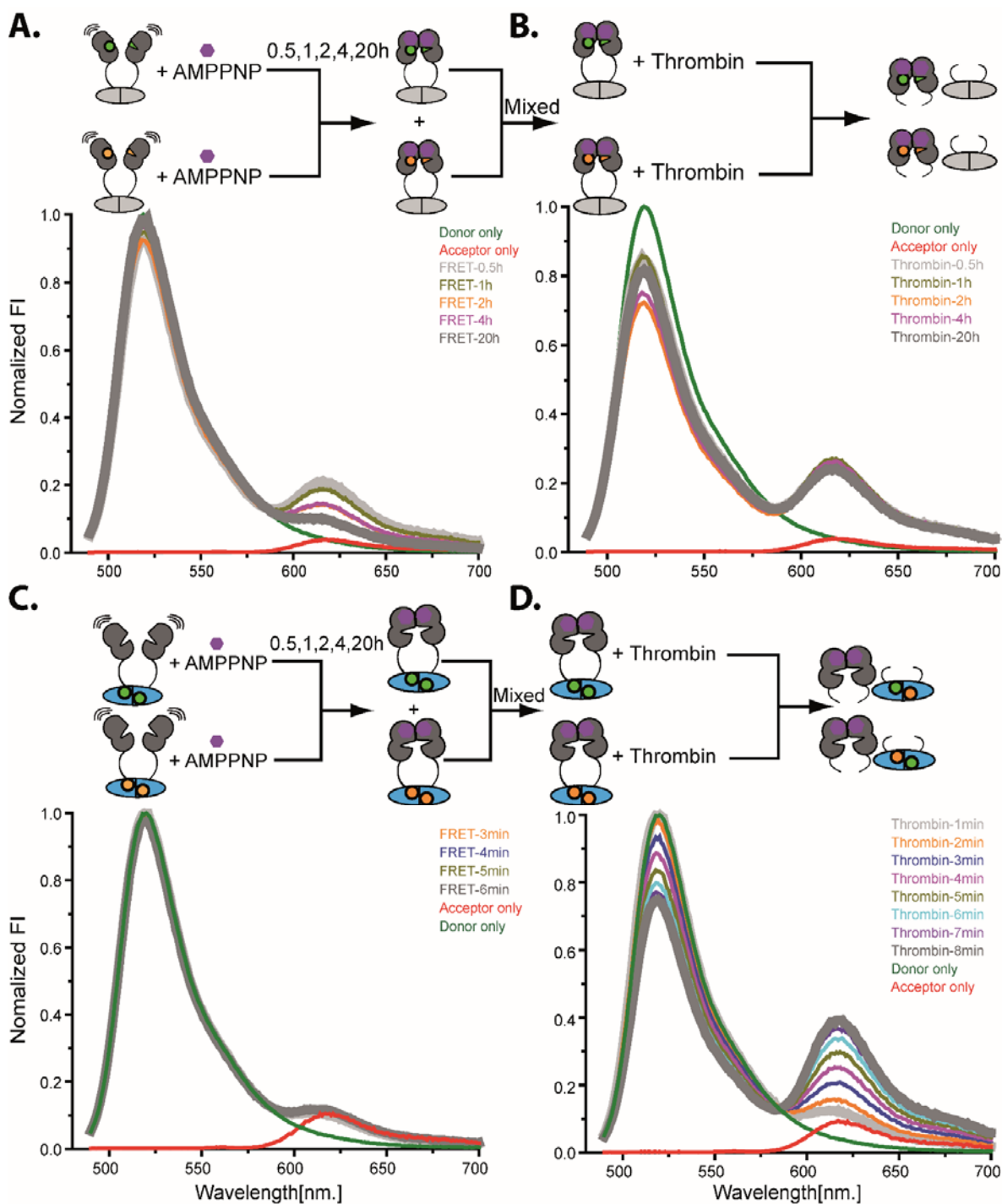


Figure 8. Fluorescence emission spectra monitor AMPPNP working time. (A) Fluorescence emission spectra of MutL297_AF488 pre-incubated with AMPPNP for 0.5, 1, 2, 4, 20 h mixed with MutL297_AF594 pre-incubated with AMPPNP for 0.5, 1, 2, 4, 20 h as well; (B) thrombin cleavage of reaction after (A); (C) Fluorescence emission spectra of MutL452_AF488 pre-incubated with AMPPNP for 20 h mixed with MutL452_AF594 pre-incubated with AMPPNP for 20 h as well; (D) thrombin cleavage of reaction after (C).

The thrombin cleavage assay is shown in Figure 9, and the thrombin cleavage site and the purified MutL CTD fragments was shown in Appendix Figure 3.6. The rationality of how long needed for

pre-incubated with 2 mM AMPPNP has been tested in Figure 8. Pre-incubating 2 mM AMPPNP with FL MutL297_AF488 and 2 mM AMPPNP with FL MutL297_AF594 separately for 0.5, 1, 2, 4 and 20 h at 4 °C (Figure 8 A). Then mixed FL MutL297_AF488-AMPPNP with FL MutL297_AF594-AMPPNP together, we found that even pre-incubated MutL and 2 mM AMPPNP for 20 h cannot 100 % prevent MutL subunit exchange but over 90 % already (Figure 8 A and B). Additionally, pre-incubated 2 mM AMPPNP with FL MutL452_AF488 and with FL MutL452_AF594 separately for 20 h at 4 °C, and then mixed together as well, we could conclude that more 95 % subunit exchange have been blocked (Figure 8 C), and the FRET signal increased while the donor signal decreased after adding thrombin (Figure 8 D).

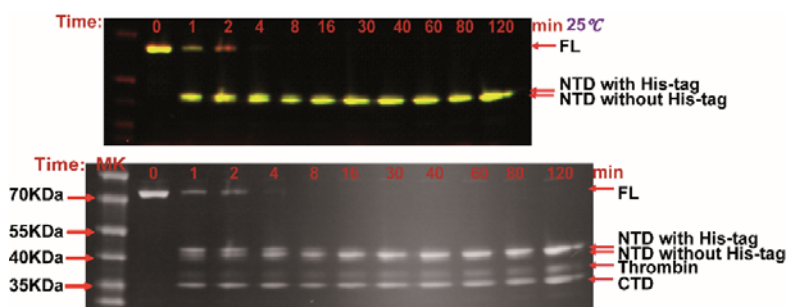


Figure 9. Thrombin cleavage kinetics by SDS-PAGE. 2 μ M full-length MutL hetero-dimer (MutL297_AF488 AF594) incubate with Thrombin at room temperature for 1-120 min, then stopped the reaction with PMSF and running 12.5 % SDS-Gel. The upper part is the merge of AF488 and AF594 images, and the lower part is the regular gel.

Discussion

Taken all data described above together, *E.coli* MMR key protein MutL undergoes slow subunit exchange which offers us the chance to monitor MutL nucleotide-dependent conformational changes and MutL dimer status, especially to monitor MutL NTD-CTD interaction, and complex formation with MutS and DNA.

Slowly, and with the concordant subunit exchange rate for all NTD-NTD, CTD-CTD, and NTD-CTD of FL MutL (Figure 3 and Figure 7), even for the trunked MutL CTD-CTD subunit exchange (Figure 2 C) have been observed. Measured with steady-state FRET illustrate that stable MutL dimer peak comes up because of the MutL subunit exchange, even though no monomer observed at sub-nanomolar level with our method. Single molecule data demonstrated that MutL forms a stable dimer and no nucleotide-induced conformational changes observed at CTD (Figure 4 J-L), whereas NTD rather dynamic even in the presence of ATP (Figure 4 B-H). From Figure 7, we show that in the presence of ATP the FRET between the labeled NTDs very slowly increases suggesting

a decrease of distance is in agreement with a closure of the NTD as reported before. The high FRET state is "resistant" to thrombin cleavage (Figure 7) suggesting that the formation of a stable NTD-NTD dimer of FL MutL by AMPPNP as observed by size-exclusion chromatography before (Ban and Yang 1998). The FRET decreased after thrombin cleavage indicating that NTD-NTD dimer appears to either dissociation or aggregation.

Until now no FL MutL crystal structure is available from the literature due to the long flexible linker. From Figure 3 C, we could observe that along with NTD and CTD labeled FL MutL subunit exchange the FRET slowly increased. We show that the FRET efficiency between donor and acceptor fluorophores attached to the NTD and CTD is non-zero (with a peak at 0.25, Figure 4 F-H) suggesting that the distance (on average) between the NTD and CTD is much smaller ($< 80 \text{ \AA}$) than that calculated before from dynamic light scattering (160 \AA ; which should result in no FRET) (Guarne, Ramon-Maiques et al. 2004). "One-arm" structure in eukaryotic MutL explaining that (Sacho, Kadyrov, et al. 2008). However higher concentration nucleotides modulated this one-armed structure shifted to the condensed structure in eukaryotic (Sacho, Kadyrov, et al. 2008), NTD-CTD FRET of FL MutL fade away after thrombin cleavage (Figure 7 F-H). However, ATP hydrolysis needed NTD-NTD dimerized (Ban and Yang 1998) indicating that this one-armed structure seems not necessary to the MutL function, but MutL conformational changes. Generating FL MutL hetero-dimer from stable dimer (even down to pico-molar level) is very important to study MutL nucleotides dependent conformational changes, especially for the NTD-CTD interaction in the future.

Method

Protein Expression and purification

Transferring 15 ml pre-culture into 500 ml LB culture containing 100 $\mu\text{g/ml}$ Ampicillin and incubating at 37 $^{\circ}\text{C}$ until OD_{600} to 1.0-1.2 for MutL, and 0.8-1.0 for MutS. Then adding 1mM IPTG (for MutL and MutS) into the culture and produce the proteins at 27 $^{\circ}\text{C}$ overnight. Recombinant His₆-tagged MutS and MutL proteins purified with Protino® Ni-IDA 2000 packed columns. After the proteins purified through gel-filtration on a Superdex 200 10/300 GL, thrombin was added into MutS to cleavage the His₆-tagged. Taking aliquots of 2-6 μl at various time intervals and running SDS PAGE (12.5 % for MutS) to make sure the cut is complete. Then, 1mM PMSF was added into the MutS before loaded into the Superdex 200 10/300 GL again. Finally, MutL and MutS proteins

were snap-frozen in liquid nitrogen and stored at -80 °C in 10 mM HEPES/KOH, 200 mM KCl, 1 mM EDTA, and pH 8.0. Protein concentrations were determined using theoretical extinction coefficients. (Toedt, Krishnan et al. 2003, Winkler, Marx, et al. 2011)

Protein labeling and degree of labeling (DOL) determination

Proteins labeled in HPLC buffer (10 mM HEPES/KOH (pH 8.0), 200 mM KCl and 1 mM EDTA) with AF488 maleimide (Invitrogen) and AF594 maleimide (Invitrogen) and excess unbound dye removed by gel filtration and buffer exchanged. For MutL change to buffer M/M (40.5 mM K₂HPO₄, 9.5 mM KH₂PO₄ (pH 7.4 at 25 °C) 50 mM KCl, 0.1 mM EDTA, 5 mM MgCl₂) and for MutS change to buffer FB150T (HEPES/KOH (pH 7.5 at 25 °C) 25 mM, KCl 150 mM, MgCl₂ 5 mM, Tween 20 0.005 %, 1 mg/ml BSA, 1 mM DTT) using Zeba Desalt Spin Columns (Pierce, Thermo Scientific). After that MutS and MutL were aliquoted and flash-frozen in liquid nitrogen and stored at -80 °C. Buffer M was used as it had been shown before to prevent self-assembly of MutL (Jia, Korolev, et al. 2011). FB150T was used as it had been shown before MutS/L complex formation (Groothuizen, Winkler, et al. 2015).

The DOL determined using absorbance spectroscopy

$$C_{\text{prot}} = (A_{280} - A_{\text{max}} \times CF) / \epsilon_{\text{prot}}$$

where A₂₈₀ is the absorbance at 280 nm, A_{max} is the absorbance of the Alexa 594 or Alexa 488, CF is the correction factor for the used dye CF_{AF488} = 0.12 and CF_{AF594} = 0.56 and ϵ_{prot} is the theoretical molar extinction coefficients of the respective protein.

The degree of labeling (DOL) was determined using the following equation:

$$\text{DOL} = (A_{\text{max}} \times \epsilon_{\text{prot}}) / ((A_{280} - A_{\text{max}} \times CF) \times \epsilon_{\text{max}})$$

Where ϵ_{max} is the molar extinction coefficients of Alexa 488 (71,000 M⁻¹cm⁻¹) and Alexa 594 (92,000 M⁻¹ cm⁻¹).

Analytical Ultracentrifugation (AUC)

Sedimentation velocity experiments performed in a Beckman Coulter Optima XL-I analytical ultracentrifuge equipped with a fluorescence detection system (AU-FDS, Aviv Biomedical, NJ, USA) using an An50Ti rotor at 20 °C and speeds from 22,000 to 33,000 rpm. The concentration profiles were measured using the AU-FDS with an excitation wavelength of 488 nm, and emission detected through a pair of long-pass (> 505 nm) dichroic filters. Programming of the centrifuge and data recording was performed using the AOS software (Aviv Biomedical, NJ, USA) on a computer attached to the centrifuge. Special cell housings (Nanolytics, Germany) used which allow the

placement of standard 3 mm double sector centerpieces directly beneath the upper window of the cell. The cells filled with 100 μ l sample. The experiments were performed in buffer M/M without or with 0.05 % (v/v) Tween20 to prevent protein adsorption to surfaces. For MutL-452-CTD he Alexa Fluor 488 labeled proteins was examined at concentrations between 2 nM and 100 nM. The measured concentration profiles were evaluated using the program package SEDFIT (Schuck 2000), which provides a model for diffusion-corrected differential sedimentation coefficient distributions (C(s) distributions). For hydrodynamic analyses measured s-values corrected to s_{20} . We are using the partial specific volumes calculated from amino acid composition (Durchschlag 1986). Since the partial specific amount of complexes of different macro-molecules with the unknown composition cannot be calculated, such a correction could not perform, and uncorrected sedimentation coefficients (s_{exp}) given in these cases (Manelyte, Urbanke, et al. 2006, Heinze, Giron-Monzon, et al. 2009).

DNA substrates

To generate a 932-bp covalently closed circular DNA containing a G: T mismatch, we used a PCR-based method substantially as described before (Xiao, Jung, et al. 2011). Our approach based on the nicking of PCR products resulting in single-stranded 3' overhangs, which form DNA circles after annealing and ligation (Xiao, Jung, et al. 2011). Briefly, λ -DNA (position 40236–41146) is amplified using primers 5'-CTC AAG CTT CAC TGC ATC GCA GAA ATC AAA GCT AA-3' and 5'-AAG CTC GAG CAC TGC TTG CTC CAT TAG CCA GAG CA-3' (5'-overhangs shown in bold; the site for the nicking enzyme Nb.BtsI is underlined). PCR products were nicked by Nb.BtsI, annealed, ligated by DNA ligase and any remaining DNA containing ends or nicks removed by treatment with exonuclease I and exonuclease III.

The smFRET

We used smFRET (single molecule Förster Resonance Energy Transfer) to study the conformation of MutL hetero-dimers and the modulation by nucleotide co-factors. The smFRET experiments were performed in a home-built confocal microscope with spectral detection windows for the donor (520/66 nm) and acceptor (630/60 nm) at Prof. Dr. D. Klostermeier's group (Institut für Physikalische Chemie, Universität Münster). All measurements were performed in buffer M/M at room temperature in absence or presence of ATP or AMPPNP with 100 pM donor and acceptor labeled hetero-dimer of MutLH297C or MutL452C (MutL452), or MutLH297C (MutL297), acceptor and MutL452C donor. 10 mM MutLH297C or MutL452C donor/acceptor labeled hetero-

dimer were pre-incubated with 50 mM AMPPNP at 4 °C for 12 h before doing the single molecular experiment.(Hilbert, Keibel, et al. 2010, Andreou and Klostermeier 2012)

Thrombin cleavage assay

Added 20 µl (1000 U/ml) Thrombin to pre-generated 200 µl, 2 µM full-length MutL hetero-dimer (MutL297_AF488 pre-incubated with MutL297_AF594 with 1:1 ratio for 25 min at room temperature) in buffer M and incubated at room temperature for 1-120 min. After that taking out 20 µl at 0, 1, 2, 4, 8, 16, 30, 40, 60, 80, and 120 min mixed with 5 µl, 0.5 mM PMSF to stop the reaction the reaction. Then running 12.5 % SDS-Gel at 150 V, 170 A for 1 h.

References

- Aksentijevich, I., D. P. C, E. F. Remmers, J. L. Mueller, J. Le, R. D. Kolodner, Z. Moak, M. Chuang, F. Austin, R. Goldbach-Mansky, H. M. Hoffman and D. L. Kastner (2007). "The clinical continuum of cryo-pyrino pathies: novel CIAS1 mutations in North American patients and a new cryopyrin model." *Arthritis Rheum* 56(4): 1273-1285.
- Anbazzhagan, R., H. Fujii and E. Gabrielson (1999). "Microsatellite instability is uncommon in breast cancer." *Clin Cancer Res* 5(4): 839-844.
- Andreou, A. Z. and D. Klostermeier (2012). "Conformational changes of DEAD-box helicases monitored by single-molecule fluorescence resonance energy transfer." *Methods Enzymol* 511: 75-109.
- Baitinger, C., V. Burdett and P. Modrich (2003). "Hydrolytically deficient MutS E694A is defective in the MutL-dependent activation of MutH and the mismatch-dependent assembly of the MutS center dot MutL center dot heteroduplex complex." *Journal of Biological Chemistry* 278(49): 49505-49511.
- Ban, C., M. Junop and W. Yang (1999). "Transformation of MutL by ATP binding and hydrolysis: a switch in DNA mismatch repair." *Cell* 97(1): 85-97.
- Ban, C. and W. Yang (1998). "Crystal structure and ATPase activity of MutL: implications for DNA repair and mutagenesis." *Cell* 95(4): 541-552.
- Brar, S. S., E. J. Sacho, I. Tessmer, D. L. Croteau, D. A. Erie and M. Diaz (2008). "Activation-induced deaminase, AID, is catalytically active as a monomer on single-stranded DNA." *DNA Repair (Amst)* 7(1): 77-87.
- Brino, L., A. Urzhumtsev, M. Mousli, C. Bronner, A. Mitschler, P. Oudet and D. Moras (2000). "Dimerization of *Escherichia coli* DNA-gyrase B provides a structural mechanism for activating the ATPase catalytic center." *J Biol Chem* 275(13): 9468-9475.
- Dong, K. C. and J. M. Berger (2007). "Structural basis for gate-DNA recognition and bending by type IIA topoisomerases." *Nature* 450(7173): 1201-U1204.
- Drotschmann, K., A. Aronshtam, H. J. Fritz and M. G. Marinus (1998). "The *Escherichia coli* MutL protein stimulates binding of Vsr and MutS to heteroduplex DNA." *Nucleic Acids Res* 26(4): 948-953.

Duppatla, V., C. Bodda, C. Urbanke, P. Friedhoff and D. N. Rao (2009). "The C-terminal domain is sufficient for endonuclease activity of *Neisseria gonorrhoeae* MutL." *Biochem J* 423(2): 265-277.

Dutta, R. and M. Inouye (2000). "GHKL, an emergent ATPase/kinase superfamily." *Trends Biochem Sci* 25(1): 24-28.

Fass, D., C. E. Bogden and J. M. Berger (1999). "Quaternary changes in topoisomerase II may direct orthogonal movement of two DNA strands." *Nat Struct Biol* 6(4): 322-326.

Giron-Monzon, L., L. Manelyte, R. Ahrends, D. Kirsch, B. Spengler and P. Friedhoff (2004). "Mapping protein-protein interactions between MutL and MutH by cross-linking." *J Biol Chem* 279(47): 49338-49345.

Guarne, A. and J. B. Charbonnier (2015). "Insights from a decade of biophysical studies on MutL: Roles in strand discrimination and mismatch removal." *Prog Biophys Mol Biol* 117(2-3): 149-156.

Guarne, A., S. Ramon-Maiques, E. M. Wolff, R. Ghirlando, X. Hu, J. H. Miller and W. Yang (2004). "Structure of the MutL C-terminal domain: a model of intact MutL and its roles in mismatch repair." *EMBO J* 23(21): 4134-4145.

Gubaev, A., M. Hilbert and D. Klostermeier (2009). "The DNA-gate of *Bacillus subtilis* gyrase is predominantly in the closed conformation during the DNA supercoiling reaction." *Proc Natl Acad Sci U S A* 106(32): 13278-13283.

Gueneau, E., C. Dherin, P. Legrand, C. Tellier-Lebegue, B. Gilquin, P. Bonnesoeur, F. Londino, C. Quemener, M. H. Le Du, J. A. Marquez, M. Moutiez, M. Gondry, S. Boiteux and J. B. Charbonnier (2013). "Structure of the MutL α C-terminal domain reveals how Mlh1 contributes to Pms1 endonuclease site." *Nat Struct Mol Biol*.

Hackman, P., P. Tannergard, S. Osei-Mensa, J. Chen, M. F. Kane, R. Kolodner, B. Lambert, D. Hellgren and A. Lindblom (1997). "A human compound heterozygote for two MLH1 missense mutations [letter]." *Nature Genetics* 17(2): 135-136.

Heinze, R. J., S. Sekerina, I. Winkler, C. Biertümpfel, T. Oretskaya, E. Kubareva and P. Friedhoff (2012). "Covalently trapping MutS on DNA to study DNA mismatch recognition and signaling." *Molecular Biosystems*.

Kosinski, J., I. Steindorf, J. M. Bujnicki, L. Giron-Monzon and P. Friedhoff (2005). "Analysis of the quaternary structure of the MutL C-terminal domain." *J Mol Biol* 351(4): 895-909.

Lanz, M. A. and D. Klostermeier (2011). "Guiding strand passage: DNA-induced movement of the gyrase C-terminal domains defines an early step in the supercoiling cycle." *Nucleic Acids Res.*

Li, J. and J. Buchner (2013). "Structure, function, and regulation of the hsp90 machinery." *Biomed J* 36(3): 106-117.

Miguel, V., E. M. Correa, L. De Tullio, J. L. Barra, C. E. Argarana and M. A. Villarreal (2013). "Analysis of the interaction interfaces of the N-terminal domain from *Pseudomonas aeruginosa* MutL." *PLoS One* 8(7): e69907.

Minami, Y., Y. Kimura, H. Kawasaki, K. Suzuki and I. Yahara (1994). "The carboxy-terminal region of mammalian HSP90 is required for its dimerization and function in vivo." *Molecular and cellular biology* 14(2): 1459-1464.

Niedziela-Majka, A., N. K. Maluf, E. Antony and T. M. Lohman (2011). "Self-assembly of *Escherichia coli* MutL and its complexes with DNA." *Biochemistry* 50(37): 7868-7880.

Pang, Q., T. A. Prolla and R. M. Liskay (1997). "Functional domains of the *Saccharomyces cerevisiae* Mlh1p and Pms1p DNA mismatch repair proteins and their relevance to human hereditary nonpolyposis colorectal cancer-associated mutations." *Mol Cell Biol* 17(8): 4465-4473.

Pillon, M. C., V. M. Babu, J. R. Randall, J. Cai, L. A. Simmons, M. D. Sutton and A. Guarne (2015). "The sliding clamp tethers the endonuclease domain of MutL to DNA." *Nucleic Acids Res.*

Richter, K., P. Muschler, O. Hainzl and J. Buchner (2001). "Coordinated ATP hydrolysis by the Hsp90 dimer." *J Biol Chem* 276(36): 33689-33696.

Sacho, E. J., F. A. Kadyrov, P. Modrich, T. A. Kunkel and D. A. Erie (2008). "Direct visualization of asymmetric adenine-nucleotide-induced conformational changes in MutL alpha." *Mol Cell* 29(1): 112-121.

Taisheng Wang,^a N. Z.^a, Ruke Bai^{*a} and Yinyin Bao^{*b} Taisheng Wang,^a Na Zhang,^a Ruke Bai^{*a} and Yinyin Bao^{*b} (2018). "Aggregation-Enhanced FRET-Active Conjugated Polymer Nanoparticles for Picric Acid Sensing in Aqueous Solution.pdf." *J. Mater. Chem. C*,(6): 266-270

Yamamoto, T., H. Iino, K. Kim, S. Kuramitsu and K. Fukui (2011). "Evidence for ATP-dependent structural rearrangement of nuclease catalytic site in DNA mismatch repair endonuclease MutL." *J Biol Chem* 286(49): 42337-42348.

Chapter 2

Methods for monitoring MMR and protein-DNA interaction

Abstract

In addition to the Förster Resonance Energy Transfer (FRET), single-molecule FRET, co-localization, and others fluorescence-based methods produced to study protein and nucleic acid interaction, a general approach to stain nucleic acid which not restricted to specific position, no selectivity of different types of nucleic acid, and to be flexible with colors to label at proteins has been needed. Under this condition, SYTOX blue (SB) excited/emitted at 435/470 nm while excited/emitted at 444/470 nm for SB-DNA complexes, has been used to stain different types of DNA and RNA. The rapid association and dissociation kinetics (equilibrium established within 30 ms) which have been captured by stopped-flow fluorescence apparatus making this method suitable as a non-interfering dye to study protein-DNA interaction base on FRET. The main advantages of SB staining DNA described as follows: Fast apparent association and dissociation (<30 ms) rates for DNA staining processes and that will not overlap with fast DNA and MMR proteins interaction; Weaker interaction between SB DNA may result in less alternating and stabilize DNA specific structure artificially; No labeling positions limited; possible used to stain all types of nucleic acids (ssDNA and RNA) have been noticed as well.

An example of using FRET between SYTOX blue (blue dye) and AF594 (red dye) is the multiphasic BR FRET kinetics of MutS_AF594 binding SB stained, mismatched dsGT59DF DNA (DF: Digoxin-Fab fragment blocked the end). The kinetics reach the saturation within 1 s in the presence of ATP in FB150T buffer. The recruitment of MutL (labeled with AF594, red) to mismatch DNA (stained with SB, blue) by MutS is demonstrated that established the equilibrium within 10 s, revealing an apparent KD around 50 nM and a fast bimolecular association rate constant of about $10 \mu\text{M}^{-1}\text{s}^{-1}$. Finally, the ATP-dependent formation of ternary complexes between mismatched DNA, MutS and MutL are shown as the GR FRET (FRET between AF488 and AF594 labeled MutS and MutL), the BR FRET (FRET between SB and AF594 colored mismatched DNA and MutL), and the BG FRET (FRET between SB and AF488 colored mismatched DNA and MutS). With a SB stained circular mismatched-containing 932 bp DNA we observed the mismatch discrimination complexes formation.

Keywords: MutL, ssDNA, dsDNA, RNA, SB, MutS, cation, FRET

Introduction

SYTOX family intercalating dyes (SYTOX blue, SYTOX orange, SYTOX green, and SYTOX red) are commonly used as dead-cell markers (Richard Wombacher, Sebastian van de Linde, et al. 2010, Shi, Vu et al. 2017). This SYTOX family's intercalating dyes share the similar Molecular Weight around 400-600 (Invitrogen) and exhibit a significant fluorescence enhancement over 500 fold (Invitrogen). SYTOX family intercalating dyes are generally used for DNA fragment sizing, DNA fragment sizing flow cytometry, and recently used for single-cell, single-molecular, Förster resonance energy transfer (FRET) studies (Yan, Habbersett et al. 2000, Heller, Sitters, et al. 2013, Thakur, Cattoni, et al. 2015). As the other cyanine dyes, SB possesses essential spectroscopic and physical properties, such as significant fluorescence enhancement, very low intrinsic fluorescence and high quantum yield (Invitrogen). Another advantage for SB staining nucleic acid much faster than the other intercalating dyes, such as YOYO-1 (Thakur, Cattoni, et al. 2015), and even SYBR Green I (SG) which was shown in the appendix (Appendix Figure 2.3, B). Except all that were described above, the literature report that intercalators change DNA in the following ways: 1, Intercalators except increase the contour length of DNA (produce ~ 0.34 nm per mono- intercalator such as SYTOX orange and SYTOX green, and ~ 0.68 nm per bis-intercalator like YOYO and POPO); 2, Intercalators are reported could alternate the structure and mechanical properties of DNA (Hurley 2002, Koster, Palle et al. 2007, Paramanathan, Vladescu, et al. 2012); 3, Stabilizing and protecting DNA against unwinding caused by different monovalent concentration (King, Gross et al. 2013, Biebricher, Heller, et al. 2015) as well. All these changes to DNA will cause perturbation of enzymatic reactions with DNA, and hence affect conformational changes in proteins.

Intercalation and external electrostatic binding to the phosphate backbone are the two distinct binding modes have been identified during the last decades (Cosa G 2001, Record, Anderson, et al. 2009, Dragan, Casas-Finet et al. 2010, Biebricher, Heller, et al. 2015). The former is the principal way at low dye/base pair ratios, and the affinity at the nano-molar range based on SYTOX orange, Pico Green, while the latter approach starting to contribute at high dye/base ratios and the affinity is the micro-molar range (Yan, Habbersett et al. 2005). Whereas these two binding modes will be misleading when the binding is cooperatively (McGhee 1974, Stephen C. Kowalczykowski, Nils Lonberg, et al. 1985). Based on the SYTOX orange association mode, the dissociation rate and the concentration of the reactants in solution (Yan, Habbersett et al. 2000, Yan, Habbersett, et al. 2005). However, related the kinetics of SB staining double strand DNA and single-strand DNA and how

this kinetics affected by the cation is still unclear. While these may cause great misunderstanding during FRET which rises comes from the donor quench and could be caused by adding Mg^{2+}/KCl as well.

An GHKL (Gyrase, Hsp90, Histidine kinase, MutL) family member, MutL and its homologs (Mlh1-Pms1 in yeast and MLH1-PMS2 in human) are essential for DNA mismatch repair (MMR)(Gorbalenya and Koonin 1990, Ban and Yang 1998, Ban, Junop et al. 1999, Friedhoff, Li et al. 2015). As indicated in the literature, all MutL homologs share around 300 conserved residues at NTD (Ban and Yang 1998). While dimerized at the divergent C-terminal domain (CTD) (Pang, Prolla, et al. 1997, Ban and Yang 1998, Drotschmann, Aronshtam et al. 1998, Ban, Junop, et al. 1999). Except together with MutS and MutH involved in methyl-dependent DNA mismatch repair in *E.coli* (Modrich and Lahue 1996), MutL implicated in other DNA repair pathways as well. These pathways are TCR (transcription-coupled repair pathway) (Mellon, Rajpal et al. 1996, Chakraborty and Alani 2016) and VSR (very short repair pathway) (Drotschmann, Aronshtam et al. 1998, Monastiriakos, Doiron, et al. 2004). Notably, MutL was recruited by MutS on DNA in physical ionic conditions, binding nucleotide and proceeding ATPase activity are all needed in these three DNA repair pathways (Ban and Yang 1998, Heinze, Giron-Monzon, et al. 2009). Mismatch deficiency will cause Lynch syndrome and sporadic tumors (Martin-Lopez and Fishel 2013).

Wild-type MutL ATP hydrolysis rate is 0.4 min^{-1} , which could be seven fold faster by adding ssDNA ($\sim 3 \text{ min}^{-1}$) at room temperature (Ban, Junop, et al. 1999) and 9 min^{-1} at $37 \text{ }^\circ\text{C}$ (90 mM KCl) with the similar affinity to ATP (Spampinato and Modrich 2000). However, how these affect MutL interact with DNA, and processing conformational changes on DNA still unclear. With SB stained DNA offer us the possibility in the future to study all these processes. Here we measure the kinetics of MutL loading on dsGT59DF DNA which starts $\sim 0.1 \text{ s}$, and wtMutS is necessary for this processes under physiological ionic strength buffer. The affinity of SB to DNA has been severely affected by the cation strength, especially Mg^{2+} . Mg^{2+} and K^+ could decrease the SB-DNA complex fluorescence intensity by changing both the association and dissociation rates that may cause severe misunderstanding in FRET calculation with the concentration of Mg^{2+} changing. Analyzed non-linear of the association and dissociation rates curves indicating that SB interact with DNA is complicated, and maybe in multiple ways, which could be shown by SB could stain ss (single-strand)/ds (double-strand) DNA and different type of RNA as well.

SYTOX blue (SB) is cell-impermanent cyanine dyes with little quantum yield when not bond to nucleic acids while around 10 fold increased in quantum yield after binding nucleic acids

(Invitrogen). Excitation (Ex.) wavelength rather than Emission (Em.) wavelength changing when forms SB-DNA or SB-RNA complexes (from 435/470 nm to 444/470 nm) (Figure 1).

Results

1, Associating SB on the different type of nucleic acids in different buffer

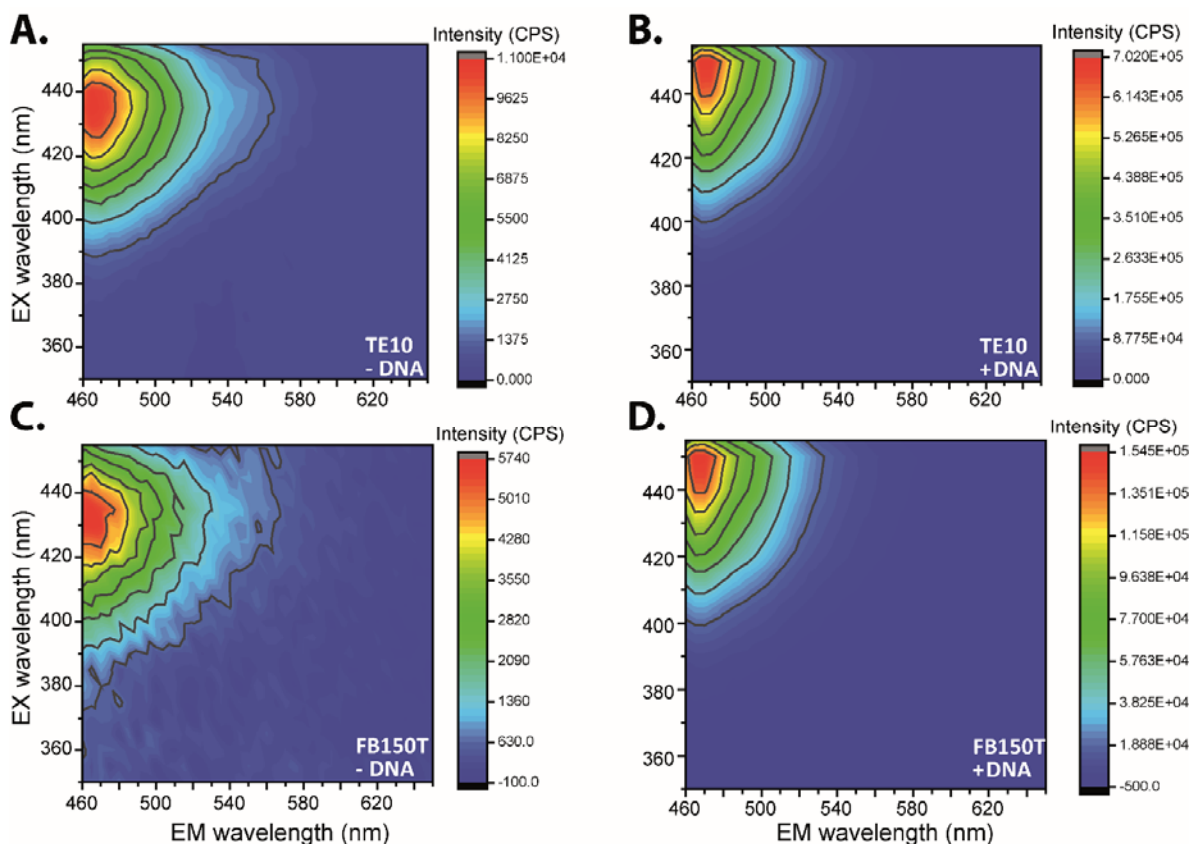


Figure 1. Spectra of Excitation and Emission of 200 nM SB free dye or/and binding 1 μ M GT30 DNA in TE10 and FB150T buffer (Slit: Ex./Em. 2 nm/2 nm). (A) 200 nM SB free dye in TE10 buffer; (B) 200 nM SB free dye with 1 μ M GT30 DNA in TE10 buffer; (C) 200 nM SB free dye in FB150T buffer; (D) 200 nM SB free dye with 1 μ M GT30 DNA in FB150T buffer.

SYTOX blue (SB) is cell-impermanent cyanine dye with meager quantum yield when not bond to nucleic acids while around 10 fold enhancement in quantum yield after binding nucleic acids (Invitrogen). Excitation (Ex.) wavelength rather than Emission (Em.) wavelength changing when forms SB-DNA or SB-RNA (from 435/470 nm to 444/470 nm) complexes (Figure 1) but no change observed due to the different types of nucleic acids and different buffers condition (Figure 2). The affinity of SB to dsDNA is around 0.9 μ M bp DNA in TE10 buffer containing 10 mM KCl which calculated from titration dsGT30 DNA to 0.1 or 0.5 μ M SB (Figure 3 A-B). Moreover, the affinity ($K_D \sim 9 \mu$ M bp DNA) will 10 fold decrease as the salt concentration increasing to 150 mM KCl,

and 100 fold lower ($K_D \sim 90 \mu\text{M}$ bp DNA) when the salt concentration increased to 150 mM KCl plus 5 mM Mg^{2+} in TE10 buffer (Figure 3 A.-C). The similar affinities of SB to ds DNA in different

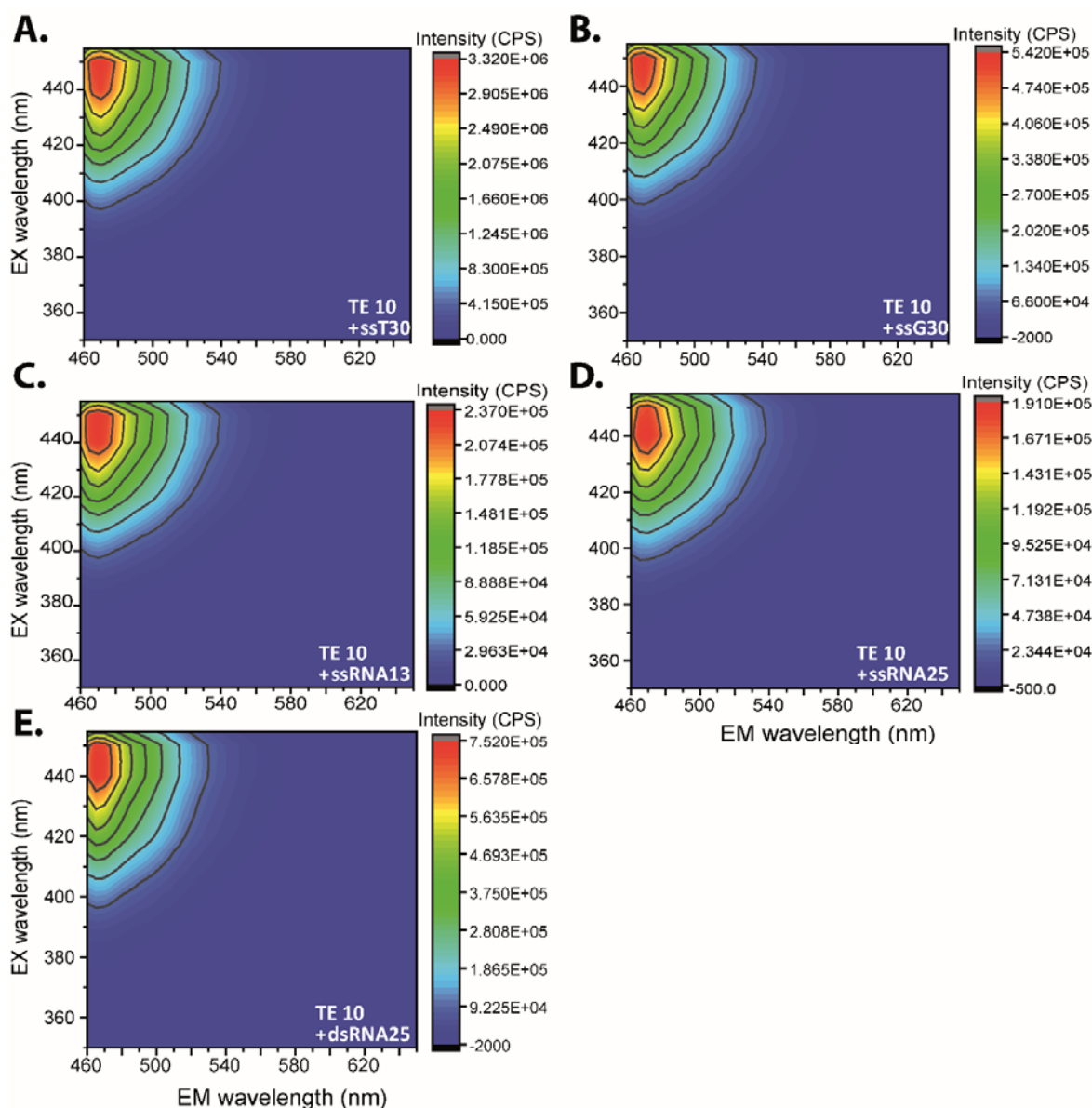


Figure 2. Spectra of Excitation and Emission of 200 nM SB free dye or/and binding 1 μM ssT30 DNA/ssG30/ssRNA13/ssRNA25/dsRNA25 in TE10 buffer (Slit: Ex. / Em. 2 nm/2 nm). (A) 200 nM SB free dye 1 μM ssT30 DNA in TE10 buffer; (B) 200 nM SB free dye with 1 μM ssG30 DNA in TE10 buffer; (C.) 200 nM SB free dye with 1 μM ssRNA13 in TE10 buffer; (D) 200 nM SB free dye with 1 μM ssRNA25 in TE10 buffer; (E) 200 nM SB free dye with 1 μM dsRNA25 in TE10 buffer.

buffers derived from analyzing the kinetics of titration SB to 50 nM dsGT30 DNA with the conditional probability of non-cooperative model. This mode was derived by McGhee and von Hippel (McGhee 1974, Stephen C. Kowalczykowski, Nils Lonberg, et al. 1985). The binding site size of SB to dsGT30 DNA and ssT30 DNA/ssG30 DNA are around 5 bp, and seems not affected

by the salt (Appendix Figure 2.1). Except for large fluorescence enhancements (over 500 fold) (Invitrogen), another advantage of SB is that it could stain single strand DNA (ssDNA) with less ability compared to double strand DNA. As titrating dsGT30/ ssT30/ssG30 DNA to 0.2 μM SB in TE10 buffer, we obtained the similar K_D value for dsGT30 as titration SB, while with around 2-3 fold lower affinity for both two different single strand DNA of dsGT30 (Figure 3 C). When titrating dsGT30/ssT30/ ssG30 DNA to 1 μM SB in TE10 buffer, we found that at high dye/base pair ratio (GT30 <10 μM bp), the kinetics fit to the high affinity mode as well (Figure 3 D, solid line). However, at low dye/base pair ratio (GT30 >10 μM bp), the binding affinities of dsGT30/ssT30/ ssG30 are all lower, and the kinetics fit to the lower affinities better (Figure 3 D, dash line). In reverse, when titration SB to 200nM ssT30 DNA/ssG30 DNA, the binding site size (n) and the

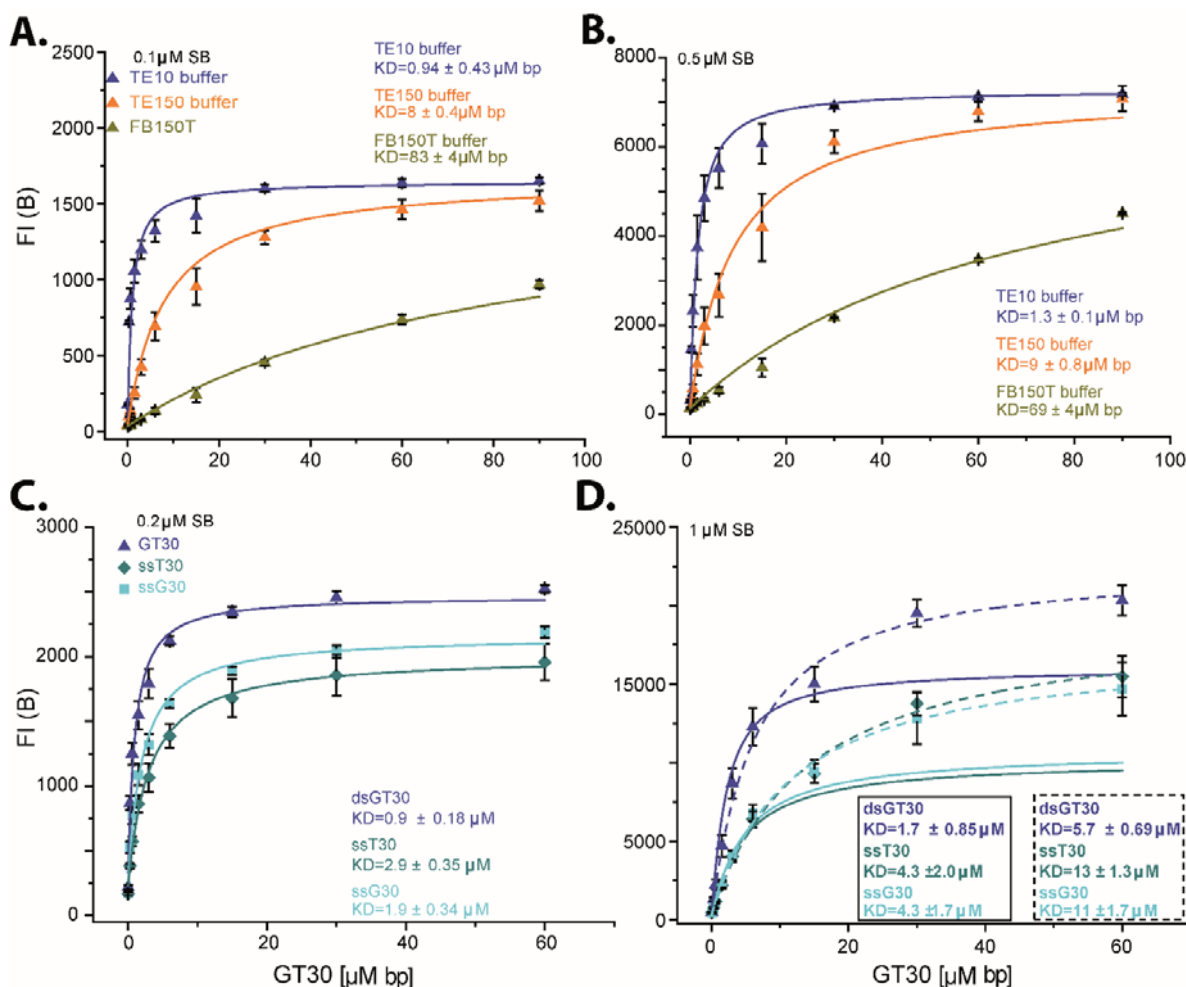


Figure 3. SB binding dsDNA and ssDNA in different buffers. (A) Titration dsGT30 DNA to 0.1 μM SB in TE10 (10 mM KCl)/TE150 (150 mM KCl)/FB150 (150 mM KCl and 5 mM Mg^{2+}) buffers; (B) Titration dsGT30 DNA to 0.5 μM SB in TE10/TE150/FB150 buffer; (C) Titration dsGT30 DNA/ssT30 DNA/ssG30 DNA to 0.2 μM SB in TE10 buffer; (D) Titration dsGT30 DNA/ssT30 DNA/ssG30 DNA to 1 μM SB in TE10 buffer, the solid lines are the fixed K_D to the data points fitting, and the dash lines are the fitting depending on the data.

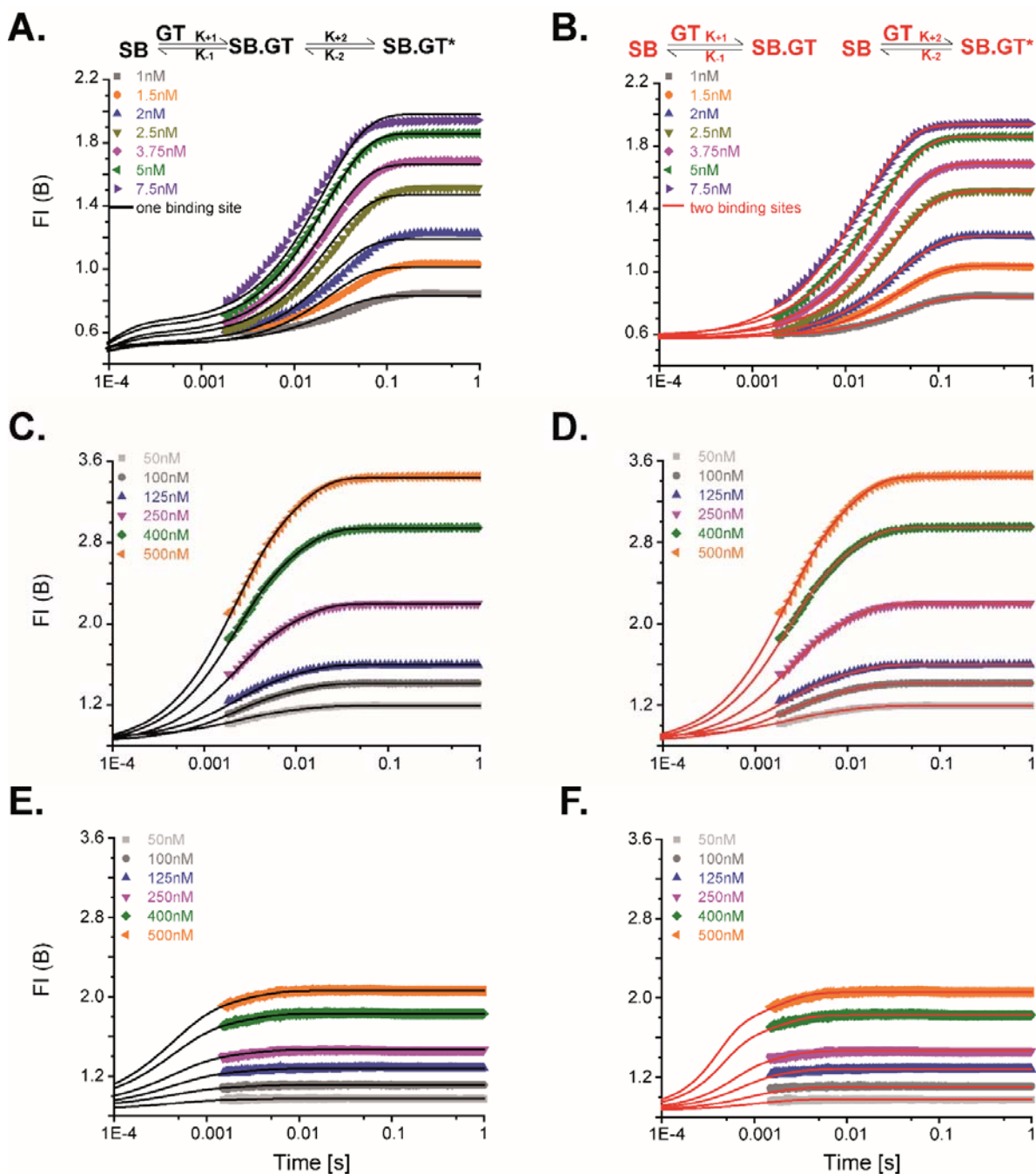


Figure 4. Kinetics of SB binding to ds or ss DNA monitored by stopped-flow. (A-B) Kinetics of titration dsGT30 DNA to 2.5 nM SB in TE10 buffer and analyzed with KinTek explorer (one binding site and two steps model, black line A; And two binding sites one step bind model, red line B; (C-D) Kinetics of titration dsGT30 DNA binding 25 nM SB in FB150T buffer and kinetics analyzed with KinTek explorer (one binding site and two steps model, black line C; And two binding sites one step bind model, red line D; (E and F) Kinetics of titration ssG30 DNA into 25 nM SB in FB150T buffer, and kinetics analyzed with KinTek explorer (one binding site and two steps model, black line E.; and two binding sites one step bind model, red line F).

affinity (KD) are $n=6.3 \pm 1.8$ nt/KD = 3.8 ± 0.99 μ M nt for ssT30, and $n=7.5 \pm 2.1$ nt/KD = 3.8 ± 0.99 μ M nt for ssG30 DNA in TE10 buffer with 10 mM KCl (Appendix Figure 2.1E and F). While

increased KCl to 150 mM, the binding site size (n) and the affinity (KD) are $n=4.6\pm 0.2$ nt/KD = 48 ± 0.5 μ M nt for ssT30 DNA, and $n=4.5\pm 0.7$ nt/KD = 51 ± 1.8 μ M nt (Appendix Figure 2.1G and I). Except for ds and ss DNA, we investigate the property of SB binding ds/ss RNA as well. As shown in Appendix Figure 2.2 A and B we conclude that SB binding dsRNA with 3 ± 0.1 bp binding site size and with KD around 160 nM. Moreover, from the graph of titration RNA into 200 nM SB, we conclude that the KD for overhang dsRNA25, ssRNA25, and ssRNA13 are 380 ± 120 nM, 690 ± 230 nM, and 730 ± 250 nM separately, and the Fluorescence intensity for overhang dsRNA25 are doubling as ss RNA (Appendix Figure 2.2 D). Only increased the concentration of KCl in buffers will block SB associating on RNA (Appendix Figure 2.2 C).

When analyzing data of titration SB to different types of nucleic acids in different buffers, we limited SB concentration within 1 μ M in case the fluorescence intensity of SB binding to the nucleic acids effected by the primary and secondary inner filter effect (Lakowicz 2006, Fabian, Rente, et al. 2010). The complication is that when SB is binding dsDNA no inner filter effect is observed while appears only in the free SB (Appendix Figure 2.1 J and K). However, compare Appendix Figure 2.1 B and D we could conclude that within 1 μ M SB, almost no SB binding dsGT30 DNA observed in FB150T (containing 150 mM KCl and 5 mM Mg^{2+}) buffer which mainly because of the high concentration of Mg^{2+} .

2, The kinetics of SB associating on ds/ssDNA assessed by Stopped-flow

After knowing the affinity (KD) and binding site size (n) of SB to dsGT30 DNA in different buffers as described above, the rates of SB associate on and dissociate from ds/ss DNA in different buffers are critical in measurement. Because if the association and dissociation rates of SB to DNA are slow, the processes of SB and DNA interaction will overlap with the processes of protein-protein interaction or protein-DNA interaction or both. From Figure 4 we could observe that SB binding ds/ss DNA and reach equilibrium within 30 ms in both TE10 and FB150T buffers. Analyzed the binding kinetics of SB to dsGT30 DNA with exponential fits after correcting 2 ms' dead time of stopped-flow instrument still not works due to the binding is too fast. Therefore, we analyze the kinetics of SB associating on DNA (Figure 4) and titration DNA to SB (Figure 1) at the same time with KinTek explorer (Johnson 2009, Johnson, Simpson, et al. 2009, Johnson, Simpson, et al. 2009). However, the kinetics of SB binding both the ds and ss DNA in FB150T buffer fit to both one binding site mode (with conformational change, black) and two binding sites (red) mode (Figure 4 C-F). While the kinetics, with titration dsGT30 DNA to 2.5 nM SB in TE10 buffer (containing 10 mM KCl), fit to two binding sites mode (Figure 4 B) better than one binding site

model (Figure 4 A). We could find that increasing the concentration of K^+ and Mg^{2+} not only decrease the association rates but also increase the dissociation rates. Even though the apparent rates for dsGT30 DNA, which are derived from the KinTek explorer, are not very well constrained, neither in TE10 buffer nor in FB150T buffer. However, the apparent association and dissociation rates are better constrained in two binding sites model than single binding site model for ssG30 DNA in FB150T (Table 1).

Table 1 Kinetics parameters derived from KinTek explorer fits (professional version)

Mechanistic model		SB $\xrightleftharpoons[K_1]{GT}$ SB.GT $\xrightleftharpoons[K_2]{}$ SB.GT*		SB $\xrightleftharpoons[K_1]{GT}$ SB.GT SB $\xrightleftharpoons[K_2]{GT}$ SB.GT*	
		Global best fit (lower-upper limit)		Global best fit (lower-upper limit)	
		TE10	FB150	TE10	FB150
k_{+1}	ds	9350-151000 $\mu M^{-1}s^{-1}$	37-1600 $\mu M^{-1}s^{-1}$	600-3000 $\mu M^{-1}s^{-1}$	3.1-9.4 $\mu M^{-1}s^{-1}$
	ss		0.001-904 s^{-1}		0.06-200 $\mu M^{-1}s^{-1}$
k_{-1}	ds	116-15800 s^{-1}	291-38000 s^{-1}	600-1000 s^{-1}	109-125 s^{-1}
	ss		1450-20400 s^{-1}		549-1070 s^{-1}
k_{+2}	ds	0.1-1420 s^{-1}	3-457 s^{-1}	5750-7490 $\mu M^{-1}s^{-1}$	24.5-56.7 $\mu M^{-1}s^{-1}$
	ss		122-71600 s^{-1}		5280-948000 $\mu M^{-1}s^{-1}$
k_{-2}	ds	8.8-33.9 s^{-1}	33-223 s^{-1}	5.9-9.3 s^{-1}	510-586 s^{-1}
	ss		321-843 s^{-1}		38-88500 s^{-1}

3, Mg^{2+}/K^+ dominating SB staining by changing the apparent K_{on} and K_{off}

As described above, K^+/Mg^{2+} to a large extent affect the binding kinetics of SB to DNA. To investigate the way that how K^+/Mg^{2+} affect SB and DNA interaction, we titration K^+/Mg^{2+} to SB-dsGT30 DNA complex in TE10 buffer and Mg^{2+} to TE150 buffer (Figure 5 A and B). Titration KCl into SB-dsGT30 DNA complex in TE10 buffer which will drive SB dissociates from DNA, around 80 % of SB dissociating from DNA when the concentration of KCl reach to 150 mM and almost no SB binding DNA when the level of KCl is over 300 mM (Figure 5 A). When titration Mg^{2+} to SB-dsGT30 DNA complex in TE10 buffer we could observe that the effect of 2.5 mM Mg^{2+} equal to 150 mM KCl. Moreover, 7 mM Mg^{2+} could block SB binding dsGT30 DNA entirely (Figure 5 B), this phenomenon could be rescued by titration ATP which could chelate Mg^{2+} (Appendix Figure 2.3, A). Due to the low affinity and weak interaction between SB and dsGT30 DNA and these were manipulated by K^+/Mg^{2+} which might catch problem during the measurement, therefore how fast the interaction between SB and dsGT30 DNA could reach equilibrium after adding K^+/Mg^{2+} is critical.

Based on this point, we are monitoring kinetics of titrating K^+/Mg^{2+} induced SB dissociation from dsGT30 DNA with the stopped-flow (Appendix Figure 2.1 C and E). The kinetics of K^+/Mg^{2+}

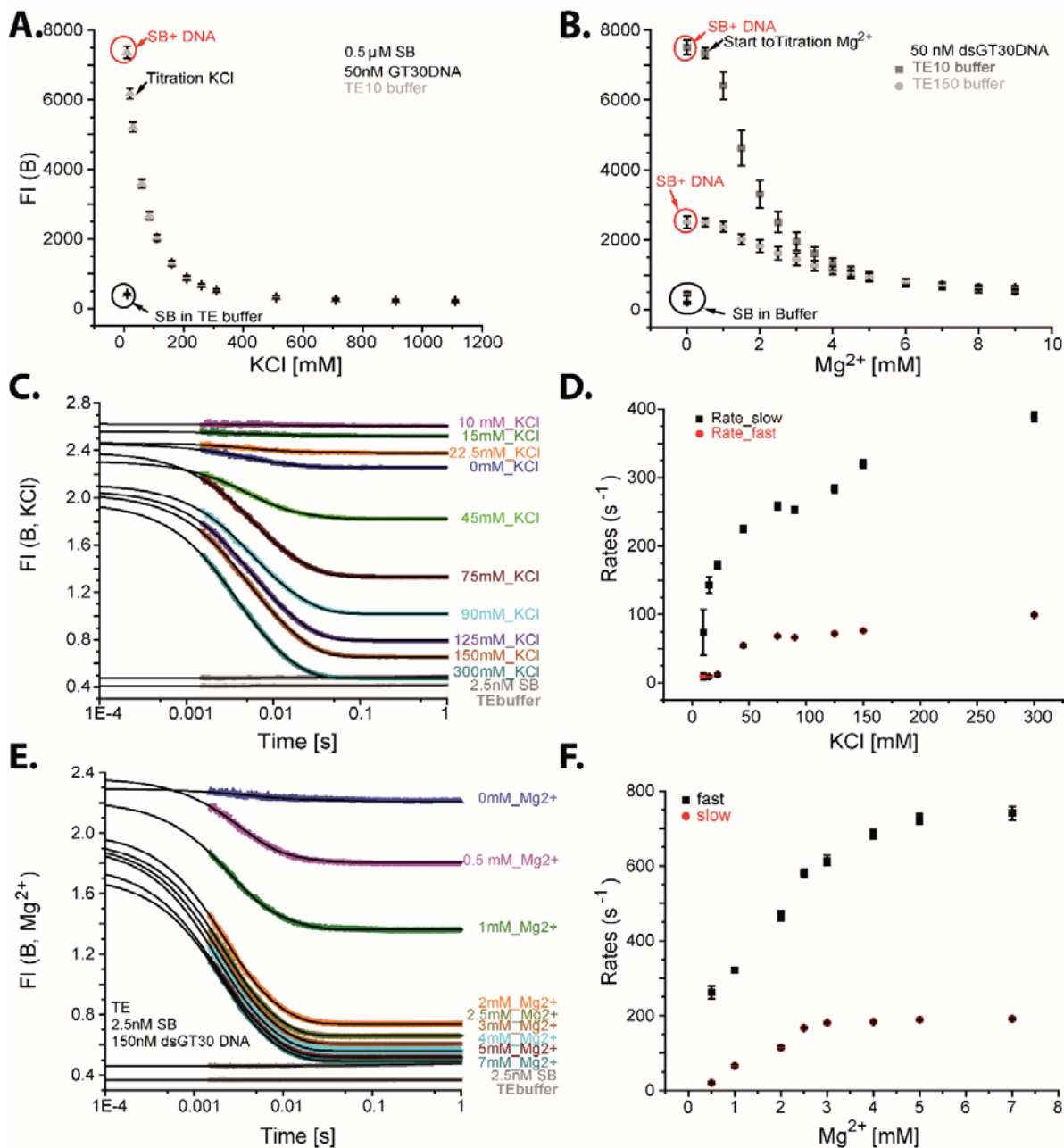


Figure 5. The effect of KCl and Mg²⁺ on SB association on/dissociation off dsGT30 DNA. (A) titration KCl to 0.5 μM SB and 1.5 μM bp dsGT30 DNA complex in TE10 (10 mM KCl) buffer; (B) titration Mg²⁺ to 0.5 μM SB and 1.5 μM bp dsGT30 DNA complex in TE10 and TE150 (150 mM KCl) buffer; (C) stopped-flow monitoring the kinetics of titration K⁺ to 2.5 nM SB/4.5 μM bp dsGT30 DNA in TE buffer and analyzed with two exponential fits after correcting the dead time of instrument (2.2 ms); (D) the fast and slow rates derived from two exponential fits to the kinetics of C; (E) stopped-flow monitoring the kinetics of titration Mg²⁺ to 2.5 nM SB/4.5 μM bp dsGT30 DNA in TE10 buffer and analyzed with two exponential fits after correcting the dead time of instrument (2.2 ms); (F) the fast and slow rates derived from two exponential fits of E.

induced SB dissociation from dsGT30 DNA indicated that these processes are rather fast and finish in 30 ms (Appendix Figure 2.1 C and E). After corrected 2 ms' dead time of the instrument, two exponential fits reveal that the effect of Mg²⁺ is simpler and linearly increase with apparent off

rates within 5 mM (3 mM for the slow rate, Appendix Figure 2.1 F), while the effect of K^+ fits two exponential fits also but the kinetics are complicated, and the apparent off rates behave non-linearly even though the slow off rates almost not change after 50 mM KCl (Appendix Figure 2.1 D).

4, Kinetics of MutS associating on SB stained DNA

One of the critical advantages of SB is that the kinetics of SB staining dsDNA is very fast (<30 ms) and could reach saturation far more before the enzymes and DNA interaction processes finished. Therefore, SB applying in studying mismatch repair proteins MutS and MutL associating on G: T mismatch-containing double strand GT59DF DNA (DF: Dig-Fab fragments). Accounting for the low affinity of SB to double strand DNA in FB150T buffer (which closes to physiological conditions), we increased the concentration of SB to 1.6 μ M to obtain more SB binding to DNA. Then we were monitoring how AF594 labeled MutS_R449C/D835R (MutS_R449C/D835R which lost the ability to form the tetramer (Groothuizen, Fish, et al. 2013)) associating on 1.6 μ M SB stained dsGT59DF DNA in the absence or presence of 10 μ M ADP or 0.5 mM ATP (Figure 6 A and B). From Figure 6 A, we could observe that accompanied the FRET signal rising (upper part) the donor signal anti-parallelled (lower part), and MutS_R449C/D835R_AF594 pre-incubated with 10 μ M ADP binding faster to GT59DF DNA than no nucleotides, while the amplitude is reduced one in tenth (Figure 6 A Upper part). Besides the binding kinetics of both are fitting to two exponential fits which indicated by cartoons at Figure 6 E depending on Figure 6 A and the literature (Groothuizen, Winkler et al. 2015, Monakhova, Ryazanova, et al. 2015). However, the kinetics of MutS_R449C/D835R_AF594 binding GT59DF DNA in the presence of ATP is more complicated, pre-incubated with ATP makes the binding faster than encountered ATP later (Figure 6 B upper part, blue and orange). After using ATP against pre-assembled complex of MutS_R449C/D835R_AF594 and GT59DF DNA with 10 μ M ADP (Figure 6 B upper part, olive), we could conclude that the down phase due to the ATP induced conformational changes in MutS which resulted DNA moves away from residues 449 at the DNA-clamp position, and that consistent with the literature as well (Groothuizen, Winkler et al. 2015). The donor signal entirely anti-correlated (Figure 6 B and interpreted by cartoons in Figure 6 E). MutS_R449C_AF594 (MutS449_AF594) which gain the ability to form the tetramer (Groothuizen, Fish, et al. 2013) could be binding dsGT59DF DNA without ATP (Figure 6 C grey) as well. The kinetics behave more complicated in the presence of ATP for MutS449 (Figure 6 C blue and orange), and faster when pre-incubated with ATP (Figure 6 C orange) as well. Even though MutS449_AF594 behaves similar to MutS_R449C/D835R_AF594 (MutS449/D835R_AF594) observed from the binding

kinetics, the total amplitudes of MutS_R449C are lower compare to MutS_R449C/D835R_AF594 (Figure 6).

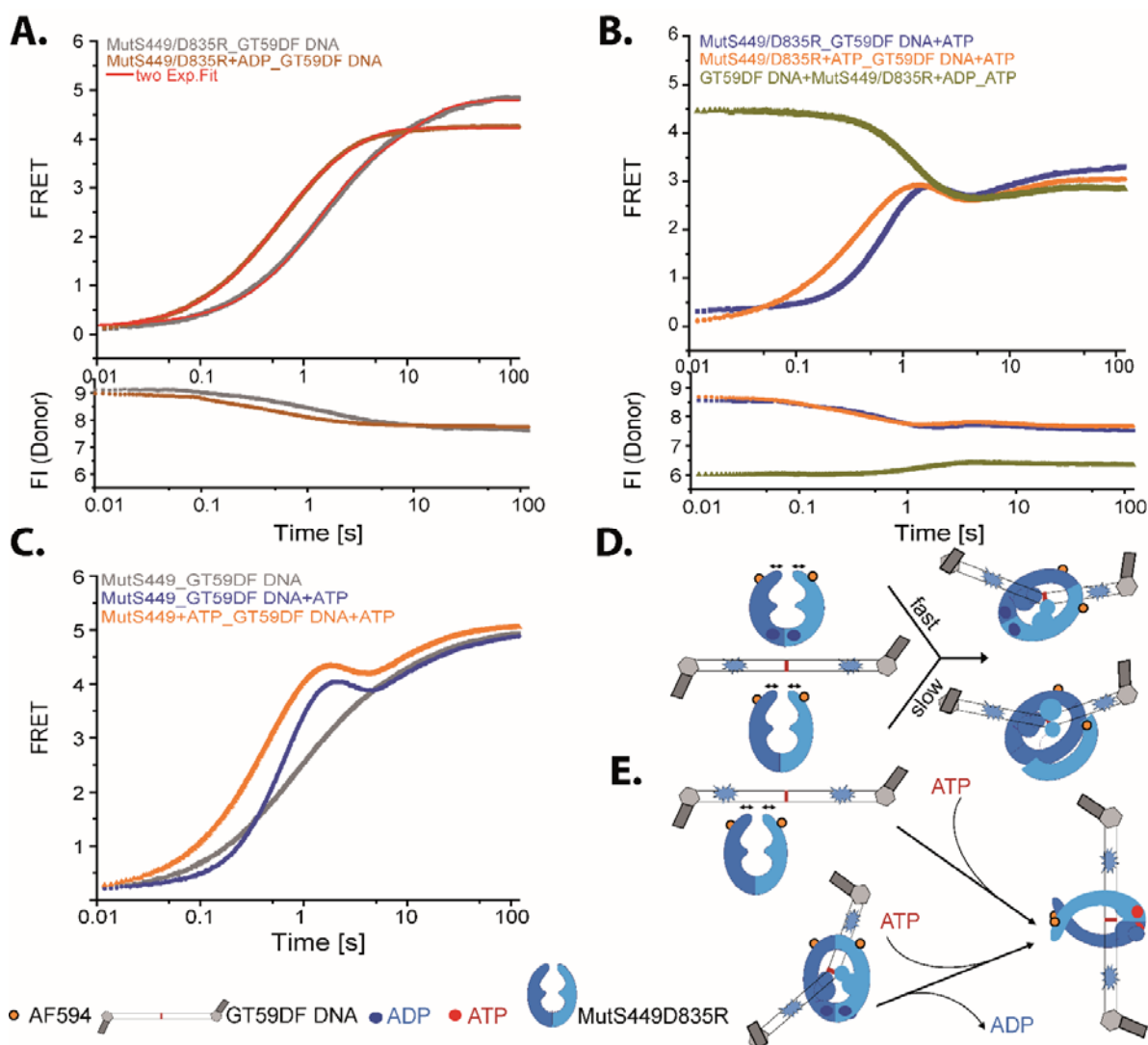


Figure 6. Monitoring MutS binding SB stained DNA assessed with stopped-flow. (A) Kinetics of 200 nM MutS449/D835R_AF594 (R) binding SB stained dsGT59DF DNA; (B) in the absence/presence of 10 μ M ADP in FB150T buffer with (brown)/without (grey), and lower part is the donor signal; (B) Kinetics of ATP effects to MutS449/D835R_AF594 binding SB stained dsGT59DF DNA in FB150T buffer (orange, MutS449/D835R_AF594 pre-incubated with 0.5 mM ATP then against 50 nM dsGT59DF DNA with 0.5 mM ATP; blue is 200 nM MutS449_AF594 encounging SB stained 50 nM dsGT59DF DNA plus 1 mM ATP; olive is pre-assembled 200 nM MutS449/D835R_AF594 on SB stained 50 nM dsGT59DF DNA with 10 μ M ADP for 2 min, then against with 1 mM ATP, and lower part is the donor signal); (C) Kinetics of 200 nM MutS449_AF594 binding SB stained dsGT59DF DNA in the absence of FB150T buffer (grey) and the effect of 0.5 mM ATP to MutS449 binding DNA; (D) Cartoons indicating the behaviors of MutS449/D835R_AF594 interacted with dsGT59DF DNA observed from A; (E) Cartoons displaying the MutS449/D835R_AF594 interacted with dsGT59DF DNA in the presence of ATP that found from B.

5, Kinetics of associating on SB stained DNA MutL

Another critical MMR (mismatch repair) protein is MutL. From Figure 7 A we could observe that nearly no AF594 labeled MutL_297 binding Lambda DNA observed, irrelevant of the absence

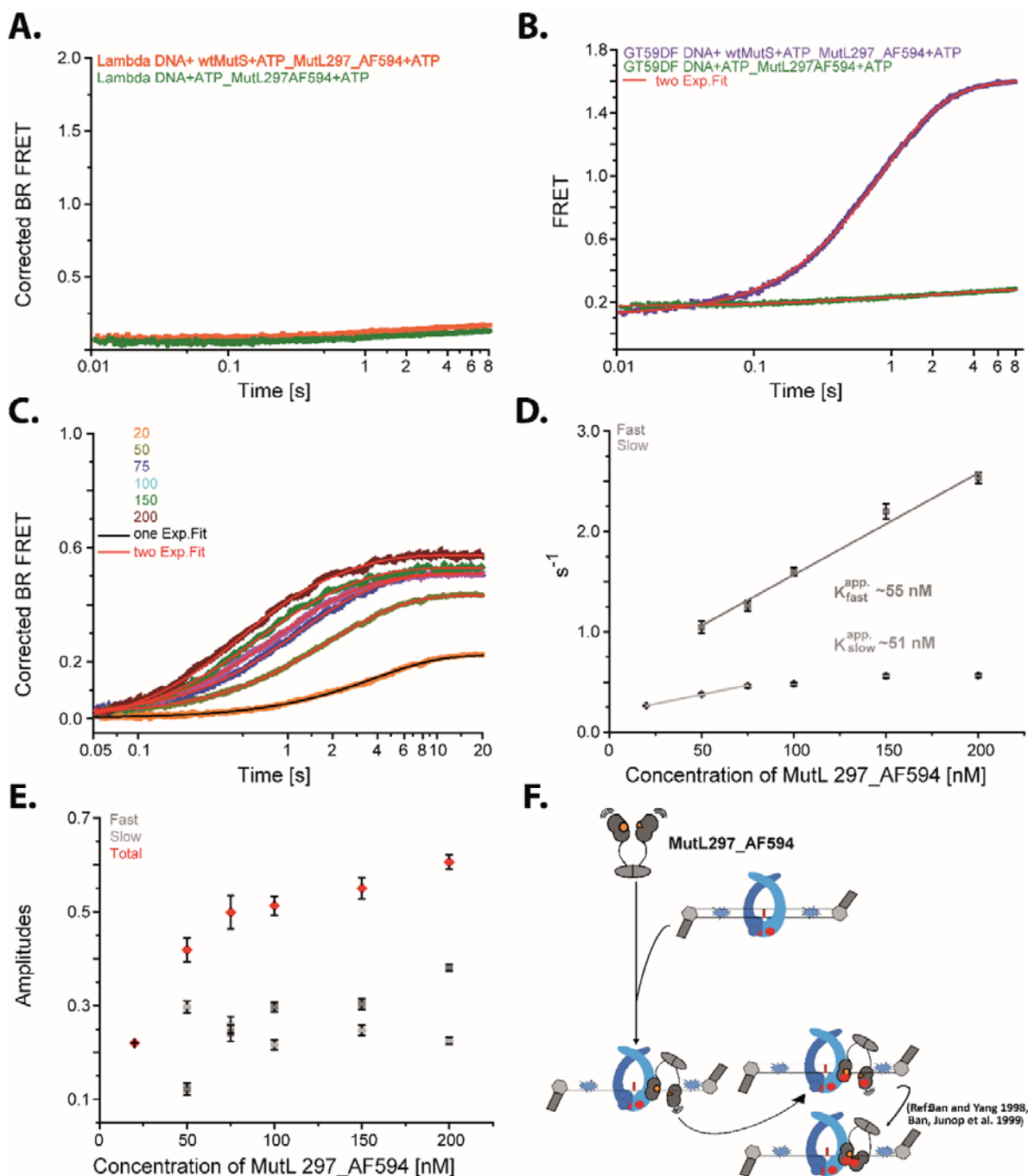


Figure 7. MutL297_AF594 associating on DNA. (A) stopped-flow kinetics of 200nM MutL297_AF594 associating on 0.122 nM Lambda DNA in the absence (light purple)/presence (light green) wtMutS with 0.5 mM ATP in FB150T buffer; (B) stopped-flow kinetics of 200 nM MutL297_AF594 associating on 50 nM GT59DF DNA in the absence (dark green) /presence (dark purple) 200 nM wtMutS with 0.5 mM ATP in FB150T buffer; (C) Titration MutL297_AF594 to 20 nM wtMutS/10 nM GT59DF DNA/ 0.5 mM ATP complexes in FB150T buffer assessed by stopped-flow; (D) the fast and slow rates derived from the kinetics of C; (E) Amplitudes derived from titration MutL297_AF594 to wtMutS and GT59DF DNA complexes; (F) cartoons depicted how MutS loaded MutL on GT59DF DNA.

(Figure 7 orange) and presence (Figure 7 green) of wtMutS. Therefore, G: T mismatch- containing double strand GT59DF DNA was used to investigate MutL binding DNA. From kinetics in Figure 7 B we could observe that MutL297_AF594 could not bind GT59DF DNA without wtMutS (Figure 7 B, dark green) in FB150T buffer, while the kinetic strikingly heads up (<5 s) when pre-incubate wtMutS with GT59DF DNA and ATP in 10s (Figure 7 B dark purple) in FB150T buffer, and the binding kinetics fit to two exponential fit better (Figure 7 B red). Therefore, we could conclude that MutL needs to be loaded by MutS in physiological ionic strength condition.

In order to obtain the apparent affinity of MutL to GT59DF DNA, we titration AF594 labeled MutL_297 binding 10 nM GT59DF DNA, 20 nM wtMutS and 0.5 mM ATP (Figure 7 C). After analyzing kinetics with two exponential fits, we could find that the fast apparent binding rate is $0.01 \pm 0.0006 \text{ s}^{-1} \text{ nM}^{-1}$ (Figure 7 D, dark grey) and the slow apparent binding rate is $0.0037 \pm 0.00011 \text{ s}^{-1}$ within 75 nM, and after 75 nM the slow binding rate reaches the saturation around 0.5 s^{-1} (Figure 7 D, light grey). In contrast to almost three folds difference in the fast and slow binding rates, both the fast and slow steps share the similar the apparent KD around 50 nM (Figure 7 D). Interestingly, two binding steps share the similar amplitudes (Figure 7 E). The binding processes indicated by the cartoons in Figure 7 F.

6, Multiple Loading MutS and MutL on SB stained G: T mismatch-containing nano- circular DNA (GT932 DNA)

As we know from the description above, MutS stay at the mismatch and kinking the DNA (Lebbink, Fish, et al. 2010) in the presence of ADP, and MutS undergoes conformational changes and sliding away from the mismatch after encountering ATP (Groothuizen, Winkler, et al. 2015). So MutL cannot bind DNA without MutS in FB150T buffer. Here we labeled MutL297 with AF594, MutS449/D835R with AF488, and SB staining G: T mismatch-containing nano-circular DNA (GT932 DNA), and monitoring MutS/DNA (BG), MutL/DNA (BR) and MutS/MutL (GR) interaction at the same time. In the presence of 2 mM ADP, only tiny proportion of MutL297_AF594 could load on GT932 DNA (Figure 8 A, blue) compared to the kinetics in the presence of 2 mM ATP (Figure 8 A, orange) and 10 μM ATP (Figure 8 A, olive). However, after adding 2 mM ATP the kinetics immediately rising to the similar level of high ATP (Figure 8 A, blue). While after adding 2 mM ATP to 10 μM ATP (Figure 8 A, olive), the kinetics decreased to the same level of adding 2 mM ATP at the beginning (Figure 8 A, orange). Paralleled to the behavior of MutL297_AF594 with GT932 DNA, the interaction kinetics between MutL297_AF594 and MutS449/D835R_AF488 behaves similarly in the presence of 2 mM ADP or 10 μM

ATP before and after adding 2 mM ATP (Figure 8 B, blue and olive). While the difference smaller between ADP and high ATP (Figure 9 B, blue and orange) and larger between low ATP and high ATP (Figure 8 B, olive, and orange) for the first 6 min.

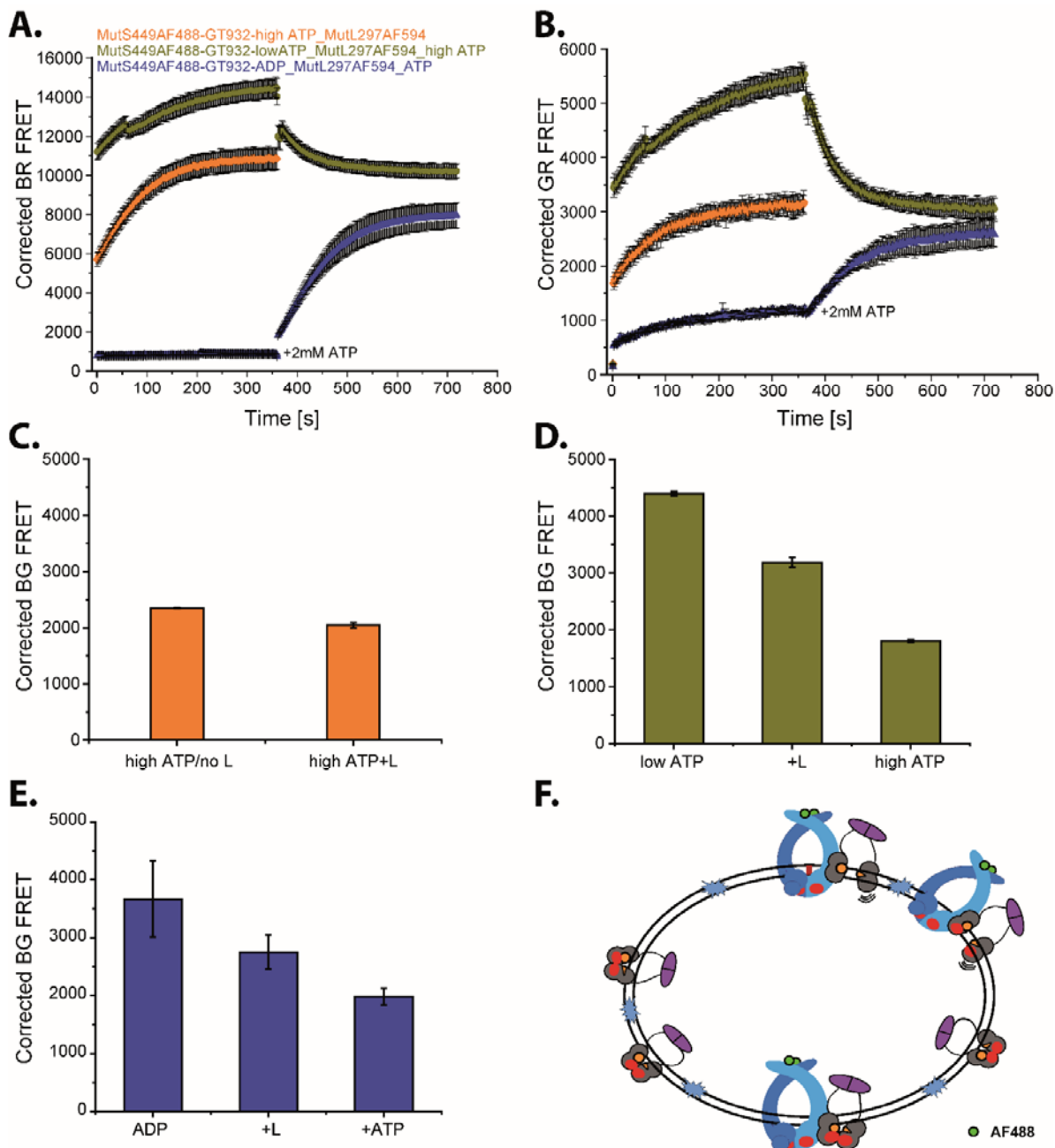


Figure 8. Multi-loading MutS and MutL on nano-circular DNA. (A) MutL/DNA FRET (BR FRET) with adding 200 nM MutL297_AF594 (R) to 200 nM MutS449/D835R_AF488 (G)-5 nM GT932 DNA (B) complexes with 2 mM ADP/10 μ M ATP/2 mM ATP in 200 μ l buffer M at beginning, and later added 2 mM ATP into ADP/10 μ M ATP (low ATP) samples and assessed by TECAN; (B) MutL-MutS FRET (GR FRET) monitored at the same conditions as A; (C-E) adding 200 nM MutS449/D835R_AF488 to 200 nM MutL297_AF594-5 nM GT932 DNA complexes with 2 mM ADP/10 μ M ATP/2 mM ATP in 200 μ l buffer M at beginning, and later added 2 mM ATP to ADP/10 μ M ATP (low ATP) samples; (F) cartoons depicted how MutS loaded MutL on GT932 nano-circular DNA.

However, MutS449/D835R_AF488 to GT932 DNA with high FRET with 10 μ M ATP (Figure 8 D) a little bit lower with ADP (Figure 8 E.) and after adding MutL both signals decreased and continuously decreased after adding 2 mM ATP (Figure 8 D and E). Compared A and B, for 10 μ M ATP to 2 mM ATP (olive), the GR FRET decreased for almost 50 %, but the BR FRET decreased only one-third which indicate that more MutL load on DNA than MutS. This observation could support by the ADP signal (Figure 8 A and B, blue) as well. The GR FRET only increased around 65 % while the BR FRET increased approximately 80 % from 2 mM ADP to 2 mM ATP state. Except that the BG FRET decreased nearly 50% when add high ATP to ADP or 10 μ M ATP state (Figure 8 C-E). Therefore, the number of MutL load on GT932 nano-circular DNA is more than the number of MutS (Figure 8 F).

Discussion

Until now, no SB chemical structure has been published, even through the binding site size seems no significant change in different salt buffer, the big error bar observed when use McGhee and von Hippel (McGhee 1974, Stephen C. Kowalczykowski, Nils Lonberg et al. 1985, Dragan, Casas-Finet et al. 2010) model to analyze the data, and differs from the other intercalation dyes like Pico Green more extended in high salt buffer (Dragan, Casas-Finet et al. 2010). SB and DNA interaction is complicated, as we show that the free dye is always existing primary and secondary inner filter effect while SB-dsGT30 DNA complex no inner filter observed as titration SB the fluorescence intensity (FI) linearly increased (Appendix Figure 2.1 J and K). Moreover, the maximum excitation shifted from 435 nm to 444 nm when SB free dye form dye-DNA complexes, while the maximum emission does not change around 470 nm (Figure 1). But we always measured with the filter of Ex./Em. at 405/485 nm, that is more close to the maximum excitation for the free dye. We consistent using this filter because with this filter less crosstalk from AF594 which applied to label MutL or MutH proteins in our system. Besides, as was pointed out at Figure 3 D, the kinetic fits to the high-affinity mode (solid line) at high dye/base pair ratio, while it fits to the low-affinity mode (dash line) at low dye/base pair ratio as well. That's consistent with the literature that both the pattern of electrostatic binding to the phosphate backbone and intercalating mode exist at high dye/base pair ratio, while the binding mode mainly consists with the primary of intercalation mode at low dye/base pair ratio (Yan, Habbersett et al. 2005). Moreover, the kinetics of the SB binding dsGT30 DNA in both TE10 and FB150T buffers fit to the two binding sites mode better than the single binding mode which includes the conformational change step (Figure 4 A-D), even though no noticeable difference observed for the kinetics of SB binding ssG30 DNA in FB150T buffer fit

to both modes (Figure 4 E-F). Compared with other Sytox family mono-intercalating cyanine dyes, such as SYTOX orange and SYTOX green (Yan, Habbersett et al. 2005, Biebricher, Heller et al. 2015, Thakur, Cattoni et al. 2015), SB has a lower affinity to DNA even it shares the similar Molecular Weight around 400-600 (Invitrogen) as other Sytox family members. However, the fast rates of associating and dissociating on DNA are one of significant advantage for SB (Figure 4). Even though the complexes of SB-DNA are easy to be affected by cations, the kinetics will reach the equilibrium before 30 ms (Figure 4, Figure 5 C and E). The result of using KinTek explores analyses the kinetics fit to the two binding sites mode better indicate that more than one way exist for SB and DNA interaction (Figure 4). Reaching the saturation fast indicating that the interaction between SB and DNA rather weak. However, one of the advantage for this weak interaction is that it will not alternate the structure of DNA and perturb enzymatic reaction with DNA (Hurley 2002, Koster, Palle, et al. 2007, Vladescu, McCauley, et al. 2007, Paramanathan, Vladescu et al. 2012, Biebricher, Heller, et al. 2015). As reported in the literature, except increase the contour length of DNA (produce ~ 0.34 nm to DNA per mono-intercalator such as SYTOX orange and SYTOX green, and ~ 0.68 nm to DNA per bis-intercalator like YOYO and POPO), intercalators could stabilized the DNA and protected DNA against unwinding which caused by different monovalent concentration as well (King, Gross et al. 2013, Biebricher, Heller et al. 2015). That is not suitable for DNA unwinding study while SB is one of the good options attributed to the advantage of weak interaction with DNA. Additionally, SB binding DNA reach saturation before 30 ms, and that makes it suitable for MutS and MutL binding mismatch-containing DNA which starts after 50 ms (Figure 6 and Figure 7).

Mismatch repair (MMR) system plays a central role in promoting genetic stability by repairing DNA replication errors, inhibiting recombination between non-identical DNA sequences, and participating in responses to DNA damage (Harfe and Jinks-Robertson 2000). One of the critical steps in DNA mismatch repair is discriminates the new daughter strand from the parental DNA strands (Guarne 2012). Two crucial proteins MutS and MutL both interact with DNA, but how these two proteins are interact on the mismatch-containing DNA and are adapt to ATP dependent functional conformation are still unclear, especially for MutL. Here we show the kinetics of tetra- and di- merized MutS, and stable dimerized MutL binding DNA at physiological ionic strength (FB150T) buffer. As we described before, MutS449/D835R (only forms dimer with nucleotide) binding mismatch-containing DNA faster if pre-incubate with nucleotides (ADP/ATP). MutS449/D835R adopting different conformational changes in the presence of ATP (Figure 6 A and B)

which is consistent with the literature (Qiu, DeRocco, et al. 2012, Groothuizen, Winkler, et al. 2015). MutS449 shares the similar kinetics as MutS449/D835R except with the lower amplitudes (Figure 6 C), that could contribute to the formation of MutS tetramer which results that not all MutS449 dimer binding directly on the DNA but close to the DNA by hooked with another MutS dimer (Groothuizen, Fish, et al. 2013).

In the absence of wtMutS, MutL hardly load on the GT59DF DNA (Figure 7 B). The binding kinetics of MutL reach the saturation in 10 s and fit to two exponential fit with the amplitudes of these two steps are similar, and that could be understood as two different N-terminal domains (NTDs) within the same MutL dimer binding DNA not (Figure 7 B-E). The first NTD binding with the apparent rate of $0.01 \pm 0.001 \text{ s}^{-1}$ and the affinity is around 55nM, and the second NTD with similar affinity around 51 nM as well while with the slower apparent rate which is $0.004 \pm 0.0001 \text{ s}^{-1}$ (Figure 7 D). However, titration AF594 labeled MutL indicate that 10 nM GT59DF DNA and 10 nM dimeric wtMutS complexes need 75 nM MutL (Figure 7 C blue) to reach the saturation. That is suggesting that around one MutL dimer loaded on one GT59DF DNA molecule.

As we described above, only one MutL dimer loaded on 59 bp end blocked G: T mismatch-containing oligo DNA. However, multiple loading of MutS and MutL have been reported in the literature both for the eukaryotic (Hombauer, Campbell et al. 2011, Li 2014) and prokaryotic (*E.coli*) (Acharya, Foster et al. 2003, Qiu, Sakato et al. 2015, Liu, Hanne et al. 2016). However, no kinetics of multiple loading MutL on G: T mismatch-containing DNA have published. Here, we are the first time published the kinetics of MutL and MutS on G: T mismatch-containing nano-circular DNA (GT932) (Figure 8).

As we describe above, the ATP binding deficient proportion of MutL still interacts with MutS in the presence of ADP and hence loaded on DNA, but only limit at the mismatch (Figure 8 A and B, blue). As literature reported, *E.coli* MutS hydrolysis ATP with the rate of 1 min^{-1} which is equivalent to 33 μM apparent affinity per monomer (Bjornson, Allen, et al. 2000). Three years later the same group found that one with higher affinity for ADP and another with higher affinity to ATP for the two nucleotide binding sites within the same MutS dimer (Bjornson and Modrich 2003). While another group from Professor Joyce Lebbink reported that almost 100 % of MutS dimers released as sliding clamps from the mismatch (Groothuizen, Fish, et al. 2013) in the presence of 10 μM ATP. Under this condition, MutS is slow dissociating for the ATP- independent release, but faster dissociation due to sliding clamps releasing from the free DNA ends (Groothuizen, Fish, et

al. 2013). Therefore, more MutS accumulated on the more extended mismatch-containing DNA without open ends (blocked or circular).

Moreover, the affinity of MutL to ATP is around 90 μM (Ban, Junop, et al. 1999). In the presence 10 μM ATP, most MutS assembled on the end blocked DNA, MutL are recruited on the DNA with ATPase inactive state (Figure 8 A olive), so MutL forms complex with MutS (Figure 8 B olive) and stabilized MutS on DNA at mismatch for certain time until more ATP added which resulted MutL NTD dimerized (Groothuizen, Winkler et al. 2015). Additionally, MutS still could binding and kink the DNA at the mismatch in the absence of nucleotides or the presence of ADP (Groothuizen, Winkler, et al. 2015). Therefore, except unassembled MutS bond at DNA mismatch, low ATP condition multiple MutS have been assembled on DNA. Hence the more inactive state of MutL loaded on nano-circular DNA, and more MutS-MutL complexes are formed compared to the state of in the presence of ADP (Figure 8 A-B olive). While MutS to DNA FRET (BG) at low (10 μM) ATP conditions is only slightly higher than in the presence of 2 mM ADP, because after MutS bond to ATP it undergoes conformational changes which results the DNA moves away from the residue of 449 at the DNA-clamp domain (Groothuizen, Winkler et al. 2015). As titration 2 mM ATP to ADP more MutS assembled on DNA and more MutL loaded on DNA (Figure 8). Whereas, when titration 2 mM ATP to low (10 μM) ATP, all FRET signals (BR, GR, and BG) are decreased (Figure 8). The MutL-DNA (BR) FRET decreased around 30 % owing to the high ATP induced closure at NTD of MutL resulted the distance from DNA to 297 residues changed, and slow MutL self-dissociation from the end of DNA as well (Figure 8 A). The MutS-MutL (GR) FRET decreased nearly 55 % that because both MutS and MutL undergo conformational changes after encountering high ATP, and the separation between MutS and MutL occurs as MutL NTD closed, which consistent with the literature (Liu, Hanne, et al. 2016). Besides that the MutS-DNA (BG) FRET nearly 55 % decreased as well due to three main reasons: Firstly, high ATP induced conformational changes in MutS resulted DNA moves away from the residue of 449 at the DNA-clamp domain (Groothuizen, Winkler et al. 2015); Secondly, a slow ATP-independent dissociation from the DNA (Groothuizen, Fish et al. 2013); Thirdly, high ATP prompt MutL exist in an NTD closed active state, that together with mismatch-containing circular DNA could increase the ATPase activity from MutS. Hence consistent with the literature, MutL ATPase activity is required to catalyzed dissociation of MutS sliding clamps (Heo, Ku et al. 2009). Therefore, we speculated that there are more MutL dimers on DNA than MutS (Figure 8 F).

Material and methods

Protein Expression and purification

Transferring 15 ml pre-culture to 500 ml LB culture containing 100 µg/ml Ampicillin and incubating at 37 °C until OD₆₀₀ to 0.8-1.2 (1.0-1.2 for MutL and 0.8-1.0 for MutS). Then produce proteins at the 27°C overnight with IPTG. Recombinant His₆-tagged MutS and MutL proteins were purified with Protino® Ni-IDA 2000 packed columns first and then were purified by gel-filtration on a Superdex 200 10/300 GL. Finally, MutL and MutS proteins were snap-frozen in liquid nitrogen and stored at -80 °C in 10 mM HEPES/KOH, 200 mM KCl, 1 mM EDTA, and pH 8.0. Protein concentrations were determined using theoretical extinction coefficients. (Toedt, Krishnan et al. 2003, Heinze, Giron-Monzon, et al. 2009, Winkler, Marx, et al. 2011)

Protein labeling and degree of labeling (DOL) determination

Proteins labeled in HPLC buffer (10 mM HEPES/KOH (pH 8.0), 200 mM KCl and 1 mM EDTA) with AF488 maleimide (Invitrogen) and AF594 maleimide (Invitrogen). The excess unbound dye was removed through the gel filtration with Zeba Desalt Spin Columns (Pierce, Thermo Scientific). After that MutS and MutL were aliquoted and flash-frozen in liquid nitrogen and stored at -80 °C.

$$C_{\text{prot}} = (A_{280} - A_{\text{max}} \times CF) / \epsilon_{\text{prot}}$$

where A₂₈₀ is the absorbance at 280 nm, A_{max} is the absorbance of the AF594 or AF 488, CF is the correction factor for the used dye CFA488 = 0.12 and CFA594 = 0.56 and ϵ_{prot} is the theoretical molar extinction coefficients of the respective protein.

The degree of labeling (DOL) was determined using the following equation (ATTO-TEC):

$$\text{DOL} = (A_{\text{max}} \times \epsilon_{\text{prot}}) / ((A_{280} - A_{\text{max}} \times CF) \times \epsilon_{\text{max}})$$

Where ϵ_{max} is the molar extinction coefficients of Alexa 594 (92,000 M⁻¹ cm⁻¹).

Titration

Titration experiments were performed using a TECAN Infinite F200 PRO fluorescence plate reader. Titration of 0.001-3 µM dsGT30 DNA (ssT30: AAT-TGC-ACC-GAG-CTT-GAT-CCT-CGA-TGA-TCC; ssG30: GGA-TCA-TCG-AGG-ATC-GAG-CTC-GGT-GCA-ATT melted together) or ssT30 DNA or ssG30 DNA in SB solution with buffer of TE10 (10 mM Tris-HCl, 10 mM KCl, 1 mM EDTA•Na₂, pH 8.0) or TE150 buffer (10 mM Tris-HCl, 150 mM KCl, 1 mM EDTA•Na₂, pH 8.0) or FB150T buffer (25 mM HEPES/KOH, 150 mM KCl, 1 mg/ml BSA, 5 mM MgCl₂, 1 mM DTT pH 7.5) at room temperature. Titration of 0.001-30 µM SB to dsGT30 DNA in

three different buffers at room temperature. The excitation filter 405 nm wavelength with 10 nm bandwidth, emission filter is 485 nm wavelength with 20 nm bandwidth and 50 % mirror channel. The fluorescence intensity (FI) of free SB from 0.001 μM to 30 μM in three different buffers have been measured as well. Titration of ssRNA13 (AGC-ACC-GUA-AAG-A), ssRNA25 (UCU-UUA-CGG-UGC-UUA-AAA-CAA-AAC-AAA-ACA-AAA-CAA-AA) or dsRNA (annealing from ssRNA13 and ssRNA25 with 12 nt overhangs) to 0.2 μM SB or titration SB to the different types of RNA monitored with TECNA in TE10 or TE150 buffers at room temperature as well.

Stopped-flow Fluorescence kinetics

The stopped-flow kinetics were carried out in SF-61SX2 (TgK Scientific, Bradford-on-Avon, UK) apparatus. Binding of SYTOX blue to DNA have been monitored the instantaneously increase in the fluorescence intensity which emission at 436 nm with the filter of GG445 at 25 $^{\circ}\text{C}$ in TE10 or FB150T buffer. While the binding of AF594 labeled MutS and MutL were monitored by the increase in fluorescence intensity when emission at 436 nm with filters of OG 590 and ET525/50 M separately in FB150T buffer at 25 $^{\circ}\text{C}$. The final data were corrected the crosstalk from the buffer and the red labeled protein.

MutL binding GT59DF DNA

20-200 nM AF594 labeled MutL with 1.6 μM SB were titrated in pre-incubated wtMutS-GT59DF DNA complex (0.5 mM ATP, 20 nM wtMutS, 10nM GT59DF DNA, 1.6 μM SYTOX blue, final concentration) assessed by SF-61SX2 (TgK Scientific, Bradford-on-Avon, UK) with ET525/50M and OG 590 filters. These experiment were performed in FB150T (25 mM HEPES/KOH, 150 mM KCl, 1 mg/ml BSA, 5 mM MgCl_2 , 1 mM DTT, pH7.5) buffer at 25 $^{\circ}\text{C}$.

MutS-MutL complex multiple loaded on nano-circular DNA

200 nM MutL297_AF594 added to 200 nM MutS449/D835R_AF488 and 5 nM G: T mismatch-containing nano-circular DNA (GT932 DNA) (Xiao, Jung et al. 2011) in the presence of 7.5 μM SB and 2 mM ATP in 200 ul buffer M (KH_2PO_4 40.5 mM, K_2HPO_4 9.5 mM, KCl 50 mM, EDTA 0.1 mM, pH 7.4) at room temperature assessed by TECAN Infinite F200 PRO fluorescence plate reader. The ADP and low ATP experiments are processed adding 200 nM AF594 labeled MutL297 to 2 mM ADP or 10 μM ATP which is pre-incubated with 200 nM AF488 labeled MutS449/ D835R and 5 nM GT932 DNA separately. Then added 2 mM ATP at the end. The FRET between MutL and DNA called the BR FRET and measured with 450 nm (20 nm width) of excitation filter and

620 nm (10 nm width) of emission filter. The FRET between MutS and DNA called the BG FRET and was measured with 405 nm (10 nm width) of excitation filter and 535 nm (25 nm width) of emission filter. And the FRET between MutL and MutS called GR FRET and was measured with 485 nm (20 nm width) of excitation filter and 620 nm (10 nm width) of emission filter. The FRET was corrected as the follows.

FRET correction

Signals corrected for buffer and spectral crosstalk to obtain the correct signal intensities.

Crosstalk $\alpha_{Channel}^{dye}$

All these crosstalk's ($\alpha_{Channel}^{dye}$) parameters (described above) derived from a series of experiments with single labeled (AF488 or AF594) different positioned proteins (in case affected by protein structure). SB is (Free SB, or in SB-DNA complex to compare the difference), measured at different channels which described as the followed table.

Signals were corrected for crosstalk using a correction matrix similar as described before (Hoppe, Scott, et al. 2013).

Calculating the 100 % binding of the dye

The fluorescence intensity of 100 % bound 0.001-30 μ M SB to 2 nM lambda DNA (97 μ M bp DNA) were measured in TE10 buffer at room temperature. In this case, the fluorescence intensity linearly increased as titrating SB to solution (Dragan, Casas-Finet, et al. 2010). The fluorescence intensity of free SB measured in the solution (in TE10, TE150, and FB150T buffers) without nucleotides, with filters of Ex./Em. are 405 nm/485 nm, and with 50 % mirror.

The fraction of bound state (θ) at different K^+/Mg^{2+} conditions

The fraction of bound SB (θ) expressed as:

$$\theta = (F_t - F_f)/(F_b - F_f)$$

Where the F_t is the total fluorescence intensity of SB that observed, F_f is the free SB fluorescence intensity, and F_b is the fluorescence intensity of 100% bound in the solution. And

$$F_t = f * C_f + b * C_b$$

$$F_t = f * (C_t - C_b) + b * C_b$$

$$C_b = (F_t - f * C_t)/(b - f)$$

C_t is the total concentration of SB in solution; C_f is the concentration of the free SB in solution and C_b is the concentration of the bound SB in solution. b and f are the fluorescence parameters for the free and bound dye in solution separately.

Due to the filter reasons, we measure at 405 nm/485 nm and 50 % mirror, and the enhancement of fluorescence intensity after binding to the nucleic acid only around 40 fold, under this condition

we cannot neglect the fluorescence intensity. Therefore, the fraction of bound SB (θ) can be expressed as:

$$\theta = b * C_b / F_b$$

The concentration of free SB (L) in solution at equilibrium is:

$$L = (1 - \theta) * C_t$$

The SB binding density (ν) which is the number of bound SB per base pair DNA is:

$$\nu = \theta C_{sb} / C_d$$

Where C_d is the total concentration of DNA (bp) and C_{sb} is the total concentration of SB in solution (McGhee 1974, Stephen C. Kowalczykowski, Nils Lonberg, et al. 1985, Dragan, Casas-Finet, et al. 2010)

References

- Acharya, S., P. L. Foster, P. Brooks and R. Fishel (2003). "The coordinated functions of the E. coli MutS and MutL proteins in mismatch repair." *Mol Cell* 12(1): 233-246.
- Ban, C., M. Junop and W. Yang (1999). "Transformation of MutL by ATP binding and hydrolysis: a switch in DNA mismatch repair." *Cell* 97(1): 85-97.
- Ban, C. and W. Yang (1998). "Crystal structure and ATPase activity of MutL: implications for DNA repair and mutagenesis." *Cell* 95(4): 541-552.
- Biebricher, A. S., I. Heller, R. F. Roijmans, T. P. Hoekstra, E. J. Peterman and G. J. Wuite (2015). "The impact of DNA intercalators on DNA and DNA-processing enzymes elucidated through force-dependent binding kinetics." *Nat Commun* 6: 7304.
- Bjornson, K. P., D. J. Allen and P. Modrich (2000). "Modulation of MutS ATP Hydrolysis by DNA Cofactors." *Biochemistry* 39(11): 3176-3183.
- Bjornson, K. P. and P. Modrich (2003). "Differential and simultaneous adenosine di- and triphosphate binding by MutS." *J Biol Chem* 278(20): 18557-18562.
- Chakraborty, U. and E. Alani (2016). "Understanding how mismatch repair proteins participate in the repair/anti-recombination decision." *Fems Yeast Research* 16(6).
- Cosa G, F. K., McLean JR, McNamee JP, Scaiano JC (2001). "Photophysical properties of fluorescent DNA-dyes bound to single- and double-stranded DNA in aqueous buffered solution.pdf." *Photochem Photobiol.* 73(6): 585–599.
- Dragan, A. I., J. R. Casas-Finet, E. S. Bishop, R. J. Strouse, M. A. Schenerman and C. D. Geddes (2010). "Characterization of PicoGreen interaction with dsDNA and the origin of its fluorescence enhancement upon binding." *Biophys J* 99(9): 3010-3019.
- Drotschmann, K., A. Aronshtam, H. J. Fritz and M. G. Marinus (1998). "The Escherichia coli MutL protein stimulates binding of Vsr and MutS to heteroduplex DNA." *Nucleic Acids Res* 26(4): 948-953.
- Fabian, A. I., T. Rente, J. Szoellosi, L. Matyus and A. Jenei (2010). "Strength in Numbers: Effects of Acceptor Abundance on FRET Efficiency." *Chemphyschem* 11(17): 3713-3721.
- Friedhoff, P., P. Li and J. Gotthardt (2015). "Protein-protein interactions in DNA mismatch repair." *DNA Repair (Amst)*.

Gorbalenya, A. E. and E. V. Koonin (1990). "Superfamily of UvrA-related NTP-binding proteins. Implications for rational classification of recombination/repair systems." *J Mol Biol* 213(4): 583-591.

Groothuizen, F. S., A. Fish, M. V. Petoukhov, A. Reumer, L. Manelyte, H. H. Winterwerp, M. G. Marinus, J. H. Lebbink, D. I. Svergun, P. Friedhoff and T. K. Sixma (2013). "Using stable MutS dimers and tetramers to quantitatively analyze DNA mismatch recognition and sliding clamp formation." *Nucleic Acids Res* 41(17): 8166-8181.

Groothuizen, F. S., I. Winkler, M. Cristovao, A. Fish, H. H. Winterwerp, A. Reumer, A. D. Marx, N. Hermans, R. A. Nicholls, G. N. Murshudov, J. H. Lebbink, P. Friedhoff and T. K. Sixma (2015). "MutS/MutL crystal structure reveals that the MutS sliding clamp loads MutL onto DNA." *Elife* 4: e06744.

Guarne, A. (2012). "The Functions of MutL in Mismatch Repair: The Power of Multitasking." *Prog Mol Biol Transl Sci* 110: 41-70.

Harfe, B. D. and S. Jinks-Robertson (2000). "DNA mismatch repair and genetic instability." *Annu Rev Genet* 34: 359-399.

Heinze, R. J., L. Giron-Monzon, A. Solovyova, S. L. Elliot, S. Geisler, C. G. Cupples, B. A. Connolly and P. Friedhoff (2009). "Physical and functional interactions between *Escherichia coli* MutL and the Vsr repair endonuclease." *Nucleic Acids Res* 37(13): 4453-4463.

Heller, I., G. Sitters, O. D. Broekmans, G. Farge, C. Menges, W. Wende, S. W. Hell, E. J. Peterman and G. J. Wuite (2013). "STED nanoscopy combined with optical tweezers reveals protein dynamics on densely covered DNA." *Nat Methods* 10(9): 910-916.

Heo, S. D., J. K. Ku and C. Ban (2009). "Effect of *E. coli* MutL on the steady-state ATPase activity of MutS in the presence of short blocked end DNAs." *Biochemical & Biophysical Research Communications* 385(2): 225-229.

Hombauer, H., C. S. Campbell, C. E. Smith, A. Desai and R. D. Kolodner (2011). "Visualization of eukaryotic DNA mismatch repair reveals distinct recognition and repair intermediates." *Cell* 147(5): 1040-1053.

Hoppe, A. D., B. L. Scott, T. P. Welliver, S. W. Straight and J. A. Swanson (2013). "N-way FRET microscopy of multiple protein-protein interactions in live cells." *PLoS One* 8(6): e64760.

Hurley, L. H. (2002). "DNA and its associated processes as targets for cancer therapy." *Nat Rev Cancer* 2(3): 188-200.

Johnson, K. A. (2009). "Chapter 23 Fitting Enzyme Kinetic Data with KinTek Global Kinetic Explorer." *Methods Enzymol.* 467: 601-626.

Johnson, K. A., Z. B. Simpson and T. Blom (2009). "FitSpace explorer: an algorithm to evaluate multidimensional parameter space in fitting kinetic data." *Anal Biochem* 387(1): 30-41.

Johnson, K. A., Z. B. Simpson and T. Blom (2009). "Global kinetic explorer: a new computer program for dynamic simulation and fitting of kinetic data." *Anal Biochem* 387(1): 20-29.

King, G. A., P. Gross, U. Bockelmann, M. Modesti, G. J. Wuite and E. J. Peterman (2013). "Revealing the competition between peeled ssDNA, melting bubbles, and S-DNA during DNA overstretching using fluorescence microscopy." *Proc Natl Acad Sci U S A* 110(10): 3859-3864.

Koster, D. A., K. Palle, E. S. Bot, M. A. Bjornsti and N. H. Dekker (2007). "Antitumour drugs impede DNA uncoiling by topoisomerase I." *Nature* 448(7150): 213-217.

Lakowicz, J. R. (2006). *Principles of Fluorescence Spectroscopy*. Boston, MA, Springer US: ... S.

Lebbink, J. H., A. Fish, A. Reumer, G. Natrajan, H. H. Winterwerp and T. K. Sixma (2010). "Magnesium coordination controls the molecular switch function of DNA mismatch repair protein MutS." *J Biol Chem* 285(17): 13131-13141.

Li, G. M. (2014). "New insights and challenges in mismatch repair: getting over the chromatin hurdle." *DNA Repair (Amst)* 19: 48-54.

Liu, J., J. Hanne, B. M. Britton, J. Bennett, D. Kim, J. B. Lee and R. Fishel (2016). "Cascading MutS and MutL sliding clamps control DNA diffusion to activate mismatch repair." *Nature* 539(7630): 583-587.

Martin-Lopez, J. V. and R. Fishel (2013). "The mechanism of mismatch repair and the functional analysis of mismatch repair defects in Lynch syndrome." *Fam Cancer*.

McGhee, J. D., and P. H. von Hippel (1974). "Theoretical Aspects of DNA-Protein Interactions: Co-operative and Non-co-operative Binding of Large Ligands to a One-dimensional Homogeneous Lattice." *J. Mol. Biol.* (86): 469-489.

Mellon, I., D. K. Rajpal, M. Koi, C. R. Boland and G. N. Champe (1996). "Transcription-coupled repair deficiency and mutations in human mismatch repair genes." *Science* 272(5261): 557-560.

Modrich, P. and R. Lahue (1996). "Mismatch repair in replication fidelity, genetic recombination, and cancer biology." *Annu Rev Biochem* 65: 101-133.

Monakhova, M., A. Ryazanova, A. Hentschel, M. Viryasov, T. Oretskaya, P. Friedhoff and E. Kubareva (2015). "Chromatographic isolation of the functionally active MutS protein covalently linked to deoxyribonucleic acid." *J Chromatogr A* 1389: 19-27.

Monastiriakos, S. K., K. M. Doiron, M. I. Siponen and C. G. Cupples (2004). "Functional interactions between the MutL and Vsr proteins of *Escherichia coli* are dependent on the N-terminus of Vsr." *DNA Repair (Amst)* 3(6): 639-647.

Monti, M. C., S. X. Cohen, A. Fish, H. H. Winterwerp, A. Barendregt, P. Friedhoff, A. Perrakis, A. J. Heck, T. K. Sixma, R. H. van den Heuvel and J. H. Lebbink (2011). "Native mass spectrometry provides direct evidence for DNA mismatch-induced regulation of asymmetric nucleotide binding in mismatch repair protein MutS." *Nucleic Acids Res* 39(18): 8052-8064.

Pang, Q., T. A. Prolla and R. M. Liskay (1997). "Functional domains of the *Saccharomyces cerevisiae* Mlh1p and Pms1p DNA mismatch repair proteins and their relevance to human hereditary nonpolyposis colorectal cancer-associated mutations." *Mol Cell Biol* 17(8): 4465-4473.

Paramanathan, T., I. Vladescu, M. J. McCauley, I. Rouzina and M. C. Williams (2012). "Force spectroscopy reveals the DNA structural dynamics that govern the slow binding of Actinomycin D." *Nucleic Acids Res* 40(11): 4925-4932.

Qiu, R., V. C. DeRocco, C. Harris, A. Sharma, M. M. Hingorani, D. A. Erie and K. R. Weninger (2012). "Large conformational changes in MutS during DNA scanning, mismatch recognition and repair signaling." *EMBO J* 31(11): 2528-2540.

Qiu, R., M. Sakato, E. J. Sacho, H. Wilkins, X. Zhang, P. Modrich, M. M. Hingorani, D. A. Erie and K. R. Weninger (2015). "MutL traps MutS at a DNA mismatch." *Proc Natl Acad Sci U S A* 112(35): 10914-10919.

Record, M. T., C. F. Anderson and T. M. Lohman (2009). "Thermodynamic analysis of ion effects on the binding and conformational equilibria of proteins and nucleic acids: the roles of ion association or release, screening, and ion effects on water activity." *Quarterly Reviews of Biophysics* 11(02): 103.

Richard Wombacher, M. H., M. P. S. Sebastian van de Linde, V. W. C. Mike Heilemann and M. Sauer (2010). "Live-cell super-resolution imaging with trimethoprim conjugates.pdf." BRIEF COMMUNICATIONS.

Shi, W., T. Vu, D. Boucher, A. Biernacka, J. Nde, R. K. Pandita, J. Straube, G. M. Boyle, F. Al-Ejeh, P. Nag, J. Jeffery, J. L. Harris, A. L. Bain, M. Grzelak, M. Skrzypczak, A. Mitra, N. Dojer, N. Crosetto, N. Cloonan, O. J. Becherel, J. Finnie, J. R. Skaar, C. R. Walkley, T. K. Pandita, M. Rowicka, K. Ginalski, S. W. Lane and K. K. Khanna (2017). "Ssb1 and Ssb2 cooperate to regulate mouse hematopoietic stem and progenitor cells by resolving replicative stress." *Blood* 129(18): 2479-2492.

Spampinato, C. and P. Modrich (2000). "The MutL ATPase Is Required for Mismatch Repair." *J. Biol. Chem.* 275(13): 9861-9869.

Stephen C. Kowalczykowski, g. L. S. P., **, t. Nils Lonberg, i John W. Newport,\$,# James A. McSwiggen, to and Peter H. von Hippel* (1985). "Cooperative and Noncooperative Binding of Protein Ligands to Nucleic Acid Lattices: Experimental Approaches to the Determination of Thermodynamic Parameters."

Thakur, S., D. I. Cattoni and M. Nollmann (2015). "The fluorescence properties and binding mechanism of SYTOX green, a bright, low photo-damage DNA intercalating agent." *Eur Biophys J* 44(5): 337-348.

Toedt, G. H., R. Krishnan and P. Friedhoff (2003). "Site-specific protein modification to identify the MutL interface of MutH." *Nucleic Acids Res* 31(3): 819-825.

Vladescu, I. D., M. J. McCauley, M. E. Nunez, I. Rouzina and M. C. Williams (2007). "Quantifying force-dependent and zero-force DNA intercalation by single-molecule stretching." *Nat Methods* 4(6): 517-522.

Winkler, I., A. D. Marx, D. Lariviere, L. Manelyte, L. Giron-Monzon, R. J. Heinze, M. Cristovao, A. Reumer, U. Curth, T. K. Sixma and P. Friedhoff (2011). "Chemical trapping of the dynamic MutS-MutL complex formed in DNA mismatch repair in *Escherichia coli*." *J Biol Chem* 286(19): 17326-17337.

Xiao, Y., C. Jung, A. D. Marx, I. Winkler, C. Wyman, J. H. Lebbink, P. Friedhoff and M. Cristovao (2011). "Generation of DNA nanocircles containing mismatched bases." *BioTechniques* 51(4): 259-262, 264-255.

Yan, X., R. C. Habbersett, J. M. Cordek, J. P. Nolan, T. M. Yoshida, J. H. Jett and B. L. Marrone (2000). "Development of a mechanism-based, DNA staining protocol using SYTOX orange nucleic acid stain and DNA fragment sizing flow cytometry." *Anal Biochem* 286(1): 138-148.

Yan, X., R. C. Habbersett, T. M. Yoshida, J. P. Nolan, J. H. Jett and B. L. Marrone (2005). "Probing the kinetics of SYTOX Orange stain binding to double-stranded DNA with implications for DNA analysis." *Anal Chem* 77(11): 3554-3562

Chapter 3

Multiple-loading combined conformational changes of MutL on mismatch-containing DNA, and the ionic strength effect to these processes

Abstract

GHKL ATPase's protein MutL is one of the critical protein bridges mismatch recognition and mismatch repair during MMR processes. Plenty of literature investigated the conformational changes of MutS, and the interaction between MutS and MutL. Seldom publications related MutL conformational changes in the presence of mismatch-containing DNA and MutS, as well as the effect of MutS and MutL interaction on MutL conformational changes. Based on the method of FRET, we investigate MutL conformational changes through EfA (FRET efficiency of MutL/MutL interaction), and interaction of MutL-DNA through the BR FRET in real-time.

A slow and robust increase in FRET efficiency over the MutL297_AF488 and MutL297_AF594 subunit exchange only appears on the mismatched DNA in the presence of MutS449/D835R and ATP. The rise in that FRET efficiency was dependent on the types of DNA (being the strongest with the 932 bp circular mismatched GT932 DNA, and lower with 100 bp end-blocked GT100DF DNA) and MutL concentration. While with the CTD (452) labeled MutL, the increase in FRET efficiency was only observed on GT932 circular DNA but absent on the end-blocked GT100DF DNA. On circular DNA with a single mismatch, multiple MutS were loaded in an ATP-dependent manner and formed ternary complex with MutL. In the condition of 10 μ M ATP, no increase in GR FRET efficiency (EfA) of AF488 and AF594 labeled MutL hetero-dimers observed. That due to the MutS sliding complex (with ATP at its ATPase pocket) bind MutL on DNA, but with no ATP binding at MutL's ATPase binding site. The similar result further proofed with ATP binding deficient variant N33A. Moreover, the BR FRET between SYTOX blue stained DNA and NTD labeled MutL is in agreement with the postulated structure of the ternary complex among MutS, MutL, and mismatched DNA. Adding more ATP to this ternary complexes (at low ATP state) lead to MutL closure via its NTD which resulted the slowly rise up of EfA kinetic while decrease in the BR FRET.

A variety of stopped-flow kinetics analyzes using different labeled MutL variants and buffer conditions to monitor either DNA binding (the BR FRET) or conformational changes in MutL (the

GR FRET) lead to the following conclusions: Firstly, MutL binding to DNA is fast (within 2 s) when preformed the MutS-DNA complexes with ATP; The BR FRET kinetics of MutL binding to DNA are multiphasic (at least three distinct phases), and the first two phases (the first NTD of MutL bind to MutS on DNA, followed the second NTD of MutL close to DNA) occur within 10 s are related to load MutL on DNA and are not ATP dependent in MutL; Depending on the different combinations of labeled MutL, the amplitudes of the first phase of the BR FRET kinetics can be positive (297/297) neutral (452/452) or negative (452/297 or 4/297); the slow phase is dependent on ATP-binding to MutL (which cannot observed with ATP binding deficient mutant MutL297N33A) and induced closer of MutL via its NTD, and is independent on the positions of labels and the amplitude of this phase always positive (even for the 452/452) suggesting the formation of a more compact structure of MutL.

Keywords: MutL, MutS, GT932 DNA, GT100DF DNA, GT59DF DNA, FRET, conformational changes, K^+ , Mg^{2+} , ionic strength

Introduction

DNA mismatch repair (MMR) corrects errors, e.g., arise due to misincorporation by the DNA polymerase (Iyer, Pluciennik, et al. 2000) which enhances the overall replication fidelity by 100-1000 fold (Iyer, Pluciennik et al. 2006). MMR repair starts when MutS binds to a mismatch and forms a ternary complex with MutL in an ATP-dependent manner. The basic steps in MMR involve error recognition by MutS followed by ATP-dependent recruitment of MutL (Galio, Bouquet, et al. 1999). MutS and MutL both contain sites for DNA binding and ATPase activity are evolutionarily conserved from bacteria to human. Absence or failure of MutS and MutL function will lead to a mutation phenotype (Pang, Lundberg, et al. 1985) and in humans to Lynch syndrome which is a hereditary form of cancer (Auranen and Joutsiniemi 2011). Except its function in MMR, MutS and MutL's other roles in DNA metabolism are, e.g., somatic hypermutation of immunoglobulin genes, and anti-recombination (Pena-Diaz and Jiricny 2012, Tham, Hermans, et al. 2013). Extensive structure-function analysis has been performed on bacterial and eukaryotic MutS down to the single-molecule level (reviewed in Lee, Cho, et al. 2014).

We are focusing on the *E. coli* MMR system. As it introduced above, two essential proteins of MMR MutS and MutL form the ternary complex on mismatch-containing DNA in an ATP-dependent manner. MutS and MutL proteins are both homodimers that undergo significant ATP-

and/or DNA induced conformational changes (Ban, Junop, et al. 1999, Guarne 2012). *E. coli* MutS is a homo-dimeric ABC-family ATPase that can bind to single base mismatches and small insertion/deletions loops (up to four nucleotides) in the absence of nucleotide or the presence of ADP (Su and Modrich 1986, Parker and Marinus 1992, Putnam 2015). *E. coli* MutL belongs to the GHKL (Gyrase, Hsp90, Histidine Kinases, and MutL) ATPase family which members share a common ATP-binding domain (the so-called Bergerat fold) with low ATPase hydrolysis rates (0.4–0.9 min⁻¹) and due to ATP binding and/or hydrolysis induce significant conformational changes (Bergerat, deMassy et al. 1997, Ban, Junop et al. 1999, Dutta and Inouye 2000, Spampinato and Modrich 2000, Polosina and Cupples 2010). MutL, eukaryotic as well as prokaryotic, could physically bridge interactions between MutS and many effectors that are crucial to repairing and non-repair pathways, and it undergoes ATPase conformational changes to transduce information from the lesion to the appropriate effectors via the MutS in a regulated manner (Polosina and Cupples 2010). These two characteristics that make MutL becomes a strong candidate in MMR web (Polosina and Cupples 2010).

Abundant literature related ATP and DNA-dependent MutS conformational changes, the interaction between MutS and MutL, and the effect of MutS-MutL interaction on MutS during MMR processes (Sharma, Doucette et al. 2013, Lee, Cho et al. 2014, Groothuizen, Winkler et al. 2015, Qiu, Sakato et al. 2015, Liu, Hanne et al. 2016). Several models of MMR proposed while the mismatch-bound MutS recruit MutL to the protein-DNA complex has been accepted in both *E. coli* and Eukaryotic MMR system. The confusions existed in different MMR models as Guo-Min Li summarized in 2014, especially for the interaction between MutS and MutL during finding the mismatch, correct mismatch and associated from the DNA (Li 2014). Therefore, the interaction between MutS and MutL, and the effect of this interaction on MutS ATPase and DNA dependent conformational changes, especially for the impact of this interaction on MutL loaded on mismatch-containing DNA, maturation on DNA, activated MutH, and later MMR processes still elusive.

We established fluorescence resonance energy transfer (FRET) assays (chapter 2) that allow us to monitor the loading of MutL on DNA by wtMutS as well as conformational changes in MutL (chapter 1). With single G: T mismatch-containing GT932 circular DNA, both multiple loading of MutL and conformational changes in MutL exist. Hence, we investigated MutL conformational changes on single G: T mismatch-containing and end blocked GT59DF DNA. However, both the BR FRET (between MutL and GT59DF DNA) kinetics and the EfA (GR FRET efficiency between MutL and MutL) kinetics varied dependent on the ionic strength. Hence, we monitored the effect

of different ionic strength FB buffers on MutL loaded on GT59DF DNA and MutL conformational changes during MMR processes.

Results

1, Multi-loading combined conformational changes MutL on G: T mismatch-containing GT932 circular DNA

1.1 The Extra FRET over MutL subunit-exchange observed in the presence of MutS, ATP, and GT932 circular DNA

From Figure 1 A we could find that GT932 DNA/ATP ($0.12 \pm 0.002 \text{ min}^{-1}$) and MutS-ATP ($0.10 \pm 0.001 \text{ min}^{-1}$) do not affect MutL NTD-NTD subunit exchanges compared to the APO ($0.08 \pm 0.001 \text{ min}^{-1}$). While the rates in the presence of GT932 DNA, MutS449/D835R and $10 \mu\text{M}$ or 2 mM ATP at the same time increased 2 fold to $0.15 \pm 0.001 \text{ min}^{-1}$, but the EfA of 2 mM ATP is 1.5 fold of $10 \mu\text{M}$ ATP (Figure 1 A. dark grey and dark brown). After adding thrombin, the EfA value decreased to the starting value except the kinetics in the presence of GT932 DNA, MutS449/D835R and 2 mM ATP at the similar level for NTD-NTD FRET efficiency in the absence of GT932 DNA, MutS449/D835R, and 2 mM ATP (Figure 1 A, B, and C).

Besides, GT932 ($0.064 \pm 0.006 \text{ min}^{-1}$), ATP ($0.085 \pm 0.0004 \text{ min}^{-1}$) and dimeric MutS/D835R ($0.086 \pm 0.0003 \text{ min}^{-1}$) do not affect AF488 and AF594 NTD labeled full-length (FL) MutL297 subunit exchange while the FRET efficiency (EfA) increase rates doubled after adding the missing components (Figure 1 B and C). The extra FRET between MutL NTD-CTD (MutL452_AF488/MutL297_AF594) and MutL CTD-CTD (MutL452_AF488AF594) are rather small change due to the distance between NTD-CTD is too large (the EfA lower, Figure 1 D and E) while the distance is too short between CTD-CTD (the EfA almost close to 1, Figure 1 F and G).

Furthermore, spectra assessment monitor ATP/GT932 DNA, dimeric MutS449/D835R and thrombin effect to MutL subunit exchange have been shown in Figure 1.2 A, the FRET efficiency demonstrated at 1.2 B. The donor fluorescence intensity excited at 470 nm and emitted at 519 nm , while the FRET intensity signal excited at 590 nm and emitted at 617 nm . After adding ATP and GT932 DNA, the donor signal decreased while the FRET signal increased at the same time,

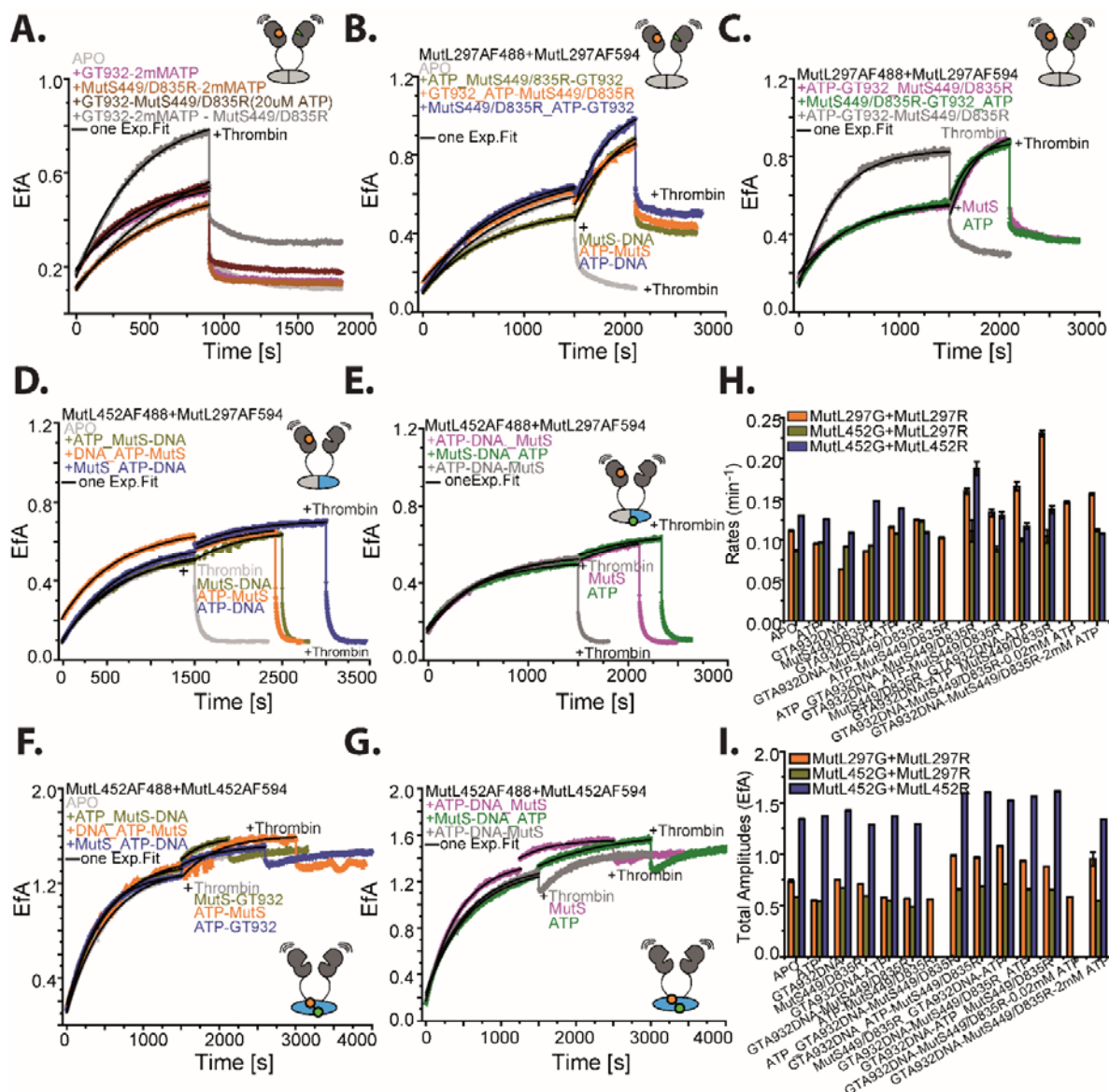


Figure 1.1 Effect of MutS and nano-circular DNA on MutL Subunit Exchange. (A) mixed 100 nM MutL297_AF488 with 100 nM MutL297_AF594 in the presence of different compositions of 2 nM GT932 DNA, 200 nM MutS449/D835R, and 20 μM or 2 mM ATP in buffer M and later added thrombin; (B and C) mixed 100 nM MutL297_AF488 with 100 nM MutL297_AF594 in the presence of different composition of 2 nM GT932 DNA, 200 nM MutS449/D835R, and 20 μM or 2 mM ATP in buffer M and later added the missing items, and added thrombin at final; (D and E) mixed 100 nM MutL452_AF488 with 100 nM MutL297_AF594 in the presence of different composition of 2 nM GT932 DNA, 200 nM MutS449/D835R, and 20 μM or 2 mM ATP in buffer M and later added the missing items, and added thrombin finally; (F and G) mixed 100 nM MutL452_AF488 with 100 nM MutL452_AF594 in the presence of different composition of 2 nM GT932 DNA, 200 nM MutS449/D835R, and 20 μM or 2 mM ATP in buffer M and later added the missing items. Finally, added thrombin to all systems. (H and I) the rates and amplitudes of MutL NTD-NTD, NTD-CTD and CTD-CTD kinetics (averaged from different chapters) under different conditions.

so the FRET efficiency increased (Figure 1.2 B purple and orange). After adding dimeric MutS449/D835R, both the donor and FRET channels are decreased, while the FRET efficiency stay no change (Figure 1.2 A brown and B). Whereas, both the donor and the FRET signal

increased, but the donor signal augmented more, so the FRET efficiency decreased a little bit (both the FRET channel and FRET efficiency corrected the degree of labeling of proteins) after adding thrombin (Figure 1.2 A grey and B).

1.2 The quantity of MutS on DNA contribute to the delay of extra FRET appears

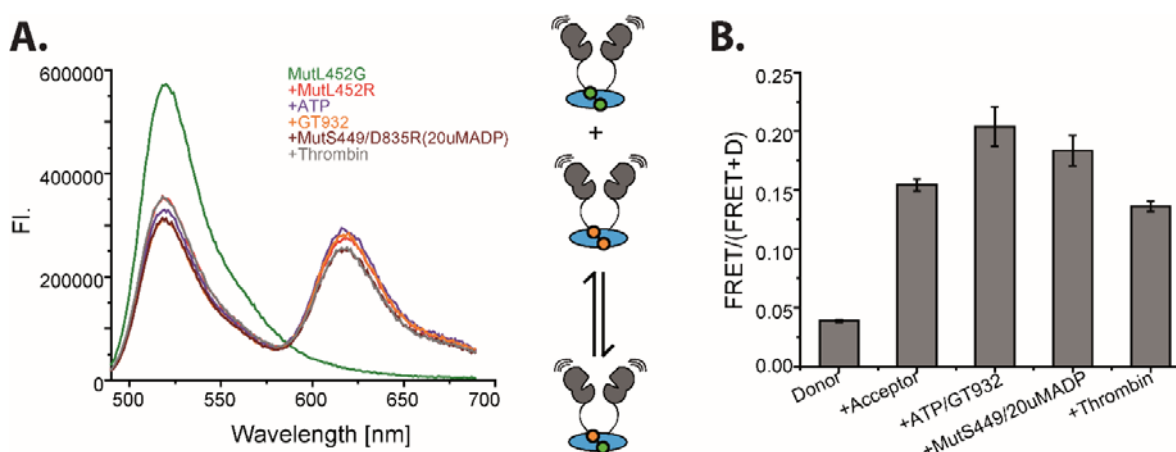


Figure 1.2 How dimeric MutS, ATP and GT932 DNA affect MutL-MutL interaction (A) mixed 100 nM MutL452_AF488 with 100 nM MutL452_AF594 in 200 μ l buffer M and later sequentially added 2 mM ATP-10 nM GT932 DNA, 400 nM MutS449/D835R and thrombin; (B) FRET intensity (emission at 470 nm and excited at 617 nm) divide donor (excited at 470 nm and emission at 519 nm) intensity plus FRET intensity, both FRET and donor channel corrected the crosstalk from buffer and acceptor (excited at 590 nm and emission at 617 nm).

As described above, the extra FRET over the MutL subunit exchange existing only in the presence of MutS, mismatch-containing circular DNA (GT932), and ATP at the same time. Nevertheless, about 30 s delays appear to the EfA when added the missing components to MutL- ATP, MutL-GT932 DNA, and MutL-MutS449/D835R observed (2 nM GT932 DNA, Figure 1 B). This 30 s' delay for the EfA always existing when added 5-400 nM MutS449/D835R (no tetramer living for this MutS mutant) to 200 nM MutL297_AF488AF594 which incubating with 2 nM GT932 DNA and 2 mM ATP in buffer M (Figure 1.3 A). And the apparent KD value is 593 ± 188 nM (Figure 1.3 B). However, as shown in Figure 1.5 C and D, only tiny change appears to the EfA and the BR FRET of MutL297 when added 2 μ M wtMutS to the system of 200 nM MutL297_AF488AF594 incubating with 10 nM GT932 DNA, 200 nM wtMutS (could form tetramer) and 2 mM ATP. Besides, the final amplitudes of kinetics for adding 200 or 400 nM MutS449/D835R are reach the similar value at the end (Figure 1.3 A dark grey and magenta). Hence, we need at least 200 nM MutS to load 200 nM MutL on GT932 circular DNA.

Moreover, the 30 s' delay of EfA only observed at lower concentration of G: T mismatch-containing GT932 DNA (< 10 nM, Figure 1.3 C grey, olive, and orange) when varied the

concentrations of GT932 circular DNA from 1 to 20 nM in the presence of 200 nM MutL297_AF488AF594 incubating with 200 nM MutS449/D835R and 2 mM ATP in buffer M (Figure 1.3 C). The apparent rates and amplitudes for the EfA kinetics reach the saturation since 10 nM GT932 DNA, and the apparent KD value is 13 ± 5.6 nM (Figure 1.3 D). At last, the 30 s' delay disappeared no matter titration MutL297_AF488AF594 to 200 nM MutS449/D835R, 2 mM ATP and with 5 or 10 nM GT932 circular DNA (Figure 1.3 E). Additionally, the changing rates for titration MutL to 5 or 10 nM GT932 circular DNA incubating with 200 nM MutS449/D835R and 2 mM ATP which derived from signal exponential fits the kinetics fluctuated at 0.75 min^{-1} independent of the concentration of MutL (Figure 1.3 G). The 30 s' delay disappeared when pre-incubated MutS449/D835R with GT932 DNA in the presence of ATP, whereas it disappeared as well when increasing the number of mismatches (G:T) (the instrument dead time is around 15 s, so the delay within 20 s cannot be measured with TECAN). Except that, the corrected BR FRET doubled with wtMutS than with MutS449/D835R for recruiting 200 nM MutL297_AF488AF594 hetero-dimers on 5 nM GT932 DNA (Figure 1.4 A and B, green and purple). Therefore, the quantity of MutS449/D835R on mismatch-containing DNA contributed to the 30 s' delay.

1.3, Multiple loading MutL on DNA mainly contribute to the Extra FRET

As we know from above, the 30 s delay disappeared when pre-incubated 200 nM MutS448/D835R with 5 nM G: T mismatch-containing GT932 circular DNA together for 2 min (Figure 1.3 E). Moreover, the MutS maturation only contribute to maximum 2 s' delay for loading MutL on GT59DF DNA (Figure 2.2 A). Then what is the critical reason for the 30 s' delay for loading MutL on GT932 DNA? Moreover, the FRET efficiency (EfA) of MutL297_AF488AF594 with 5 nM GT932 DNA is always higher than with 10 nM GT932 DNA, even though both of them share the similar corrected BR FRET (MutL to DNA FRET) when titrated 50-400 nM MutL297_AF488AF594 to 5 or 10 nM GT932 circular DNA in the presence of 200 nM MutS449/D835R, and 2 mM ATP (Figure 1.3 E and F, red and olive). The FRET efficiency (EfA) of MutL297_AF488AF594 with 10 μM ATP stay the same as the beginning until added 2 mM ATP to the system (Figure 1.3 E, dark grey), then it strikingly heading up to the similar level as with 2 mM ATP at the beginning (Figure 1.3 E, olive and dark grey). However, the corrected BR FRET of titration MutL297_AF488AF594 to 10 nM GT932 DNA with 10 μM ATP is always higher than with 2 mM ATP at the beginning, the corrected BR FRET reach the similar level only after titrated 400 nM MutL297_AF488AF594 (Figure 1.3 F, olive, and dark grey). Besides, the down phase appears to kinetics of the correct BR FRET of MutL to DNA with 2 mM ATP which are irrelevant

with 5 or 10 nM GT932 DNA (Figure 1.3 F, red and olive) and seems not appear to the low ATP situation (Figure 1.3 F, dark grey). Substituted the GT932 DNA with 59 bp G: T mismatch-containing DNA, no extra EfA observed when added 50-200 nM GT59D DNA (DNA without blocking the end) or GT59DF DNA (the end of DNA blocked with four-fold Fab-fragment) (Figure 1.3 H).

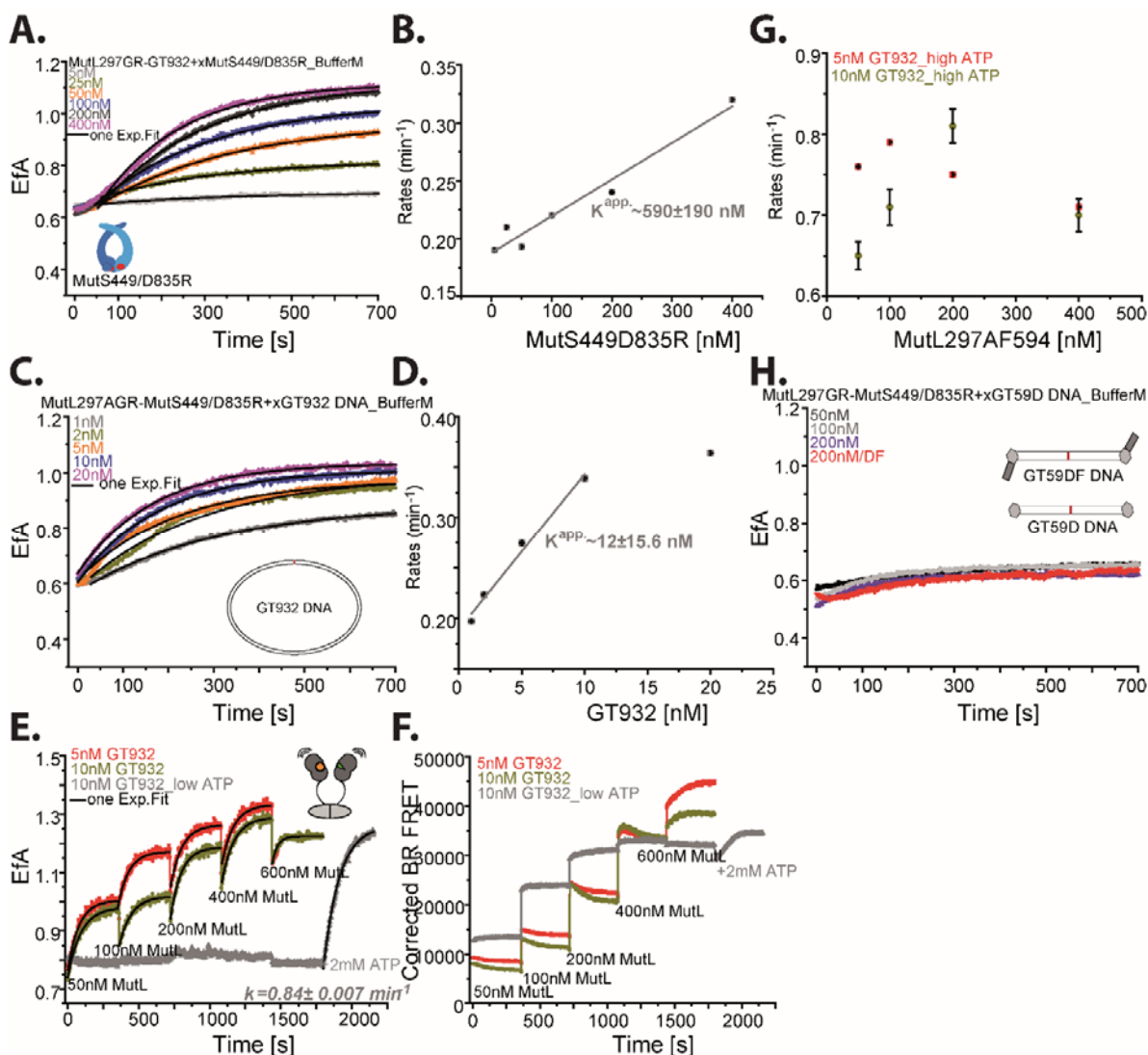


Figure 1.3 Titration MutS/MutL/GT932 DNA to MutL297_AF488AF594 (GR) hetero-dimers (A) 200 nM MutL297_AF488AF594 incubate with 2 nM GT932 DNA and 2 mM ATP in buffer M, then added 5-400 nM MutS449/D835R to start the reaction; (B) the rates derived from kinetics of titration MutS449/D835R with single exponential fits (A); (C) 200 nM MutL297_AF488AF594 incubate with 200 nM MutS449/D835R and 2 mM ATP in buffer M, then added 1- 20 nM GT932 DNA to start the reaction; (D) the rates derived from kinetics of titration GT932 DNA with single exponential fits (C); (E and F) titration 50-600 nM MutL297_AF488AF594 to pre-incubated 200 nM MutS449/D835R and 10 μ M/2 mM ATP with 5/10 nM GT932 DNA in buffer M; (G) the rates derived from kinetics of titration MutL297_AF594 to 5 or 10 nM GT932 DNA with single exponential fits (E); (H) 200 nM MutL297_AF488AF594 incubate with 200 nM MutS449/D835R and 2 mM ATP in buffer M, then added 50- 200 nM GT59D DNA or 200 nM GT59DF DNA to start the reaction

Added 20-200 nM MutL297_AF488AF594 to 5 or 10 nM GT932 DNA with 200 nM MutS449/D835R and 2 mM ATP in buffer M, we could observe that the EfA is higher when MutL-GT932 DNA ratio is higher (Figure 1.4 A). Both the EfA and the corrected BR FRET reached the saturation slower for 200 nM MutL297_AF488AF594 with 5 nM GT932 DNA in the presence of 200 nM MutS449/D835R and 2mM ATP (Figure 1.4 A and B, grey). The corrected BR FRET intensities are 2 fold lower compared Figure 1.4 D (green and olive) to Figure 1.4 B (green and olive), when mixed 10 or 100 nM MutL297_AF488 with 10 or 100 nM MutL297_AF594 in the presence of 200 nM MutS449/D835R and 2 mM ATP with 5 or 10 nM GT932 DNA. The EfA was lower as well when compared Figure 1.4 C to 1.4 A (grey and olive).

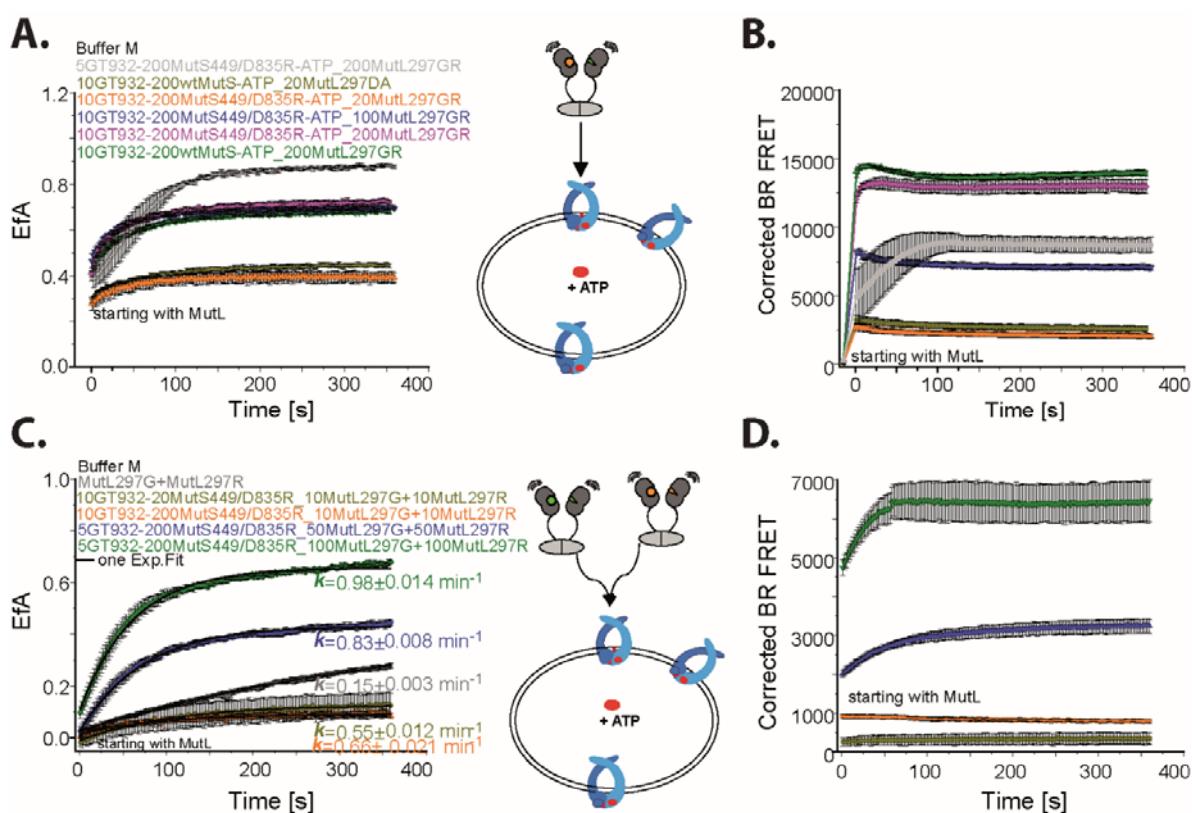


Figure 1.4 Dimeric/tetrameric MutS and different concentration of GT932 nano-circular DNA effect different MutL mutants' hetero-dimer FRET. (A and B) added 20-200 nM MutL297_AF488AF594 hetero-dimer to pre-incubated 200 nM wtMutS/MutS449/D835R and 2 mM ATP with 5/10 nM GT932 DNA in buffer M; (C and D) pre-incubated 200 nM MutS449/D835R and 2 mM ATP with 5/10 nM GT932 DNA in buffer M, then added 10-100 nM MutL297_AF488 and 10-100 nM MutL297_AF594 at the meantime to start the reaction.

The subunit exchange rate of 100 nM MutL297_AF488 with 100 nM MutL297_AF594 is $0.15 \pm 0.003 \text{ min}^{-1}$, while rates of the EfA increased 2-3 fold at lower MutL concentration (Figure 1.4 C, orange and olive) and increased 6-7 fold at higher MutL concentration (Figure 1.4 C, green and blue) in the presence of MutS, GT932 circular DNA and 2 mM ATP. In addition, mixed 10 nM MutL297_AF488 with 10 nM MutL297_AF594 together in the presence of 20 or 200 nM

MutS449/D835R with 10 nM GT932 and 2 mM ATP, we could conclude that the rate with 200 nM MutS449/D835R ($0.66 \pm 0.21 \text{ min}^{-1}$) is faster than with 20 nM MutS449/D835R ($0.55 \pm 0.12 \text{ min}^{-1}$) (Figure 1.4 C orange and olive). MutL cannot be loaded on DNA by MutS without mismatch as no observation of MutL binding lambda DNA in buffer M while the EfA and the corrected BR FRET strikingly increased after adding 5 nM GT932 circular (Appendix Figure 3.1 A and B). As we known from the literature, MutL297N33A is deficient in binding nucleotides,

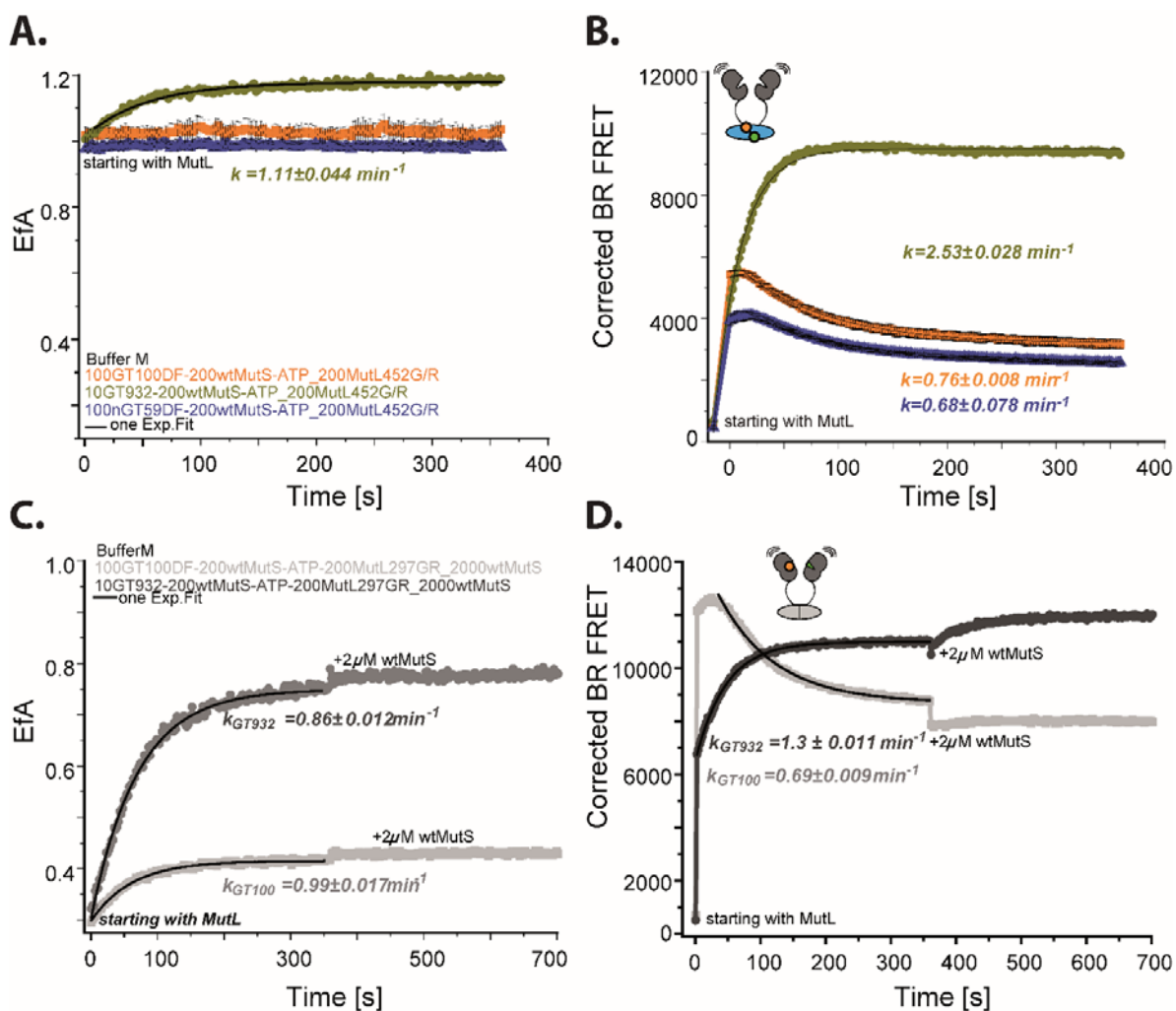


Figure 1.5 GT932 nano-circular DNA or end blocked oligoes' effect MutL452_AF488AF594/MutL297_AF488 AF594 hetero-dimers subunit interaction (A and B) added 200 nM MutL452_AF488AF594 hetero-dimer to pre-incubated 200 nM wtMutS and 2 mM ATP 10 nM GT932 DNA or 100 nM GT100DF DNA/GT59DF DNA in buffer M; (C and D) added 200 nM MutL297_AF488AF594 hetero-dimers to pre-incubated with 200 nM wtMutS and 2 mM ATP 10 nM GT932 DNA or 100 nM GT100DF DNA in buffer M, and later continually added 2 μ M wtMutS.

and MutL297E29A is deficient in hydrolysis ATP which will cause MutL NTD dimerized forever (Ban and Yang 1998, Guarne, Ramon-Maiques et al. 2004, Robertson, Pattishall, et al. 2006). Even through 200 nM MutL297N33A_AF488AF594 or MutL297_AF488/ MutL297- N33A_AF594

hetero-dimers could be loaded on 5 nM GT932 DNA as well by 200 nM wtMutS in the presence of ATP, the EfA stay no change (Appendix Figure 3.1 C and D). Similarly, 200 nM MutL297E29A_AF488AF594 could be loaded on 5 nM GT932 circular DNA by 200 nM wtMutS in the presence of ATP as well, while no observation for the EfA changing (Appendix Figure 3.1 E and F).

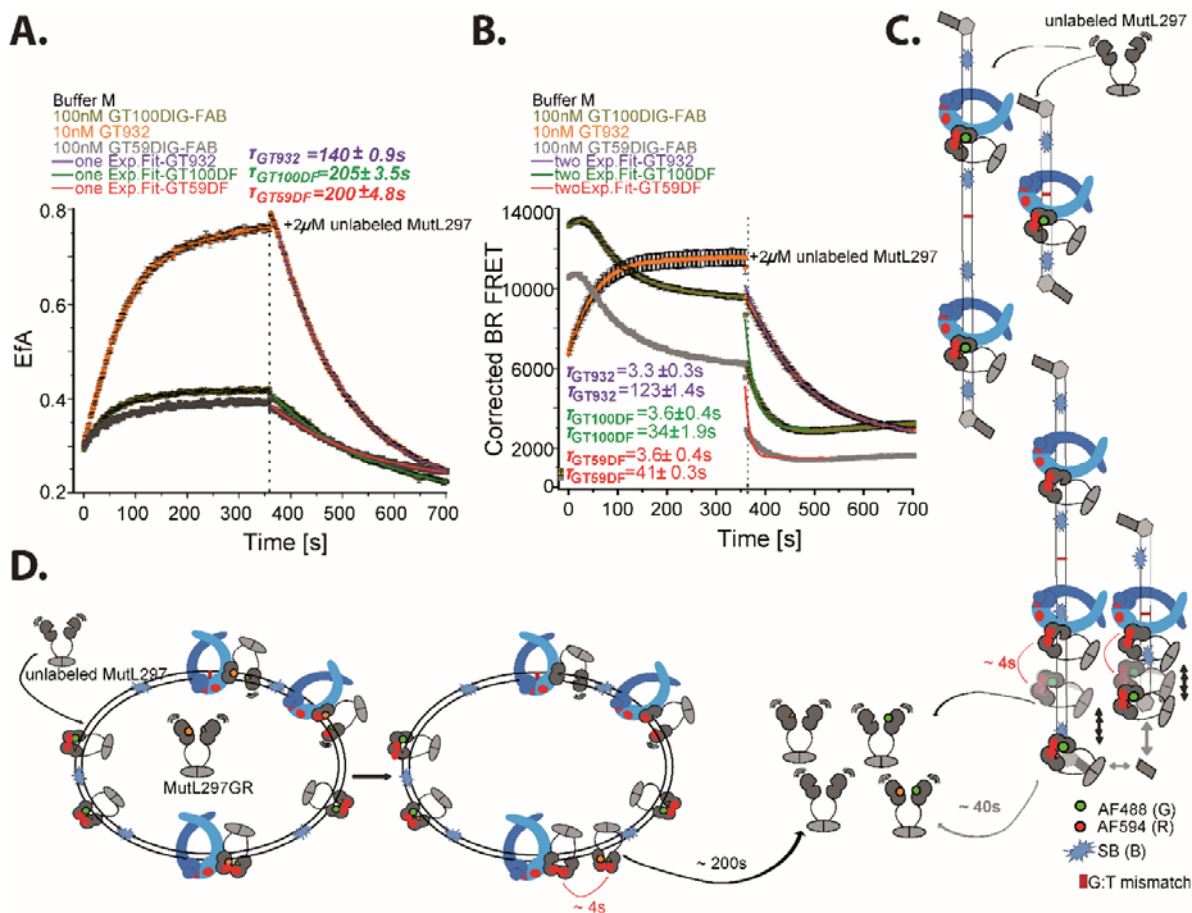


Figure 1.6 MutL297_AF488AF594 off rates from GT932 nano-circular DNA or end blocked oligoes' DNA. (A and B) added 200 nM MutL297_AF488AF594 hetero-dimers to pre-incubated 200 nM wtMutS and 2 mM ATP 10 nM GT932 DNA or 100 nM GT100DF DNA/GT59DF DNA in buffer M, and later continually added 2 μ M unlabeled MutL297; (C) cartoons depiction of MutL dissociation from Fab-fragment blocked single mismatch-containing GT59DF DNA or GT100DF DNA in the graph A and B; (D) cartoons depiction of MutL dissociation from single mismatch-containing GT932 circular DNA in the graph A and B.

To sum up, we could conclude that the extra EfA over subunit exchange is due to MutL conformational changes combined with multiple loading of MutL on GT932 circular DNA. We could observe that the BR FRET with GT932 DNA is two-fold higher than with GT100DF DNA (Figure 1.5 B olive and orange), and the EfA increased 20 % with GT932 DNA (Figure 1.5 A and B, olive and orange), even though 100 nM GT100DF DNA and 10 nM GT932 DNA are share the similar base pairs when added 200 nM MutL452_AF488AF594 to 10 nM GT932 DNA or 100 nM

GT100DF DNA or 100 nM GT59DF DNA incubating with 200 nM wtMutS and 2 mM ATP. Besides 100 nM GT100DF DNA base pairs almost doubled as GT59DF DNA, while both of them share the similar BR FRET and the EfA of both stay at the same level as the starting points (Figure 1.5 A and B, orange and blue). The distance between donor and acceptor labeled MutL452 residue is ~ 28 angstrom, and the single molecule FRET efficiency is close to 0.9 (Chapter 1 Figure 4 J-L). Moreover, the rate of loading MutL452_AF488AF594 on GT932 DNA (the corrected BR FRET) is $2.53 \pm 0.028 \text{ min}^{-1}$ (Figure 1.5 B, olive) which is twofold faster than the increase of EfA which is $1.11 \pm 0.044 \text{ min}^{-1}$ (Figure 1.5 A, olive). Therefore, one reason for the extra EfA for MutL452_AF488AF594 over the subunit exchanges is the multiple loading of MutL on GT932 DNA, which enable the FRET exist for both inter- and intra- MutL hetero-dimers.

1.4, Out-of-step dissociation rates for MutL hetero-dimers, and for MutL/DNA complex

After measuring the rate of loading MutL on GT932 DNA or GT100DF DNA or GT59DF DNA by wtMutS, we estimate the off rate of MutL297_AF488AF594 from the different types of DNA. We could observe that the EfA (FRET efficiency) of MutL297_AF488AF594 decrease with the similar lifetime around 200 s when added 2 μM unlabeled MutL297 as competitor to 200 nM MutL297_AF488AF594 hetero-dimers which incubated with 10 nM GT932 DNA or 100 nM GT100DF DNA or GT59DF DNA, 2 mM ATP, and 200 nM wtMutS in buffer M (Figure 1.6 A), while MutL297_AF488AF594 hetero-dimers dissociated from all kinds of DNA with binary steps (Figure 1.6 B). At the beginning, the fast phases appeared at 3-4 s which is irrelevant with the different types of mismatch-containing DNA (Figure 1.6 B). However, the slow steps are evidently different (3 to 4 fold) from GT932 DNA ($123 \pm 1.4 \text{ s}$, Figure 1.6 B orange) to oligoes ($34 \pm 1.9 \text{ s}$ for GT100DF DNA, Figure 1.6 B olive; and $41 \pm 8.3 \text{ s}$ for GT59DF DNA, Figure 1.6 B dark grey).

1.5, Multiple loading versus conformational changes derived from the different combination of NTD-NTD, NTD-CTD, and CTD of MutL

As we know from the above description, 200 nM AF488 and AF594 labeled MutL hetero-dimers could be multiply loaded on G: T mismatch-containing circular GT932 DNA, and together with its conformational changes contributed to the extra EfA over the MutL subunit exchange. While in this part, we monitored the EfA and the corrected BR FRET changes with the different combinations of the various single labeled residues at both the NTD and the CTD of MutL. The

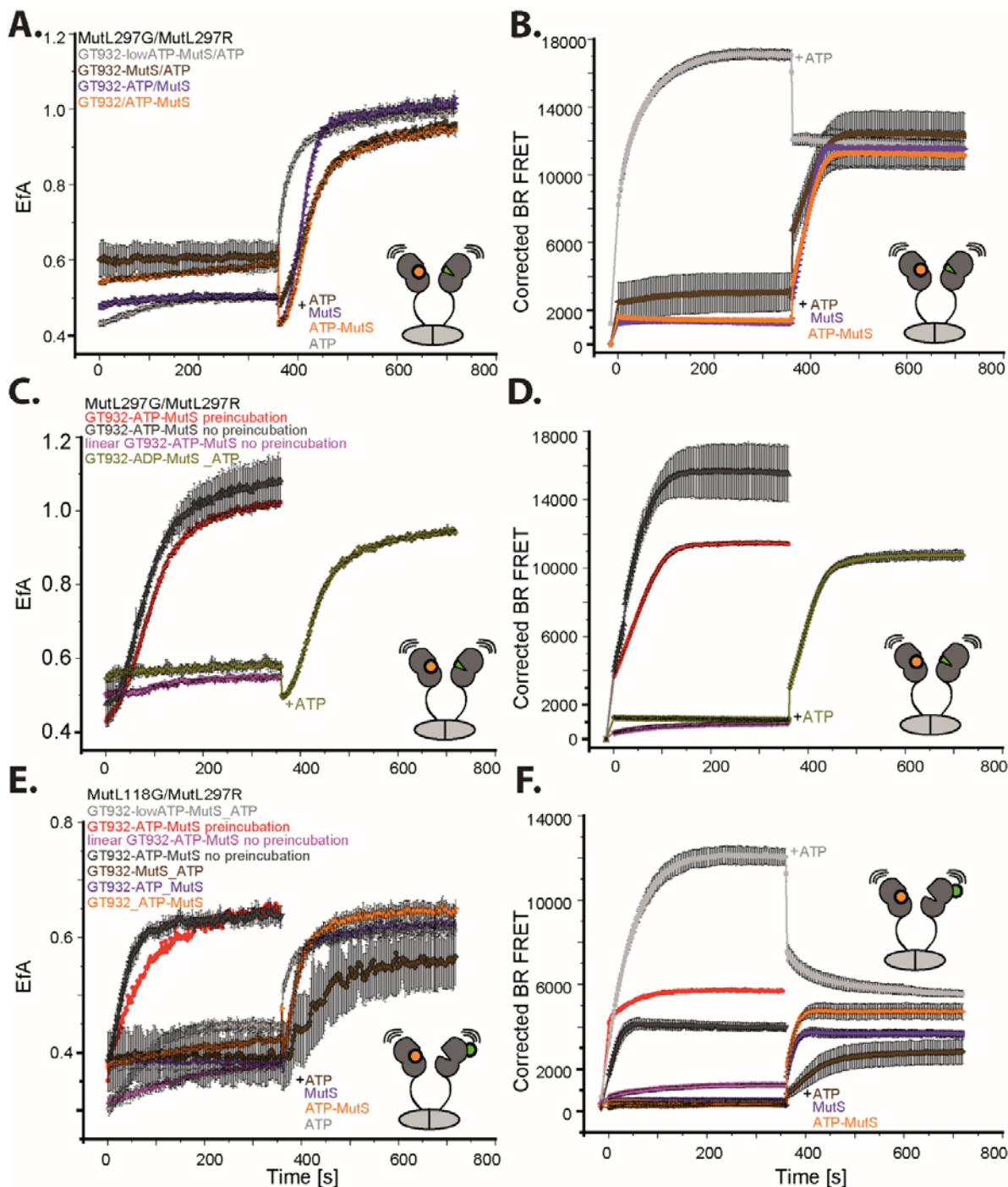


Figure 1.7 The effect of dimeric MutS, ATP and nano-circular/linearized GT932 DNA effect MutL297_AF488AF594 or MutL118_AF488/MutL297_AF594 hetero-dimers subunit interaction. (A and B) 200 nM MutL297_AF488AF594 hetero-dimers added to system with different composition of 5 nM GT932 DNA, 200 nM MutS449/D835R, and 10 μ M or 2 mM ATP in buffer M and later added the missing items; (C and D) added pre-incubated or non-incubated 5 nM GT932 DNA (circular or linear), 200 nM MutS449/D835R, and 2 mM ATP/ADP to 200 nM MutL297_AF488AF594 hetero-dimers in buffer M to start the reaction; (E and F) the same procedure as described above from A-D which added to 200 nM preformed MutL118_AF488/MutL297_AF594 hetero-dimers in buffer M to initiate the reaction.

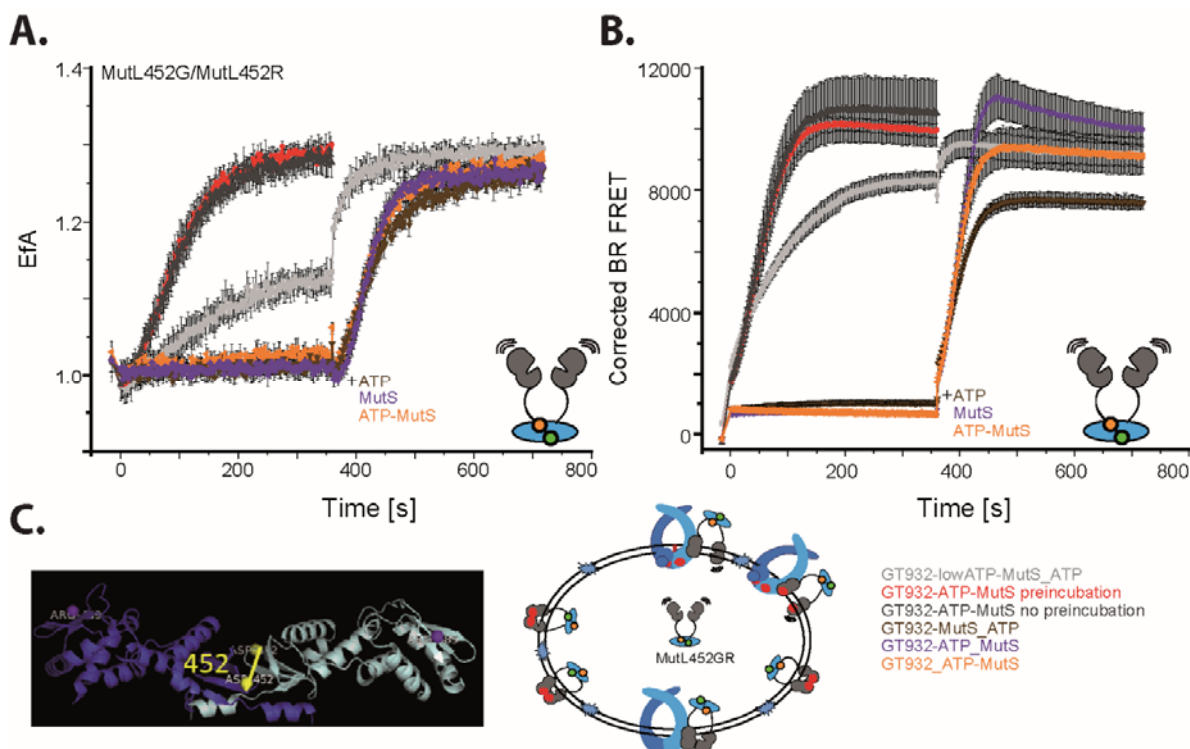


Figure 1.8 Subunit interaction of MutL452_AF488AF594 (GR, CTD-CTD) hetero-dimers in the presence of dimeric MutS, ATP and nano-circular GT932 DNA. Added pre-/non- incubated different composition of 5 nM GT932 DNA, 200 nM MutS449/D835R and 10 μ M or 2 mM ATP to 200 nM pre-incubated AF488 and AF594 labeled MutL452 hetero-dimers. (A) the GR FRET efficiency between CTD labeled MutL hetero-dimers (Efa); (B) the BR FRET between he labeled MutL452 to SYTOX blue stained GT932 circular DNA; (C) upper part is 452 position on MutL CTD dimer ternary structure, and the lower part is the cartoons depiction of CTD labeled MutL conformational changes and binding on GT932 circular DNA.

different orders to add 5 nM GT932 DNA, 200 nM MutS449/D835R, and 10 μ M/2 mM ATP in buffer M were tested as well. Firstly, we test two positions at NTD of MutL: 297 (H297C, mutant of histidine to cysteines and removed other cysteines of MutL at the same time, is close to the ATP binding pocket and positioned at the five disordered loops) and 118 (Q118C, mutant of glutamine to cysteine and removed other cysteines of MutL at the same time, and is positioned away from the five disordered loops at the top shoulders of MutL NTD). As we could observe from Figure 1.7 A-B and E-F, only GT932 circular DNA or GT932 DNA-ATP or GT932 DNA- MutS449/D835R cannot cause the Efa and the BR FRET changing for both MutL297_AF488- AF594 and MutL118_AF488A/MutL297_AF594 hetero-dimers. However, the Efa are very tiny increased in the presence of GT932 DNA-MutS449/D835R and 10 μ M ATP, while the corrected BR FRET are strikingly increased for both two MutL hetero-dimers. The slowly loading rate for MutL on the GT932 DNA is due to the reaction starting with MutS449/D835R, which need to wait MutS449/D835R switch to the sliding clamp to recruit MutL. Both the Efa and the BR FRET

increased significantly after adding the missing components, such as 2 mM ATP, or MutS449/D835R, or 2 mM ATP and MutS449/ D835R (Figure 1.7 A-B and E-F).

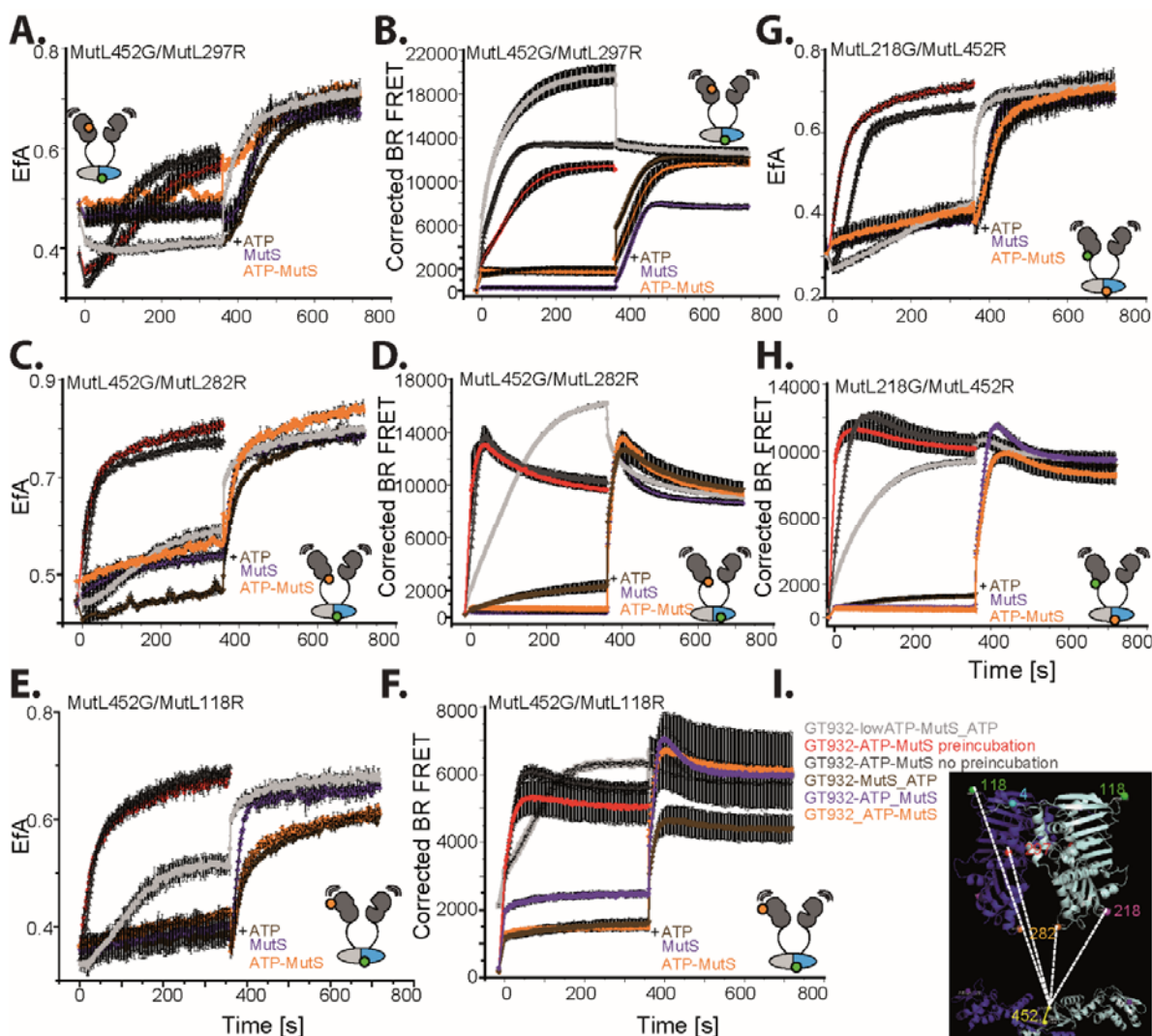


Figure 1.9 Subunit interaction of AF488 (G) and AF594 (R) labeled CTD-CTD/CTD-NTD of MutL hetero-dimers in the presence of dimeric MutS, ATP, and nano-circular GT932 DNA. Added pre-/non- incubated different composition of 5 nM GT932 DNA, 200 nM MutS449/D835R, and 10 μ M or 2 mM ATP. The followed combinations are measured in buffer M and start the reaction with the missing items. (A and B) 200 nM pre-incubated MutL452_AF488AF594 hetero-dimers; (C and D) 200 nM pre-incubated MutL452_G/MutL297_R hetero-dimers; (E and F) 200 nM pre-incubated MutL452_G/MutL282_R hetero-dimers; (G. and H.) 200 nM pre-incubated MutL452_G/MutL118_R hetero-dimers; (I) 200 nM pre-incubated MutL218_G/MutL452_R hetero-dimers.

As adding 2 mM ATP to the system of GT932-MutS449/ D835R-10 μ M ATP, the Efa notably increased the rate of that much faster than others (Figure 1.7 A-B and E-F). That supports the opinion that the maturation of MutS on mismatch-containing DNA is imperative for loading MutL on mismatch-containing DNA. And consistent with the observation that only MutS and GT932 DNA, without ATP, cannot load MutL on DNA (Figure 1.7 A-B and E-F). MutS, GT932 DNA,

and ADP cannot load MutL on GT932 DNA as well (Figure 1.7 C and D, Chapter 2 Figure 9 A and B). In contrast to the EfA, added 2 mM ATP to MutL297_GR or MutL118_G/ MutL297_R hetero-dimers incubated with GT932 DNA-MutS449/D835R-10 μ M ATP induced the BR FRET immediately decreased to the same level as other kinetics with 2 mM ATP at the beginning (Figure 1.7 B and F). These down phases of the BR FRET are due to ATP resulted in a series of conformational change on GT932 circular DNA (Figure 1.7 B and F grey) as we know that 200 nM MutS is sufficient loaded 200 nM MutL on this GT932 circular DNA (Figure 1.5 C and D). However, neither the EfA nor the BR FRET increased when we linearized the GT932 circular DNA for both the MutL297_AF488AF594 and MutL118_AF488/MutL297_AF594 hetero-dimers. That supports the opinion of MutL were multiple-loaded on GT932 circular DNA (Figure 1.7 C-F). Additionally, compared to add pre-incubated samples (including 5 nM GT932 DNA, 2 mM ATP and 200 nM MutS449/D835R pre-incubated in 50 μ l buffer M) to 200 nM MutL297_AF488AF594 or MutL118_AF488A/MutL297_AF594 hetero-dimers separately, we could observe that pre-incubation could induce MutL multiple loading on DNA and process conformational changes faster than the non-incubated samples (Figure 1.7 C-F). That supports the quantity and maturation of MutS on the GT932 DNA is the main reason for the \sim 30 s' delay for loading MutL on DNA. Compared the EfA and the BR FRET of these two hetero-dimers, we could find that the distance between MutL118_AF488 to MutL297_AF594 within the hetero-dimers is further than the distance between MutL297_AF488 and MutL297_AF594 (Figure 1.7). Hence, MutL297_AF594 gain less energy from MutL118_AF488 compared to MutL297_AF488, which is consistent with the MutL quaternary structure with AMPPNP. The same as MutL297, when added GT932 circular DNA or GT932 DNA-ATP or GT932 DNA-MutS449/D835R, cannot cause both the EfA and the corrected BR FRET changing at CTD labeled (MutL452_AF488AF594) hetero-dimers, and only increased when added the missing components (Figure 1.8 A and B). While in contrast to MutL118 and MutL 297, both the EfA and the BR FRET of MutL452_AF488AF594 hetero-dimers are slowly increased when incubating with GT932 DNA-MutS449/D835R-10 μ M ATP, and continuously increased after adding 2 mM ATP to the GT932 DNA-MutS449/D835R- 10 μ M ATP (Figure 1.8 A and B grey). Similar to MutL452_AF488AF594 CTD-CTD labeled hetero-dimers, the EfA and the corrected BR FRET of NTD-CTD labeled hetero-dimers (such as MutL452_AF488/MutL282_AF594, MutL218_AF488/MutL452_AF594, and MutL452_AF488/MutL118_AF594) showed no big changes in the presence of GT932 DNA-ATP or GT932 DNA-MutS449/D835R, both the EfA and the corrected BR FRET slowly increased when incubating with

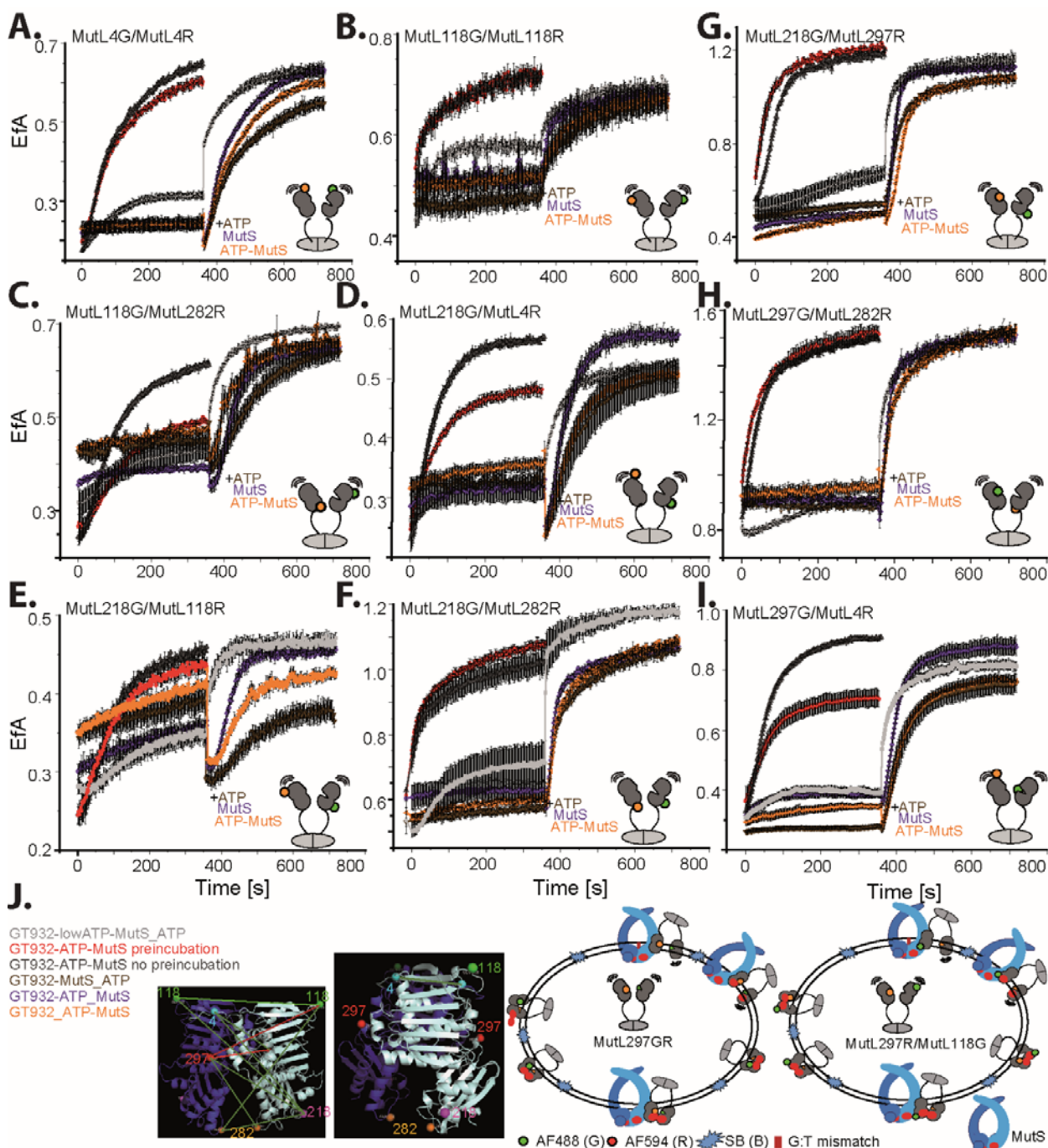


Figure 1.10 Efa of AF488 (G) and AF594 (R) labeled different positions of MutL hetero-dimers. Subunit interaction in the presence of MutS449/D835R, ATP, and nano-circular GT932 DNA. Added pre-/non- incubated with different composition of 5 nM GT932 DNA, 200 nM MutS449/D835R, and 10 μ M or 2 mM ATP in buffer M to the following combinations: (A) 200 nM pre-incubated MutL4_AF488AF594 hetero-dimers; (B) 200 nM pre-incubated MutL118_AF488AF594 hetero-dimers; (C) 200 nM pre-incubated MutL118_AF488/MutL282_AF594 hetero-dimers; (D) 200 nM pre-incubated MutL218_AF488/MutL4_AF594 hetero-dimers; (E) 200 nM pre-incubated MutL-218_AF488/MutL118_AF594 hetero-dimers; (F) 200 nM pre-incubated MutL218_AF488/MutL282_AF594 hetero-dimers; (G) 200 nM pre-incubated MutL218_AF488/MutL297_AF594 hetero-dimers; (H) 200 nM pre-incubated MutL297_AF488/MutL282_AF594 hetero-dimers; (I) 200 nM pre-incubated MutL297_AF488/MutL4_AF594 hetero-dimers; (J) different single cysteine mutant positions on MutL NTD dimer (PDB: 1b63, left) and cartoons depiction of MutL conformational changes and binding on GT932 circular DNA (right).

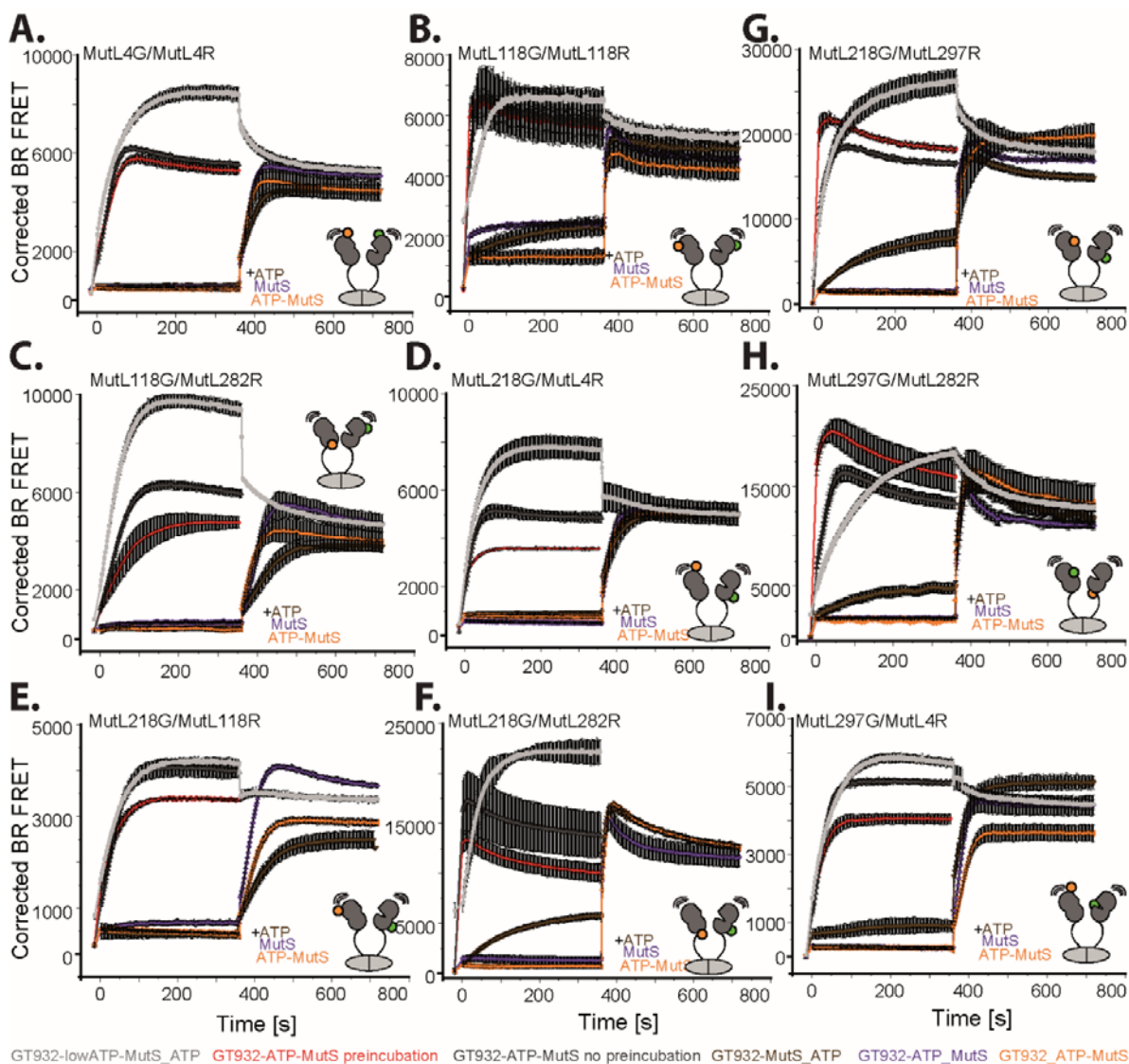


Figure 1.11 Corrected BR FRET of AF488 (G) and AF594 (R) labeled different positions of MutL hetero-dimer. Subunit interaction in the presence of MutS449/D835R, ATP, and nano-circular GT932 DNA. Added pre-/non-incubated with different composition of 5 nM GT932 DNA, 200 nM MutS449/D835R and 10 μ M or 2 mM ATP to the following combinations: (A) 200 nM pre-incubated AF488 and AF594 labeled MutL4 hetero-dimer; (B) 200 nM pre-incubated AF488 and AF594 labeled MutL118 hetero-dimers; (C) 200 nM pre-incubated AF488 labeled MutL118 and AF594 labeled MutL282 hetero-dimers; (D) 200 nM pre-incubated AF488 labeled MutL218 and AF594 labeled MutL4 hetero-dimers; (E) 200 nM pre-incubated AF488 labeled MutL218 and AF594 labeled MutL118 hetero-dimers; (F) 200 nM pre-incubated AF488 labeled MutL218 and AF594 labeled MutL282 hetero-dimers; (G) 200 nM pre-incubated AF488 labeled MutL218 and AF594 labeled MutL297 hetero-dimers; (H) 200 nM pre-incubated AF488 labeled MutL297 and AF594 labeled MutL282 hetero-dimers; (I) 200 nM pre-incubated AF488 labeled MutL297 and AF594 labeled MutL4 hetero-dimers, in buffer M to start the reaction and later added the missing items.

the GT932 DNA-MutS449/ D835R-10 μ M ATP, continuously increased after adding 2 mM ATP to the GT932 DNA- MutS449/D835R-10 μ M ATP (Figure 1.9 C-H). Except the hetero-dimers of MutL452_ AF488/MutL282_ AF594, the corrected BR FRET of which is decreased induced by adding high ATP (Figure 1.9 D).

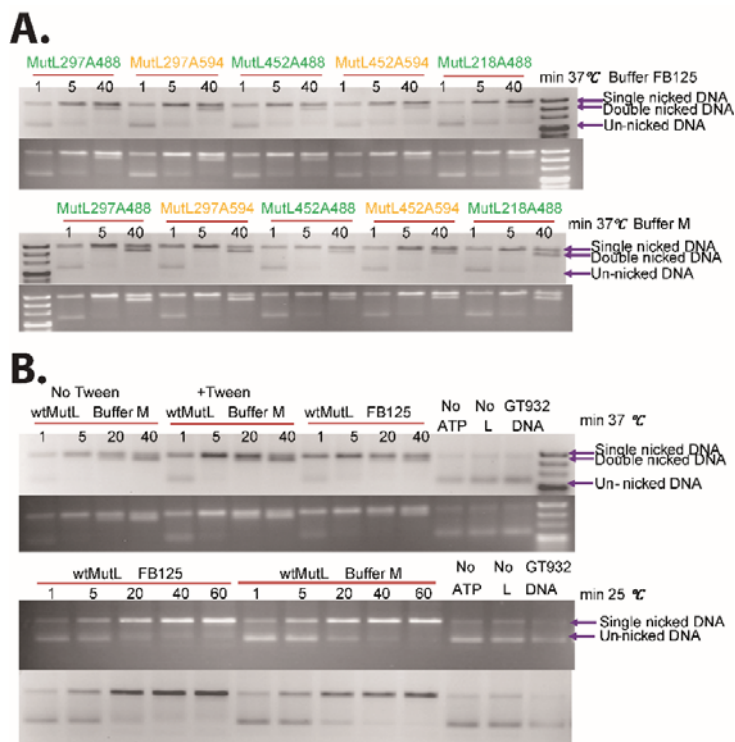


Figure 1.12 The Activity of wtMutL and labeled different NTD and CTD MutL mutants. (A) Pre-incubated 200 nM wtMutL or AF488 or AF594 labeled MutL297, MutL452 or MutL218 with 200 nM MutS449/D835R, 1 mM ATP and 10 nM GT932 DNA in buffer M or FB125 at 37 °C for 10 min and start the reaction with 100 nM wtMutH for 1-40 min then stopped the reaction with proteinase K or protein loading dye; (B) Pre-incubated 200 nM wtMutL with 200 nM MutS449/ D835R, 1 mM ATP and 10 nM GT932 DNA in buffer M or FB125 at 37 °C or 25°C for 10 min and start the reaction with 100 nM wtMutH for 1-60 min then stopped the reaction with proteinase K or protein loading dye.

Otherwise, only the corrected BR FRET increased when incubating with the GT932 DNA-MutS449/D835R-10 μ M ATP complexes for another CTD-NTD labeled hetero-dimer MutL452_A488/MutL297_A594, while the EfA stays the same as beginning (Figure 1.9 A and B, grey). The EfA only increased after adding 2 mM ATP to that system which resulted the corrected BR FRET decreased at the same time (Figure 1.9 A and B, grey). Finally, we tested different combination of the NTD-NTD labeled hetero-dimers, such as MutL4_A488AF594, MutL118_A488AF594, MutL118_A488/MutL282_A594, MutL218_A488/MutL4_A594, MutL218_A488/MutL118_A594, MutL218_A488/MutL282_A594, MutL218_A488/MutL297_A594, MutL297_A488/MutL282_A594, and MutL297_A488/MutL4_A594 hetero-dimers with the same method as we described in Figure 1.7 and Figure 1.8. Incubating with GT932 DNA-MutS449/D835R-10 μ M ATP complexes, the EfA of all MutL NTD-NTD combinations are slightly increased when the corrected BR FRET increased strikingly (Figure 1.10 and Figure 1.11). However, kinetics of the corrected BR FRET of MutL297_A488/ MutL282_A594 hetero-dimers are increased slower under 10 μ M ATP conditions than the other combinations (Figure 1.11 H). Whereas, all the corrected BR FRET immediately decreased to the similar level as the kinetics containing 2 mM ATP at beginning after adding 2 mM ATP, while the EfA increased greatly of all combinations of MutL NTD-NTD labeled hetero-dimers (Figure 1.10 and Figure 1.11). Interestingly, the EfA of MutL118_A488AF594, MutL218_A488/ MutL282_A594,

MutL218_AF488/MutL297_AF594, and MutL297_AF488/MutL282_AF594 hetero-dimers stay no change in the presence 5 nM GT932 circular DNA and 200 nM MutS449/ D835R, while the corrected BR FRET slightly increased (B, F, G, and H of Figure 1.10 and Figure 1.11).

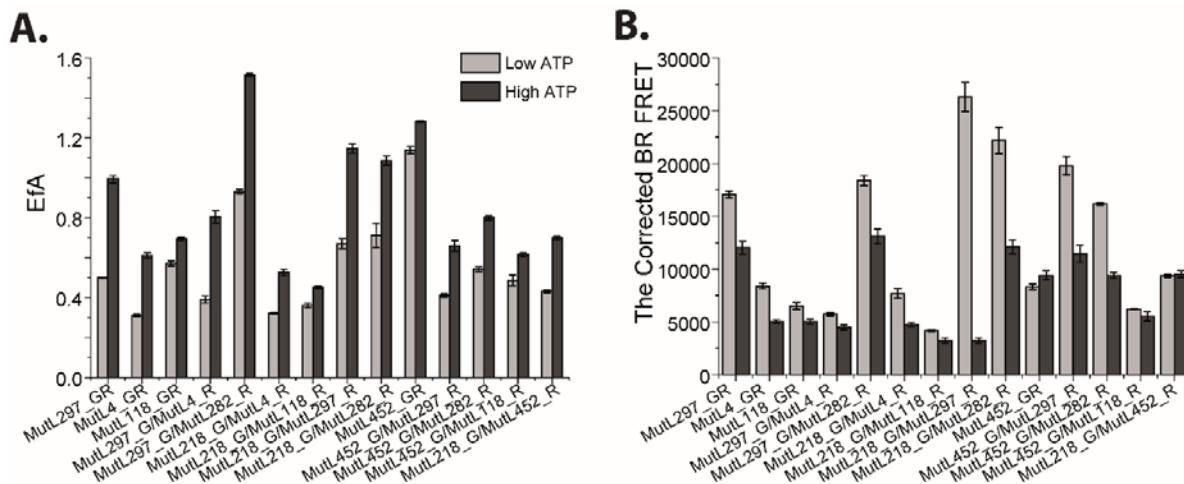


Figure 1.13 Summary of different combination of MutL/MutL interaction in the presence of GT932 DNA, MutS449/D835R, and low/high ATP. (A) MutL/MutL FRET efficiency (EfA, AF488 (G) as donor, AF594 (R) as acceptor) of MutL MutL452_GR, MutL297_GR, MutL118_GR, MutL118_G/MutL297_R, MutL118_G/MutL282_R, MutL218_G/MutL118_R, MutL218_G/MutL282_R, MutL218_G/MutL297_R, MutL297_G/MutL282_R, MutL4_GR, MutL297_G/MutL4_R, MutL218_G/MutL4_R, MutL452_G/MutL118_R, MutL452_G/MutL282_R, MutL218_G/MutL452_R heterodimers from Figure 1.7-1.10 and Table 1; (B) The BR FRET between labeled MutL heterodimers (acceptor) as described in (A) and SYTOX blue (SB) stained GT932 circular DNA from Figure 1.7-1.10 and Table 1.

As described above, the BR FRET of MutL297_G/MutL282_R hetero-dimers slowly increased in the presence of GT932 DNA-MutS449/D835R-10 μ M ATP complexes (~300 s) while the BR FRET of MutL118_G/MutL282_R and MutL218_G/MutL282_R increased faster within 100s, and all of their BR FRET decreased immediately after adding 2 mM ATP (Figure 1.11 C, F and H, and Figure 1.13 B). Similarly, the BR FRET of MutL452_G/MutL282_R and MutL218_G/MutL452_R increased slowly at low ATP state as well (Figure 1.9 D and H grey). On the contrary, the BR FRET of MutL218_G/MutL452_R (Figure 1.9 H grey and Figure 1.13 B) hetero-dimers continuously ascending after adding 2 mM ATP as well as the hetero-dimers of MutL452_GR (Figure 1.8 B grey and Figure 1.13 B). In summary, the conformational changes occurs at all processes of MutL upon loading it on DNA at low ATP to its NTD stably dimerized by adding more ATP. Even without ATP binding at MutL ATPase domain, DNA still could induce some domains of MutL movement which proofed by MutL297_GR hetero-dimers conformational changes at FB75T buffer, and conformational changes of hetero-dimers of MutL452_AF488/MutL297_AF594 at FB150T buffer.

	SE				GT932MutS449/D835R-0.01mM ATP				Rel. change to subunit exchange				GT932-MutS449/D835R-2mM ATP				Rel.change to subunit-exchange				Rel.change to 0.01mM ATP					
	Efa	SEr.	Cor. BR	SEr.	Efa	SEr.	Cor. BR	SEr.	Efa	BR	SEr.	Cor. BR	SEr.	Efa	BR	SEr.	Cor. BR	SEr.	Efa	BR	SEr.	Cor. BR	SEr.	Efa	BR	
CTD - CTD	1.02	0.002	-183	24	1.14	0.017	8328	266	12%	8304	1.28	0.006	9391	422	26%	9366	12%	1063								
NTD - NTD																										
MutL297GR	0.58	0.009	12	14	0.50	0.002	17062	296	-14%	1242	0.99	0.020	12043	604	70%	12029	99%	-5019								
MutL297N33A_GR	0.46	0.045	479	2							0.41	0.020	19681	1219	-11%	19679		2195								
MutL297G/MutL297N33A_R	0.54	0.014	455	59	0.58	0.016	22307	1487	7%	377	0.52	0.037	24502	3742	-4%	24443		-10%								
MutL297E29A_GR	0.42	0.016	325	11	0.46	0.006	17709	869	10%	1609	0.43	0.015	15962	896	2%	15951		-7%								
MutL297G/MutL297E29A_R	0.54	0.017	200	22	0.51	0.002	14622	255	-8%	664	0.51	0.027	13319	589	-6%	13297		0%								
MutL118GR	0.46	0.012	264	21	0.57	0.012	6502	304	24%	308	0.69	0.009	5010	244	51%	4989		22%								
MutL118G/MutL297R	0.39	0.017	275	42	0.45	0.009	12061	399	16%	287	0.44	0.113	4404	463	15%	4362		-1%								
MutL118G/MutL282R	0.35	0.032	352	8	0.43	0.025	9417	287	22%	1133	0.63	0.030	4649	315	78%	4641		46%								
MutL218G/MutL118R	0.36	0.006	205	11	0.36	0.012	4159	55	1%	376	0.45	0.008	3256	238	26%	3245		25%								
MutL218G/MutL282R	0.58	0.017	223	30	0.71	0.061	22190	1236	23%	741	1.09	0.021	12129	634	88%	12099		53%								
MutL218G/MutL297R	0.53	0.045	147	19	0.67	0.025	26283	1391	27%	1356	1.15	0.023	17048	517	117%	17028		71%								
MutL297G/MutL282R	0.87	0.023	-149	51	0.93	0.011	18395	487	6%	356	1.52	0.008	13111	674	73%	13060		63%								
MutL4GR	0.23	0.012	378	31	0.31	0.006	8378	277	32%	270	0.61	0.014	5028	184	160%	4997		97%								
MutL297G/MutL4R	0.36	0.014	8	9	0.39	0.018	5720	130	7%	644	0.80	0.032	4475	242	121%	4466		106%								
MutL218G/MutL4R	0.35	0.011	366	46	0.32	0.004	7687	440	-8%	166	0.53	0.014	4746	236	51%	4700		64%								
NTD - CTD																										
MutL452G/MutL297R	0.45	0.020	43	11	0.41	0.008	19805	862	-9%	1845	0.66	0.027	11465	798	47%	11455		61%								
MutL452G/MutL118R	0.36	0.005	209	20	0.49	0.030	6214	35	35%	311	0.61	0.011	5528	430	71%	5508		27%								
MutL452G/MutL282R	0.46	0.009	231	23	0.54	0.010	16171	126	19%	606	0.80	0.010	9410	295	76%	9383		48%								
MutL218G/MutL452R	0.31	0.004	43	22	0.43	0.006	9364	144	40%	417	0.70	0.009	9508	298	128%	9485		62%								

Table 1. The relative changes of Efa and Corrected BR FRET of different MutL heterodimer at different conditions.

Rel., Cor. and SE are representing relative, corrected and standard error.

B Rel. change to B was calculated with formula $Rel. changes \% = \left(\frac{B-A}{A} \right) 100\%$

Efa and Cor.BR are collected from Figure 1.7 to Figure 1.11 and Appendix Figure 1.

2. MutL conformational changes on mismatch-containing, end blocked GT59DF DNA, and buffer effect on MutL conformational changes

2.1, Effect of different length of oligo's DNA with the same number of GT mismatch

As we described in the above part, the extra EfA over the subunit exchange is owing to the multiple loading of MutL on GT932 circular DNA and MutL conformational changes. At this part, we tested the effect of different length of mismatch-containing Oligos with the four-fold concentration of Fab-fragments blocking at their ends on MutL conformational changes. We could observe that the different types of DNA did not affect the EfA increased rate, but the amplitude of the kinetics (Figure 2.1 A). The down phase for the corrected BR FRET is observed for GT59DF DNA and GT100DF DNA rather than the GT932 mismatch-containing circular DNA (Figure 2.1 B). Because of the 100 nM GT59DF DNA GT100DF DNA containing 100 G: T mismatches, while 10 nM GT932 DNA only containing 10 G: T mismatches, so the loading of MutL on GT932 DNA is much slower than the DNA of GT59DF/GT100DF (Figure 2.1 B). And no conformational changes induced down phase observed (Figure 2.1 B). Except that no EfA and corrected BR FRET increasing observed without using the Fab-fragment blocked at the end of the GT100D DNA (Figure 2.1 A and B orange).

To prevent the multiple loading of MutL, we lower the concentration of MutL297_AF488AF594 hetero-dimer to 20 nM (10 nM dimers) while keeping the concentration of DNA, ATP, and MutS no change. Then we could observe that the EfA of GT932 DNA is much higher than the end blocked 100 nM GT100DF DNA (Figure 2.1 C olive), while the MutL loading rate (the corrected BR FRET) is still slow and no down phase observed for GT932 DNA, when GT100DF DNA decreased without loading kinetics observed in TECAN's dead-time ~15s (Figure 2.1 D blue and orange). Loading 20 nM MutL297_AF488AF594 on 100 nM GT100DF DNA is much faster than 10 nM GT932 DNA (Figure 2.1 D). Moreover, loading 20 nM MutL297_AF488AF594 on 100 nM GT100DF DNA is much faster than loading 200 nM MutL297_AF488AF594 on 100 nM GT100DF DNA (Figure 2.1 B and D) as well. From Figure 2.1 C and D, we could find that no big difference of the EfA and the corrected BR FRET for using wtMutS or using MutS449/D835R observed on 100 nM end-blocked GT100DF DNA in the presence of 2 mM ATP. However, we could observe that the corrected BR FRET of 200 nM MutL297_AF488AF594 hetero-dimers to the open-end GT100D DNA with wtMutS (Figure 2.1 E and F green) is 3 fold higher than with MutS449/D835R in the presence of 2 mM ATP (Figure 2.1 E and F). That may be because the

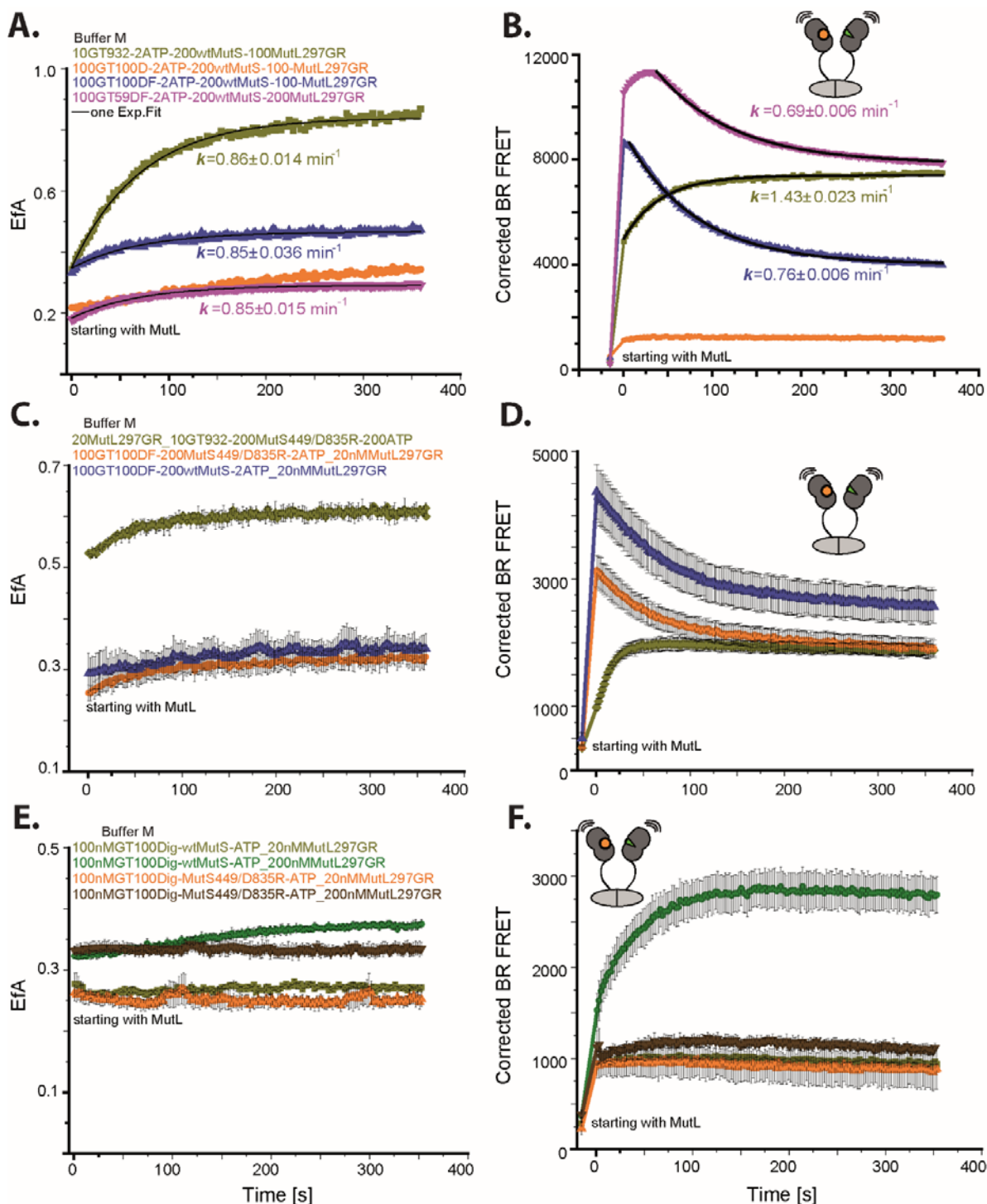


Figure 2.1 MutL-MutL interaction with different type of GT containing DNA and different concentration of AF488 (G) and AF594 (R) labeled MutL297 (A and B) added 100/200 nM MutL297_AF488AF594 hetero-dimer to pre-incubated 200 nM MutS449/D835R and 2 mM ATP with 10 nM GT932 or 100 nM GT100DF DNA/GT59DF DNA in buffer M; (C and D) mixed 20 nM MutL297_AF488AF594 hetero-dimers to pre-incubated 200 nM MutS449/D835R and 2 mM ATP with 10 nM GT932 DNA or 100 nM GT100DF DNA in buffer M; (E and F) added 20/200 nM MutL297_AF488AF594 hetero-dimers to pre-incubated 200 nM wtMutS/MutS449/D835R and 2 mM ATP with 100 nM GT100DF DNA in buffer M.

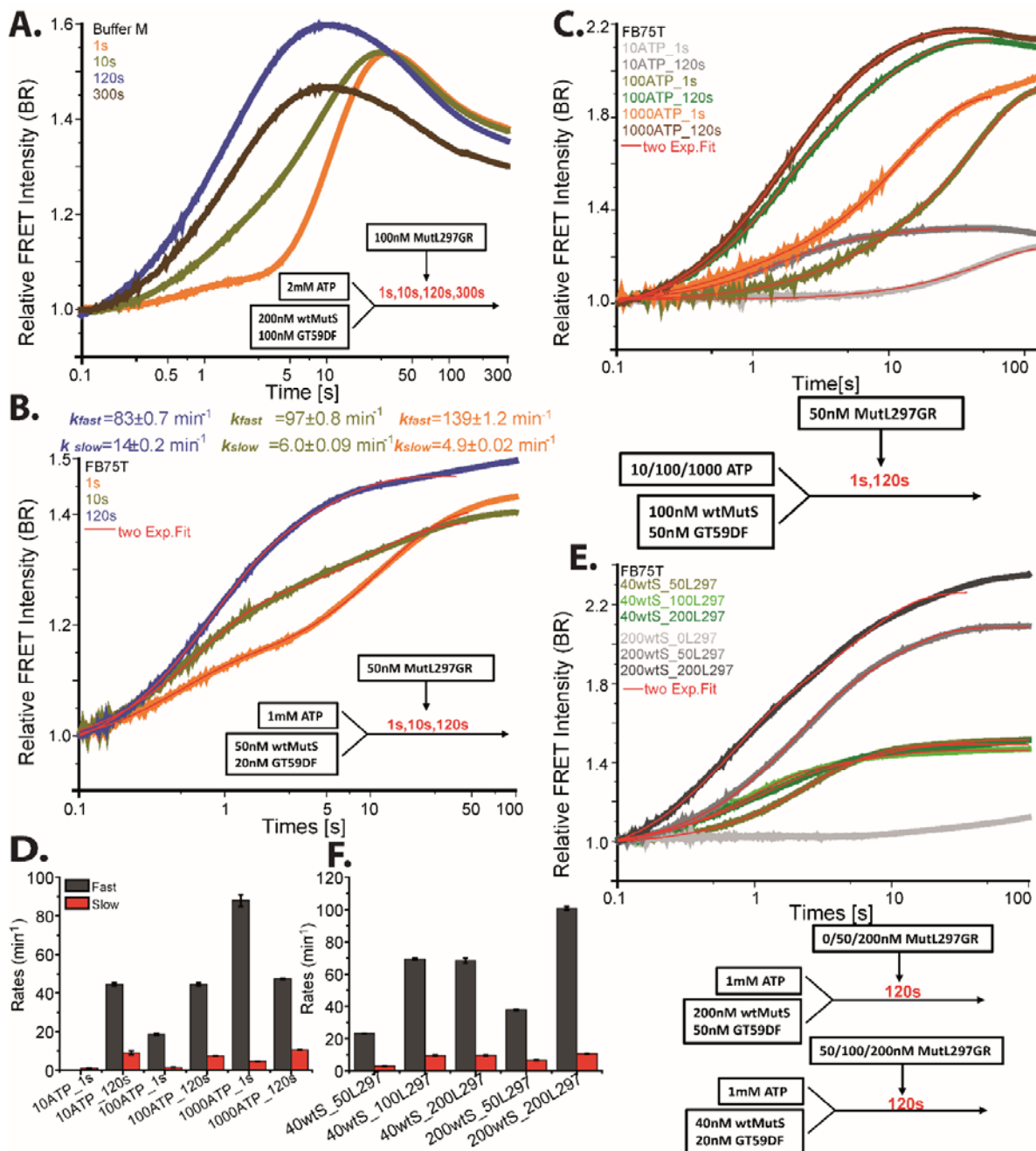


Figure 2.2 The maturation of wtMutS on DNA effect MutL recruitment on DNA in the different buffer. (A) Using Stopped-flow double mixing mode varied the aged time for pre-incubated 2 mM ATP with 100 nM GT59DF DNA and 200 nM wtMutS from 1 to 300 s, then encountered with 100 nM MutL297_AF488AF594 hetero-dimers in buffer M; (B) Using Stopped-flow double mixing mode varied the aged time for pre-incubated 0.01-1 mM ATP with 50 nM GT59DF DNA and 100 nM wtMutS for 1 or 120 s, then encountered with 50 nM MutL297_AF488AF594 hetero-dimer in FB75T buffer; (C) Using Stopped-flow double mixing mode varied the aged time for pre-incubated 1 mM ATP with 20 nM GT59DF DNA and 50 nM wtMutS from 1 to 200 s, then mixed with 50 nM MutL297_AF488 AF594 hetero-dimer in the FB75T buffer; (D) the fast and slow rates derived from double exponential fit of the kinetics from C; (E) Using Stopped-flow dual mixing mode with varied the aged time for pre-incubated 1 mM ATP, 20 or 50 nM GT59DF DNA, and 40 or 200 nM wtMutS for 120 s, then mixed with 0-200 nM MutL297_AF488AF594 hetero-dimers in FB75T buffer; (F) The fast and slow rates derived from double exponential fit of the kinetics from E. All the mixing ratios are 1:1.

wtMutS with the ability (Figure 2.1 E and F, brown) of forming tetramer (instead of dimeric MutS449/D835R) which could stabilize MutS dimers on the open end GT100D DNA in the presence of high concentration rather than the low concentration of MutL.

2.2, The maturation of wtMutS on GT59DF DNA generating delay for loading MutL on GT59DF DNA

As described above, the quantity of MutS on DNA could cause a 30 s delay for loading MutL on DNA, plus pre-incubated MutS with GT932 DNA and 10 μ M ATP could induce MutL loading on DNA and the EfA of MutL increasing much faster. Therefore, we tested different pre-incubation time for wtMutS and GT59DF DNA with 2 mM ATP for loading MutL297_AF488AF594 on GT59DF DNA in different buffers assessed by stopped-flow (with 2 ms dead time). When incubating 200 nM wtMutS and 100 nM GT59DF DNA with 2 mM ATP with 1:1 ratio for 1 s, 10 s, and 120 s, then mixed with 100 nM MutL297_AF488AF594 with 1:1 ratio in buffer M, MutL297_AF488AF594 hetero-dimers were loaded faster when the incubation time is longer (Figure 2.2 A). And ~ 3 s' delay observed with 1s incubation time (Figure 2.2 A).

When incubated 200 nM wtMutS and 100 nM GT59DF DNA with 2 mM ATP (1:1 ratio) for 300 s (Figure 2.2 A, brown), we could observe that MutL loaded slower as well than pre-incubated for 120 s (Figure 2.2 A blue). That because after 300 s pre-incubation time, the concentration of ADP (KD of MutS to ADP ~ 0.6 μ M (Lebbink, Fish, et al. 2010)) increased from MutS hydrolysis ATP (7.4 min^{-1} (Lamers, Georgijevic, et al. 2004)). That's consistent with Figure 1.7 (C and D) and Figure 9 (A and B) in Chapter 2 as well. After that, we varied the incubation time for 50 nM wtMutS with 20 nM GT59DF DNA and 1 mM ATP (1:1 ratio) for 1 s, 10 s, and 120 s in FB75T buffer. The data displayed that the different incubation time affect both the first and the second steps of loading MutL on DNA rather than the first phase (1 s: 139 ± 1.2 min^{-1} and 4.9 ± 0.02 min^{-1} ; 10 s: 97 ± 0.8 min^{-1} and 6.0 ± 0.09 min^{-1} ; 120 s: 83 ± 0.7 min^{-1} and 14 ± 0.7 min^{-1}) (Figure 2.2 B). Compared the graphs in buffer M and FB75T buffer, we could find that MutL on GT59DF DNA is more stable in FB75T buffer (Figure 2.2 A and B).

Then we varied the ATP concentration from 10 μ M to 1 mM for 1 s or 120 s' pre-incubation time with 100 nM wtMutS and 50 nM GT59DF DNA before mixing with 50 nM MutL297_AF488AF594 (with 1:1 ratio) in FB75T buffer (Figure 2.2 C). The amplitudes of the relative change for loading 50 nM MutL297_AF488AF594 is positive correlated with ATP concentration (Figure 2.2 C). The fast and slow rates for loading MutL on GT59DF DNA are similar for the different concentration of ATP, while the fast and slow binding rates are both faster with higher

concentration of ATP when with 1 s' pre-incubation time and analyze the kinetics of MutL loading on DNA with double exponential fit (Figure 2.2 D). Then we investigated that using low and high concentrations of wtMutS-GT59DF DNA complex incubated with 1 mM ATP for 120 s' pre-incubation time (with 1:1 ratio) to load 50-200 nM MutL297_AF488AF594 hetero-dimers on GT59DF DNA. From the kinetics (colored olive, green and dark green) in Figure 2.2 E, we could observe that kinetics of loading 25, 50 and 100 nM MutL297_AF488AF594 on DNA share the same relative amplitudes but the different loading rates which depending on the concentrations of MutL in the presence of 5 nM-GT59DF DNA and 10 nM wtMutS.

However, the amplitudes and loading rates of the kinetics were increased ~2 fold when using 200 nM wtMutS and 50 nM GT59DF DNA incubated with 1 mM ATP (50 nM wtMutS, 12.5 nM GT59DF DNA and 0.25 mM ATP for final) for 120 s, then loaded 50 nM MutL297_AF488- AF594 (25 nM for final concentration) on GT59DF DNA (Figure 2.2 E and F). In addition, both the amplitudes and rates of the loading kinetics are increased followed the increased concentration of MutL297_AF488AF594 after adding the pre-incubated 120 s of 200 nM wtMutS

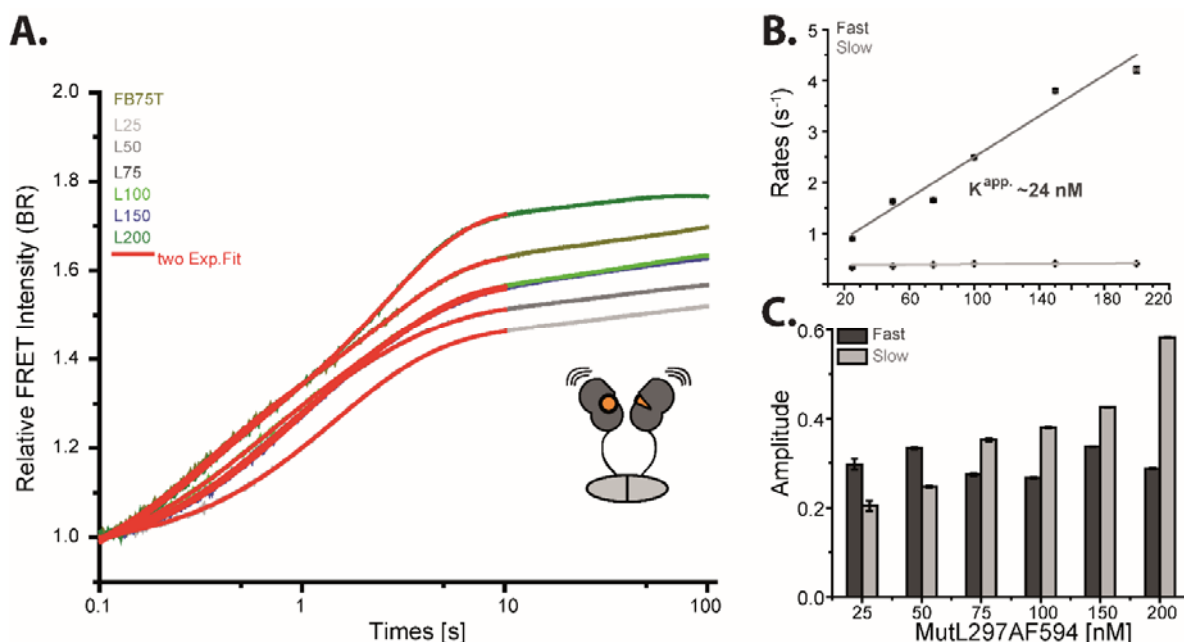


Figure 2.3 The KD value for recruiting MutL297_AF594 on DNA assessed with Stopped-flow. (A) Stopped-flow double mixing mode with the aged time for pre-incubated 1 mM ATP with 20 nM GT59DF DNA-40 nM wtMutS for 120 s, then injected 50-400 nM MutL297_AF594 hetero-dimers to start loaded MutL on DNA in FB75T buffer; all the mixing ratio are 1:1; (B) The fast and slow rates derived from two exponential fits of the kinetics of A; (C) The amplitudes obtained from two exponential fits analyzed the kinetics from A.

and 50 nM GT59DF DNA with 1 mM ATP (50 nM wtMutS, 12.5 nM GT59DF DNA and 0.25 mM ATP for final) (Figure 2.2 E and F). Then we varied the concentration of MutL297_AF594 (the final concentration are 25-200 nM) to 10 nM GT59DF-20 nM wtMutS (final concentration)

incubated ~2 min with 0.5 mM ATP (Figure 2.3 A and B). From Figure 2.3 we could observe that the apparent K_D for MutL to GT59DF DNA is ~24 nM in FB75T buffer, which is twofold of the apparent K_D for MutL to GT59DF DNA in FB150T buffer (~50 nM, chapter 2 Figure 7 C and D).

2.3, MutL conformational changes in GT59DF DNA

From the above description, we know that the quantity and maturation of wtMutS on DNA could generate 2-3 s' delay time for loading MutL on G: T mismatch-containing GT59DF DNA, and generate 30 s' delay time for multiple loading MutL on 2-5 nM GT932 circular DNA (part 1 Figures). As well we proofed the multiple loading of MutL at the previous Figures, the EfA still much higher of Mutl297_GR with 10 nM GT932DNA than with the end-blocked GT100DF DNA/GT59DF DNA after lower the concentration of MutL297_AF488AF594 to 20 nM (which is 10 nM dimers) (Figure 2.1 C and D). Therefore, we play around the different orders and different combinations of 100 nM GT59DF DNA, 2 mM ATP and 200 nM wtMutS with 200 nM MutL297_AF488AF594 or ATP binding deficient mutant MutL297N33A_AF488AF594 to specify MutL conformational changes on GT59DF DNA.

When we mixed 200 nM MutL297_AF488AF594-100 nM GT59DF DNA-0.5 mM ATP with 200 nM wtMutS-0.5 mM ATP (with 1:1 ratio) in the FB75T buffer, data shown that the kinetics (light grey) goes down firstly near the 3 s, then heading up after 4 s and over the starting value and 10 % relative change over the starting value (Figure 2.4 A grey). However when using 200 nM MutL297_AF488AF594 incubated with 1 mM ATP encountered 200 nM wtMutS incubating with 100 nM GT59DF DNA (with 1:1 ratio) in the FB75T buffer, the down phase appears earlier around 1 s then the kinetics increased 13 % over the starting value (Figure 2.4 A orange). We could observe that the kinetics is heading down much earlier within 0.2 s then increased back to the starting value (Figure 2.4 A dark grey) when mixed 200 nM MutL297_AF488AF594 with 0.5 mM ATP in the presence of 200 nM wtMutS-0.5 mM ATP-100 nM GT59DF DNA complexes (with 1:1 ratio) in FB75T buffer. The kinetics is repeatable when we used 200 nM MutL297_At390AF488 heterodimer with 0.5 mM ATP added to 200 nM wtMutS-0.5 mM ATP-100 nM GT59DF DNA complexes (with 1:1 ratio) in FB75T buffer, but the amplitude of the second phase is smaller (Figure 2.4 C light grey). Besides the anisotropy of MutL297_At390 incubating with 1 mM ATP increased after encountering wtMutS-ATP-GT59DF DNA complexes in FB75T (Figure 2.4 D).

While, when used the same procedures with 200 nM MutL297N33A_AF488 AF594 (ATP binding deficient) in the absence or presence of ATP incubated with 200 nM wtMutS-100 nM GT59DF DNA complexes (with 1:1 ratio) in FB75T buffer, the down phase appears within 0.2 s and 1 s as

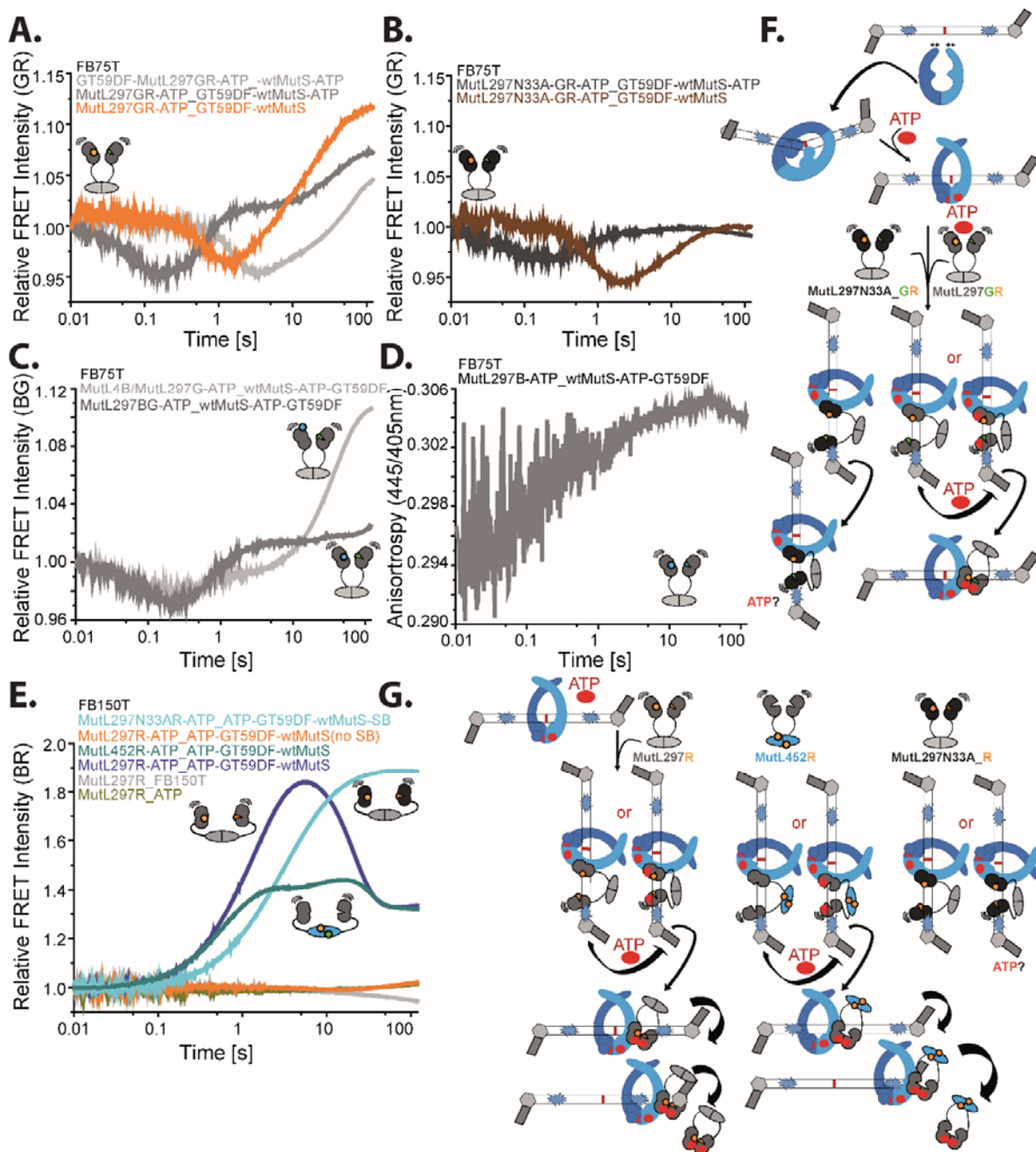


Figure 2.4 Stopped-flow monitor MutL-MutL interaction on GT59DF DNA (A) Mixing 1 mM ATP, 100 nM GT59DF DNA and 200 nM wtMutS, and with 200 nM MutL297_AF488AF594 hetero-dimer to observe MutL subunit inter-action on DNA in FB75T buffer; (B) Mixing 1 mM ATP, 100 nM GT59DF DNA and 200 nM wtMutS, and with MutL297N33A_AF488AF594 hetero-dimers in different orders to observe MutL-MutL interaction on DNA in FB75T buffer; (C) Mixing 1 mM ATP-50 nM GT59DF DNA-100 nM wtMutS, with 100 nM MutL297_AF488AF594 hetero-dimers to observe MutL-MutL interaction on DNA in FB75T buffer; (D) the anisotropy changes of 100 nM MutL297_AF488AF594 hetero-dimers encountered with 1 mM ATP-50 nM GT59DF DNA-100 nM wtMutS in FB75T buffer; (E) recruitment of 100/200 nM AF594 labeled different MutL mutants incubate with 0.5 mM ATP by pre-incubated 0.5 mM ATP-100 nM GT59DF DNA-200 nM wtMutS on DNA in FB75T buffer; all the mixing ratio are 1:1; (F) cartoons depiction of MutL297_GR or MutL297N33A_GR (ATP binding deficient) mutants conformational changes on GT59DF DNA; (G) AF594 (R) labeled MutL mutants interaction with SB stained GT59DF DNA of E.

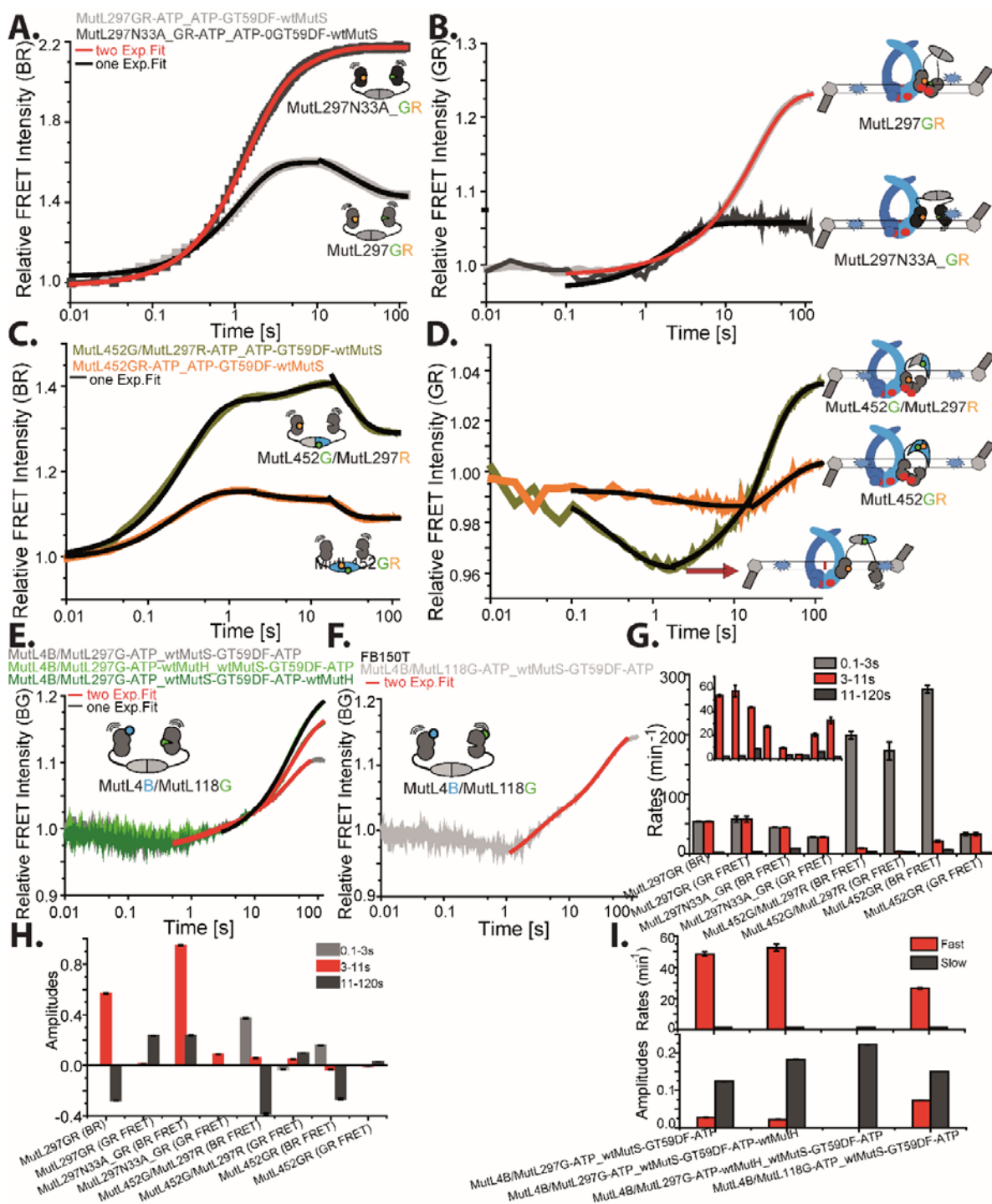


Figure 2.5 MutL conformational changes on GT59DF DNA assessed with Stopped-flow in FB150T (A and B) Mixed pre-incubated 0.5 mM ATP-100 nM GT59DF DNA-200 nM wtMutS, with 200 nM preformed MutL297_AF488AF594 or MutL297N33A_AF488AF594 hetero-dimers; (C and D) Mixing pre-incubated 0.5 mM ATP-100 nM GT59DF DNA-200 nM wtMutS, with 200 nM preformed MutL452_AF488/MutL297_AF594 or MutL452_AF488 AF594 hetero-dimers; (E) Mixed pre-incubated 0.5 mM ATP-50 nM GT59DF DNA-100 nM wtMutS in the absence/presence of 100 nM wtMutH with 100 nM preformed MutL4_At390/ MutL297_AF488 hetero-dimers in the absence/presence of 100 nM wtMutH; (F) Mixed pre-incubated 0.5 mM ATP-50 nM GT59DF DNA-100 nM wtMutS, with 100 nM preformed MutL4_At390/MutL118_AF488 hetero-dimers; (G-H) The rates and amplitudes derived from A-D; (I) The rates and amplitudes derived from E-F.

well, then only back to the starting value (Figure 2.4 B brown). From Figure 2.4 A and B, we could find that MutL start to open upon loading on GT59DF DNA by wtMutS in FB75T buffer, then undergoes conformational changes owing to binding and hydrolysis ATP which cannot observe from MutL297N33A (ATP binding deficient mutant). From Figure 2.3, we could observe that MutL297_AF594 was loaded on GT59DF DNA in 10 s and no down phase appears in FB75T. Otherwise, MutL297_AF594 loaded by wtMutS on GT59DF DNA in 10 s, then goes down and reach the saturation within 100 s in FB150T buffer (Figure 2.4 E blue). While kinetics of MutL297N33A_AF594 heading up slower than MutL297_AF594, but no down phase appears (Figure 2.4 E cyan). Moreover, when loaded MutL452_AF488AF594 hetero-dimers on GT59DF DNA, kinetics with bi-phases were observed before the down phase seems in FB150T buffer (Figure 2.4 E dark cyan).

Therefore, 200 nM NTD-NTD labeled hetero-dimers (MutL297_AF488AF594 or MutL297N33A_AF488AF594) in the presence of 0.5 mM ATP mixed together with 200 nM wtMutS-100 nM GT59DF DNA-0.5 mM ATP complexes (with 1:1 ratio) in FB150T buffer to monitor MutL loading on DNA and conformational changes in real-time. Similarly, as we described in Figure 2.4 E, DNA binding kinetics of MutL297_AF488AF594 reached the saturation within 10 s ($61.4 \pm 0.43 \text{ min}^{-1}$), then goes down ($2.4 \pm 0.01 \text{ min}^{-1}$) to reach the new saturation in 100 s (Figure 2.5 A grey and G). While kinetics of loading MutL297N33A_AF488AF594 on GT59DF DNA fit to two exponential fits ($43.7 \pm 0.26 \text{ min}^{-1}$ with 0.9 amplitude, and $8.4 \pm 0.43 \text{ min}^{-1}$ with ~ 0.3 amplitude), which in the absence of the down phase (Figure 2.5 A, G and H). Whereas the MutL297_AF488AF594 undergoes conformational changes induced by binding and hydrolysis ATP, the relative GR FRET (MutL-MutL FRET) increased 25 %, while only around 7 % for the relative GR FRET of MutL297N33A_AF488AF594 hetero-dimers (Figure 2.5 A and H). Except that, no down phase observed in GR FRET upon MutL297_AF488AF594 or MutL297N33A_AF488AF594 loaded on GT59DF DNA by wtMutS in FB150T buffer (Figure 2.5 A and B). Moreover, At390 labeled MutL4 with AF488 labeled MutL297 or MutL118 to form 200 nM MutL4_At390/MutL297_AF488 and MutL4_At390/MutL118_AF488 hetero-dimers to test MutL conformational changes on GT59DF DNA in the absence or presence of 100 nM wtMutH in FB150T buffer. Kinetics are showing that MutL4_At390/MutL297_AF488 and MutL4_At390/MutL118_AF488 hetero-dimers undergo conformational changes with rates of $40 \pm 1.5 \text{ min}^{-1}$ / $1.7 \pm 0.02 \text{ min}^{-1}$ and $26 \pm 0.5 \text{ min}^{-1}$ / $1.7 \pm 0.02 \text{ min}^{-1}$, while these two types of hetero-dimers share the similar relative changes of the BG FRET which reflect the MutL conformational changes (Figure 2.5 E grey and F light grey).

However, the amplitudes of the slow phases are increased for both incubated MutL4_At390/MutL297_AF488 hetero-dimers with ATP and 100 nM wtMutH first then mixed with wtMutS-GT59DF DNA-ATP (Figure 2.5 E light green), as well as it encountered 100 nM wtMutH with wtMutS-GT59DF DNA-ATP together (Figure 2.5 E dark green).

Finally, 200 nM MutL452_AF488AF594 or MutL452_AF488/MutL297_AF594 hetero-dimers incubated with 0.5 mM ATP have been loaded by 200 nM wtMutS on 100 nM GT59DF DNA in the presence of 0.5 mM ATP in FB150T buffer as well (Figure 2.5 C and D). As the graph shown, the CTD-CTD labeled hetero-dimer MutL452_AF488AF594 were loaded on GT59DF DNA with two phases increased kinetics (Figure 2.5 C orange). Then the kinetic heading down and reach the saturation in 100 s in FB150T buffer (Figure 2.5 C orange). Moreover, the GR FRET processed down phase in 1s, then exhibit $\sim 2\%$ relative increase over the starting value after 1 s with the rate of $1.6 \pm 0.02 \text{ min}^{-1}$ (Figure 2.5 C orange, G and H). Besides, the NTD-CTD labeled hetero-dimer MutL452_AF488 /MutL297_AF594 loaded on GT59DF DNA with clearly two phases kinetics as well (Figure 2.5 D olive). While the second phase goes down instead of continuously increased like MutL452_AF488AF594 hetero-dimers kinetics within 30 s, and then continuously goes down and reach new saturation in 100 s (Figure 2.5 D olive). The GR FRET only exhibits $\sim 4\%$ relative increase after 10 s with the rate of $1.9 \pm 0.23 \text{ min}^{-1}$ (Figure 2.5 D olive, G and H).

2.4, Salt effect on MutL conformational changes in GT59DF DNA

As described above, we could know that MutL297_AF488AF594 behaves differently in buffer FB75T and FB150T for both the BR (MutL to DNA) and GR (MutL to MutL) FRET. So in this part, we discuss that the salt effect to load MutL on GT59DF DNA and MutL conformational changes. In FB75T buffer, MutL only weakly bind GT932 DNA or Lambda DNA in the absence of ATP (Figure 2.6 A and B). More MutL loaded on DNA after adding 2 mM ATP, while both the corrected BR FRET and the EfA dramatically decrease after titrating KCl (Figure 2.6 A and B). The EfA of MutL even lower than the starting value indicated that MutL conformations stay more closed in the lower salt buffer, while more opened in the high salt buffer (Figure 2.6 A).

Moreover, this opinion supported by MutL GR FRET kinetics firstly heading down in FB75T buffer upon loaded by wtMutS on GT59DF DNA (Figure 2.4 A, B and C) which cannot observe in FB150T buffer (Figure 2.5). Whereas, Lambda DNA and ATP seems not affect the EfA (FRET efficiency) of MutL297_AF488AF594 or MutL297N33A_AF488AF594 or MutL452_AF488-AF594 hetero-dimers in FB90T buffer, while after adding 60 mM KCl induced MutL NTD-CTD FRET efficiency (EfA) slightly lower than starting value (Figure 2.6 C).

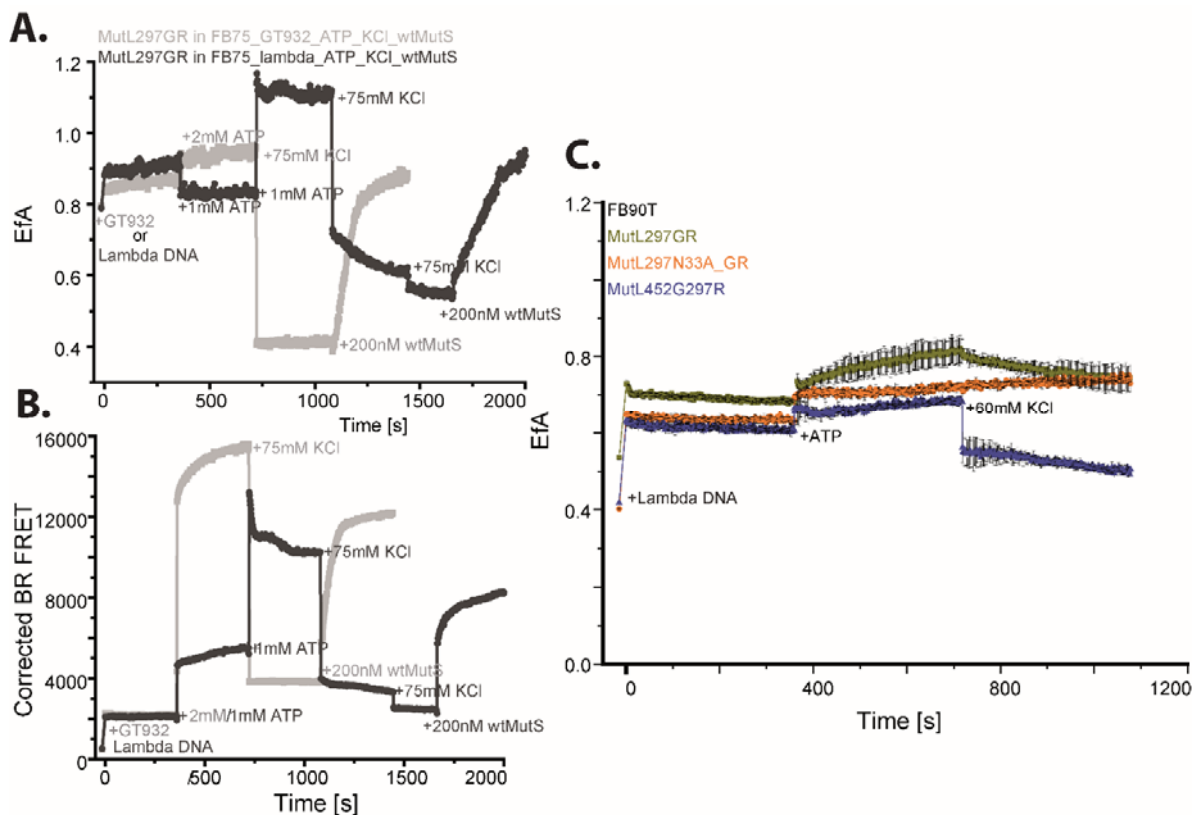


Figure 2.6 Kinetics of ionic strength effect on MutL subunit and MutL/DNA interaction (A and B) Sequentially added lambda DNA/10 nM GT932 DNA, 1/2 mM ATP, 75 mM KCl and 200 nM wtMutS (2.4 nM GT932 DNA to lambda DNA at the end) to 200 nM MutL297_AF488AF594 preformed hetero-dimers, to observe how each component effect MutL-MutL interaction and MutL/DNA interaction in different ionic strength FB buffer; (C) the reaction started with adding 20 μ l 0.3 μ g/ μ l lambda DNA to 200 nM MutL297_AF488AF594 or MutL297N33A_AF488AF594 or MutL452_AF488/MutL297_AF594 preformed hetero-dimers, then added 2 mM ATP and KCl.

Stopped-flow measurement shown that the ionic strength (K^+ and Mg^{2+}) significantly affect both the BR FRET and the GR FRET. In lower ionic strength like FB75T-2.5 Mg^{2+} (75 mM KCl, 2.5 mM Mg^{2+}) and FB75T-5 Mg^{2+} (75 mM KCl, 5 mM Mg^{2+}), kinetics of MutL binding DNA are more complicated and fit to three exponential fits (Figure 2.7 A, grey and olive). Except with the high relative amplitudes, the first binding rates are very fast while decrease (5 fold) dramatically by only doubled the concentration of Mg^{2+} (Figure 2.7 A and B, grey and olive). Whereas, the GR FRET decreased at the beginning, then increased in a biphasic and no difference observed by doubled the concentration of Mg^{2+} in these two buffers (Figure 2.7 C and D, grey and olive) After increasing KCl's concentration to 90 mM and 125 mM and in the presence of 5 mM Mg^{2+} for both, or even to 150 mM KCl with 2.5 mM Mg^{2+} , we could observe that the DNA binding kinetics fit two exponential fits (Figure 2.7 A, orange, blue and green). All kinetics of MutL bind to DNA in these three buffers are sharing the similar binding rates (Figure 2.7 B), while the relative amplitude of FB125T-5 Mg^{2+} lower than FB90T-5 Mg^{2+} and FB150T-2.5 Mg^{2+} which are similar (Figure 2.7 A

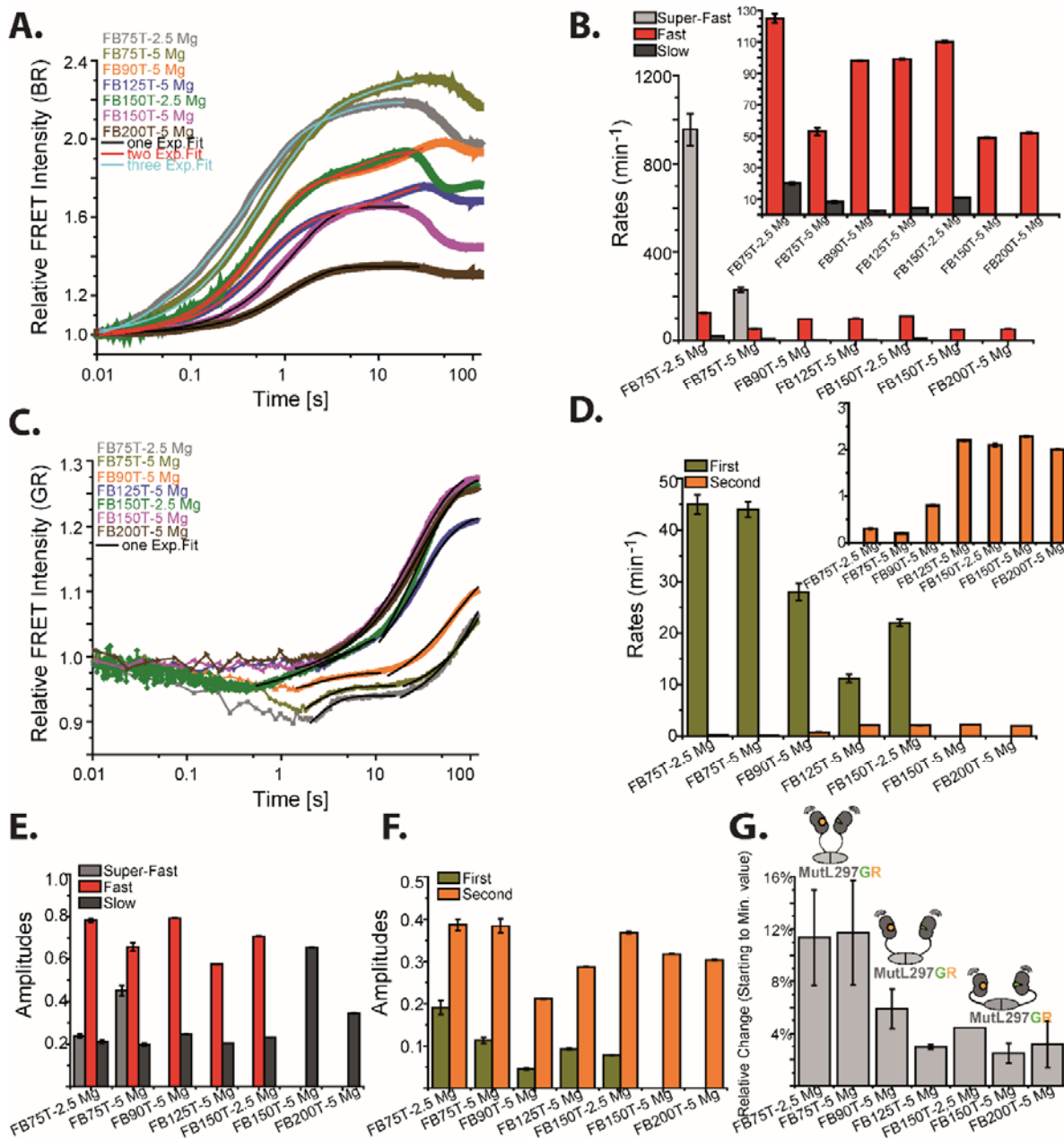


Figure 2.7 Kinetics of different K^+ and Mg^{2+} effect on MutL subunit and MutL/DNA interaction assessed with Stopped-flow. (A) Relative BR FRET (MutL297_GR to GT59DF DNA) of mixing pre-incubated 0.5 mM ATP-100 nM GT59DF DNA-200 nM wtMutS with 200 nM preformed MutL297_AF488AF594 hetero-dimers in FB buffer with the different concentration of K^+ and Mg^{2+} ; (B) the rates derived from one, two and three exponential fits of the kinetics of A; (C) Relative GR FRET under the same conditions as A; (D) The rates derived from single exponential fits kinetics of B; (E and F) The amplitudes of different phases of kinetics in A. and C; (G) The relative changes of MutL297_GR hetero-dimers at the starting point upon GT59DF DNA binding conditions (~ 1 s) DNA in FB buffers with different concentration of K^+ and Mg^{2+} .

(orange, blue and green), B and E). Similarly, the fast rates of the MutL conformational changes kinetics in FB90T-5 Mg^{2+} and FB150T-2.5 Mg^{2+} buffers are similar ~ 28 min⁻¹ which are faster than ~ 13 min⁻¹ in FB90T-5 Mg^{2+} buffer (Figure 2.7 D, olive). However, the relative GR FRET are

decreased in the following order: FB150T-2.5 Mg²⁺ > FB125T-5 Mg²⁺ > FB90T-5 Mg²⁺ (Figure 2.7 C, green, blue and orange). When the ionic strength of buffer increased to FB150T-5 Mg²⁺ and FB200T-5 Mg²⁺, the DNA binding kinetics only fit to signal exponential fits, and the loading rate is around 50 min⁻¹ for both (Figure 2.7 A and B, purple and brown). While the relative amplitudes of the GR FRET in FB150T-5 Mg²⁺ buffer is two-fold of the relative amplitude of the GR FRET in buffer FB200T-5 Mg²⁺ (Figure 2.7 C, D, and F).

Nevertheless, the GR FRET kinetics in these two buffers are share the similar relative amplitudes and slow conformational changes rates, even the fast rates in buffer FB150T-5 Mg²⁺ is much quicker than in the buff FB200T-5 Mg²⁺ (Figure 2.7 C, D, and F). Besides, we find that MutL stay in more closed conformations in the lower ionic strength buffers, while adopted in more open conformations in the higher ionic strength buffers (Figure 2.7 C and G). Eventually, except ionic strength, the pH of the buffer significantly affect the GR FRET kinetics' relative amplitude and fast phases of MutL conformational changes (Appendix Figure 3.4 A). While no dramatic changes of the relative GR FRET were observed under different concentration of Tween 20 buffers, and under the different temperatures (Appendix Figure 3.4 C-D).

Discussion

Recently, MutS is in the sliding clamp within the complex of MutS/MutL with the method of co-crystallization combined site-specifically crosslinking (Groothuizen, Winkler, et al. 2015). A new MutS-MutL interface generated by crossed MutS subunit pushed DNA down to the new channel which induced the connector domain reoriented (Groothuizen, Winkler et al. 2015); *Thermus aquaticus* MutS loaded more MutL on mismatch-containing DNA, and MutL stabilized MutS at DNA mismatch during MutS recognized mismatch to MutS convert to sliding clamp (Qiu, Sakato et al. 2015); except for MutS-MutL long-lived complex, MutL DNA clamp that oscillates between the principal MutS-MutL complex could activate MutH endonuclease as well (Liu, Hanne et al. 2016). All these literature more focused on MutS-MutL complexes formation, the effect of these complexes formation on MutS conformational changes, multiple loading MutS-MutL complexes, and activation of MutH endonuclease activity. While no information about MutL conformational changes during complexes formation, even though ATP binding could dimerize MutL NTD ATPase domain (Ban and Yang 1998, Ban, Junop, et al. 1999) have published almost 20 years ago. Here, in this chapter, we show that MutL undergoes a series of conformational changes between loaded on mismatch-containing DNA by MutS and active MutH endonuclease activity.

In the presence of MutS, ATP and circular GT932 DNA, we could observe that the increased FRET efficiency (EfA) over subunit exchange appear due to multiple loading of MutL on circular GT932 DNA (Figure 1.1 and Figure 1.2). However, this extra FRET efficiency (EfA) was not observed with 10 μ M ATP until titrated 2 mM ATP, even though the BR FRET (MutL to DNA FRET) is higher with lower ATP than with the higher ATP (2 mM) for the most MutL combinations except for MutL452_GR and MutL218_G/MutL452_R hetero-dimers (Figure 1.13 and Table 1). The BR FRET reach the similar level for both low (10 μ M) and high (2 mM) ATP when the concentration of MutL297_AF488AF594 reach to 600 nM (Figure 1.3 E and F). Therefore the extra MutL GR FRET efficiency (EfA) of MutL is due to the inter- and intra- MutL dimer interaction after multiple loading of MutL on GT932 DNA combined with MutL conformational changes. Additionally, added thrombin to MutL hetero-dimers caused the EfA of MutL297_AF488AF594 back to the starting value, while only down to the subunit exchange level in the presence of MutS, ATP and mismatch-containing circular GT932 DNA. While the EfA of MutL297_AF488AF594 back to the starting value in the absence of MutS, ATP and circular GT932 DNA. And the EfA of MutL452_AF488/MutL297_AF594 NTD-CTD hetero- dimers back to the starting value after adding thrombin in the absence or presence of MutS, ATP and circular GT932 DNA (Figure 1.1, D and E). The left EfA of MutL297_AF488AF594 in the presence of MutS, ATP and circular GT932 DNA after thrombin is owing to MutS still interact with NTD and form the interaction between MutS-NTD and MutS-NTD. That phenomenon supported by the FRET between donor labeled MutL NTD and acceptor labeled MutS even higher than the FRET between donor labeled MutL CTD and acceptor labeled MutS after adding MutL competitor (Marx 2013) as well.

Then, we investigated the different combination of MutL NTD-NTD, NTD-CTD, CTD-CTD to observe the EfA changes and MutL to SB stained GT932 G: T mismatch-containing circular DNA FRET (BR FRET) at low (10 μ M) and high (2 mM) ATP (Figure 1.7, Figure 1.11, and Figure 1.13). From Table 1 and Figure 1.13 we could find that added 2 mM ATP to low ATP system in the presence of MutS and GT932 DNA, the BR FRET immediately decreased for most combinations of MutL hetero-dimers while the BR FRET of MutL452_AF488AF594, MutL218_AF488/MutL452_AF594, and MutL297_G/MutL297N33A_R increased. Otherwise, Table 1 and Figure 1.13 indicated that low concentration of ATP was not sufficient to induce the top part of MutL NTD domains and MutL CTD domains conformational changes. While loading MutL on G: T mismatch-containing DNA caused part of MutL NTD domains (including the fives disordered loops (Ban and Yang 1998)) changing and MutL NTD (except 297) to CTD distance decreased

which means that the EfA increased. Especially for MutL452_G/MutL118_R hetero-dimers which EfA increased 64 %. After titrating 2 mM ATP, the EfA of all combinations of MutL hetero-dimers are increased notably, even for the combinations which EfA stay no change at low ATP. However, neither low ATP nor high ATP induced the EfA of MutL297N33A_GR (the ATP binding deficient mutant) and MutL297E29A_GR (ATP hydrolysis-deficient mutant) hetero-dimers increased (Table 1 and Appendix Figure 3.1). The EfA stay no change even for half wild-type hetero-dimer mutants (MutL297_G/ MutL297N33A_R, MutL297_G/MutL297E29A_R), even though all these hetero-dimers loaded on G: T mismatch-containing circular GT932 DNA as well (Table 1, Figure 1.13 and Appendix Figure 3.1). Hence, we find that MutL conformational changes start upon its loading on mismatch-containing DNA by MutS combined ATP induced MutL NTD ATPase domain dimerization and the whole MutL conformational changes.

We missed the information of MutL conformational changes upon bind DNA due to ~15-20 s dead time for TECAN instrument, so we change to use stopped-flow to assess MutL conformational changes during MutS-MutL complex formation. In FB75T buffer, multi-phases were observed for MutL297_AF488AF594 GR FRET (MutL-MutL). Upon MutL297_GR binding DNA, MutL structures immediately stay more open, then the EfA back to the starting value even for ATP binding-deficient mutants (MutL297N33A) in FB75T buffer (Figure 2.4 A and B). While the phase over the starting value only could observe with MutL297_AF488AF594 rather than MutL297N33A_AF488AF594 (Figure 2.4 A-C). Besides, two steps of binding kinetics observed for MutL297_AF594 loading on SB stained GT59DF DNA in FB75T buffer (Figure 2.3). Increasing the concentration of MutL297_AF594 accelerate the linearly increased of fast binding rates rather than the amplitudes which fluctuate around 0.3; however, the slow binding rates state the same while the amplitudes increased (Figure 2.3, B and C). Whereas, as we described in Chapter 2 Figures 7 (C and D), two steps binding kinetics of MutL297_AF594 loading on SB stained GT59DF DNA observed in FB150T buffer as well, and the first binding rates linearly increased as increased the concentration of MutL297_AF594 when the slow binding rates state no change after 75 nM. However, both amplitudes for fast and slow binding rates are similar and fluctuates around 0.3. Therefore, we could conclude that the rapid binding rate is the rates for MutS loading one NTD of MutL dimer on DNA with apparent affinity ~50 nM, and the slow rate is related to the second NTD of MutL dimer come close to DNA which shares the similar apparent affinity as the first coming NTD (chapter 2, Figure 7 C and D). Generated similar amplitudes could indicate that as the first coming NTD but the rates are not changing when MutL concentration over the

concentration of GT59DF DNA in FB 150T buffer. While in FB75T buffer, the fast binding rates are related to MutS loading one NTD of dimer on DNA as well which apparent affinity is around 24 nM (Figure 2.3). While the slow rates are associated with MutL associating on DNA itself in FB75T buffer, which consistent with the literature (Liu, Hanne, et al. 2016). That could explain the corrected BR FRET kinetics decreased after 10 s in FB150T buffer which not observed in FB75T buffer (Figure 2.3 and 2.4 E).

Another distinct difference in FB75T and FB150T buffer is that the GR FRET immediately goes down in FB75T buffer while that stay no change in FB150T buffer within 1 s for MutL297_GR (Figure 2.4 A B, and Figure 2.5 B). The amplitudes of these down phase becomes smaller as titration K^+ and Mg^{2+} into the buffer (Figure 2.7 C and G). The pH of all these buffers are 7.5, in which conditions MutL exists in dimer in all these buffers rather than oligomers (Niedziela-Majka, Maluf, et al. 2011). Therefore we could conclude that MutL adopted in more closed structures in low ionic strength buffers like FB75T, while exist in more opened conformations in higher ionic strength buffer such as FB150T. Except that, the amplitudes of the slow rates phase for the kinetics of MutL binding DNA (BR FRET) significantly decreased while the NTD conformational changes rates increased in the higher ionic strength buffer (FB150T) (Figure 2.7).

To avoid non-specific loading MutL on DNA, we assessed the NTD-NTD, NTD-CTD, and CTD-CTD labeled MutL hetero-dimers' conformational changes in FB150T buffer with stopped-flow (dead time is about 2 ms). We could find that the GR FRET of MutL NTD-CTD hetero-dimers starts at 0.1 s, and the kinetics decreased firstly upon binding DNA then heading up over the starting value (Figure 2.5 B and D). Whereas the GR FRET of MutL NTD-NTD labeled, hetero-dimers starts at 1 s and heading up directly instead of decreased (Figure 2.5 A and B). The final amplitude of the GR kinetics of MutL297_AF594AF488 is more than one fold higher than the GR FRET of MutL297N33A (ATP binding deficient mutant); however, the CTD-CTD GR FRET starts after 10 s when the processes of loading MutL on G: T mismatch-containing DNA are finished (Figure 2.5 B and D). As we know from the quaternary structure, the distance between MutL452 CTD within the dimer is 2.8 nm which means the GR FRET efficiency is around 1.0 that's supported by smFRET efficiency is 0.9 in chapter 1 Figure 2 C and Figure 4 J-L. Therefore, we speculated that the increased of the GR FRET is due to MutL CTD dimer slightly twisted.

In order to investigate the rates of MutL dissociation from different types of DNA, 10 fold excess MutL competitor was added to the system which including 200 nM MutL297_AF488AF594 hetero-dimer, 200 nM wtMutS, 2 mM ATP, and 10 nM GT932/100 nM GT100DF/GT59DF DNA

in buffer M. The graphs shown that the kinetics of the GR FRET fit to signal exponential fit, and the lifetime are around 200 s for all three types of G: T single mismatch-containing DNA (Figure 1.6 A). Nevertheless, the kinetics of the BR FRET decreased fits to two exponential fits. The first phase's lifetime is around 3 s which irrelevant with the different types of DNA (Figure 1.6 A and B). Moreover, this short lifetime represents the separation between MutL and MutS, and that consistent with the literature that the lifetime of MutL oscillates from MutS is 3.8 ± 0.3 s (Liu, Hanne, et al. 2016). The long dissociation time from GT932 circular DNA is ~ 120 s, and that consistent with the former work in our lab which monitored the FRET between acceptor labeled MutS and donor labeled MutL after added MutL competitor (Marx 2013).

As we described above, we could conclude that MutL conformational changes start at loading MutL on G: T mismatch-containing DNA. The different parts of MutL conformational changes are out of step, and these conformational changes are beyond the ATP binding and hydrolysis which induced MutL NTD ATPase domain dimerized and reopened which are critical for activated MthH endonuclease activity and recruited UvrD in later MMR processes.

Method

Steady-state Förster Resonance Energy Transfer (FRET)

Förster Resonance Energy Transfer (FRET) is a radiationless, photophysical process of energy transfer from an optically excited donor (D) to a nearby acceptor (A) via dipole-dipole interaction within 10 nm (Koontz 2013, Patowary, Pisterzi, et al. 2015). Usually, donor fluorophore with shorter wavelength emission and is excited with an external light source, while acceptor with more extended wavelength fluorophore and the emission will increase if the distance to the donor within the effective FRET range (shorter than 7-8 nm). If the distance to donor over the effective FRET range (longer than 10 nm), only the emission of the donor was observed (Koontz 2013). FRET efficiency defined as $E = I_A / (I_D + I_A) = 1 / (1 + (d/R_0)^6)$. Where I_D and I_A are the donor and acceptor emission intensities, R_0 is Förster radius and ranges 4-6 nm and that's depends on the spectral properties of the donor and acceptor fluorophores, and d is the distance between the fluorophores (Koontz 2013, Koontz 2013). The Steady-state FRET was assessed with TECAN Infinite F200 PRO fluorescence plate reader or Fluoromax 4 spectral photometer manufactured by Horiba. The dead-time for steady-state FRET is around 15 s.

Stopped-flow Fluorescence kinetics

The stopped-flow kinetics were carried out in SF-61SX2 (TgK Scientific, Bradford-on-Avon, UK) apparatus. The single mixing mode is mixing samples in Syringe C and Syringe D with 1:1 ratio and with ~11 ml/s rate at 25 °C. The dual mixing mode is firstly mixing samples in Syringe A and Syringe B with 1:1 ratio with setting different aged time (~10 ml/s rate at 25 °C). Then mixing again with samples in Syringe C with 1:1 ratio and pushed by the buffer in Syringe D into the cuvette with ~10 ml/s rate at 25 °C. The GR FRET is the FRET between AF488 (G, donor) and AF594 (R, acceptor) labeled proteins assessed with ET525/50M and OG 590 filters at 492 nm. The BR FRET is FRET between AF594 (R, acceptor) labeled protein and SYTOX blue (SB, donor) stained DNA assessed with ET525/50M and OG 590 filters at 436 nm. While the BG FRET is FRET between AF488 (G, acceptor) and At390 (R, donor) labeled proteins assessed with ET525/50M and ET450/50M filters at 436 nm.

MutL binding GT59DF DNA

20-200 nM AF594 labeled MutL with 1.6 μM SB were titrated in pre-incubated wtMutS- GT59DF DNA complex (0.5 mM ATP, 20 nM wtMutS, 10 nM GT59DF DNA, 1.6 μM SYTOX blue, final concentration) assessed by SF-61SX2 (TgK Scientific, Bradford-on-Avon, UK) with ET525/50M and OG 590 filters. These experiments were performed in FB75T (25 mM HEPES/KOH, 75 mM KCl, 1 mg/ml BSA, 2.5 mM MgCl₂, 1 mM DTT, pH7.5) buffer at 25 °C.

MutS-MutL complex multiple loaded on nano-circular DNA

200 nM MutL297_AF594 added to 200 nM MutS449/D835R_AF488 and 5 nM G: T mismatch-containing nano-circular DNA (GT932 DNA) (Xiao, Jung et al. 2011) in the presence of 7.5 μM SB and 2 mM ATP in 200 ul buffer M (KH₂PO₄ 40.5 mM, K₂HPO₄ 9.5 mM, KCl 50 mM, EDTA 0.1 mM, pH 7.4) at room temperature assessed with TECAN Infinite F200 PRO fluorescence plate reader. The ADP and low ATP experiments are processed with adding 200 nM AF594 labeled MutL297 to 2 mM ADP or 10 μM ATP pre-incubated with 200 nM AF488 labeled MutS449/D835R and 5 nM GT932 DNA separately, then added 2 mM ATP at the end. The FRET between MutL and DNA called BR FRET and measured with 450 nm (20 nm width) excitation filter and 620 nm (10 nm width) emission filter. FRET between MutS and DNA called BG FRET and measured with 405 nm (10nm width) excitation filter and 535 nm (25 nm width) emission filter, while FRET between MutL and MutS called GR FRET and measured with 485 nm (20 nm

width) excitation filter and 620 nm (10 nm width) emission filter. The FRET was corrected as follows.

Isothermal Titration

Titration experiments were performed using a TECAN Infinite F200 PRO fluorescence plate reader at room temperature. Titration 5-400 nM MutS449/D835R to the system include 200 nM MutL297_AF488-AF594, 2 nM GT932 DNA and 2 mM ATP in 200 μ l buffer M. GT932 mismatch-containing circular DNA titration titrated 1 nM to 20 nM GT932 DNA to 200 nM MutL297_AF488AF594 incubated with 200 nM MutS449/D835R and 2 mM ATP in 200 μ l buffer M. While titration of MutL was carried out 50-600 nM MutL297_AF488AF594 to pre-incubated 200 nM MutS449/D835R, 10 μ M or 2 mM ATP with 5 or 10 nM GT932 DNA in 200 μ l buffer M. The FRET between MutL and DNA called BR FRET and was measured with 450 nm (20 nm width) excitation filter and 620 nm (10 nm width) emission filter, while FRET between AF488 (G, donor) labeled MutL and AF594 (R, acceptor) labeled MutL called GR FRET (EfA is the FRET efficiency) and measured with 485 nm (20nm width) excitation filter and 620 nm (10 nm width) emission filter.

MutH activation assay

Pre-incubated 200 nM wtMutL or AF488 or AF594 labeled MutL297, MutL452 or MutL218 with 200 nM MutS449/D835R, 1 mM ATP and 10 nM GT932 DNA together in 100 μ l buffer M or FB125 buffer at 37 $^{\circ}$ C or 25 $^{\circ}$ C for 10 min, then starting the reaction with 100 nM wtMutH and sampled 20 μ l each time from 1-40 min incubation time and stopped the reaction with proteinase K or protein loading dye. The control experiment were only 10 nM in 20 μ l buffer M/FB125T, added 100 nM wtMutH to 200 nM MutS449/D835R, 1mM ATP and 10 nM GT932 DNA in 20 μ l buffer M or FB125T buffer (no L), and added 100 nM wtMutH to 200 nM wtMutL, 200 nM MutS449/D835R and 10 nM GT932 DNA in 20 μ l buffer M/FB125T (no ATP) incubating at 37 $^{\circ}$ C or 25 $^{\circ}$ C for 40 min and stopped the reaction with proteinase K or protein loading dye.

References

- Auranen, A. and T. Joutsiniemi (2011). "A systematic review of gynecological cancer surveillance in women belonging to Hereditary Nonpolyposis Colorectal Cancer (Lynch syndrome) families." *Acta Obstet Gynecol Scand*.
- Ban, C., M. Junop and W. Yang (1999). "Transformation of MutL by ATP binding and hydrolysis: a switch in DNA mismatch repair." *Cell* 97(1): 85-97.
- Ban, C. and W. Yang (1998). "Crystal structure and ATPase activity of MutL: implications for DNA repair and mutagenesis." *Cell* 95(4): 541-552.
- Bergerat, A., B. deMassy, D. Gadelle, P. C. Varoutas, A. Nicolas and P. Forterre (1997). "An atypical topoisomerase II from Archaea with implications for meiotic recombination." *Nature* 386(6623): 414-417.
- Dutta, R. and M. Inouye (2000). "GHKL, an emergent ATPase/kinase superfamily." *Trends Biochem Sci* 25(1): 24-28.
- Galio, L., C. Bouquet and P. Brooks (1999). "ATP hydrolysis-dependent formation of a dynamic ternary nucleoprotein complex with MutS and MutL." *Nucleic Acids Res* 27(11): 2325-2331.
- Groothuizen, F. S., I. Winkler, M. Cristovao, A. Fish, H. H. Winterwerp, A. Reumer, A. D. Marx, N. Hermans, R. A. Nicholls, G. N. Murshudov, J. H. Lebbink, P. Friedhoff and T. K. Sixma (2015). "MutS/MutL crystal structure reveals that the MutS sliding clamp loads MutL onto DNA." *Elife* 4: e06744.
- Guarne, A. (2012). "The Functions of MutL in Mismatch Repair: The Power of Multitasking." *Prog Mol Biol Transl Sci* 110: 41-70.
- Guarne, A., S. Ramon-Maiques, E. M. Wolff, R. Ghirlando, X. Hu, J. H. Miller and W. Yang (2004). "Structure of the MutL C-terminal domain: a model of intact MutL and its roles in mismatch repair." *EMBO J* 23(21): 4134-4145.
- Iyer, R. R., A. Pluciennik, V. Burdett and P. L. Modrich (2006). "DNA mismatch repair: functions and mechanisms." *Chem. Rev.* 106(2): 302-323.
- Iyer, R. R., A. Pluciennik, W. A. Rosche, R. R. Sinden and R. D. Wells (2000). "DNA polymerase III proofreading mutants enhance the expansion and deletion of triplet repeat sequences in *Escherichia coli*." *J Biol Chem* 275(3): 2174-2184.

- Koontz, L. (2013). "Agarose gel electrophoresis." *Methods Enzymol* 529: 35-45.
- Koontz, L. (2013). "Explanatory chapter: how plasmid preparation kits work." *Methods Enzymol* 529: 23-28.
- Koontz, L. (2013). "Explanatory chapter: introducing exogenous DNA into cells." *Methods Enzymol* 529: 29-34.
- Lee, J. B., W. K. Cho, J. Park, Y. Jeon, D. Kim, S. H. Lee and R. Fishel (2014). "Single-molecule views of MutS on mismatched DNA." *DNA Repair (Amst)* 20: 82-93.
- Liu, J., J. Hanne, B. M. Britton, J. Bennett, D. Kim, J. B. Lee and R. Fishel (2016). "Cascading MutS and MutL sliding clamps control DNA diffusion to activate mismatch repair." *Nature* 539(7630): 583-587.
- Marx, A. D. (2013). Conformational changes and complex formation in DNA mismatch repair. Dr. rer. nat Dissertation, Justus Liebig University.
- Niedziela-Majka, A., N. K. Maluf, E. Antony and T. M. Lohman (2011). "Self-assembly of Escherichia coli MutL and its complexes with DNA." *Biochemistry* 50(37): 7868-7880.
- Pang, P. P., A. S. Lundberg and G. C. Walker (1985). "Identification and characterization of the mutL and mutS gene products of Salmonella typhimurium LT2." *Journal of Bacteriology* 163(3): 1007-1015.
- Parker, B. O. and M. G. Marinus (1992). "Repair of DNA heteroduplexes containing small heterologous sequences in Escherichia coli." *Proceedings of the National Academy of Sciences of the United States of America* 89(5): 1730-1734.
- Patowary, S., L. F. Pisterzi, G. Biener, J. D. Holz, J. A. Oliver, J. W. Wells and V. Raicu (2015). "Experimental Verification of the Kinetic Theory of FRET Using Optical Microspectroscopy and Obligate Oligomers." *Biophysical Journal* 108(7): 1613-1622.
- Pena-Diaz, J. and J. Jiricny (2012). "Mammalian mismatch repair: error-free or error-prone?" *Trends in Biochemical Sciences* 37(5): 206-214.
- Polosina, Y. Y. and C. G. Cupples (2010). "Wot the 'L-Does MutL do?" *Mutat Res.*
- Putnam, C. D. (2015). "Evolution of the methyl-directed mismatch repair system in Escherichia coli." *DNA Repair (Amst)*.

Qiu, R., M. Sakato, E. J. Sacho, H. Wilkins, X. Zhang, P. Modrich, M. M. Hingorani, D. A. Erie and K. R. Weninger (2015). "MutL traps MutS at a DNA mismatch." *Proc Natl Acad Sci U S A* 112(35): 10914-10919.

Robertson, A. B., S. R. Pattishall, E. A. Gibbons and S. W. Matson (2006). "MutL-catalyzed ATP hydrolysis is required at a post-UvrD loading step in methyl-directed mismatch repair." *J Biol Chem* 281(29): 19949-19959.

Sharma, A., C. Doucette, F. N. Biro and M. M. Hingorani (2013). "Slow conformational changes in MutS and DNA direct ordered transitions between mismatch search, recognition, and signaling of DNA repair." *J Mol Biol* 425(22): 4192-4205.

Spampinato, C. and P. Modrich (2000). "The MutL ATPase Is Required for Mismatch Repair." *J. Biol. Chem.* 275(13): 9861-9869.

Su, S. S. and P. Modrich (1986). "Escherichia coli mutS-encoded protein binds to mismatched DNA base pairs." *Proceedings of the National Academy of Sciences of the United States of America* 83(14): 5057-5061.

Tham, K. C., N. Hermans, H. H. Winterwerp, M. M. Cox, C. Wyman, R. Kanaar and J. H. Lebbink (2013). "Mismatch Repair Inhibits Homeologous Recombination via Coordinated Directional Unwinding of Trapped DNA Structures." *Mol Cell* 51(3): 326-337.

Xiao, Y., C. Jung, A. D. Marx, I. Winkler, C. Wyman, J. H. Lebbink, P. Friedhoff and M. Cristovao (2011). "Generation of DNA nanocircles containing mismatched bases." *BioTechniques* 51(4): 259-262, 264-255

Chapter 4

Monitoring MutL binding nucleotides in real-time followed by conformational changes during MMR process in vitro

Abstract

E. coli MutL belongs to the GHKL (Gyrase, Hsp90, Histidine Kinases, and MutL) ATPase family which members share a common ATP-binding domain (the so-called Bergerat fold) as we know from the literature. Upon binding and hydrolysis ATP, MutL undergoes a series of conformational changes. MutL ATP hydrolysis rate in steady-state is combined ATP binding, hydrolysis, and release together. But little was known about the kinetics of ATP binding to MutL which observed with multiple-phases.

A half-maximal effective concentration of ATP to MutL binding is 50-150 μ M was obtained which similar as the K_m for MutL ATPase of 90 μ M from literature. Mant-ATP (modified at 2'/ 3'-OH group) due to cannot bind at MutL ATPase pocket (could be bound and hydrolyzed by MutS) have not effect on loading MutL to DNA (similar BR FRET as ATP) and cannot induce MutL NTD conformational changes and dimerization (the EfA only increased after adding ATP).

Binding of adenine nucleotide can be monitored by MutL NTD labeled mutants, the fluorescence dyes respond differently depending on the different labeled positions. Kinetics of MutL297_ At390 interacted with ATP, ADP and ATP γ S fit three exponential fits better. Varying the concentration of ATP and ATP γ S induced the first rates increased significantly as well as the second rates, while the third rates stay no change. Varying the concentration of ADP induced the first rates of kinetics increased dramatically within 0.2 mM and slightly rising between 0.2-2 mM. The second and the third rates both are stable. Similarly, kinetics of the relative BG FRET increased fit to three exponential fits as well when MutL4_ At390/MutL297_ AF488 hetero-dimers encountered ATP and ATP γ S. The slower hydrolysis' ATP analog ATP γ S induced both the rate and amplitude of the third phase notably increased. And the relative blue fluorescence intensity was enhanced strongly in the presence of the GT59DF DNA-wtMutS complexes which indicated that forming the ternary complex with MutS and mismatched DNA could prevent the ATP hydrolysis by MutL. In brief, with blue dye At390 labeled the residues of 4 and 297 both show strong response to ATP but little changes upon the ternary complex formation with MutS and mismatched DNA. That is in the contrary to the blue dye At390 labeled at 282.

Keywords: ATP, mant-ATP (mATP), ADP, ATP γ S, AMPPNP, MutL297, MutL4, FRET

Introduction

One of the central proteins in *E.coli* MMR system is MutL which is not only involved in DNA mismatch repair but also in other out-of-step repair pathways. Bacterial MutL protein is homo-dimeric (hetero-dimeric in eukaryotic systems) ATPase belonging to the GHKL-family (Gyrase, Hsp90, histidine-kinase and MutL homology) (Dutta and Inouye 2000). Most GHKL-ATPases are dimeric proteins and show significant conformational changes upon ATP binding involved dimerization of the ATPase domain (Dong and Berger 2007, Li and Buchner 2013). MutL also undergoes substantial conformational changes as well when binding adenine nucleotides (as visualized by hydrodynamic methods and atomic force microscopy (AFM) (Ban and Yang 1998, Ban, Junop, et al. 1999, Guarne, Ramon-Maiques, et al. 2004, Sacho, Kadyrov, et al. 2008)). However, less known about the kinetics of the conformational transitions and the role of ATP binding and hydrolysis of MutL during the MMR process.

ATP hydrolysis by MutL is slow ($k_{cat} = 0.4 \text{ min}^{-1}$ for *E. coli* MutL) but accelerated by double and single-strand DNA (Ban and Yang 1998, Ban, Junop, et al. 1999). Binding of ATP induces dimerization of the ATPase domains result in a more compact form of the MutL dimer as analyzed by size-exclusion chromatography and dynamic light scattering using the non-hydrolysable ATP-analog AMPPNP (Ban and Yang 1998, Guarne, Ramon-Maiques, et al. 2004). A dimeric form of the N-terminal domain was obtained in the presence of the non-hydrolysable ATP analog AMPPNP and ATP which in the crystal was found to be hydrolyzed to ADP (Ban, Junop, et al. 1999). However, N-terminal dimerization seems not to be entirely required for ATPase activity at least in human and yeast MutL proteins (Guarne, Junop et al. 2001, Bourniquel and Bickle 2002). In addition, nucleotide binding changes the orientation between the ATPase and DNA-binding subdomains (Anbazhagan, Fujii, et al. 1999). Noteworthy, only AMPPNP but not ATP was able to convert the N-terminal domain of *E. coli* MutL into stable dimers as analyzed by size-exclusion chromatography suggesting that upon ATP-hydrolysis the N-terminal domain dissociate rapidly (Ban and Yang 1998). Small angle X-ray scattering (SAXS) of MutL from *Thermotoga maritima*, *Aquifex aeolicus* suggested that the protein, even in the presence of nucleotides, adopts an extended conformation (Kim, Cha, et al. 2009, Iino, Hikima, et al. 2015). In contrast, a single-molecule atomic force microscopy using the full-length eukaryotic MutL proteins revealed several conformations of MutL (open, one-arm, closed and

condensed) which are modulated by adenine nucleotides (ADP, ATP or AMPPNP) with ATP leading to a mostly condensed state (Sacho, Kadyrov, et al. 2008).

In this chapter we investigated the kinetics of different nucleotides binding to At390 labeled NTD subdomain at ATP binding pocket (MutL297) or the flexible arm (MutL4) in real-time. The effect of different types of nucleotides on MutL loaded on mismatch-containing DNA by wtMutS, and subsequently conformational changes based on the FRET as well.

Results

1, Nucleotides effects on MutL subunit exchanges

We observed that ATP ($0.11 \pm 0.001 \text{ min}^{-1}$) and ADP ($0.10 \pm 0.002 \text{ min}^{-1}$) have no impact on MutL NTD-NTD (MutL297_AF488-MutL297_AF594) subunit exchanges compared to the APO ($0.08 \pm 0.001 \text{ min}^{-1}$) (Figure 1 A and B). Only MutS449/D835R-GT932 DNA complexes do not affect MutL subunit exchange as well, while the extra EfA appears with the rate of $0.27 \pm 0.004 \text{ min}^{-1}$ after adding 2 mM ATP to the system (Figure 1 C and D). Only 1/3 amplitude of the relative extra EfA over subunit exchange with a rate of $0.15 \pm 0.007 \text{ min}^{-1}$ when substituting ATP with AMPPNP (Figure 1 C and D). Also, adding 2 mM ATP or AMPPNP to MutL452_AF488-MutL297_AF594 (NTD-CTD) hetero-dimers in the presence of 200 nM MutS449/D835R and 2 nM GT932 DNA, the extra EfA only slightly over the SE with rates of $0.15 \pm 0.006 \text{ min}^{-1}$ and $0.04 \pm 0.001 \text{ min}^{-1}$ separately (Figure 1 E and F) due to the long distance between these two 452 residues within the same dimer. While the extra EfA of MutL452_AF488-MutL452_AF594 (CTD-CTD) hetero-dimers only slightly over the subunit-exchange with the rates of $0.07 \pm 0.001 \text{ min}^{-1}$ and $0.04 \pm 0.002 \text{ min}^{-1}$ for separately (Figure 1 G and H). The extra EfA increased slightly in the presence of 2 mM ATP or AMPPNP, 200 nM MutS449/D835R, and 2 nM GT932 DNA is owing to the very short distance between two subunits (2.8 nm) within the MutL dimer (Figure 1 G and H). After adding thrombin, the EfA kinetics of APO/ATP channels of MutL297_GR are back to the starting value, while the EfA of ADP is slightly higher than the starting value, while EfA of AMPPNP stays similar as before adding thrombin (Figure 1 A). While the EfA of the ATP/AMPPNP in the presence of 200 nM MutS449/D835R and 2 nM GT932 DNA were only slightly lower than the EfA after the subunit exchange for MutL297_AF488/MutL297_AF594 hetero-dimer (Figure 1 A-D). However, the EfA of MutL452_AF488/MutL297_AF594 hetero-dimer in the presence of 2 mM ATP/AMPPNP, 200 nM MutS449/D835R,

and 2 nM GT932 decreased immediately back to the starting points after adding thrombin (Figure 1 E and F). The EfA is still high for MutL452_AF488/ MutL452_AF594 hetero-dimer (Figure 1 G and H).

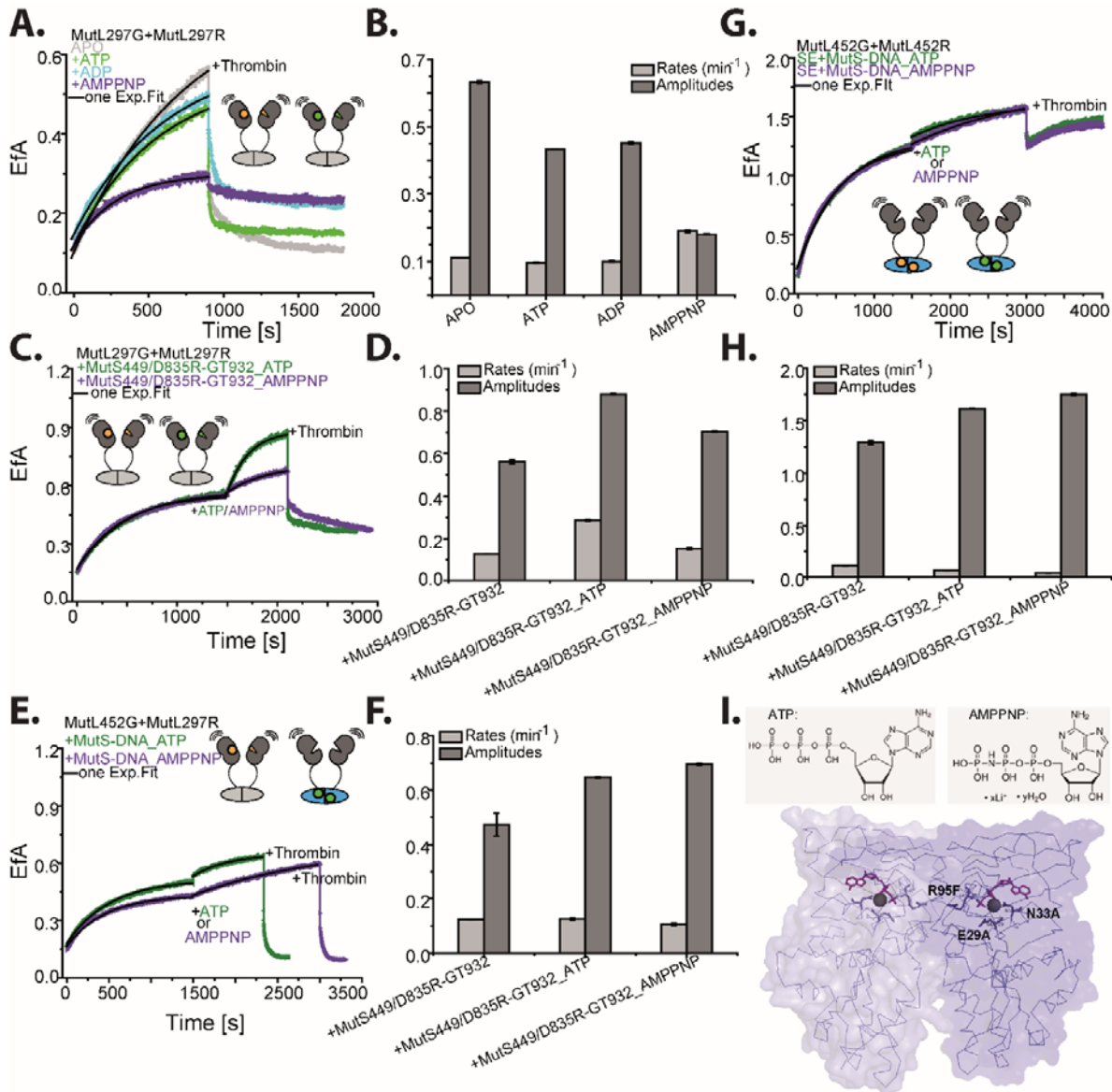


Figure 1 Nucleotides effects on MutL subunit exchange (SE) and subunits interaction in Buffer M. (A) 100 nM MutL297_AF488 and 100 nM MutL297_AF594 subunit exchange (SE) in the absence or presence 2 mM ATP/ADP/AMPPNP; (B) The rates and amplitudes of A; (C) 200 nM MutS449/D835R and 2 nM GT932 DNA effect on 100 nM MutL297_AF488 and 100 nM MutL297_AF594 subunit exchange (SE) and later added 2mM ATP or AMPPNP and thrombin added after that; (D) The rates and amplitudes of C; (E) 200 nM MutS449/D835R and 2 nM GT932 DNA effect on 100 nM MutL452_AF488 and 100 nM MutL297_AF594 subunit exchange (SE) and later added 2 mM ATP or AMPPNP and thrombin added after that; (F) The rates and amplitudes of E; (G) 200 nM MutS449/ D835R and 2 nM GT932 DNA effect on 100 nM MutL452_AF488 and 100 nM MutL452_AF594 subunit exchange (SE) and later added 2 mM ATP or AMPPNP and thrombin added after that; (H) the rates and amplitudes of G.; (I)The chemical structure of ATP and ANPPNP, as well as the AMPPNP dimerized MutL NTD (PDB code 1b63) structure.

2, Nucleotides effects on MutL conformational changes and its multiple loading on GT932 DNA

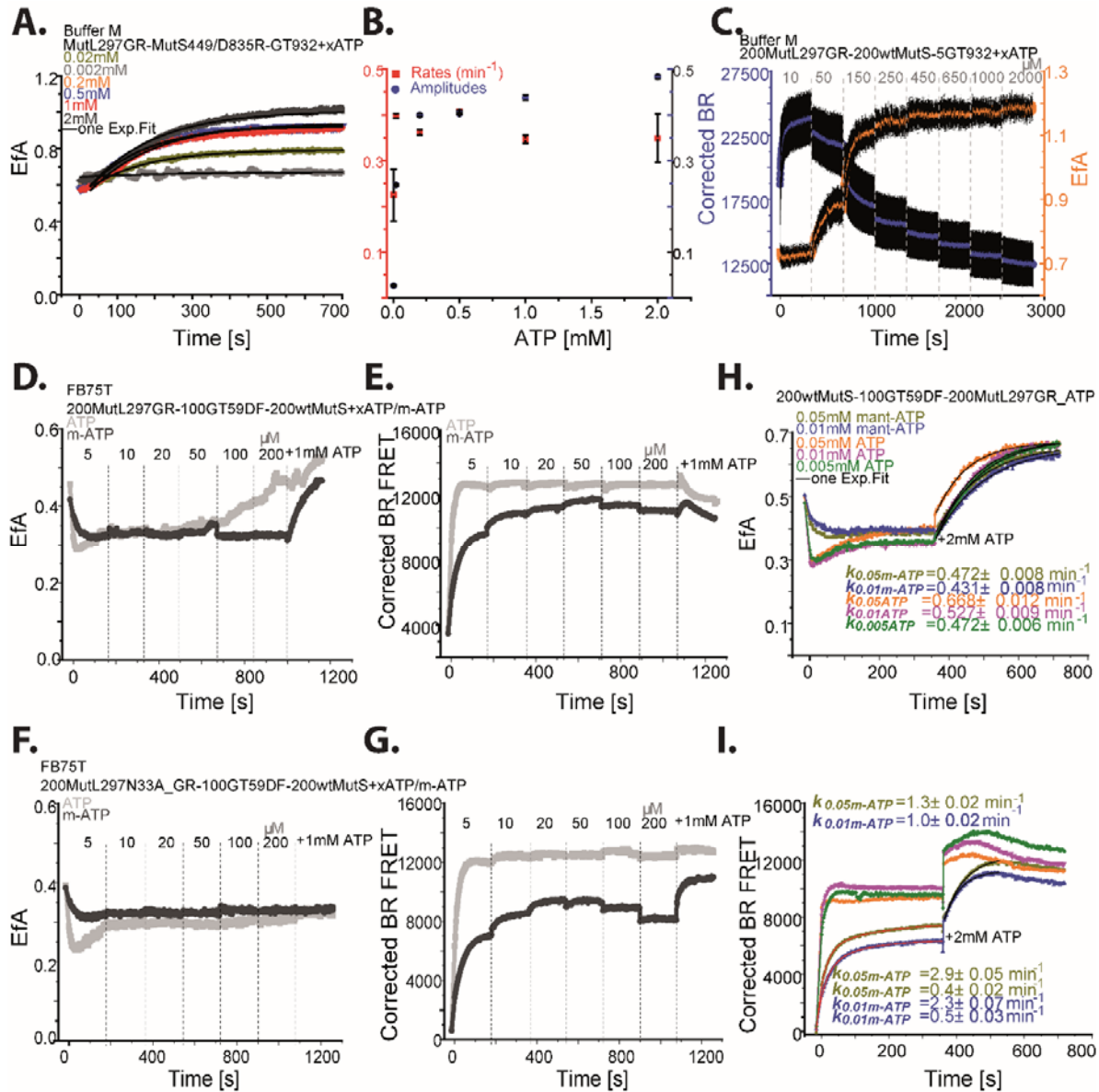


Figure 2 Titration ATP to MutL297_AF488AF594 (GR) hetero-dimers in the presence of GT932 DNA or different concentration of GT932 DNA, and MutS449/D835R or wtMutS. (A) titration 0.002-2 mM ATP to 2 nM GT932 DNA, 200 nM MutS449/D835R, and 200 nM MutL297_GR in buffer M; (B) the rates derived from single exponential fits to kinetics of A; (C) titration 0.01-2 mM ATP to 5 nM GT932 DNA, 200 nM wtMutS449 and 200 nM MutL297_GR in buffer M; (D and E) titration 0.005-1 mM ATP or mant-ATP (m-ATP) to 200 nM MutL297_GR with 100 nM GT59DF DNA and 200 nM wtMutS, D is GR FRET efficiency between MutL297_GR subunit and E is BR FRET between MutL297_GR to SYTOX blue (SB) stained DNA in FB75T buffer; (F and G) titration 0.005-1 mM ATP or mant-ATP (m-ATP) to 200 nM MutL297N33A_GR with 100 nM GT59DF DNA and 200 nM wtMutS, F is the GR FRET efficiency between MutL297N33A_GR subunit and G is the BR FRET between MutL297N33A_GR to SYTOX blue (SB) stained DNA in FB75T buffer; (H and I) Different concentration ATP or mant-ATP (m-ATP) to 200 nM MutL297_GR in the presence of 100 nM GT59DF DNA and 200 nM wtMutS in FB75T buffer.

When varied the concentration of ATP from 0.002 mM to 2 mM in the system containing 200 nM MutL297_AF488AF594, 200 nM MutS449/D835R, and 2 nM GT932 DNA in buffer M, we could observe that the amplitudes of the EfA kinetics increased, while the rates are floating around 0.38 min^{-1} (Figure 2 A and B). Titrating 0.01-2 mM ATP to 200 nM MutL297_AF488AF594, 200 nM MutS449/D835R, and 5 nM GT932 circular DNA stained by SB, the corrected BR FRET reach the highest value at low ATP concentration ($\sim 10 \mu\text{M}$), then the corrected BR FRET decreased and reach the saturation at 0.25 mM ATP, while the EfA increased and reached the saturation at 0.25 mM ATP as well (Figure 2 C).

However, the EfA kinetics of 200 nM MutL297_AF488AF594 decreased firstly, then reached the saturation in 100 s at 0.005 mM ATP after titrating 0.005-0.2 mM ATP in the presence of 100 nM GT59DF DNA and 200 nM wtMutS in FB75T buffer (Figure 2 D, light grey). While, the EfA stay no changes after decreasing upon titrating mant-ATP (mATP) at the beginning and reaching the saturation within 100 s by 0.005 mM mant-ATP (Figure 2 D, dark grey). The EfA only slowly increased after adding 1 mM ATP to mant-ATP system (Figure 2 D, dark grey). Whereas, the BR FRET kinetics heading up immediately and saturating at high value (at 0.005 mM ATP) which slightly decreased only after adding 1mM ATP for the ATP channel as well (Figure 2 D light grey). The BR FRET kinetics of mant-ATP channel increased immediately (but the rate is slower compared to in the presence of ATP) as well and saturated at 0.01 mM mATP, then slightly decreased until after adding 1 mM ATP (Figure 2 E dark grey). Nevertheless, the EfA for both channels were reduced at the beginning, then saturated at 0.3 for MutL297N33A_AF488AF594 hetero-dimers after adding 1 mM ATP at the end for titrating 0.005-0.2 mM ATP (Figure 2 F light grey) or mant-ATP (m-ATP, Figure 2 F dark grey) in the presence of 100 nM GT59DF and 200 nM wtMutS in FB75T buffer.

Moreover, the BR FRET behave the same as MutL297_AF488AF594 before adding 1 mM ATP, while after adding 1 mM ATP in FB75T buffer the BR FRET still stays no change for ATP channel (Figure 2 G, light grey) while mant-ATP channel notably increased (Figure 2 G). At the end, we investigated the effect of adding 2 mM ATP to different lower concentrations of ATP or mant-ATP for both the EfA and the corrected BR FRET of MutL297_AF488AF594 in the presence of 100 nM wtMutS, 100 nM GT59DF in FB75T buffer (Figure 2 H and I). Similar as 0.005-0.05 mM ATP, and 0.01 or 0.05 mM mant-ATP induced the EfA of the MutL297_AF488AF594 hetero-dimers decreased at beginning, but the rates of the BR FRET kinetics for loading it on GT59DF DNA with mant-ATP slower ($2.30 \pm 0.068 \text{ min}^{-1}$ and $0.476 \pm 0.033 \text{ min}^{-1}$ for 0.01 mM mant-ATP; while $2.86 \pm 0.051 \text{ min}^{-1}$ and $0.402 \pm 0.023 \text{ min}^{-1}$ for 0.05 mM mant-ATP) and the amplitudes are lower as well than with ATP (Figure 2 H and I).

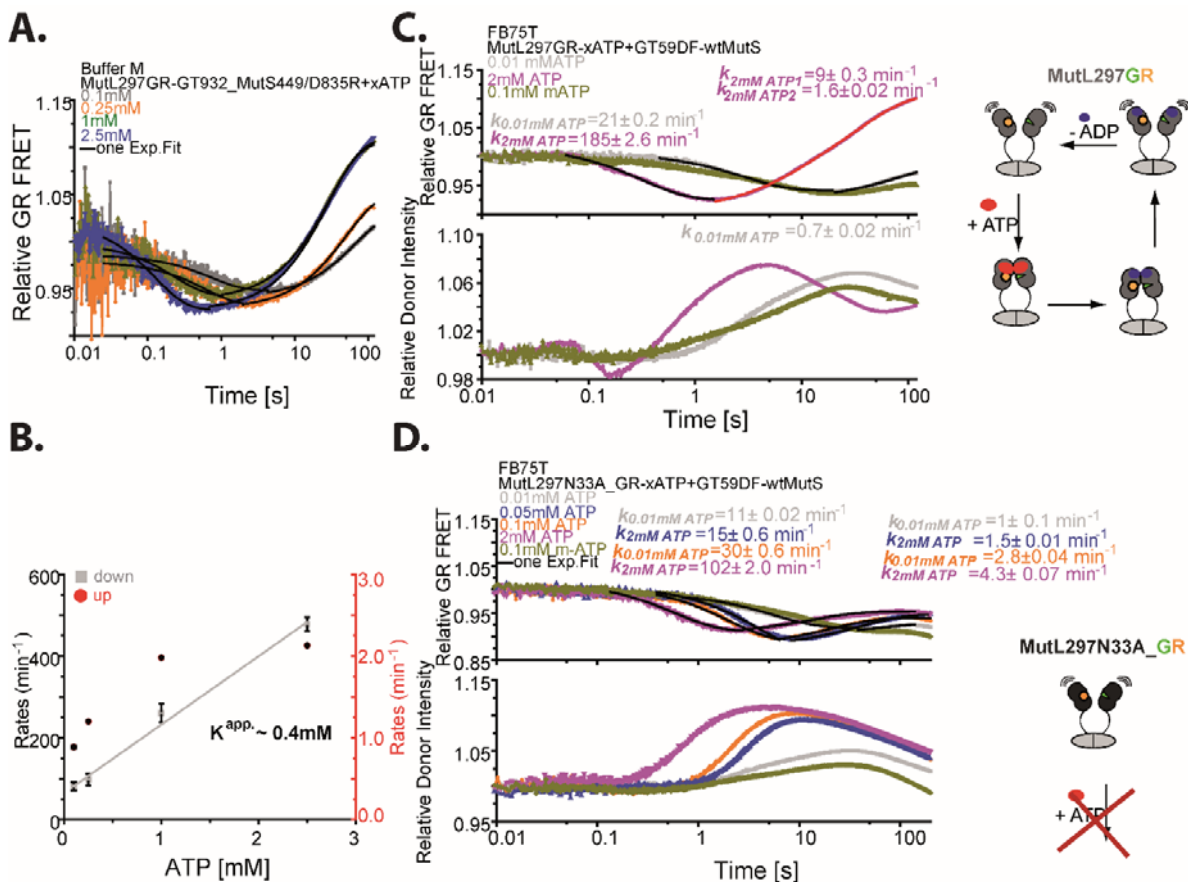


Figure 3 The ATP effects on MutL297_AF488AF594 (GR) interaction assessed by Stopped-flow. (A) 100 nM MutL297_AF488AF594 hetero-dimers against the different concentration of ATP in the presence of 4 nM GT932 and 200 nM MutS449/D835R in buffer M and all concentration diluted to half after mixing; (B) The rates derived from A; (C) 200 nM MutL297_GR pre-incubated with different concentrations of ATP against 100 nM GT59DF DNA pre-incubated with 200 nM wtMutS in buffer FB75T (the upper part is the FRET channel, and the lower part is the donor channel); (D) 200 nM MutL297N33A_GR pre-incubated with different concentrations of ATP or 100 nM mant-ATP (m-ATP) against 100 nM GT59DF DNA pre-incubated with 200 nM wtMutS in buffer FB75T. All concentrations were diluted to half after mixing, the upper part is the FRET channel, and the lower part is the donor channel.

After adding 2 mM ATP, EfA increased with the similar rates for all different concentrations of low ATP (Figure 2 H, orange, purple and green). In the presence of mant-ATP, kinetics of the EfA (as shown in Figure 2 H) fit to single exponential fit. The BR FRET increased slowly with rates of $1.0 \pm 0.02 \text{ min}^{-1}$ for kinetics of 0.01 mM mant-ATP and $1.3 \pm 0.02 \text{ min}^{-1}$ for kinetics of 0.05 mM mant-ATP which are fit to signal exponential fit as well when all three kinetics of low ATP (5 μM , 10 μM and 50 μM) slightly decreased and saturated nearly 11000 (Figure 2 H and I, orange, purple and green). Summarized from the description above, the EfA decreased while the BR FRET already reach the top value when incubating MutL297_AF488AF594 with GT59DF DNA and wtMutS at low ATP or mant-ATP, while both the EfA and the BR FRET kinetics behaves opposite after titrating 2 mM ATP.

However, no observation for the EfA decreased with lower ATP in the presence of GT932 DNA, and that increased and saturated with ~ 0.25 mM ATP. The corrected BR FRET kinetics of MutL297_AF488AF594 in the presence of GT932 circular DNA and wtMutS decreased and saturated at 0.25 mM ATP as well. Therefore, in the presence of GT932 DNA mismatch-containing circular DNA, MutL297_AF488AF594 hetero-dimers undergoes conformational changes combined multiple loading by MutS on GT932 DNA which consistent with the observation in Chapter 3.

3, Nucleotides effects on MutL conformational changes in DNA

As described above, the EfA of MutL297_AF488AF594 decrease with lower ATP concentration in the presence of GT59DF DNA and wtMutS which was not observed in the presence of GT932 DNA. Due to TECAN with 10-20 s' dead time, so we use stopped-flow (0.002 ms dead time) to investigate MutL297_AF488AF594 hetero-dimers conformational changes on GT932 DNA. When varied the concentration of ATP from 0.01 mM to 2.5 mM in the presence of 100 nM MutL297_AF488AF594, 4 nM GT932 DNA, and 200 nM MutS449/D835R (with 1:1 ratio) in buffer M, the down phase of the relative GR FRET kinetics appears earlier, and the relative GR FRET is higher when ATP concentration is higher (Figure 3 A). The down phase rates linearly increased as the ATP concentration increased (Figure 3 B grey). While the rates for the up phase of kinetics saturated at 1 mM ATP (0.5 mM for final concentration) and around 100 fold slower (Figure 3 B red). Therefore, we could find that MutL297_AF488AF594 hetero-dimers adopted more open structures upon loading on GT932 DNA. MutL undergoes a series of conformational changes until ATP bound and dimerized MutL297_AF488AF594 at NTD (Figure 3 A).

Similarly, the GR FRET kinetics goes down firstly, then turnover and heading up (Figure 3 C). While the donor channels anti-paralleled when incubated 200 nM MutL297_AF488AF594 with 0.01/0.1/2 mM ATP mixed with 100 nM GT59DF DNA-200 nM wtMutS complexes (1:1 ratio) in FB75T buffer (Figure 3 C). The concentration of ATP affect not only the rates of kinetics but also the amplitudes. As the relative GR FRET of MutL297_GR is ~ 13 % over the starting value with 2 mM ATP (1 mM at the final) while less than the starting point with 10 μ M ATP (Figure 3 C). Nevertheless, the GR FRET kinetics of MutL297N33A_GR goes down and then turnover as well, but never over the starting value even though in the presence of 2 mM ATP (Figure 3 D). Besides, the donor channels anti-paralleled as well when incubating 200 nM MutL297N33A_AF488AF594 with 0.01-2 mM ATP in the presence of 100 nM GT59DF DNA-200 nM wtMutS complexes (1:1 ratio) in FB75T buffer (Figure 3 D). Therefore, MutL stay at more open conformation upon loading on GT59DF DNA and then undergo a series of conformational changes. The wild-type MutL297_GR hetero-dimers adopted more closed

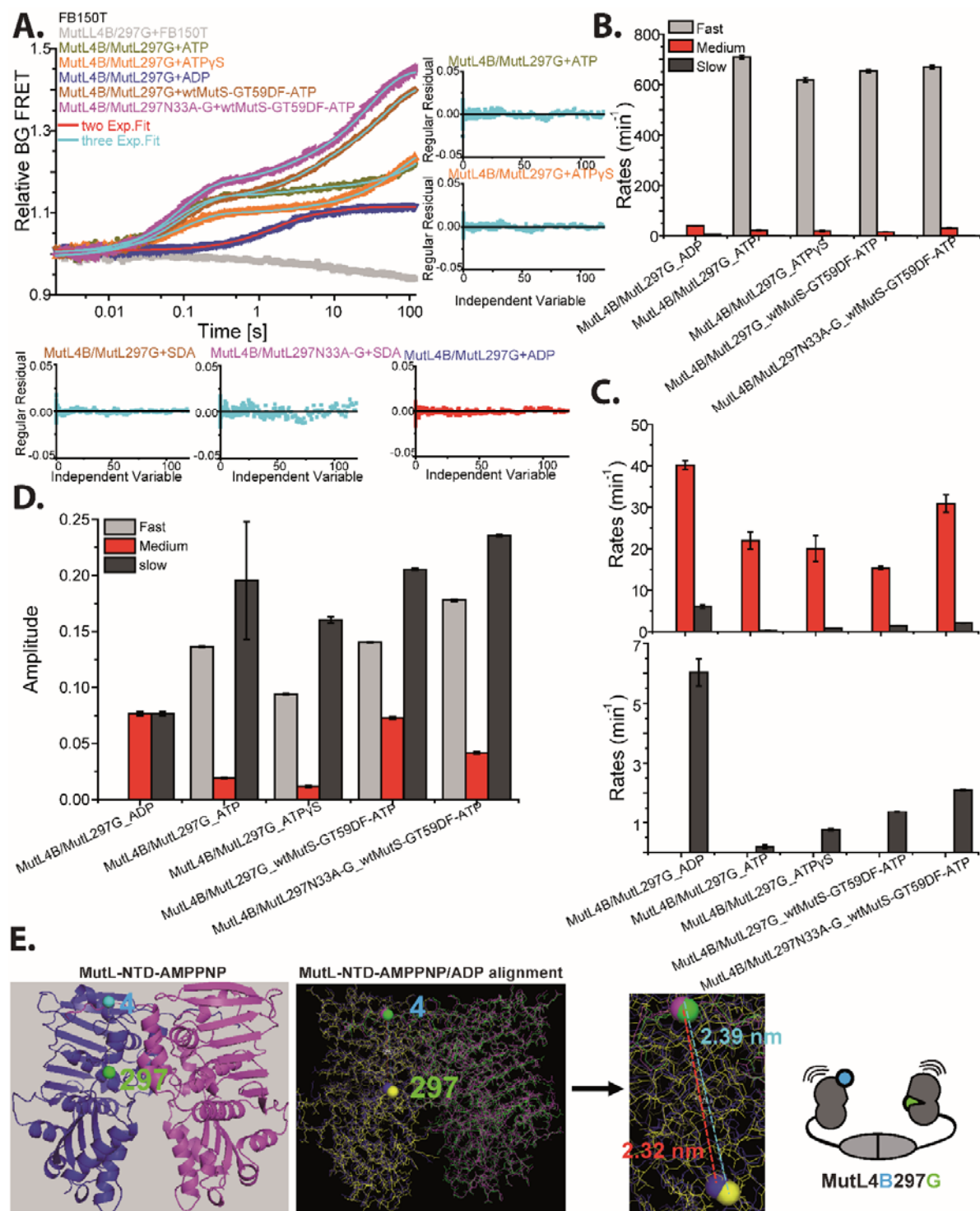


Figure 4 Different nucleotides effects on MutL NTD subunit interaction. (A) 200 nM At390 labeled MutL4 and AF488 labeled MutL297 hetero-dimer conformational change at NTD with 2 mM ATP/ATP γ S/ADP in the absence or presence 200 nM wtMutS and 100 nM GT59DF DNA in FB150T buffer; (B-D) three rates and amplitudes of changing after binding different nucleotides after fitting with two or three exponential fits; (E) quaternary structure of AMPPNP dimerized MutL NTD dimer (left, PDB:1B63), and the alignment the quaternary structure of AMPPNP/ADP dimerized MutL NTD dimer (middle, PDB:1B63/1B62), and cartoons for MutL hetero-dimer MutL4_B/297_G in FB150T buffer. The concentration of all items will be diluted to half in 2 ms after mixing.

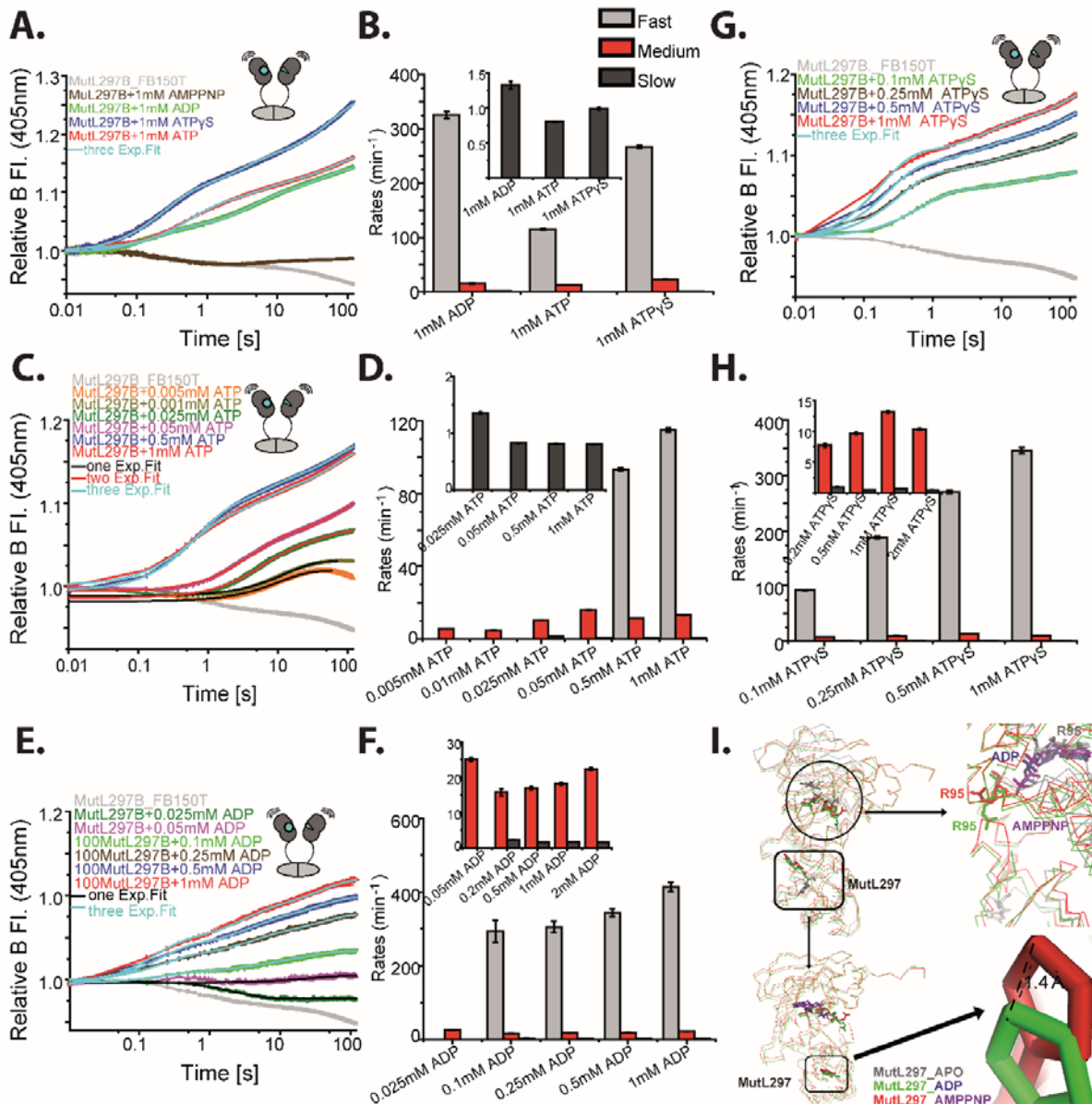


Figure 5 Different concentration of ATP/ADP/ATP γ S effect on MutL297_At390. (A) 100 nM At390 labeled MutL297 against 2 mM ATP/ADP/ATP γ S/AMPPNP in FB150T buffer; (B) Rates of derived from the three exponential fits of kinetics in A; (C) 100 nM MutL297_At390 against different concentration ATP in FB150T buffer; (D) Rates of derived from the one/two/three exponential fits of kinetics in C; (E) 100 nM MutL297_At390 against different concentration ADP in FB150T buffer; (F) Rates derived from the one and three exponential fits of kinetics in E; (G) 100 nM MutL297_At390 against different concentration ATP γ S in FB150T buffer; (H) Rates derived from the three exponential fits of kinetics in G; (I) Align the MutL structure of APO/ADP/AMPPNP together. The concentration will be diluted to half after mixing.

structure in the presence of ATP is due to the ATP induced dimerization at NTD ATPase domain which cannot be observed from ATP binding deficient mutant MutL297N33A. However, the BG FRET is much more pronounced for the inter- and intra- MutL dimer interaction compared to the GR FRET which kinetics' phases is not as clear as the BG FRET in FB150T buffer. Therefore, we use the

blue (B) and green (G) labeled MutL4/MutL297 hetero-dimer to monitor the MutL conformational changes as well. Used 200 nM MutL4/ MutL297 hetero-dimers encountered with 2 mM ATP/ADP/ATP γ S, or 2 mM ATP in the presence of 200 nM wtMutS-100 nM GT59DF DNA complexes (with 1:1 ratio) in FB150T buffer (Figure 4 A). As we observed from the graph, the kinetics slightly decreased when using 200 nM MutL4_B/MutL297_G against buffer only (Figure 4, light grey), while the kinetics of 200 nM MutL4_At390/ MutL297_AF488 hetero-dimers encountered with 2 mM ATP/ATP γ S fit three exponential fits (Figure 4 A, olive and orange) and increased since the starting point. While the kinetics fit only to two exponential fits better when mixed with ADP (Figure 4 A blue). Moreover, the kinetics of MutL4_At390/MutL297_AF488 with ADP missed the third increased phase (Figure 4 A blue), which exists for all kinetics in the presence of ATP/ATP γ S, and ATP in the presence of wtMutS and GT59DF DNA (Figure 4 A). Compared the rates of all kinetics, we could observe that the fast rates are similar and floated around 650 min⁻¹ for ATP, ATP γ S, and ATP in the presence of wtMutS and GT59DF DNA (Figure 4 B). However, the rate for ADP (Figure 4 B, grey) is \sim 50 min⁻¹, which is in the similar range as the medium rates (around 20 min⁻¹) for the kinetics of ATP, or ATP γ S, or ATP in the presence of wtMutS and GT59DF DNA (Figure 4 C upper part, red). The rate of the second phases for the kinetics of ADP is three-fold slower (around 6 min⁻¹), which is similar as the slow rates for (only \sim 0.4 min⁻¹) ATP. While the slow rates of the kinetics of ATP γ S, and of ATP in the presence of wtMutS and GT59DF DNA, are almost two and four times faster than that of the kinetics of ATP (Figure 4 A, and C lower part dark grey). However, the amplitudes of all kinetics except ADP are similar for the fast and slow phases (Figure 4 C lower part, light grey, and dark grey). The amplitudes of the medium phases are much lower for the kinetics of ATP and ATP γ S which 3 fold higher in the presence of wtMutS and GT59DF DNA.

4, Effect of different nucleotides to At390 labeled MutL297

We could observe that MutL4_At390 is sensitive to ATP binding and ATP induced a series of conformational changes (Figure 3 A grey graph with Figure 4 A olive graph). As well as the residue 297 of MutL NTD which close to ATP binding pocket (Winkler, Marx et al. 2011). Then we investigated how different concentrations and types of nucleotides' effect on the At390 labeled MutL297 or MutL4. As the graph were shown, 100 nM MutL4_At390 encountered 1mM ATP in buffer FB75T cause the relative blue intensity enhancement of \sim 9 % (Figure 6 E, grey). While only 3 % increased when using pre-incubated MutL4_At390 and ATP mixed together with ATP-wtMutS-GT59DF DNA complexes (Figure 6 E). Kinetics of both anisotropy and total blue intensity increased as well when MutL4_At390 encountered ATP in FB75T buffer (Figure 8 I and J). And the relative

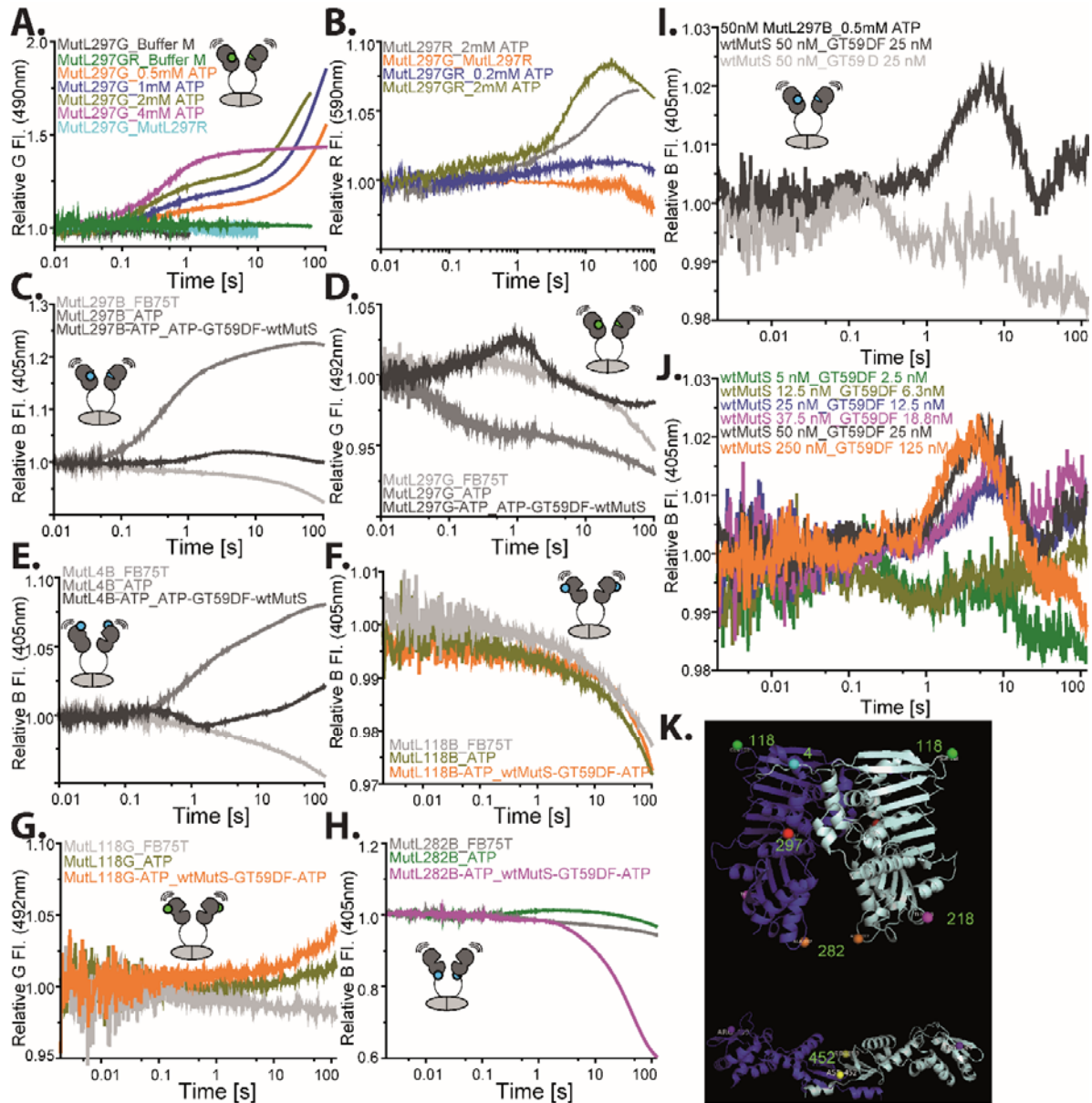


Figure 6 The ATP effects to different NTD labeled MutL. (A) 200 nM MutL297_AF488 against the different concentration of ATP in buffer M; (B) The different concentration of ATP effect to 200 nM AF488 and/or AF594 labeled MutL297 in buffer M; (C and D) ATP, 100 nM wtMutS-100 nM GT59DF DNA effect to 100 nM MutL297_At390 (C) and MutL297_AF488 (D) with/without ATP in FB75T buffer; (E) ATP and 100nM wtMutS-100 nM GT59DF DNA effect to 100 nM MutL4_At390 with/without pre-incubated with ATP in buffer FB75T; (F and G) ATP and 100 nM wtMutS-100 nM GT59DF DNA effect to 100 nM MutL118_At390 (F), MutL118_AF488 (G) with/without ATP in FB75T buffer; (H) ATP and 100nM wtMutS-100 nM GT59DF DNA effect to 100 nM MutL282_At390 with or without pre-incubated with ATP in buffer FB75T; (I) 50 nM MutL297_At390 with 500 μ M ATP against 500 μ M ATP, 100 nM wtMutS and 50 nM GT59D (Dig) DNA in the absence/presence of 200 nM Fab fragment in FB150T buffer; (J) 50 nM MutL297_At390 with 500 μ M ATP against 500 μ M ATP with different concentration of wtMutS-GT59Dig-Fab (DF) DNA in FB150T. The final concentration will be diluted to half; (K) different single cysteine position on MutL NTD dimer (PDB: 1b63) and MutL CTD dimer (PDB: 1x9z) ternary structure.

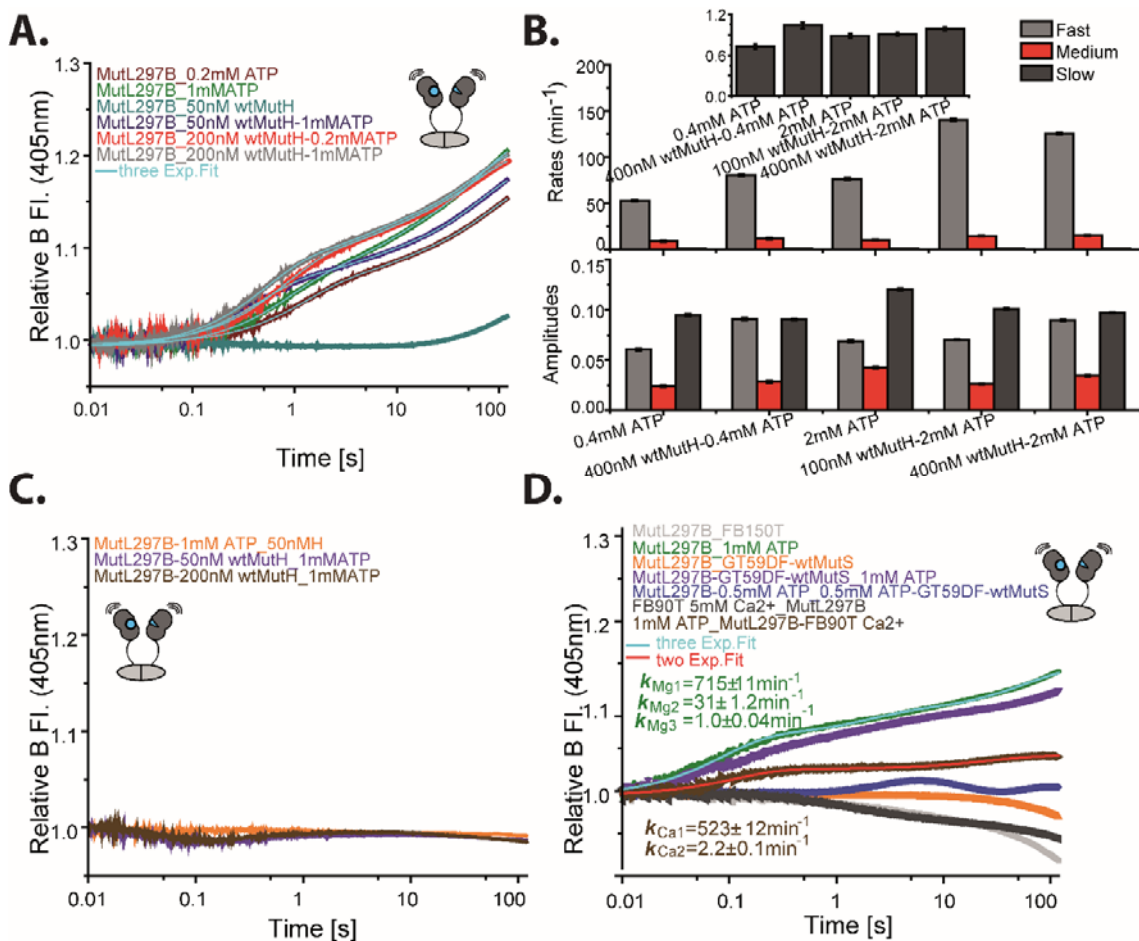


Figure 7 wtMutH mediated nucleotides effects to At390 (B) labeled MutL297 in different buffer. (A) 100 nM MutL297_At390 against 0.04 or 2 mM ATP in the absence or presence wtMutH in buffer FB75T; (B) Rates and amplitudes for three exponential fit of the kinetics in A; (C) 100 nM MutL297_At390 pre-incubated with 100 or 400 nM wtMutH against 2 mM ATP in buffer FB75T; (D) the effect of 50 nM GT59DF DNA, 100 nM wtMutS and 2 mM ATP effect to 100 nM MutL297_At390 in FB150T (5 mM Mg²⁺) and use 5 mM Ca²⁺ instead of 5 mM Mg²⁺ in FB90T buffer.

blue intensity nearly 25 % enhanced when 100 nM MutL297_At390 encountered 1 mM ATP in buffer FB75T (Figure 6 C, grey). While tenfold less when pre-incubated MutL297_At390 and ATP mixed with ATP-wtMutS-GT59DF DNA complexes (Figure 6 C, dark grey). However, no relative changes observed for MutL118_At390 when encountered ATP, or together with ATP mixed with ATP-wtMutS-GT59DF DNA complexes in FB75T buffer (Figure 6 F). Additionally, no obviously increase observed when used 100 nM MutL297_AF488 encountered with 1 mM ATP in FB 75T buffer, which is only slightly different from the buffer kinetics (Figure 6 D, grey). As well as 100 nM MutL118_AF488 encountered with 1 mM ATP in FB 75T buffer (Figure 6 G, olive). However, the kinetics with apparently biphasic increase in green intensity observed when use 200 nM MutL297_AF488 against with 1 to 8 mM ATP in buffer M (with 1:1 ratio) (Figure 6 A). While the kinetics for 200 nM MutL297_AF488 against with 200 nM MutL297_AF594 or buffer M state no change (Figure 6

A). Moreover, mixed MutL297_AF488 and MutL297_AF594 together (with 1:1 ratio) will not cause the red intensity increased in buffer M (Figure 6 B). While the red intensity slowly and slightly increase after encountered with ATP (Figure 6 B).

Furthermore, ATP did not induce the anisotropy and total intensity of green/red changes in the absence or presence of MutS449/D835R and GT932 DNA in buffer M (Figure 8 A-F). Moreover, using 100 nM MutL297_At390 against 2 mM ATP/ADP/ATP γ S/AMPPNP (final concentration will be diluted to half), and 100 nM MutL297_At390 against different levels of ATP/ADP /ATP γ S have been measured in FB150T buffer in Figure 5. As we observed that the kinetics of using MutL297_At390 mixed with 2 mM ATP/ADP/ATP γ S were fit three exponential fits (Figure 5 A and B). With the first rates are $115 \pm 1.2 \text{ min}^{-1}$, $325 \pm 6.3 \text{ min}^{-1}$, and $266 \pm 2.7 \text{ min}^{-1}$ for ATP, ADP and ATP γ S separately (Figure 5 A and B). The second rates are $13.1 \pm 0.15 \text{ min}^{-1}$, $15.0 \pm 0.37 \text{ min}^{-1}$ for ATP and ADP separately, and $23.0 \pm 0.59 \text{ min}^{-1}$ for ATP γ S (Figure 5 A and B). Whereas the third rates are all similar and close to 1.0 min^{-1} (Figure 5 A and B). However, no observation for 2 mM AMPPNP induced relative blue intensity increase for 120 s but still different from the buffer (Figure 5 A). Hence, AMPPNP not only causes MutL NTD-NTD dimerized slow but also the binding processes is much slower as well compared to ATP/ADP/ATP γ S (Figure 5 A). Kinetics of 100 nM MutL297_At390 against 0.01 or 0.02 mM ATP only fit to signal exponential fit, and the rates are only $\sim 5 \text{ min}^{-1}$ (Figure 5 D). The kinetics were fit to double exponential fit with rates of $10.3 \pm 0.09 \text{ min}^{-1}$ and $15.9 \pm 0.10 \text{ min}^{-1}$ for the first phases, and $1.4 \pm 0.02 \text{ min}^{-1}$ and $0.9 \pm 0.01 \text{ min}^{-1}$ for the second phases when increase the ATP concentration to 0.05 or 0.1 mM (Figure 5 C and D). When increase the ATP concentration to 1 or 2 mM, the kinetics were fit to three exponential fits with the rates of the first phases were increased to $93.4 \pm 0.69 \text{ min}^{-1}$ and $115 \pm 1.2 \text{ min}^{-1}$, and rates of the second phases were increased to $11.6 \pm 0.14 \text{ min}^{-1}$ and $13.1 \pm 0.15 \text{ min}^{-1}$, and the rates for the third phases is $\sim 0.8 \text{ min}^{-1}$ for both (Figure 5 C and D). Besides, both anisotropy and total blue intensity increased, and the rates and relative amplitudes of the kinetics depend on the concentration of ATP (Figure 8 G and H). Similarly, three exponential fitted kinetics which use 100 nM MutL297_At390 against 0.2-2 mM ATP γ S indicated that the first rates were increased from 92 to 346 min^{-1} while the second and third rates were fluctuate around 10 min^{-1} and 0.6 min^{-1} , separately (Figure 5 G and H). Whereas, Kinetics of 100 nM MutL297_At390 against 0.05 or 0.1 mM ADP were fit to single exponential fit better, and with a rate of $3.5 \pm 0.13 \text{ min}^{-1}$ (Figure 5 E and F). When increase the ADP concentration from 0.2 mM to 2 mM, kinetics were fit three exponential fits and with the first rates were increased from 293 to 414 min^{-1} , the second rates increased from 16 min^{-1} to 23 min^{-1} , and $\sim 1.4 \text{ min}^{-1}$ for the rates of the third phase for both (Figure 5 E and F). Otherwise, changing buffer to

FB90T will not inhibit ATP induced the relative blue fluorescence intensity MutL297_At390 (green) enhancement.

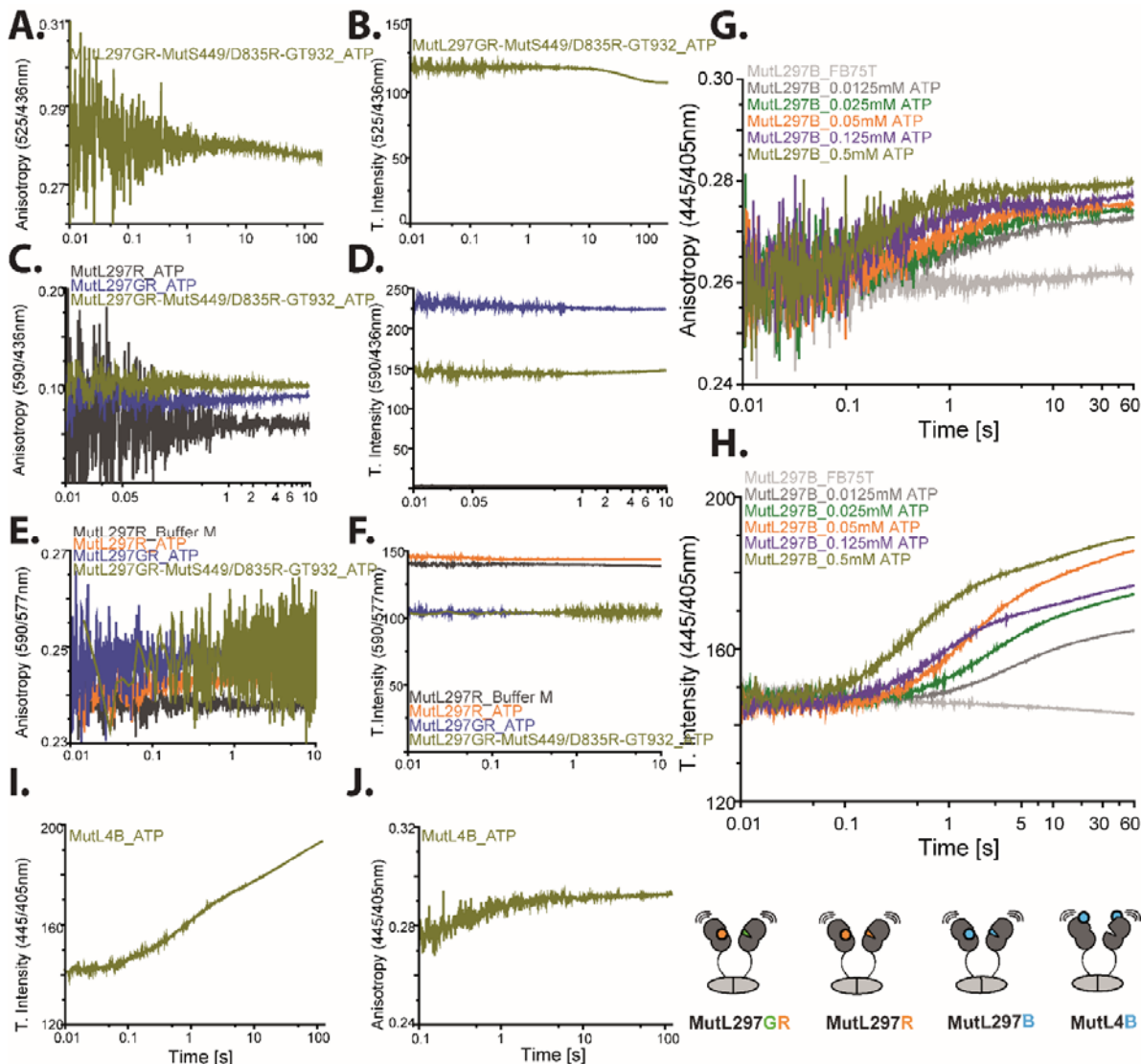


Figure 8 The Anisotropy and total intensity changes of different labeled MutL297. (A and B) Anisotropy and total intensity for pre-incubated with 200 nM MutL297_AF488AF594 with 200 nM MutS449/D835R and 3 nM GT932 DNA against 4 mM ATP in buffer M assessed at 436 nm with 525 nm filter; (C and D) Anisotropy and total intensity for pre-incubated 200 nM MutL297_AF488AF594 with or without 200 nM MutS449/D835R and 3 nM GT932 DNA against 4 mM ATP in buffer M assessed at 436 nm with 590 nm filter; (E and F) Anisotropy and total intensity for pre-incubated 200 nM MutL297_AF488AF594 with or without 200 nM MutS449/D835R and 3 nM GT932 DNA against 4 mM ATP in buffer M assessed at 577 nm with 590 nm filter; (G and H) Anisotropy and total intensity for 100 nM MutL297_At390 against the different concentration of ATP in FB75T buffer assessed at 405 nm with 445 nm filter; (I and J) Anisotropy and total intensity for 100 nM MutL297_At390 against 1 mM ATP in FB75T assessed at 405 nm with 445 nm filter.

Even pre-incubated MutL297_At390 with GT59DF DNA and wtMutS (purple), the kinetics were fit to three exponential fits ($715 \pm 11 \text{ min}^{-1}$, $31 \pm 1.2 \text{ min}^{-1}$, $1.0 \pm 0.04 \text{ min}^{-1}$) as well, while the first binding rate increased compared to that in FB150T buffer (Figure 7 D). Nevertheless, kinetics was fit to two

exponential fits rather than three exponential fits when using 5 mM Ca^{2+} substitute 5 mM Mg^{2+} in FB90T buffer (Figure 7 D brown), the rate for the first phase is $523 \pm 12 \text{ min}^{-1}$ which is 0.7 fold decreased, while the rate for the second phase is $2.2 \pm 0.1 \text{ min}^{-1}$ which is almost 15 fold reduced (Figure 7 D, Brown).

5, MutL conformational changes induced by wtMutS-GT59DF-ATP complexes

The last phase which starts since 10 s was much more strengthened when compared 200 nM MutL4_At390/MutL297_AF488 hetero-dimer to MutL297_At390AF488 hetero-dimer (Figure 2.4 C grey and light grey), which was incubated with 1mM ATP and mixed with 100 nM wtMutS- 1 mM ATP- 50 nM GT59DF DNA complexes (with 1:1 ratio) in FB75T buffer (Figure 2.4 C in Chapter 3). Besides, both the relative BG FRET kinetics' amplitudes and the rates for the third phase strongly enhanced when 200 nM MutL297_At390AF488 pre-incubated with 2mM ATP encountered with 200 nM wtMutS-100nM GT59DF complexes in FB150T buffer (with 1: 1 ratio, Figure 4, brown). The similar kinetics observed as well even for 200 nM MutL4_At390/ MutL297N33A_AF488 hetero-dimers which one unit of the dimer (MutL297N33A_AF488) is ATP binding deficient (Figure 4 A magenta). The relative blue intensity was $\sim 2\%$ increased after pre-incubated MutL297_At390 and ATP mixed with ATP-wtMutS-GT59DF DNA complexes (Figure 6 C, dark grey). However, in the presence of 50 nM wtMutS-50 nM GT59DF DNA (after dilution) arouse a small peak with nearly 3 % relative amplitudes appears at 1 s with ATP incubated with both MutL297_AF488 and wtMutS-GT59DF DNA complexes (Figure 6 D, dark grey). This small peak will disappear when use GT59DF DNA (without four-fold Fab-fragment blocked the end at Dig) instead of GT59DF DNA (Figure 6 I). Moreover, the amplitudes of the relative blue fluorescence intensity (B FI.) peaks changed and appeared time is earlier when added a series of concentrations of wtMutS-GT59DF DNA-0.5mM ATP complexes to 50 nM MutL297_At390-0.5 mM ATP (Figure 6 J). Otherwise, this phenomenon was observed in FB90T buffer as well (Figure 7 D blue). However, no apparent difference of MutL118_AF488 encountered ATP (olive) or confronted with ATP-wtMutS- GT59DF DNA complexes (orange) in FB75T buffer observed (Figure 6 G). Nevertheless, in the presence of 50 nM wtMutS-50 nM GT59DF DNA (after dilution) causes the relative blue fluorescence intensity tremendously decreased (40 %, magenta) when incubating ATP with both wtMutS-GT59DF DNA and 50 nM MutL282_At390 (grey) channels (Figure 6 H).

6, MutH mediating nucleotides effect on MutL297 changes

As described above, ATP could cause the blue intensity of MutL297_At390 and MutL4_At390 increased in FB75T buffer. Then we observed that ATP could cause the blue intensity of MutL297_At390 increased in the absence or presence of wtMutH in FB75T buffer (Figure 7 A). Adding 100 nM or 400 nM wtMutH not only increased the relative amplitudes of the kinetics but also increase the first rates almost two-fold as well as the second rates, while the third rate does not change (Figure 7 B). Whereas, 2 mM ATP cannot cause the relative blue intensity increased when incubating MutL297_At390 with 100 nM or 400 nM wtMutH together in FB75T buffer (Figure 7 C purple and brown). Even though 100 nM wtMutH induced relative blue intensity of MutL297_At390 slightly increased after 10 s, 100 nM wtMutH cannot induce the relative blue intensity of MutL297_At390 increased probability because the increase of relative blue intensity already finished in FB75T buffer (Figure 7 C orange).

Discussion

The most singular unifying feature for GHKL-family (Gyrase, Hsp90, histidine-kinase and MutL homology) is the unconventional Bergerat ATP-binding fold (Dutta and Inouye 2000) which includes four conserved motifs: Motif I (uubEuuaNouDA), MotifII (uxuDNGxGuxb-aauxxu), Motif III (uGxxGxouxSxxxuoxbuTuxT) and MotifIV (TxnGT) where's u, conserved bulky hydrophobic residues; o, small residues; b, basic residues; a, acidic residues (Dutta and Inouye 2000). Apart from magnesium ion, both Na⁺ and K⁺ (in BCK: branched-chain K-ketoacid dehydrogenase kinase and involves four carbonyl oxygen atoms emanating from the hinges of the ATP lid and non-bridging oxygen of the bound nucleotide) are critical for MutL ATPase activity as well (Hu, Machius et al. 2003). From Figure 1, AMPPNP dimerized *E.coli* MutL NTD dimer we could observe that the position of nucleotide and Mg²⁺ in MutL dimerized NTD (PDB: 1b63).

As we know from the literature, *Aquifex aeolicus* MutL NTD binds AMPPNP in a monomeric state which is irrelevant the presence of CTD, and this uncoupling of dimerization of NTD and ATP binding phenomenon is a standard feature among bacterial and eukaryotic MutL with small-angle X-ray scattering analysis combined gel-filtration (Iino, Hikima, et al. 2015). However, we could not observe AMPPNP induced the relative blue (405 nm) intensity of MutL297_At390 dramatically increased within 120 s (Figure 5 A brown), which may indicate that AMPPNP not only dimerized MutL NTD ATPase domain slowly (Ban, Junop, et al. 1999) but also the binding slower compared to other ligands. Otherwise, when aligning APO (PDB: 1bkn), ADP (PDB: 1b62) and ATP (PDB: 1b63) together

(Figure 5 I) we find that the residue of H297C changes the direction which may cause the environment (hydrophilic and hydrophobic) changes, hence cause the blue intensity significantly increased. ADP binding faster than ATP and ATP γ S, the amplitude of the fast and the slow phase of ADP were smaller than ATP and ATP γ S, while the amplitudes of the medium phases were similar for all three ligands (Figure 5 and Appendix Figure 4.2). Even though the crystal structure indicated that the distance between two 297 residues within the ADP or AMPNP dimerized MutL NTD was only 1.4 angstroms difference (Figure 5 and Appendix Figure 4.2). When AF488 and At390 labeled MutL4/MutL297 hetero-dimer encountered different nucleotides, ADP only induced two phases kinetics of BG FRET while ATP and ATP γ S BG FRET kinetics fit to three exponential fits better even in the presence of wtMutS, ATP and GT59DF DNA (Figure 4A). Compared to the kinetics of ADP, the amplitudes of ATP kinetics and ATP γ S kinetics were decreased, while the amplitudes increased in the presence of wtMutS, ATP and GT59DF DNA (Figure 4 D). The medium and slow phases' amplitudes are similar for ADP and smaller than others (Figure 4 C lower part and D). That may due to miss the γ phosphate induced changes to MutL NTD.

The amplitudes of slow phases for all component GT59DF DNAs are similar (Figure 4 D.). While the rates increased in order of MutL4_B/MutL297_G-ATP < MutL4_B/MutL297_G-ATP γ S < MutL4_B/MutL297_G-ATP-wtMutS-GT59DF DNA < MutL4_B/MutL297N33A_G-ATP- wtMutS-GT59DF DNA (Figure 4 D). As reported in the literature, ATP hydrolysis ATP need MutL NTD dimerized (Ban and Yang 1998, Ban, Junop, et al. 1999). The *Aquifex aeolicus* MutL NTD binds AMPNP in a monomeric state which irrelevant with the presence of CTD, and this uncoupling of dimerization and ATP binding phenomenon at NTD is common feature for both bacterial and eukaryotic MutL (Iino, Hikima et al. 2015). Additionally, no extra EfA for both MutL297_G/MutL297N33A_R and MutL297_G/MutL297E29A_R observed in the presence of high ATP, wtMutS, and GT59DF DNA (Appendix Figure 3.1). All these phenomena indicated that the third phase was related to the state that ATP/ATP γ S induced MutL NTD ATPase domain tightly dimerized, which need to be further study in future.

The difference in ADP and AMPNP bound state of MutL NTD at R95 and H297 (Figure 5 I) indicating that ADP induced MutL NTD ATPase dimerization different from AMPNP which could explain that MutL4_B/MutL297_G with ADP missing the tightly dimerized phase as ATP bound MutL on DNA. The medium and slow binding rates which amplitudes are similar correspond to the fast and medium rates for ATP/ATP γ S and may be related to the first and second MutL NTD monomer in dimer binding ligands (Figure 4). We speculated that the second NTD monomer binding nucleotides, which could be accelerated by wtMutS and mismatch-containing DNA, resulted in the two NTD of MutL dimer

loosely interact. Additionally, from Figure 2 D-I, we conclude that MutL loaded on GT mismatch-containing DNA by MutS not necessarily binding ATP. While dimerized its NTD ATPase domain and multiple loading MutL needed ATP, and these MutL-MutL-DNA complexes formation (EfA) reach the saturation at ATP concentration around 300nM (Figure 2 C), that is about ten-fold lower than the affinity for MutL hydrolyzed ATP's $K_m=0.41\pm 0.11$ mM (Spampinato and Modrich 2000). Therefore, more proofs needed in the future to dissect for MutS, mismatch-containing DNA even MutH effect on two NTD monomer within MutL dimer binding and hydrolysis ATP synchronized or independently like another GHKL family member Hsp90 (Mayer and Le Breton 2015).

Method

Isothermal Titration

Titration experiments were performed using a TECAN Infinite F200 PRO fluorescence plate reader at room temperature. Titration 0.02-2 mM ATP to the system which including 200 nM MutL297_AF488AF594 with 200 nM MutS449/D835R, 2 nM or 5 nM GT932 mismatch-containing circular DNA in 200 μ l buffer M. Similarly, varied the concentration of 0.005-1 mM ATP or mant-ATP (m-ATP) in the system containing 200 nM MutL297_GR, SYTOX blue (SB) stained 100 nM GT59DF DNA and 200 nM wtMutS in FB75T buffer. The FRET between MutL and DNA called the BR FRET which was measured with 450 nm (20 nm width) excitation filter and 620 nm (10 nm width) emission filter. While the intra- and inter- MutL FRET called the GR FRET and measured with 485 nm (20 nm width) excitation filter and 620 nm (10 nm width) emission filter.

Stopped-flow Fluorescence kinetics

The stopped-flow kinetics were carried out in SF-61SX2 (TgK Scientific, Bradford-on-Avon, UK) apparatus with the single mixing mode is mixing samples in Syringe C and Syringe D with 1:1 ratio and with ~ 11 ml/s rate at 25 °C. The GR FRET is the FRET between AF488 (G, donor) and AF594 (R, acceptor) labeled proteins assessed with ET525/50M and OG 590 filters at 492 nm. The BR FRET is FRET between AF594 (R, acceptor) labeled protein and SYTOX blue (SB, donor) stained DNA assessed with ET525/50M and OG 590 filters at 436 nm. While the BG FRET is FRET between AF488 (G, acceptor) and At390 (R, donor) labeled MutL proteins assessed with ET525/50M and ET450/50M filters at 436 nm. The blue (At390, B) labeled MutL297 or MutL4 were assessed at 405 nm with the

filter of ET450/50M in FB150T buffer when encountered different types of and different concentration of nucleotides.

Steady-state Förster Resonance Energy Transfer (FRET)

Förster Resonance Energy Transfer (FRET) is a radiation less, photo physical process of energy transfer from an optically excited donor (D) to a nearby acceptor (A) via dipole-dipole interaction within 10 nm (Koontz 2013, Patowary, Pisterzi, et al. 2015). Normally, donor fluorophore with the shorter wavelength emission and is excited with an external light source, while acceptor with the longer wavelength fluorophore and the emission will increase if the distance to the donor within the effective FRET range (shorter than 7-8 nm). If the distance between donor and acceptor over the effective FRET range (longer than 10 nm), only the emission of the donor will observe (Koontz 2013). FRET efficiency defined as $E=I_A/(I_D+I_A)=1/(1+(d/R_0)^6)$. Where I_D and I_A are the donor and acceptor emission intensities, R_0 is Förster radius and ranges 4-6 nm that depends on the spectral properties of the donor and acceptor fluorophores, and d is the distance between the fluorophores (Koontz 2013, Koontz 2013). The Steady-state FRET assessed with TECAN Infinite F200 PRO fluorescence plate reader or Fluoromax 4 spectral photometer manufactured by Horiba. The dead-time for steady-state FRET is around 15 s.

References

- Anbazhagan, R., H. Fujii and E. Gabrielson (1999). "Microsatellite instability is uncommon in breast cancer." *Clin Cancer Res* 5(4): 839-844.
- Ban, C., M. Junop and W. Yang (1999). "Transformation of MutL by ATP binding and hydrolysis: a switch in DNA mismatch repair." *Cell* 97(1): 85-97.
- Ban, C. and W. Yang (1998). "Crystal structure and ATPase activity of MutL: implications for DNA repair and mutagenesis." *Cell* 95(4): 541-552.
- Bourniquel, A. A. and T. A. Bickle (2002). "Complex restriction enzymes: NTP-driven molecular motors." *Biochimie* 84(11): 1047-1059.
- Dong, K. C. and J. M. Berger (2007). "Structural basis for gate-DNA recognition and bending by type IIA topoisomerases." *Nature* 450(7173): 1201-U1204.
- Dutta, R. and M. Inouye (2000). "GHKL, an emergent ATPase/kinase superfamily." *Trends Biochem Sci* 25(1): 24-28.
- Guarne, A., M. S. Junop and W. Yang (2001). "Structure and function of the N-terminal 40 KDa fragment of human PMS2: a monomeric GHL ATPase." *EMBO J* 20(19): 5521-5531.
- Guarne, A., S. Ramon-Maiques, E. M. Wolff, R. Ghirlando, X. Hu, J. H. Miller and W. Yang (2004). "Structure of the MutL C-terminal domain: a model of intact MutL and its roles in mismatch repair." *EMBO J* 23(21): 4134-4145.
- Hu, X., M. Machius and W. Yang (2003). "Monovalent cation dependence and preference of GHKL ATPases and kinases." *FEBS Letters* 544(1-3): 268-273.
- Iino, H., T. Hikima, Y. Nishida, M. Yamamoto, S. Kuramitsu and K. Fukui (2015). "Small-angle X-ray scattering analysis reveals the ATP-bound monomeric state of the ATPase domain from the homodimeric MutL endonuclease, a GHKL phosphotransferase superfamily protein." *Extremophiles* 19(3): 643-656.
- Kim, T. G., H. J. Cha, H. J. Lee, S. D. Heo, K. Y. Choi, J. K. Ku and C. Ban (2009). "Structural Insights of the Nucleotide-Dependent Conformational Changes of *Thermotoga maritima* MutL Using Small-Angle X-ray Scattering Analysis." *Journal of Biochemistry* 145(2): 199-206.
- Li, J. and J. Buchner (2013). "Structure, function, and regulation of the hsp90 machinery." *Biomed J* 36(3): 106-117.

Mayer, M. P. and L. Le Breton (2015). "Hsp90: breaking the symmetry." *Mol Cell* 58(1): 8-20.

Sacho, E. J., F. A. Kadyrov, P. Modrich, T. A. Kunkel and D. A. Erie (2008). "Direct visualization of asymmetric adenine-nucleotide-induced conformational changes in MutL alpha." *Mol Cell* 29(1): 112-121.

Spampinato, C. and P. Modrich (2000). "The MutL ATPase Is Required for Mismatch Repair." *J. Biol. Chem.* 275(13): 9861-9869.

Winkler, I., A. D. Marx, D. Lariviere, L. Manelyte, L. Giron-Monzon, R. J. Heinze, M. Cristovao, A. Reumer, U. Curth, T. K. Sixma and P. Friedhoff (2011). "Chemical trapping of the dynamic MutS-MutL complex formed in DNA mismatch repair in *Escherichia coli*." *J Biol Chem* 286(19): 17326-17337.

Chapter 5

Two *Escherichia coli* MMR essential proteins: MutL and MutH interaction and maturation

Abstract

MutS, MutL, and MutH are three critical proteins in *E.coli* MMR system. Previously, the site-specific photo cross-linking between MutL and MutH obtained that both the NTD and the CTD of MutL interact with MutH. The CTD fragments of MutL is sufficient to interact with MutL obtained through the yeast two-hybrid analysis. At low ionic strength, MutL is adequate to active MutH in an ATP dependent manner. However, little was known about how MutL recruited MutH on the mismatched DNA at high ionic strength buffer and lead to the activation of MutH endonuclease activity. In this chapter, we are the first time using the FRET method to monitor MutL and MutH interaction in real-time.

The interaction between MutL and MutH depends on the presence of both the NTD and CTD of MutL monitored by FRET, and cleavage of MutL by thrombin into NTD and CTD fragments resulted the loss of FRET. The apparent association and dissociation rates between MutL and MutH are very fast ($>15 \text{ nM}^{-1}\text{s}^{-1}$) and independent of DNA, MutS, and ATP. The apparent affinity (KD) between MutL and MutH is around 200 nM in dependent of ionic strength, ATP, MutS, and mismatched DNA. MutL297N33A (ATP binding deficient) share the similar apparent affinity (KD) with MutH as the wild-type of MutL297, but the apparent affinity is much lower (~500 nM) in the presence GT59DF DNA and wtMutS. The less GR FRET state monitored between MutH and NTD labeled MutL (297) with MutS on mismatched DNA at low (10 μM) ATP state as well, but the opposite result obtained between MutH and CTD labeled MutL (452). The BR FRET (FRET between MutH and SB stained DNA) kinetics are similar under all these conditions. Therefore, the interaction between MutL and MutH on mismatched DNA-MutS complexes is highly dynamic.

Nevertheless, the BR FRET between MutH156_AF594 and SB stained GT932 mismatched circular DNA is almost five-fold higher than the BR FRET between MutH156_AF594 and SB stained, mismatched end blocked oligo (GT59DF DNA) DNA in the presence of MutS and MutL indicated that the loops formation may exist. Moreover, recruitment of MutH to DNA by MutL with mismatched DNA-MutS complexes slower in the higher ionic strength buffer (buffer M or

FB150T) than, the lower ionic strength buffer on account of the slow ATP dependent MutL transition.

Keywords: MutH156, MutH77, MutH223, MutL452, MutL297, MutL297N33A, MMR

Introduction

MutL and MutH are two critical proteins in *Escherichia coli* (*E.coli*) MMR system. MutL bridges mismatch recognition and repair. A methyl-directed endonuclease of MutH could generate a nick on the un-methylated or transiently hemi-methylated GATC sites on DNA shortly after its replication. This methyl-directed nicking by MutH ensures that MMR in *E. coli* is directed to the newly synthesized DNA strand containing the error instead of generating mutations in the genome. Eukaryotic MutL homolog MutL α harbor latent endonuclease activity which nicks the discontinuous strand of the mismatched duplex in a MutS α -, PCNA-, RFC-, and an ATP-dependent manner (Fukui 2010). *E. coli* MMR is bi-directional processes and helps MutL to utilize the nick on both sides of the mismatch to interact with UvrD (DNA helicase II) to unwind the nascent strand (Robertson, Pattishall et al. 2006, Hsieh and Yamane 2008, Fukui 2010, Polosina and Cupples 2010). This process is generating an open end which is exposed to ExoI, ExoVII, ExoX, or RecJ in 3'-5' or 5'-3' polarity (Burdett, Baitinger, et al. 2001). As a result, a DNA gap has been produced by the exonuclease, and this gap will be remedied by polymerase III and ligase, thereby restoring the duplex to its intact parental genotype (Hsieh and Yamane 2008). The first evidence of MutL and MutH interaction applied deletion analysis combined with two-hybrid assay identified that the residues from 398 to 615 located at CTD of *E. coli* MutL was sufficient for communication with the MutH as well as the UvrD helicase (Hall, Jordan et al. 1998, Hall and Matson 1999). However, full-length MutL was necessary for fully activating the MutH endonuclease activity, even though MutL NTD is sufficient to physically and functionally interact with MutH (Ban and Yang 1998). The method of site-specific chemical and photo-chemical cross-linking coupled mass spectrometry identified that residues 217–331 of MutL NTD and residues 475–569 of CTD both interact with MutH (Ye, O'Neil et al. 2004, Ahrends, Kosinski, et al. 2006). XVPAXLRXXXLXXLIXX which is a MutH interaction sequence motif (Banasik and Sachadyn 2014) interacted with the “C-arm” of MutH (Ban and Yang 1998, Toedt, Krishnan, et al. 2003, Giron-Monzon, Manelyte et al. 2004, Ahrends, Kosinski, et al. 2006). In this chapter, we first monitored the interaction between AF488 labeled MutL297 (NTD single-cysteine mutant) or MutL452 (CTD single-cysteine mutant) interact with AF594 labeled MutH156,

MutH223 or DNA endonuclease deficient mutant MutH77 (MutH_C96S/S85C/E77A) in real-time based on FRET method. The interaction between MutL and MutH is highly dynamic, independent of ATP, wtMutS, and mismatch-containing DNA, even though with a slightly low affinity.

Results

1, MutL and MutH interact independently of ATP, DNA, and MutS

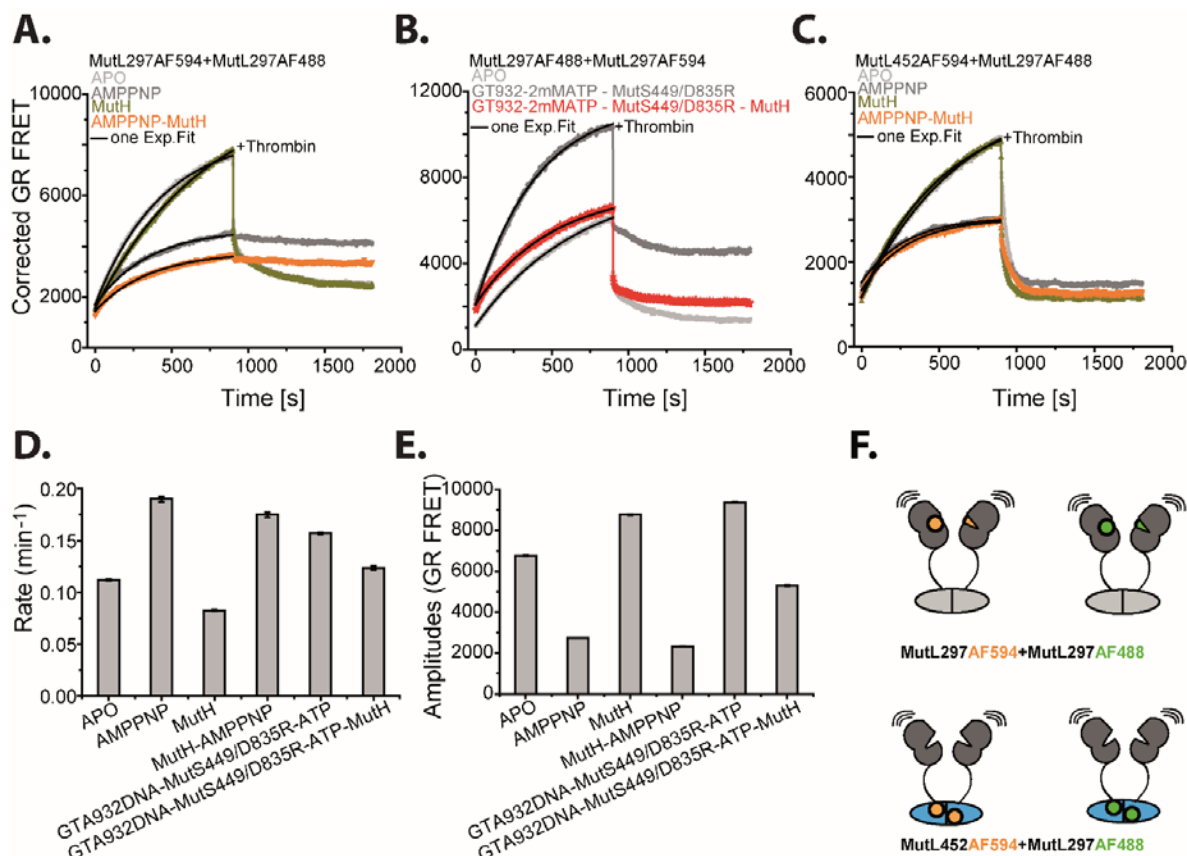


Figure 1 MutH effect on MutL subunit exchange (SE). (A) Effect of 200 nM MutH to subunit exchange between 100 nM MutL297_AF488 and 100 nM MutL297_AF594 with or without 2 mM AMPPNP in buffer M, and added thrombin at the end; (B) Effect of 200 nM MutH to subunit exchange between 100 nM MutL297_AF488 and 100 nM MutL297_AF594 with or without 2 mM ATP-200 nM MutS449/D835R-2 nM GT932 DNA in buffer M and later added thrombin; (C) Effect of 200 nM MutH to subunit exchange between 100 nM MutL297_AF488 and 100 nM MutL452_AF594 with or without 2 mM AMPPNP in buffer M and later added thrombin; (D-E) the rates, relative amplitudes for the kinetics of A-C; (F) cartoons for AF488 or AF594 labeled MutL297 and MutL452.

From Figure 1 A we could observe that the subunit exchange (SE) between 100 nM MutL297_AF488 and 100 nM MutL297_AF594 has been slow down ($0.082 \pm 0.0006 \text{ min}^{-1}$) compared to APO state ($0.138 \pm 0.0007 \text{ min}^{-1}$) in the presence of 200 nM MutH. In the presence of AMPPNP, the amplitude is less than half, even though the rate seems accelerated (Figure 1 A, grey) at the same time. While the amplitude is only one-third of APO state but the rate of kinetics stay

no change in the presence of AMPPNP and MutH (Figure 1 A, orange). Even after adding thrombin, the amplitudes were remains unchanged for both kinetics of AMPPNP and kinetics of AMPPNP- MutH (Figure 1 A, grey and orange). Otherwise, no effect of MutH on the subunit exchange between 100 nM MutL452_AF488 and 100 nM MutL297_AF594 NTD-CTD observed (Figure 1 C). As we described in chapter 3 part 1, the extra FRET over 100nM MutL297_AF488 and 100 nM MutL297_AF594 subunit exchange (SE) in the presence of 2 nM GT932 DNA, 200 nM MutS449/D835R, and 2 mM ATP is due to MutL conformational changes combined MutL multiple loading on GT932 circular DNA. Nevertheless, the extra FRET disappeared in the presence of 200 nM MutH, 2 nM GT932 DNA, 200 nM MutS449/D835R, and 2 mM ATP at the same time (Figure 1 B). The rates of kinetics are slow down slightly as well (Figure 1 B).

Then AF594 labeled MutH156, MutH223, and MutH85 were used to study the interaction with MutL452_AF488 in the absence of MutS and mismatch-containing DNA in buffer M (Figure 2). At the beginning, we titrated 50-1000 nM MutH156_AF594 to 200 nM MutL452_AF488 in the absence or presence of 2 mM ATP in buffer M. As we observed from Figure 2 A, 200 nM MutL452_AF488 needed at least 600 nM MutH156_AF594 to reach the saturation of the GR FRET. Besides, ATP did not cause the changes between MutL CTD and MutH156, while the GR FRET decreased dramatically after thrombin chopped MutL at linker region, and the GR FRET vanished after adding proteinase K. The different ionic strength buffers have no big effect on the interaction between 200 nM MutL452_AF488 and 600 nM MutH156_AF594, and this interaction seems only slightly strengthened in high ionic strength buffer (Figure 2 B). Owing to almost 6 MutH interact with one MutL452_AF488 or MutL297_AF488 dimer, no obviously changing in the GR FRET intensity between 600 nM MutH156_AF594 or MutH223_AF594 or MutH85_AF594 to 200 nM MutL452_AF488 (CTD) or MutL218_AF488 (NTD edge) as well as 600 nM MutH156_AF594 to 200 nM MutL297_AF488 (NTD), were observed after adding ATP, except the GR FRET between 600 nM MutH223_AF594 or MutH85_AF594 and 200 nM MutL297_AF488 (NTD) which remarkably increased (Figure 2 C).

Whereas after lowering MutH concentration to 200 nM, the GR FRET between 200 nM MutL452_AF488/MutL297_AF488 and MutH156_AF594/MutH223_AF594 notably increased, while the GR FRET intensity between MutH85_AF594 and MutL297_AF488 stay unchanged, after adding the ATP (Figure 2 D). The kinetics for 200 nM MutH156_AF594 or MutH223_AF594 interacting with 200 nM MutL452_AF488 shown in Figure 2 E, the GR FRET kinetics immediately

reach the saturation and no processes have observed after adding MutH to MutL452_AF488, as well as added 2 μ M wtMutH competitor. And after adding thrombin the FRET intensity even lower.

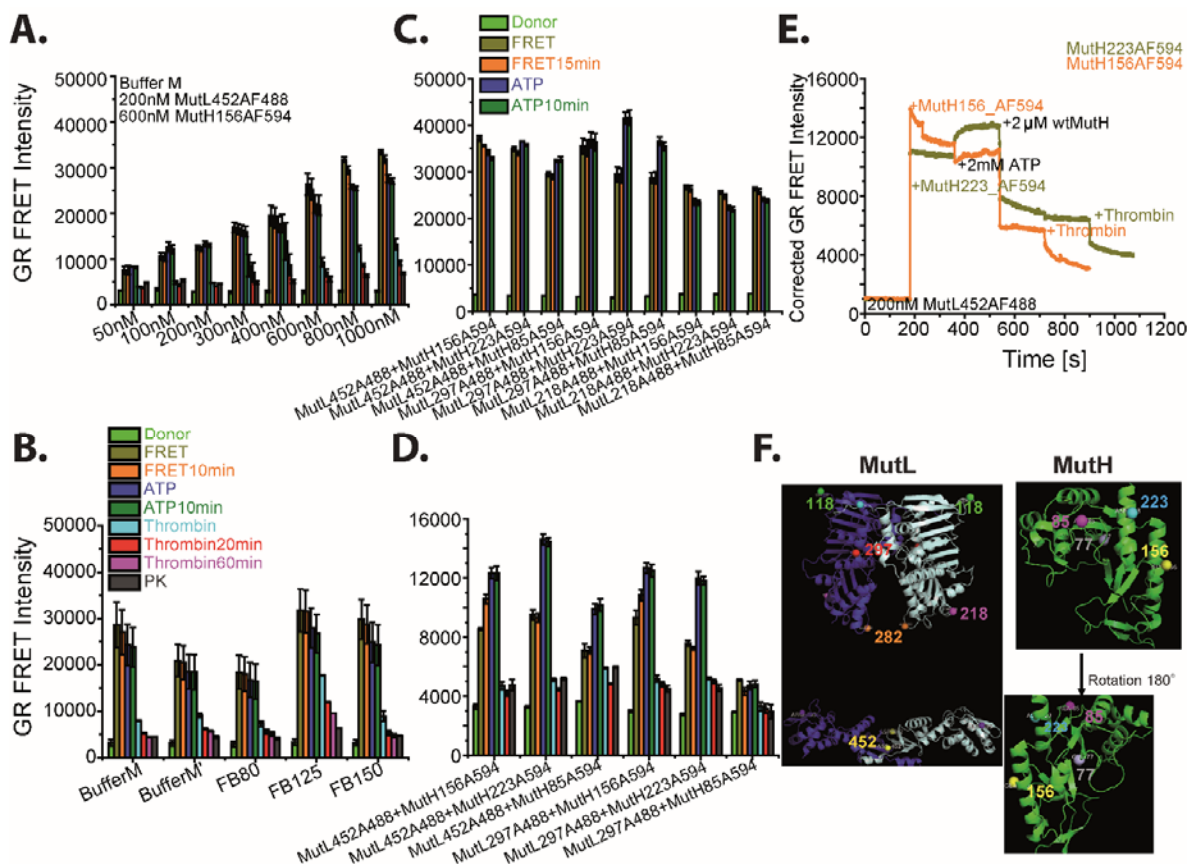


Figure 2 The interaction between AF488 (G) labeled MutL, and AF594 (R) labeled MutH. (A) Titration 50-1000 nM MutH156_AF594 to 200 nM MutL452_AF488, successively added 2 mM ATP, thrombin and proteinase K successively at the end in buffer M; (B) Added 600 nM MutH156_AF594 to 200 nM MutL452_AF488, later successively added 2 mM ATP, thrombin and proteinase K at the end in different buffers; (C) Added 600 nM AF594 labeled MutH156/MutH85/MutH223 to 200 nM MutL452_AF488 or MutL297_AF488, later successively added 2 mM ATP, thrombin, and proteinase K at the end in different buffer M; (D) Added 200 nM AF594 labeled MutH156/MutH85/MutH223 to 200 nM MutL452_AF488 or MutL297_AF488, later successively added 2 mM ATP, thrombin, and proteinase K at the end in different buffer M; (E) Kinetics of adding 200 nM AF594 labeled MutH223 or MutH156 to 200 nM AF488 labeled MutL297, and later successively added 2 mM ATP, 2 μ M wtMutH, and thrombin in buffer M.

2, MutH wreaking MutL inter-dimer interaction on GT932 circular DNA

Consistent with Chapter 3 part 1, MutL loaded faster when MutS449/D835R matured on G: T mismatch-containing GT932 DNA, the extra FRET over subunit exchange is due to MutL conformational changes and MutL multiple loading for both MutL297_AF488AF594 (NTD-NTD) and MutL452_AF488/MutL297_AF594 (NTD-CTD) interactions (Figure 3). However, when added 200 nM MutH to preloaded MutL297_AF488AF594 (NTD-NTD) hetero-dimer and MutL452_AF488/MutL297_AF594 (NTD-CTD) hetero-dimers on 5 nM GT932 circular

mismatch-containing DNA could induce the kinetics slowly decreased with the rate of $0.036 \pm 0.005 \text{ min}^{-1}$ for both the EfA of MutL NTD-NTD hetero-dimers and the EfA of MutL NTD-CTD hetero-dimers (Figure 3 A and C). Nevertheless, no observation for the BR FRET decrease during these processes, especially for the BR FRET between MutL452_AF488/MutL297_AF594 hetero-dimers and SB stained GT932 DNA (Figure 3 B and D).

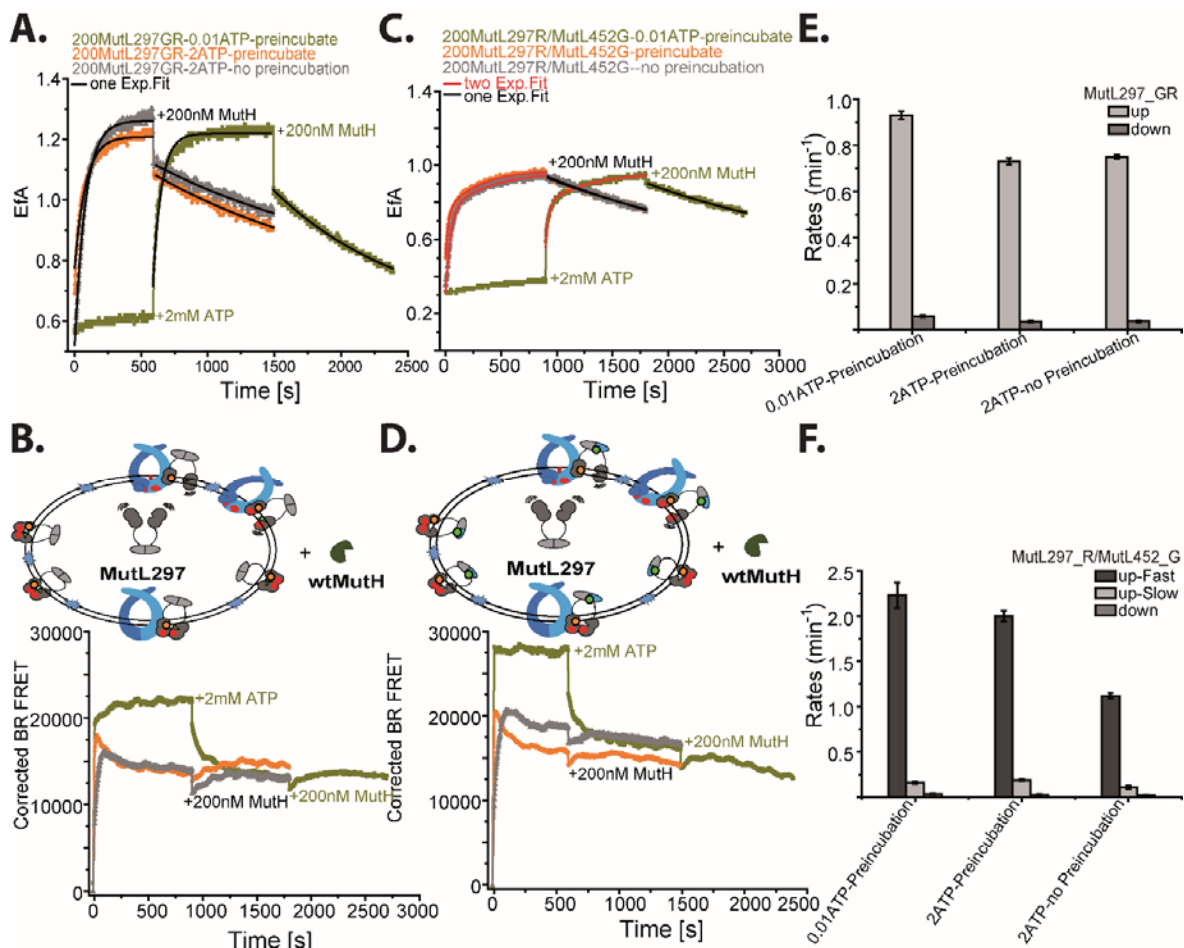


Figure 3 MutH effect to MutL NTD-NTD and NTD-CTD subunit interaction in the presence of MutS, GT932 DNA, and ATP. (A and B) 200 nM unlabeled MutH156 effects 200 nM MutL297_AF488AF594 hetero-dimer subunit interaction and interaction with 5 nM GT932 DNA in the presence 200 nM MutS449/D835R and 2 mM ATP in buffer M; (C and D) 200 nM unlabeled MutH156 effects 200 nM MutL452_AF488/MutL297_AF594 hetero-dimers subunit interaction and interaction with 5 nM GT932 DNA in the presence 200 nM MutS449/D835R and 2 mM ATP in buffer M; (E) The rates of MutL297_GR EfA increase and decrease kinetics; (F) the rates of MutL297_R/MutL452_G EfA kinetics.

Moreover, no noticeable change for both the EfA and the BR FRET observed when added 100 nM wtMutH to 200 nM MutL297_AF488AF594 incubated with 2 mM ATP, 100 nM GT100DF DNA, and tetrameric 200 nM wtMutS or dimeric MutS449/D835R in buffer M (Figure 10 H and I). Then, we investigated the interaction between MutL297_AF488 or MutL297N33A_AF488 (ATP binding deficient mutant), and MutH156_AF594 or MutH77_AF594 (nicking deficient mutant) which

labeled at residue of 85 in buffer M (Figure 4). We could observe that MutH156_AF594 interact with MutL297_AF488 in the absence of ATP, MutS, and GT932 DNA (Figure 4 A and B, olive). Even the ATP binding deficient mutant Mutl297N33A_AF488 interact with MutH156_AF594 immediately as well (Figure 4 A and B, orange). After adding ATP induced the GR FRET immediately decreased for both MutL297_AF488 and Mutl297N33A_AF488, while the EfA slowly increased between MutH156_AF594 and MutL297_AF488 but the EfA continuously reduced almost back to the starting value between MutH156_AF594 and Mutl297N33A_AF488 after adding 10 nM GT932 DNA to the system (Figure 4 A).

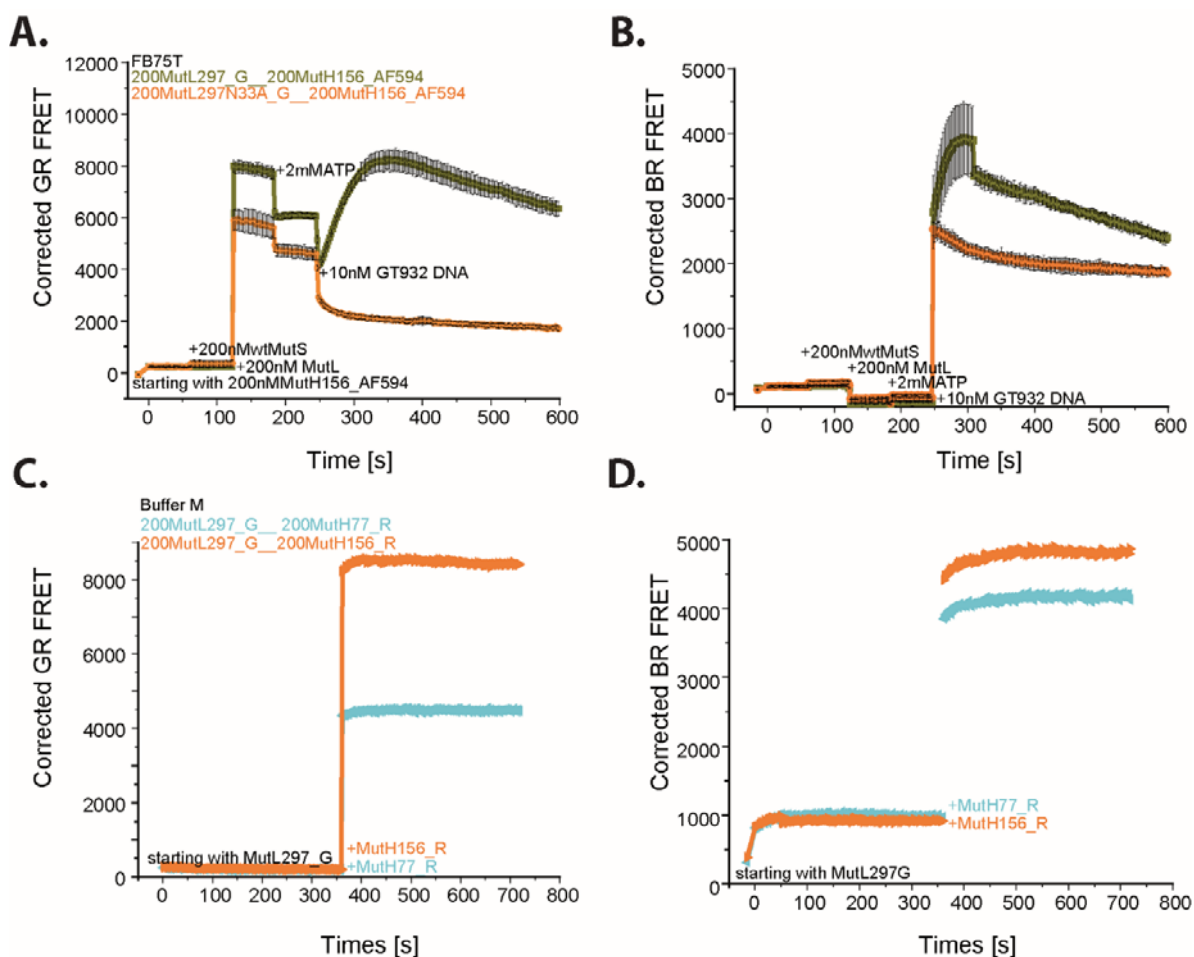


Figure 4 AF488 (G) labeled MutL interacting with AF594 (R) labeled MutH in presence of DNA, ATP and MutS (A and B) the interaction kinetics of the effect of 200 nM wtMutS, 2 mM ATP and 10 nM GT932 DNA to 200 nM MutH156_AF594 interact with 200 nM MutL297_AF488 or Mutl297N33A_AF488 (GR) and interact with DNA (BR) in FB75T buffer; (C and D) the interaction kinetics between 200 nM MutH156_AF594 or MutH77_AF594 and 200 nM MutL297_AF488 (GR FRET) with pre-interact with 200 nM wtMutS, 2 mM ATP and 10 nM GT932 DNA (BR FRET) in buffer M.

Even though the GR FRET increased slowly after adding 10 nM GT932 mismatch-containing DNA, the BR FRET between MutH156_AF594 to SB stained GT932 DNA dramatically increased

then slightly and gradually decreased (Figure 4 A and B). Whereas, both the GR FRET and the BR FRET increased immediately after added 200 nM MutH156_AF594 or MutH77_AF594 (DNA nicking deficient mutant, labeled at residue 85) to 200 nM MutL297_AF488 in the presence of 10 nM GT932 DNA, 200 nM wtMutS, and 2 m ATP (Figure 4 C and D). Even though the amplitude of the GR FRET between MutH77_AF594 and MutL297_AF488 is only half of the amplitude of the GR FRET between MutH156_AF594 and MutL297_AF488, the BR FRET are similar (Figure 4 C-D).

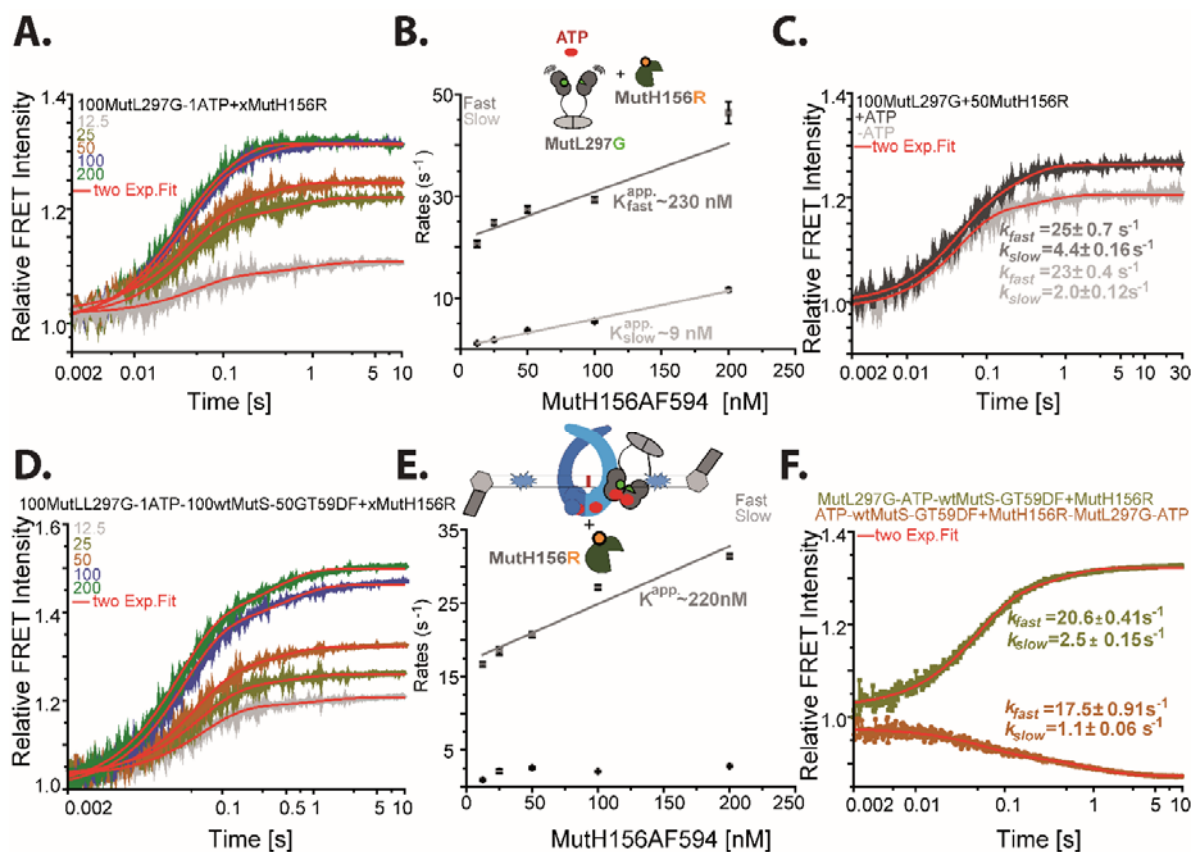


Figure 5 the kinetics and KD value between MutH156_AF594 (G) and MutL297_AF488 (R) in the absence or presence of GT59DF-wtMutS-ATP (A) Kinetics of added 12.5-200 nM MutH156_AF594 to 100 nM MutL297_AF488 incubate with 1 mM ATP in FB75T buffer; (B) the fast and slow rates derived from A; (C) Kinetics of added 50 nM MutH156_AF594 to 100 nM MutL297_AF488 with/without incubate with 1 mM ATP in FB75T buffer; (D) Kinetics of added 12.5-200 nM MutH156_AF594 to 100 nM MutL297_AF488 incubate with 1mM ATP, 50nM GT59DF DNA and 100 nM wtMutS in FB75T buffer; (E) the fast and slow rate derived from D.; (F) the green line kinetic is added 50 nM MutH156_AF594 to 100 nM MutL297_AF488 incubate with 1 mM ATP, 50 nM GT59DF DNA and 100 nM wtMutS in FB75T buffer, while the brown line kinetics is added pre-incubated 1 mM ATP, 50 nM GT59DF DNA and 100 nM wtMutS to 50 nM MutH156_AF594-100 nM MutL297_AF488 complex in FB75T buffer. Then use two exponential fit to analyze all kinetics above.

3, Highly dynamic with lower affinity

As we described above, MutL and MutH interact immediately when mixed together. Hence the AF594 labeled MutH mutants could be loaded on mismatch-containing DNA immediately by MutL as well. Owing to about 20 s dead time for TECAN instrument cannot overcome, so we use stopped-flow which dead time only 0.002 s to investigate MutL and MutH interaction in this part. All the kinetics were observed heading up immediately and reach the saturation within 0.1 s after added 12.5-200 nM MutH156_AF594 to 100 nM MutL297_AF488 which incubated with 1 mM ATP in buffer FB75T, and the amplitudes reach the saturation at 100 nM (Figure 5 A). The fast and slow rates derived from analyzing all kinetics with double exponential fits (Figure 5 A) which are shown at Figure 5 B. Fitting the rates of different concentrations of MutL with linear fit, we derived that the apparent affinity between MutH and MutL are around 225 nM and 9 nM separately for the fast and the slow phases (Figure 5 B). Even though the fast binding rates are the same, the slow rate is only half when compared the kinetics of 50 nM MutL297_AF488 and 50 nM MutH156_AF594 interaction in the absence of ATP with in the presence of ATP (Figure 5 C). However, the total relative amplitudes smaller as well in the absence of ATP (Figure 5 C).

Nevertheless, the apparent affinity between MutH156_AF594 to MutL297_AF488 is around 216 nM, and no second apparent affinity observed in the presence of 100 nM wtMutS and 50 nM GT59DF DNA in buffer FB75T (Figure 5 D and E). Besides, the binding kinetics reached the saturation within 0.1 s at lower concentration and reached the saturation at 1 s at higher concentration (Figure 5 E). However, the GR FRET kinetics goes down with rates of $17.5 \pm 0.91 \text{ s}^{-1}$ and $1.1 \pm 0.06 \text{ s}^{-1}$ when pre-incubated 50 nM MutH156_AF594, 100 nM MutL297_AF488, and 0.5 mM ATP with 100 nM wtMutS-50 nM GT59DF DNA-0.5 mM ATP complexes together (Figure 5 F, brown). While the GR FRET kinetics heading up with rates of $20.6 \pm 0.41 \text{ s}^{-1}$ and $2.5 \pm 0.15 \text{ s}^{-1}$ when adding 50 nM MutH156_AF594 to 100 nM MutL297_AF488-100 nM-wtMutS-50 nM-GT59DF DNA-1 mM-ATP complexes (Figure 5 F). The apparent KD value between MutH156_AF594 and ATP binding deficient mutant MutL297N33A_AF488 is around 200 nM for the fast phases as well, and 60 nM for the slow phase (Figure 6 A and B). Noticeable the amplitudes of the kinetics between MutH156_AF594 and MutL297N33A_AF488 are only half of the kinetics between MutH156_AF594 and MutL297_AF488 (Figure 5 A and Figure 6 A).

However, the apparent affinity between MutH156_AF594 and 100 nM MutL297N33A_AF488-100 nM wtMutS-50 nM GT59DF DNA-1 mM ATP complexes was almost 2 fold lower (KD ~ 486 nM) (Figure 6, C and D) compared to the apparent affinity both for MutH156_AF594 and 100 nM

MutL297_AF488 (Figure 5, D and F), and MutH156_AF594 and 100 nM MutL297N33A_AF488 (Figure 6, A and B) without wtMutS and GT59DF DNA in FB75T buffer. As the kinetics shown, both the GR FRET and the BR FRET immediately decreased without kinetics could be observed after adding 1.6 μ M wtMutH to 200 nM MutL297_AF488- 100 nM MutH77_AF594 complexes in the presence of 1 mM ATP, 200 nM wtMutS, and 5 nM GT932 DNA (Figure 7 C and D). As well as the GR FRET and the BR FRET between 50 nM MutL297_AF488 or MutL452_AF488 in the presence of 25 nM MutH77_AF594, 1 mM ATP, 50 nM wtMutS and 100 nM GT59DF DNA (Figure 7 E and F). Besides, the BR FRET disappeared completely, while around 20 % of the GR FRET exist after titration 100-2000 nM wtMutH to 200 nM MutL452_AF488 incubated with 100 nM MutH156 AF594 in the presence of 100 nM GT59DF DNA, 200 nM wtMutS, and 20 μ M mant-ATP (Figure 7 I). However, when added 2 μ M wtMutL to 100 nM MutH77_AF594 incubated with 200 nM MutL452_AF488, 5 nM GT932 DNA, 200 nM wtMutS and 1 mM ATP in FB75T buffer induced the BR FRET increased while the GR FRET decreased (Figure 7 G and H). In conclusion, MutL and MutH interaction with low apparent affinity (\sim 200 nM), and 2 fold lower when MutH loaded on mismatch-containing DNA by MutL which NTD may not be closed.

4, Out-of-Step recruited MutL and MutH on DNA

As described above, the GR FRET between MutH156_AF594 and MutL297_AF488 only increased slightly, while BR FRET (MutH156_AF594 to SB stained GT932 DNA) increased immediately when incubating MutL297_AF488 with MutH156_AF594, wtMutS and ATP then encountered

GT932 mismatch-containing circular DNA in the 50 s (Figure 4 A and B). Besides, the GR FRET goes down when MutH156_AF594-MutL297_AF488 complexes encountered wtMutS-GT59DF-ATP complexes (Figure 5 F). Therefore, if MutH and MutL loading on mismatch-containing DNA together is a critical point for all these observations. Another critical point is the GR FRET between MutH and MutL decreased almost back to the background (Figure 4 A, orange) while the BR FRET between MutH and DNA dramatically increased to the similar level as MutL297_AF488 (Figure 4 B, orange) when added 10 nM GT932 DNA to MutL297N33A_AF488- MutH156_AF594-wtMutS-ATP complexes. From this point, we cannot help thinking that if MutH interact with MutL CTD and DNA when encountered MutL which opened NTD on DNA?

As we know from Chapter 3 and Chapter 4, MutL cannot bind mant-ATP while MutS could utilize mant-ATP load MutL on DNA. Therefore, 20 μ M mant-ATP was added to 200 nM MutL297_AF488 or MutL452_AF488 incubated with 100 nM MutH156_AF594, 200 nM wtMutS and 100

nM GT59DF DNA in FB75T buffer. From Figure 7 A and B, we could observe that the GR FRET is slowly decreased while the BR FRET increased after adding 20 μ M mant-ATP, and the GR and BR FRET continuously increased after adding 2 mM ATP. However, the GR FRET between MutL452_AF488 and MutH156_AF594 firstly decreased then increased (Figure 8 G and H), while the GR FRET between MutL297_AF488 and MutH156_AF594 decreased and only slightly turn over in 50 s (Figure 8 A and B).

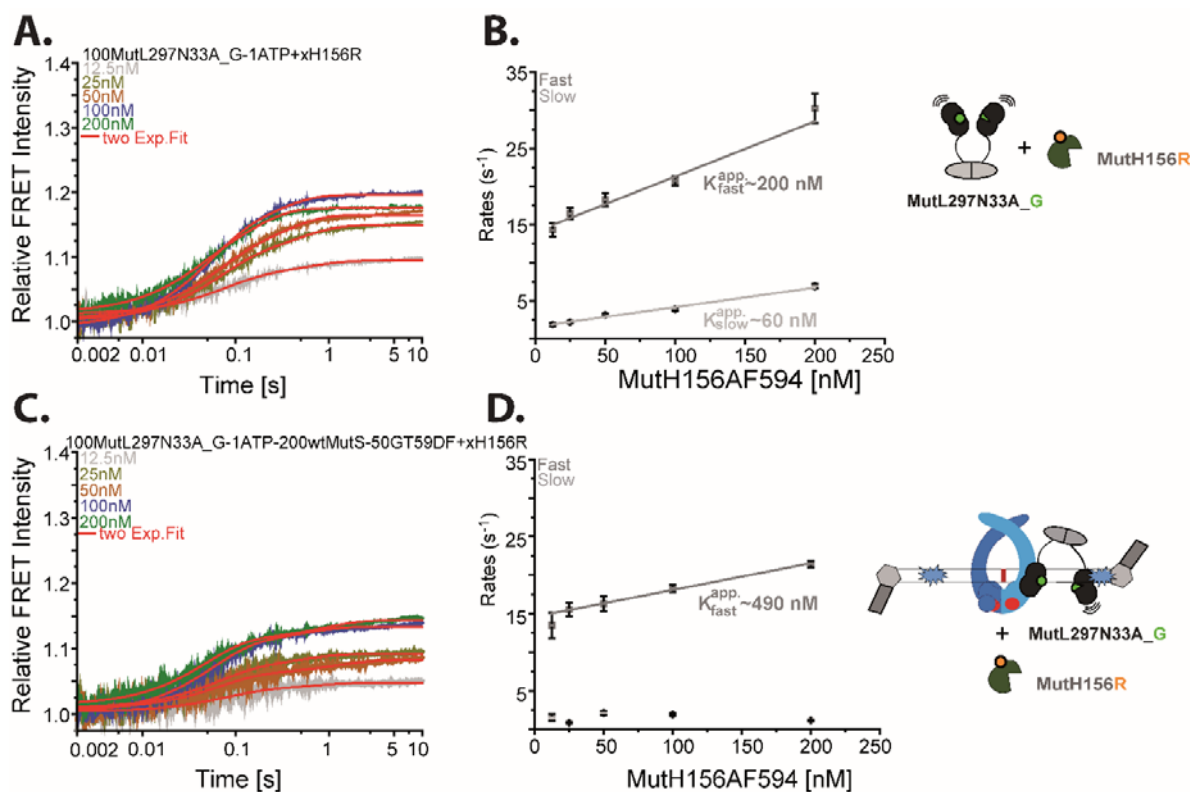


Figure 6 the kinetics and KD value between MutH-156_AF594 and MutL297-N33A_AF488 in the absence or presence of GT59DF DNA-wtMutS-ATP (A) Kinetics of added 12.5-200 nM MutH156_AF594 to 100 nM MutL297N33A_AF488 incubate with 1 mM ATP in FB75T buffer; (B) the fast and slow rates derived from A; (C) Kinetics of added 12.5-200 nM MutH156_AF594 to 100 nM MutL297N33A_AF488 incubate with 1 mM ATP, 50 nM GT59DF DNA and 100 nM wtMutS in FB75T buffer; (D) the fast and slow rate derived from C. Then use two exponential fits to analyze all kinetics above, and the concentration describe here is the final concentration.

Even though the BR FRET for both increased immediately when added 10 μ M ATP to 200 nM MutL297_AF488 or MutL452_AF488 incubated with 100 nM MutH156_AF594, 200 nM wtMutS, and 100 nM GT59DF DNA in buffer FB75T to start the reaction (Figure 8 A, B, G, and H). Moreover, after adding 2 mM ATP, the GR FRET between MutL297_AF488 and MutH156_AF594 increased greatly but almost stay no change for the GR FRET between MutL452_AF488 and MutH156_AF594 (Figure 8, A and G). And the BR FRET for both were continuously increased (Figure 8 B and H). Besides, the GR FRET decreased slowly between MutH156_AF594 and

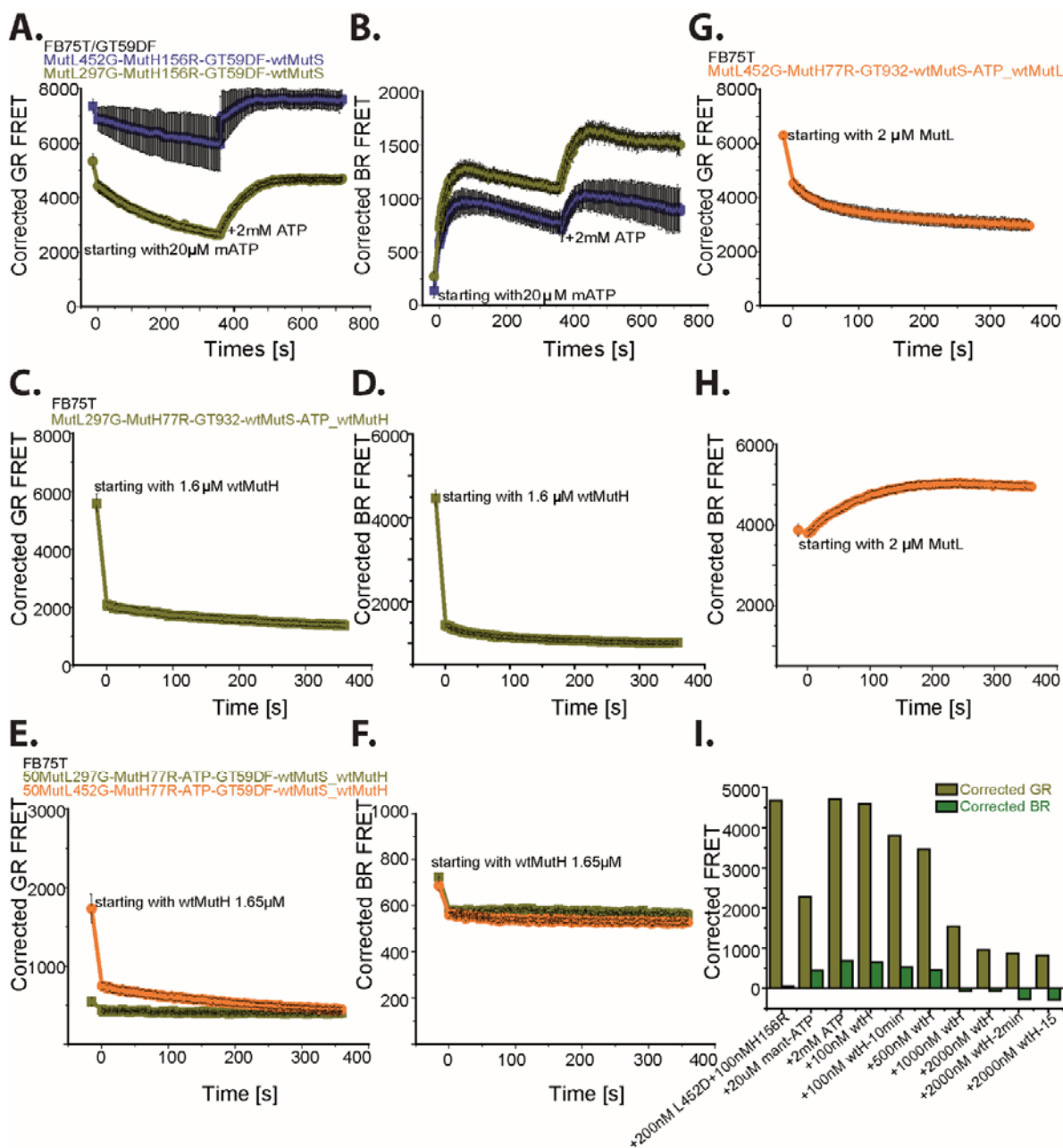


Figure 7 the interaction between AF594 (R) labeled MutH with AF488 (G) labeled MutL NTD or CTD (A and B) added 20 μ M mant-ATP (m-ATP) to pre-incubated 200 nM MutL452_AF488 and 100 nM MutH156_AF594 in the presence of 100 nM GT59DF DNA and 200 nM wtMutS in FB75T buffer, and later added 2 mM ATP; (C and D) 1.65 μ M wtMutH was added to 100 nM MutH77_AF594 pre-incubated with 200 nM MutL297_AF488 in the presence of 5 nM GT932 DNA, 200 nM wtMutS and 1 mM ATP; (E and F) 1.65 μ M wtMutH was added to 25 nM MutH77_AF594 pre-incubated with 50 nM MutL297_AF488 in the presence of 100 nM GT59DF DNA, 50 nM wtMutS and 1 mM ATP; (G and H) 2 μ M wtMutL was added to 100 nM MutH77_AF594 pre-incubated with 200 nM MutL452_AF488 in the presence of 5 nM GT932 DNA, 200 nM wtMutS and 1 mM ATP. BR FRET is the FRET between MutH and SB stained DNA, while the GR FRET is the FRET between MutH and MutL; (I) The reaction started with 2 mM ATP after pre-incubated 200 nM MutH156_AF594 with 200 nM MutL452_AF488 in the presence of 100 nM GT59DF DNA, 200 nM wtMutS in buffer FB75T and later titration 100-2000 nM wtMutH.

MutL297N33A_AF488 (ATP binding deficient mutant) or MutL297E29A_AF488 (ATP hydrolysis-deficient mutant), while the BR FRET immediately increased to the same level as with wildtype MutL297_AF488 (Figure 8 C-F). However, the BR FRET between MutH156_AF594 and SB stained GT59DF DNA slightly increased after adding 2 mM ATP (Figure 8, D and F), the GR FRET between MutH156_AF594 and MutL297N33A_AF488 continuously decreased (Figure 8, C) while the GR FRET between MutH156_AF594 and MutL297E29A_AF488 slowly and obviously increased (Figure 8, E).

Moreover, the GR FRET between MutH_AF594 and MutL297_AF488 dramatically and kinetically increased then turnover, that's similar as the BR FRET which reaches the highest FRET intensity immediately when starting the reaction in the presence of 200 nM MutH156_AF594 with 200 nM MutL297_AF488, 10 nM GT932 DNA, and 200 nM wtMutS with 2 mM ATP in buffer FB75T (Figure 9 A and B, olive). Even though the BR FRET behave similarly, while the GR FRET decreased after adding 2 mM ATP to 200 nM MutH156_AF594 incubated with 200 nM MutL297N33A_AF488, 10nM GT932 DNA and 200 nM wtMutS (Figure 9 A and B, orange). Except for the description above, we found that 200 nM MutL297_AF488 loaded 200 nM MutH156_AF594 on 10 nM GT932 in the presence of 200 nM wtMutS and ATP in FB75T buffer faster than in buffer M (Figure 9, C and D). Moreover, both the GR and BR FRET decreased after thrombin separated MutL NTD and CTD, while the BR FRET decreases much faster in buffer M (Figure 9 C and D, light green). As usual, the GR FRET decreased while BR FRET increased between MutH156_AF594 and MutL297N33A_AF488 after adding 2 mM ATP starting the reaction in buffer FB75T, and both the GR and BR FRET decreased obviously after thrombin (Figure 9 E and F, green and magenta). Whereas both the GR FRET and BR FRET between MutH156_AF594 and MutL297N33A_AF488 stay no change after added 2 mM ATP to start the reaction in buffer M, but the amplitudes of the GR and BR FRET much lower in buffer M than buffer FB75T (Figure 9 E and F).

Finally, the GR FRET decreased firstly until titrated 2 mM ATP to the system after starting the reaction with 10 μ M ATP when substituted 10 nM GT932 circular DNA with 100 nM GT59DF end blocked oligo DNA (Figure 10 A). While the GR FRET decreased firstly, then turn over and slowly increased when starting the reaction with 2 mM ATP, even though the BR FRET intensity were similar for both (Figure 10 A and B). Different from Appendix Figure 5.4 A and B green kinetics in buffer M, after added thrombin, the GR FRET decreased dramatically while the BR FRET only slightly decreased with 100 nM GT59DF DNA in buffer FB75T (Figure 10 A and B).

Even though the BR FRET were similar, the GR FRET between 200 nM MutH77_AF594 (which deficient in nicking DNA at GATC site) and 200 nM MutL297_AF488 is one fold lower than the GR FRET which used 200 nM MutH156_AF594 instead of MutH77_AF594 in the presence of 200 nM wtMutS, 100 nM GT100DF DNA, and the reaction started with 2 mM ATP in buffer FB75T

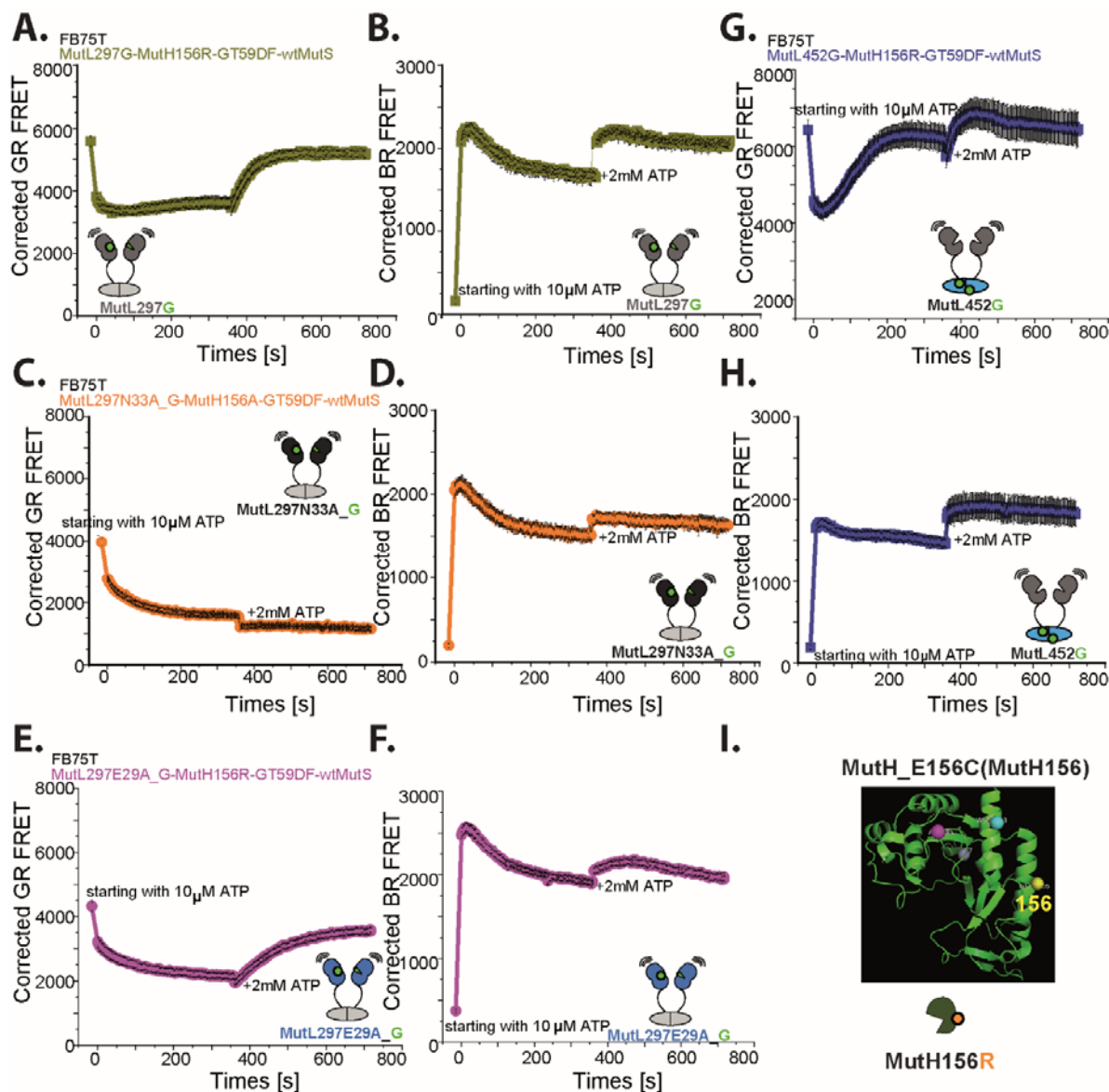


Figure 8 the interaction between AF594 (R) labeled MutH156 with AF488 (G) labeled different MutL mutants (A and B) added 10 μM ATP to pre-incubated 200 nM MutL297_AF488 and 100 nM MutH156_AF594 in the presence of 100 nM GT59DF DNA and 200 nM wtMutS in FB75T buffer, and later added 2 mM ATP; (C and D) added 10 μM ATP to pre-incubated 200 nM MutL297N33A_AF488 (ATP binding deficient mutant) and 100 nM MutH156_AF594 in the presence of 100 nM GT59DF DNA and 200 nM wtMutS in FB75T buffer, and later added 2 mM ATP; (E and F) added 10 μM ATP to pre-incubated 200 nM MutL297E29A_AF488 (ATP hydrolysis deficient mutant) and 100 nM MutH156_AF594 in the presence of 100 nM GT59DF DNA and 200 nM wtMutS in FB75T buffer, and later added 2 mM ATP; (G and H) added 10 μM ATP to pre-incubated 200 nM MutL452_AF488 and 100 nM MutH156_AF594 in the presence of 100 nM GT59DF DNA and 200 nM wtMutS in FB75T buffer, and later added 2 mM ATP. The BR FRET is the FRET between MutH and SB stained DNA, while the GR FRET is the FRET between MutH and MutL.

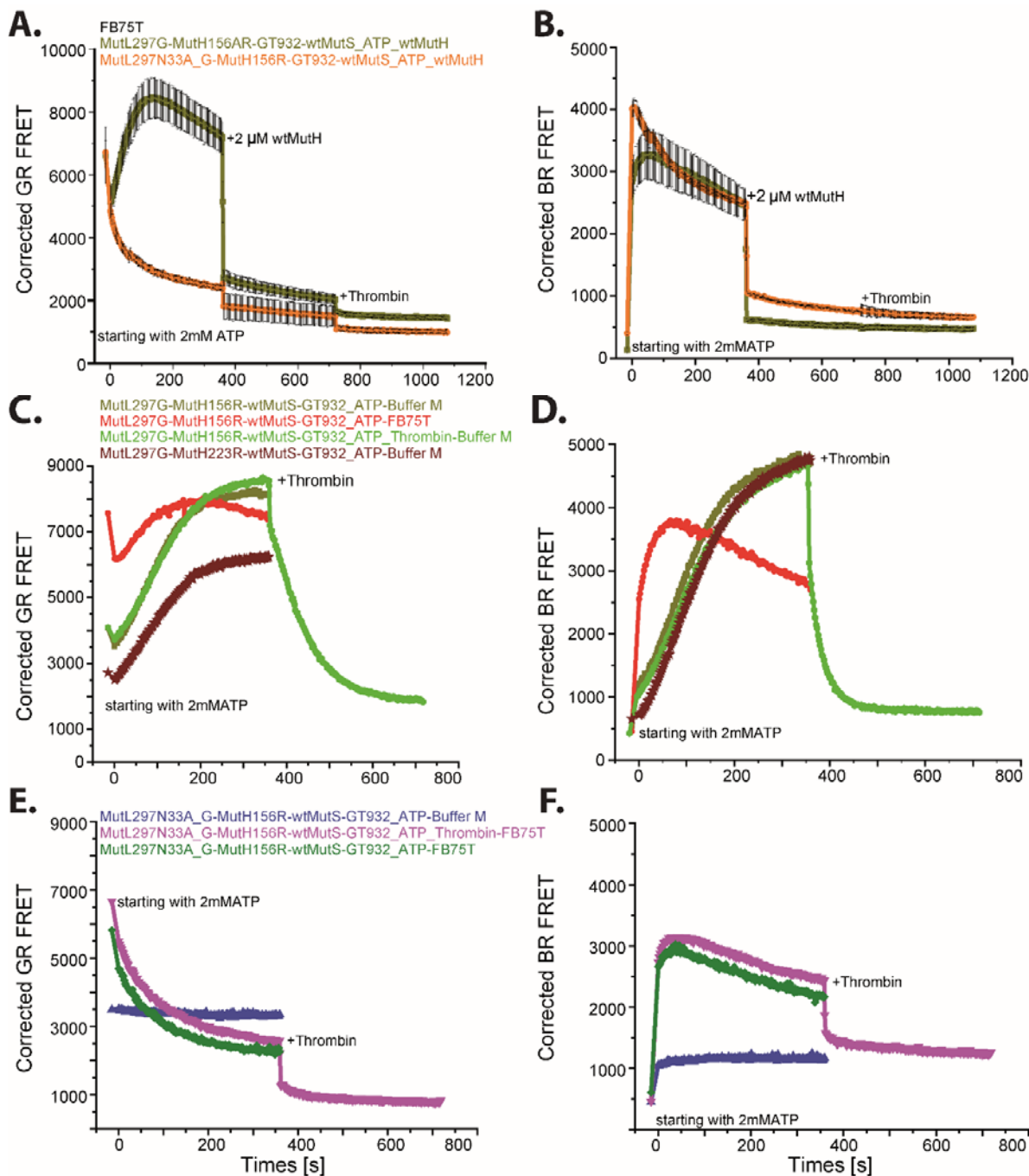


Figure 9 Different buffer effect to the interaction between MutH and MutL. (A and B) the reaction started with 2 mM ATP after pre-incubated 200 nM MutH156_AF594 with 200 nM MutL297_AF488 or MutL297N33A_AF488 in the presence of 10 nM GT932 DNA, 200 nM wtMutS and 2 μ M wtMutH and Thrombin in buffer FB75T; (C and D) The reaction started with 2 mM ATP after pre-incubated 200 nM MutH156_AF594 with 200 nM MutL297_AF488 in the presence of 100 nM GT100DF DNA, 200 nM wtMutS in different buffer. The FRET is the FRET between MutH and SB stained DNA, while the GR FRET is FRET between MutL and MutH.

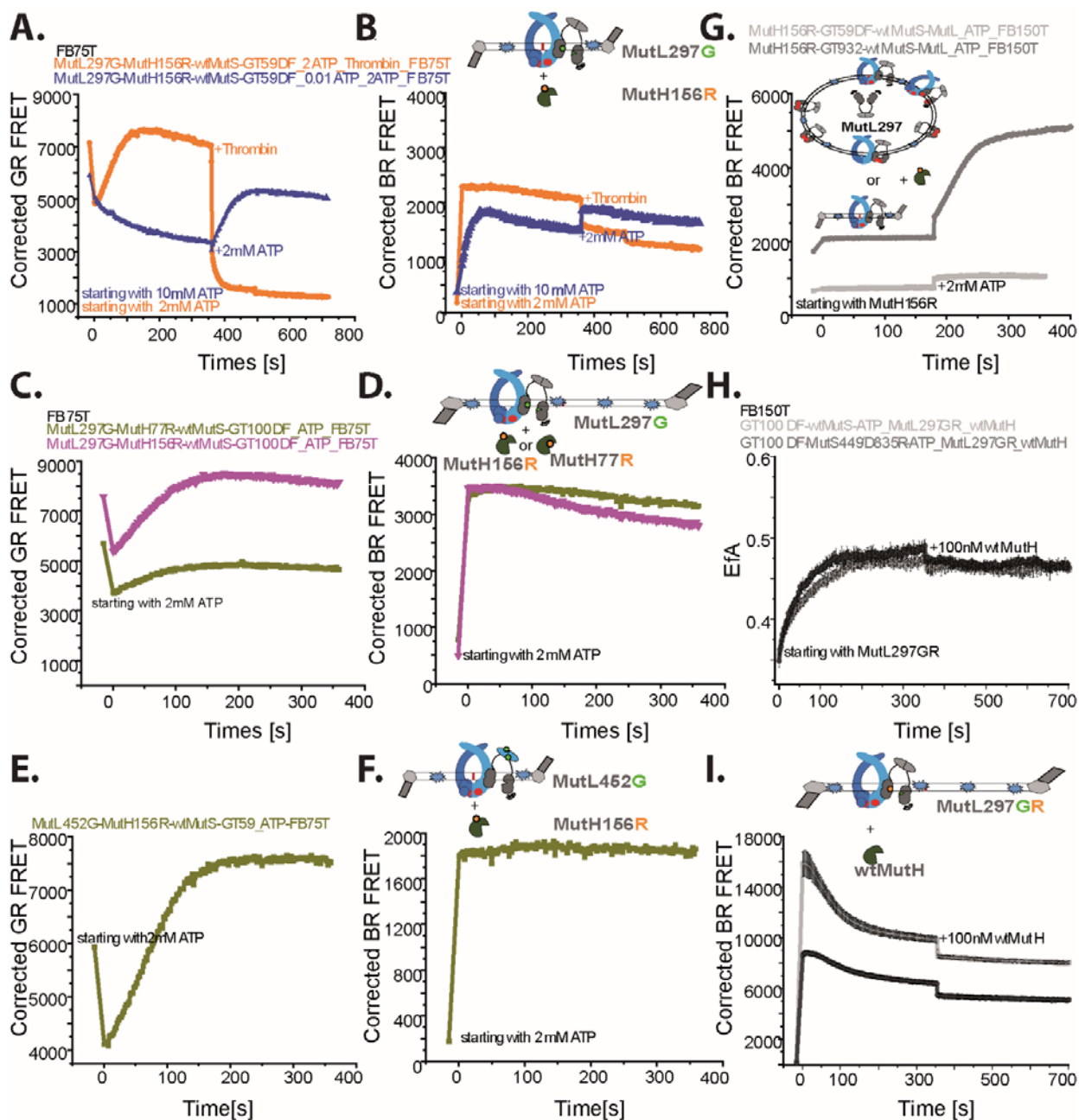


Figure 10 Different MutS and low high ATP effect to the interaction between MutL and MutH (A and B) The reaction started 200 nM MutL297_AF488AF594 after pre-incubated 2 mM ATP, 100 nM GT100DF DNA, 200 nM wtMutS or MutS449/D835R in FB75T; (C and D) the reaction started with 2 mM ATP after pre-incubated 200 nM MutH77_AF594 with 200 nM MutL297_AF488 in the presence of 100 nM GT100DF DNA, 200 nM wtMutS in buffer FB75T; (E and F) the reaction started with 2 mM or 10 μ M ATP after pre-incubated 200 nM MutH156_AF594 with 200 nM MutL297_AF488 in the presence of 100 nM GT59DF DNA, 200 nM wtMutS in buffer FB75T and added 2 mM ATP or Thrombin into the reaction; (G) the reaction started with 100 nM MutH156_AF594 after pre-incubated 200 nM MutL297 with 10 nM GT932 DNA/or 100 nM GT59DF DNA and 200 nM wtMutS in FB150T buffer and later added 2 mM ATP; (H and I) the reaction started with 2 mM ATP after pre-incubated 200 nM MutH156_AF594 with 200 nM MutL452_AF488 in the presence of 100 nM GT59DF DNA, 200 nM wtMutS in buffer FB150T. The BR FRET is the FRET between MutH and SB stained DNA, while the GR FRET is the FRET between MutH and MutL.

(Figure 10 C and D). Both the GR and the BR FRET between 200 nM MutH156_AF594 and 200 nM MutL452_AF488 in the presence of 200 nM wtMutS, 100nM GT100DF DNA, and starting with 2 mM ATP in buffer FB75T behave similar as with 200 nM MutL297_AF488 in FB75T buffer (Figure 10 E and F). Compared Figure 9 to Figure 10, we could find that the BR FRET between 200 nM MutH156_AF594 and MutL297_AF488 was higher with 10 nM GT932 circular DNA than with 100 nM GT100DF or GT59DF DNA in FB75T buffer. Moreover, the orange kinetics in Figure 10 C and D shows that the GR FRET decreased dramatically while the BR FRET only slightly reduced after thrombin was added. In order to avoid MutH interact with GT932 DNA or GT59DF DNA directly (without loaded by MutL), we investigated 100 nM MutH156_AF594 loaded on 10 nM GT932 circular DNA or 100 nM GT59DF DNA in buffer FB150T. From Figure 10 G, we could observe that the BR FRET between MutH156_AF594 and GT932 DNA or GT59DF DNA have no significant change observed compared to the starting value in the absence of ATP. After adding 2 mM ATP, the BR FRET between MutH156_AF594 and GT59DF DNA only slightly increased (but no kinetics observed), while the BR FRET between MutH156_AF594 and GT932 DNA dramatically (~ 10 fold relative change) and kinetically increased (Figure 10 G).

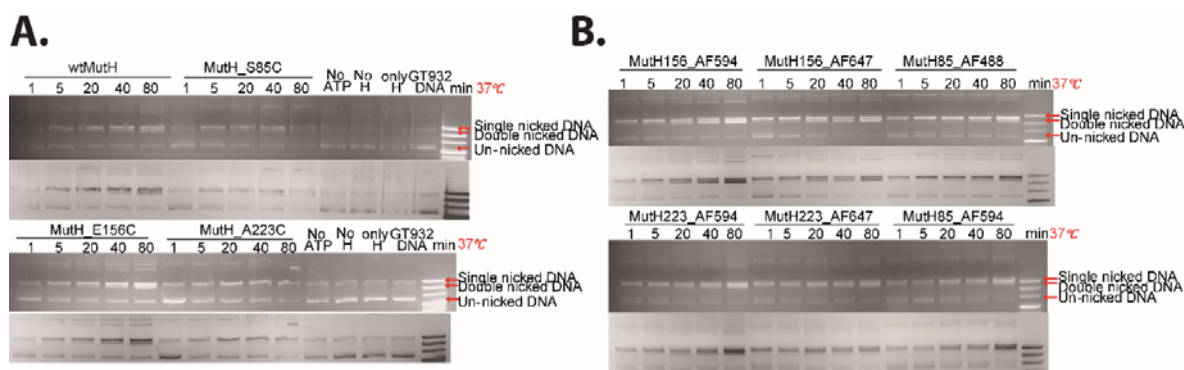


Figure 11 The Activity of wtMutH and labeled or un-labeled different MutH mutants. (A) Pre-incubated 200 nM wtMutL, 200 nM MutS449/D835R, 1 mM ATP and 10 nM GT932 DNA in buffer M at 37 °C for 10 min and start the reaction with 100 nM wtMutH, MutH_S85C (MutH85), MutH_E156C (MutH156) or MutH_A223C (MutH223) for 1-80 min then stopped the reaction with proteinase K; (B) Pre-incubated 200 nM wtMutL, 200 nM MutS449/D835R, 1 mM ATP and 10 nM GT932 DNA in buffer M at 37 °C for 10 min and start the reaction with 100 nM AF594, AF488 or AF647 labeled MutH_S85C (MutH85), MutH_E156C (MutH156) or MutH_A223C (MutH223) for 1-80 min then stopped the reaction with proteinase K.

Discussion

MutL and MutH ternary structure formation have been studied with methods of yeast two-hybrid (Hall and Matson 1999), affinity co-purification (Spampinato and Modrich 2000), and site-specific

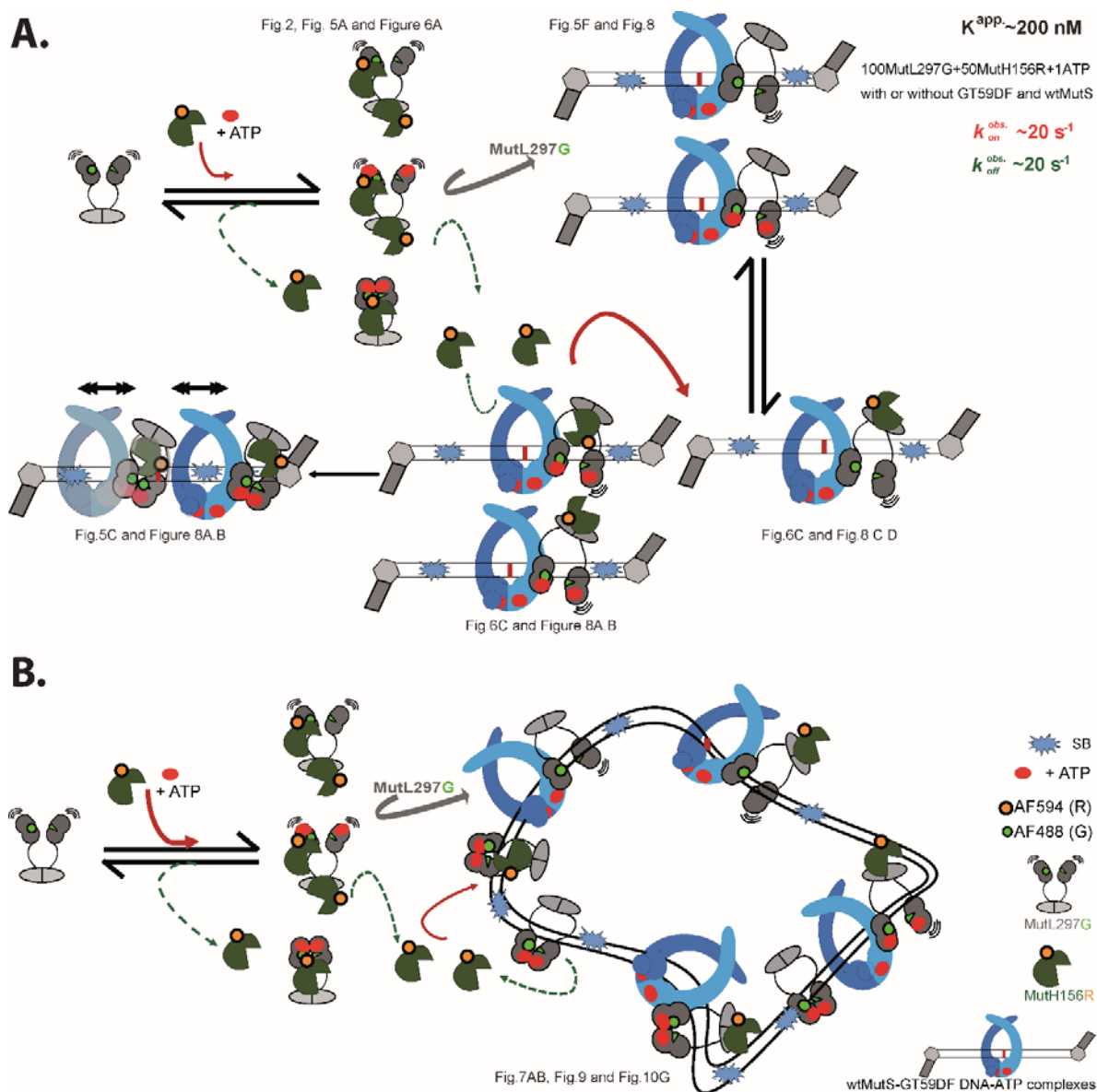


Figure 12 Cartoons depicted MutL297_AF488 (G) and MutH156_AF594 (R) interaction (A) MutL297_AF488 (G) and MutH156_AF594 (R) interaction in the presence of wtMutS, ATP, and GT59DF DNA; (B) MutL297_AF488 (G) and MutH156_AF594 (R) interaction in the presence of wtMutS, ATP, and GT932 nano-circular DNA.

photo-cross-linking and cross-linking combined mass spectrometry (Toedt, Krishnan et al. 2003, Giron-Monzon, Manelyte et al. 2004, Ahrends, Kosinski et al. 2006). Moreover, the MutH only binds clamped MutL which enhanced its DNA association rates more than 1000 fold and activated its endonuclease accurately introduce a scission into a transiently hemi-methylated newly synthesized daughter strand DNA at GATC site (Liu, Hanne, et al. 2016). As it was shown in Figure 11 and Appendix Figure 5.3, site-specific modified MutH156 did not affect its endonuclease activity. That is consistent with the literature (Toedt, Krishnan, et al. 2003). So we use endonuclease

activity-deficient mutant MutH77 (Toedt, Krishnan, et al. 2003) to control the interaction between MutH and MutL, in case the changes are caused by MutH nicking the GATC site containing DNA (GT59DF or GT932, Figure 4 C and D, Figure 7 C and Figure 10 C). Beyond all these control experiments, we found that MutL and MutH interaction is independent of MutS, G: T mismatch-containing and GATC site containing DNA, and ATP (Figure 1 and Figure 2). Besides, one MutL dimer seems bound more than one molecule of MutH which observed by other groups with gel mobility shift assay (Joseph, Sawarkar, et al. 2004). MutH induced MutL297_GR and MutL452_GR EfA slowly decrease, while no change to the BR FRET indicated that MutL undergoes conformational changes after encountering MutH (Figure 3). Mixed MutH156_AF594 with donor labeled MutL (MutL297 or MutL297N33A) indicated that MutL and MutH interaction with very fast association and dissociation rates ($\sim 20 \text{ s}^{-1}$) (Figure 5 and Figure 6). While the affinity is rather low $\sim 200 \text{ nM}$ for wild-type MutL297 in the absence or presence of wtMutS-ATP-GT59DF DNA, and even lower $\sim 500 \text{ nM}$ for ATP binding deficient mutant MutL297N33A in the presence of wtMutS-ATP-GT59DF DNA (Figure 5 and Figure 6). This low affinity is indirectly supported by the micro molar range affinity for MutH to DNA in the absence/presence of MutL (Wu, Loh et al. 2002).

The GR FRET between MutL and MutH decreased after adding $10 \mu\text{M}$ ATP to the pre-incubated MutH56_R and MutL297N33A_G (ATP binding deficient) complexes, or MutH56_R and MutL297E29A_G (ATP hydrolysis deficient) complexes (Guarne, Ramon-Maiques et al. 2004, Robertson, Pattishall et al. 2006) in the presence of wtMutS and GT59DF DNA (Figure 8 A-F). While the BR FRET between MutH156_R and SB stained, GT59DF DNA reached the top value and slowly reduced and reach the saturation later (Figure 8 A-F). However, the GR kinetics of adding $10 \mu\text{M}$ ATP to pre-incubated MutH56_R and MutL452_G complexes decreased firstly then turnover back to the starting value, while the BR reach the same level as NTD labeled MutL (Figure 8 G and H). Therefore, we could conclude that with NTD opened MutL could load MutH close to DNA as well. One of reasons for cannot activate MutH endonuclease activity due to its bind between DNA and MutL CTD, or hang on MutL CTD near the DNA. That means without dimerized at NTD, MutL only bring MutH near the DNA instead of tightly interacting with DNA. Titrating 2 mM ATP into the system induced the GR FRET increased for MutH156_R/MutL297_G complexes, while the GR FRET stay no change for MutH156_R/MutL452_G complexes, and slightly decreased for MutH156_R/MutL297N33A_G complexes, while the BR FRET were similarly for all combinations (Figure 8).

Therefore, we could observed that the interaction between MutH and MutL exist at almost all possible structures of MutL (Figure 12). Nevertheless, MutL and MutH complexes cannot be loaded on GT59DF DNA by MutS at the same time. That's coincidence for both starting the reaction with 10 μ M/2 mM ATP (Figure 8, Figure 9 and Figure 10) and 20 μ M mant-ATP (Figure 7 A and B), as well as the decreased kinetics of mixed wtMutS-GT59DF DNA-ATP clamps with MutH156_R/MutL297_G-ATP complexes which assessed with stopped-flow (Figure 5 F).

MutL could stimulate MutH methyl-directed endonuclease activity more than 60-fold (Joseph, Sawarkar, et al. 2004). Even though MutL297N33A could load MutH156_R close to DNA, which is not sufficient to activate MutH endonuclease activity due to MutL fail to active MutH in the absence of ATP (Joseph, Sawarkar et al. 2004). Therefore, bring MutH close to GATC site-containing G: T mismatch DNA is not sufficient to activate its endonuclease activity. Besides, the dimerized MutL NTD not only bring MutH more tightly interact with DNA but ATP induced MutL conformational changes (as described in chapter 3) may cause the changes of the MutH as well, which is still unclear and need to investigate in future. Even though MutL hydrolysis ATP seems not required, which derived from MutLE29A and non-hydrolysable analog AMPPNP could activate MutH endonuclease activity (Ban and Yang 1998, Junop, Yang, et al. 2003, Robertson, Pattishall, et al. 2006).

Method

Protein Expression and purification

MutL and MutS' purification procedure is the same as we described in Chapter 1. The process for transferring 15 ml pre-culture into 500 ml LB culture containing 100 μ g/ml Ampicillin and incubating at 37 $^{\circ}$ C until OD₆₀₀ to 1.0-1.2, then adding 2 g/L Arabinose (for MutH) into the culture and incubated at 27 $^{\circ}$ C overnight. Recombinant His₆-tagged MutH proteins were purified with Protino® Ni-IDA 2000 packed columns. After that those proteins purified through gel-filtration on a Superdex 200 10/300 GL, Thrombin was added into MutH to cleavage the His₆-tagged. Taking aliquots of 2-6 μ l at various time intervals and running SDS PAGE (15 %) to make sure the remove of is complete. Then, 1 mM PMSF was added into the MutH and MutS separately before loaded into the Superdex 200 10/300 GL again. Finally, MutH proteins were snap-frozen in liquid nitrogen and stored at -80 $^{\circ}$ C in 10 mM HEPES/KOH, 500 mM KCl, 1 mM EDTA, 1 mM DTT, 150 %

glycerol, pH 8.0 concentrations were determined using theoretical extinction coefficients (Toedt, Krishnan et al. 2003, Heinze, Giron-Monzon, et al. 2009, Winkler, Marx, et al. 2011).

MutH activation assay

Pre-incubated 200 nM wtMutL, 200 nM MutS449/D835R, 1 mM ATP and 10 nM GT932 DNA in buffer M at 37 °C for 10 min, then starting the reaction with 100 nM wtMutH, AF488/AF594 /AF647 labeled or unlabeled MutH_S85C (MutH85), MutH_E156C (MutH156) or MutH_A223C (MutH223), 10 µl samples were taken from 1-80 min separately. The reaction was stopped with proteinase K and NEB protein loading dye.

Stopped-flow Fluorescence kinetics

The stopped-flow kinetics were carried out in SF-61SX2 (TgK Scientific, Bradford-on-Avon, UK) apparatus with single mixing mode which is mixing samples in Syringe C and Syringe D with 1:1 ratio and with ~11 ml/s rate at 25 °C. The GR FRET is the FRET between AF488 (G, donor) and AF594 (R, acceptor) labeled proteins (MutL and MutH156) assessed with stopped-flow with ET525/50M and OG 590 filters at 492 nm. The BR FRET is the FRET between AF594 (R, acceptor) labeled MutH156 and SYTOX blue (SB, donor) stained DNA assessed with ET525/50M and OG 590 filters at 436 nm.

Titration

Titration experiments were performed using a TECAN Infinite F200 PRO fluorescence plate reader at room temperature. Titrated 50-1000 nM MutH156_AF594 (R, acceptor) to 200 µl 200 nM MutL452_AF488 (G, donor) in buffer M, after about 10 min, added 2 mM ATP and measure GR FRET with 485 nm (20 nm width) Excitation filter and 620 nm (10 nm width) Emission filter.

While vary MutH156_AF594's concentration from 25 to 400 nM mixed with 200 nM MutL297_AF488 or MutL297N33A_AF488 which incubated with 1 mM ATP in the absence or presence of 100 nM GT59DF DNA and 200 nM wtMutS in the FB75T buffer, the final concentration will dilute to half.

References

- Ahrends, R., J. Kosinski, D. Kirsch, L. Manelyte, L. Giron-Monzon, L. Hummerich, O. Schulz, B. Spengler and P. Friedhoff (2006). "Identifying an interaction site between MutH and the C-terminal domain of MutL by crosslinking, affinity purification, chemical coding and mass spectrometry." *Nucleic Acids Res* 34(10): 3169-3180.
- Ban, C. and W. Yang (1998). "Crystal structure and ATPase activity of MutL: implications for DNA repair and mutagenesis." *Cell* 95(4): 541-552.
- Ban, C. and W. Yang (1998). "Structural basis for MutH activation in *E. coli* mismatch repair and relationship of MutH to restriction endonucleases." *EMBO J.* 17(5): 1526-1534.
- Banasik, M. and P. Sachadyn (2014). "Conserved motifs of MutL proteins." *Mutat Res* 769: 69-79.
- Burdett, V., C. Baitinger, M. Viswanathan, S. T. Lovett and P. Modrich (2001). "In vivo requirement for RecJ, ExoVII, ExoI, and ExoX in methyl-directed mismatch repair." *Proc Natl Acad Sci U S A* 98(12): 6765-6770.
- Fukui, K. (2010). "DNA mismatch repair in eukaryotes and bacteria." *J Nucleic Acids* 2010.
- Giron-Monzon, L., L. Manelyte, R. Ahrends, D. Kirsch, B. Spengler and P. Friedhoff (2004). "Mapping protein-protein interactions between MutL and MutH by cross-linking." *J Biol Chem* 279(47): 49338-49345.
- Guarne, A., S. Ramon-Maiques, E. M. Wolff, R. Ghirlando, X. Hu, J. H. Miller and W. Yang (2004). "Structure of the MutL C-terminal domain: a model of intact MutL and its roles in mismatch repair." *EMBO J* 23(21): 4134-4145.
- Hall, M. C., J. R. Jordan and S. W. Matson (1998). "Evidence for a physical interaction between the *Escherichia coli* methyl- directed mismatch repair proteins MutL and UvrD." *EMBO J* 17(5): 1535-1541.
- Hall, M. C. and S. W. Matson (1999). "The *Escherichia coli* MutL protein physically interacts with MutH and stimulates the MutH-associated endonuclease activity." *J Biol Chem* 274(3): 1306-1312.
- Hsieh, P. and K. Yamane (2008). "DNA mismatch repair: Molecular mechanism, cancer, and ageing." *Mech Ageing Dev* 129(7-8): 391-407.

Joseph, N., R. Sawarkar and D. N. Rao (2004). "DNA mismatch correction in *Haemophilus influenzae*: characterization of MutL, MutH and their interaction." *DNA Repair (Amst)* 3(12): 1561-1577.

Junop, M. S., W. Yang, P. Funchain, W. Clendenin and J. H. Miller (2003). "In vitro and in vivo studies of MutS, MutL and MutH mutants: correlation of mismatch repair and DNA recombination." *DNA Repair (Amst)* 2(4): 387-405.

Liu, J., J. Hanne, B. M. Britton, J. Bennett, D. Kim, J. B. Lee and R. Fishel (2016). "Cascading MutS and MutL sliding clamps control DNA diffusion to activate mismatch repair." *Nature* 539(7630): 583-587.

Polosina, Y. Y. and C. G. Cupples (2010). "Wot the 'L-Does MutL do?" *Mutat Res*.

Robertson, A. B., S. R. Pattishall, E. A. Gibbons and S. W. Matson (2006). "MutL-catalyzed ATP hydrolysis is required at a post-UvrD loading step in methyl-directed mismatch repair." *J Biol Chem* 281(29): 19949-19959.

Spampinato, C. and P. Modrich (2000). "The MutL ATPase Is Required for Mismatch Repair." *J. Biol. Chem.* 275(13): 9861-9869.

Toedt, G. H., R. Krishnan and P. Friedhoff (2003). "Site-specific protein modification to identify the MutL interface of MutH." *Nucleic Acids Res* 31(3): 819-825.

Wu, T. H., T. Loh and M. G. Marinus (2002). "The function of Asp70, Glu77 and Lys79 in the *Escherichia coli* MutH protein." *Nucleic Acids Res* 30(3): 818-822.

Ye, X., P. K. O'Neil, A. N. Foster, M. J. Gajda, J. Kosinski, M. A. Kurowski, J. M. Bujnicki, A. M. Friedman and C. Bailey-Kellogg (2004). "Probabilistic cross-link analysis and experiment planning for high-throughput elucidation of protein structure." *Protein Sci* 13(12): 3298-3313.

Material

1. Table for all Markers, Kits, Columns and Chemical reagents

Categories	Items	Name	Supplier
Markers	Protein markers	Page Ruler Pre-stained protein ladder	ThermoFisher Scientific
		Page Ruler unstained protein ladder	ThermoFisher Scientific
	DNA Markers		ThermoFisher Scientific
			ThermoFisher Scientific
Kits	DNA purification Kits	Wizzard Plus SV Minipreps	Promega
		Wizzard SV Gel and PCR clean-up system	Promega
Columns	Protein Purification	Protino® Ni-IDA 2000 packed columns	MACHEREY-NAGEL
		Superdex 75 10/300 GL	GE Healthcare Life Science
		Superdex 200 10/300 GL	GE Healthcare Life Science
	Protein desalting, Free dye removing and buffer exchanging column	Zeba Desalting spin columns 0.5 ml 40 KDa	Pierce
		Zeba Desalting spin columns 0.5 ml 7KDa	Pierce
	Protein Concentrator	Vivaspin 2 column 10 KDa	GE Healthcare Life Science
		Vivaspin 2 column 20 KDa	GE Healthcare Life Science
	Enzymes	Restriction Enzymes	Nb.BtsI
MboI			
Nt.BspQI			New England Biolabs
Exonuclease I			New England Biolabs
Exonuclease III			New England Biolabs
Reagents		RecJF	New England Biolabs
		Lambda Exonuclease	New England Biolabs
		Phusion-Polymerase	New England Biolabs
		Proteinase K	New England Biolabs
		TaqI-Methyltransferase	New England Biolabs
		T4 Ligase	New England Biolabs
		BSA	New England Biolabs
	Nucleotides	ADP	Sigma
		ATP	Sigma
		ADPnP (AMPPNP)	Jena Bioscience
		ATP γ S	Jena Bioscience
		Mant-ATP	Jena Bioscience
		dNTPs	Roth
		Oligodeoxyribonucleotides	IBA, Eurogentec, and Purimex
	Protein labeling or Containing Dyes	Alexa Fluor R-maleimide	ThermoFisher Scientific
Atto Fluor R-maleimide		Sigma	
InstantBlue		Expedeon	
Coomassie brilliant blue (G250)		AppliChem	

Material

DNA labeling or Staining Dyes	SYTOX blue	ThermoFisher Scientific
	Sybr Green I	
	Ethidium Bromide (BE)	Merck
Antibiotic	Ampicillin	AppliChem
Protein Inhibitor	Benzamidine	Sigma
	PMSF	AppliChem
Chemical Reagents	Acrylamid / BisAcrylamid 40%, 29:1	AppliChem
	Agarose (Ultra PURE™)	AppliChem
	Acetic acid	Roth
	APS	Merck
	Bromphenolblue	Merck
	DMSO	ThermoFisher Scientific
	DTT	AppliChem
	EDTA	Roche
	Ethanol	Roche
	Glycerol	AppliChem
	HEPES	AppliChem
	HCl	Merck
	H ₃ PO ₄	Roth
	Imidazole	AppliChem
	IPTG	Merck
	MgCl ₂	Merck
	K ₂ HPO ₄	Merck
	KH ₂ PO ₄	Merck
	KCl	Roth
	KOH	Merck
	SDS	Roth
	NaCl	Merck
	TCEP	Merck
	TEMED	Merck
	Tris	AppliChem
	Tween 20	Merck and AppliChem
β-Mercaptoethanol		

2. Table for all Oligonucleotides

Name	Length	Sequence	Modification	Applicat ion
MutH GATC1 2 Beacon	36	TGC GGA TCC GGC TTT TTT TTT TTT GCC GGA TCC GCA	5'-HEX 3'-Black Hole Quencher1	MutH activity test
A2-X- Nb.BtsI- R41146	35	AAG CTC GAG CAC TGC TTG CTC CAT TAG CCA GAG CA		GT932/ AT932 nano- circular DNA
A-X- Nb.BtsI- F40236	35	CTC GAG CTT CAC TGC ATC GCA GAA ATC AAA GCT AA		

Material

A-H-Nb.BtsI-F40236	35	CTC AAG CTT CAC TGC ATC GCA GAA ATC AAA GCT AA	generation
G30	30	GGA-TCA-TCG-AGG-ATC-GAG-CTC- GGT-GCA-ATT	GT30 DNA
T30	30	AAT-TGC-ACC-GAG-CTT-GAT-CCT- CGA-TGA-TCC	generation
59G30	59	TGA-AGC-TTA-GCT-TAG-GAT-CAT- CGA-GGA-TCG-AGC-TCG-GTG-CAA- TTC-AGC-GGT-ACC-CAA-TT	GT59D DNA generation
59T29_ DIG2	59	AAT-TGG-GTA-CCG-CTG-AAT-TGC- ACC-GAG-CTT-GAT-CCT-CGA-TGA-TCC- TAA-GCT-AAG-CTT-CA	DIG on

Oligonucleotides were purchased from the companies IBA, Purimex, and Eurogentec.

3. Table for all mismatch repair protein information

Name	Molecular Weight (gM ⁻¹)	Extinction Coefficient (cm ⁻¹ M ⁻¹)	Physical state	Single Cysteine Mutants	Tag	T. sites	Vector	<i>E.coli</i> Strains
MutS	97300	73430	Tetramer / Dimer	R449CD835 R; R449C	His6		pTX 412	HMS174 (λDE3)
MutL	67500	54890	Dimer	H297C, H297CN33A H297CE29A T218C, A282C, N131C, Q4C, Q118C, 489C, 573C, 480C, 452C	His6	376	pTX 418	HMS174 (λDE3)
MutH	28000	37470	Monomer	E156C, A223C, C96S/S85C/ E77A	His6		pMQ 402	XL1Blue MRF'

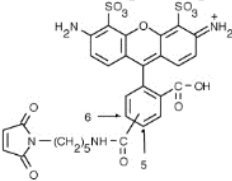
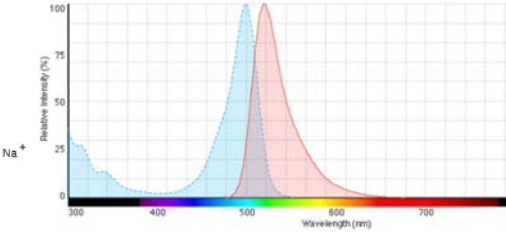
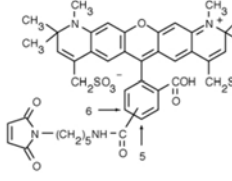
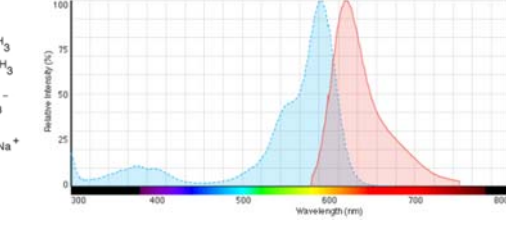
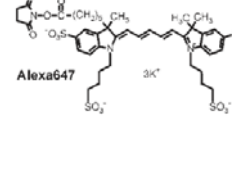
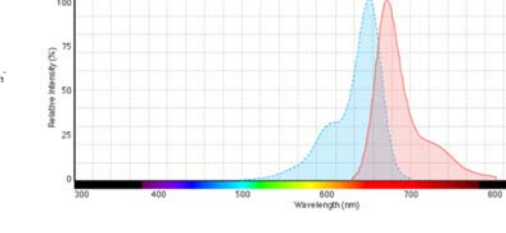
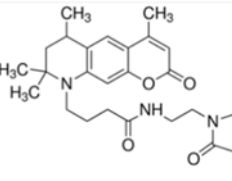
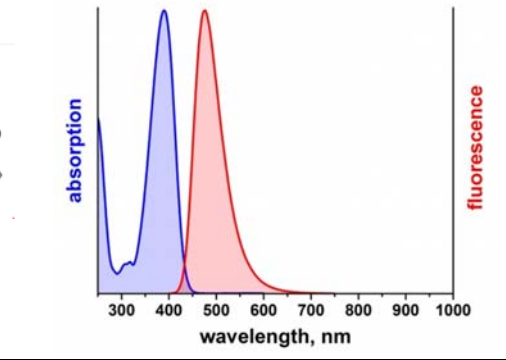
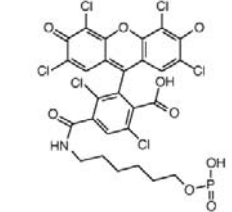
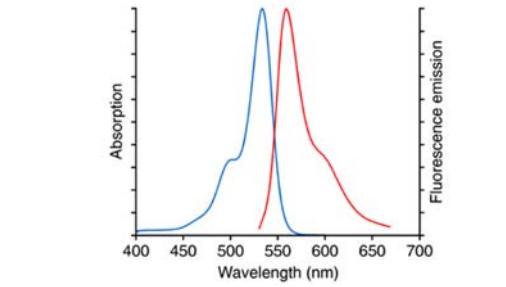
Single Cysteine mutants of MutS/L/H were generated by the former doctoral student in this Lab. T. site is the Thrombin cleavage site. For all these three proteins, the His6-tag was linked to the N-terminal domain. pTX418 (Feng and Winkler 1995); MutS449/D835R (Friedhoff, Manelyte et al. 2017); MutL (Giron-Monzon, Manelyte, et al. 2004, Kosinski, Steindorf, et al. 2005); MutH (Toedt, Krishnan et al. 2003)

References

- Feng, G. and M. E. Winkler (1995). "Single-step purifications of His₆-MutH, His₆-MutL and His₆-MutS repair proteins of *Escherichia coli* K-12." *Biotechniques* 19(6): 956-965.
- Friedhoff, P., L. Manelyte, L. Giron-Monzon, I. Winkler, F. S. Groothuizen and T. K. Sixma (2017). "Use of Single-Cysteine Variants for Trapping Transient States in DNA Mismatch Repair." *Methods Enzymol* 592: 77-101.
- Giron-Monzon, L., L. Manelyte, R. Ahrends, D. Kirsch, B. Spengler and P. Friedhoff (2004). "Mapping protein-protein interactions between MutL and MutH by cross-linking." *J Biol Chem* 279(47): 49338-49345.
- Kosinski, J., I. Steindorf, J. M. Bujnicki, L. Giron-Monzon and P. Friedhoff (2005). "Analysis of the quaternary structure of the MutL C-terminal domain." *J Mol Biol* 351(4): 895-909.
- Toedt, G. H., R. Krishnan and P. Friedhoff (2003). "Site-specific protein modification to identify the MutL interface of MutH." *Nucleic Acids Res* 31(3): 819-825.

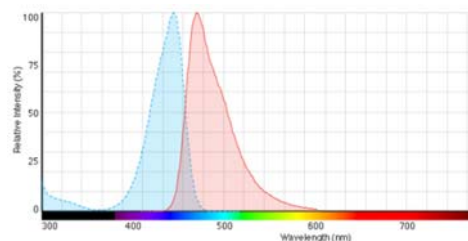
Material

4. Table for all Protein and DNA labeling dyes

Name	Specification	Structure	Fluorescence Spectra
AF488 (G)	λ_{abs} : 495 nm EM: 519nm ϵ_{max} : 71,000 cm ⁻¹ M ⁻¹ CF ₂₆₀ : 0.30 CF ₂₈₀ : 0.11 Chemical Reactivity: Thiol Supplier: ThermoFisher Scientific		
AF594 (R)	λ_{abs} : 590 nm EM: 617 nm ϵ_{max} : 73,000 cm ⁻¹ M ⁻¹ CF ₂₆₀ : 0.43 CF ₂₈₀ : 0.56 Chemical Reactivity: Thiol Supplier: ThermoFisher Scientific		
AF647	λ_{abs} : 650 nm EM: 668 nm ϵ_{max} : 239,000 cm ⁻¹ M ⁻¹ CF ₂₆₀ : 0.00 CF ₂₈₀ : 0.03 Chemical Reactivity: Thiol Supplier: ThermoFisher Scientific		
At390 (B)	λ_{abs} : 390 nm EM: 479 nm ϵ_{max} : 24,000 cm ⁻¹ M ⁻¹ CF ₂₆₀ : 0.52 CF ₂₈₀ : 0.08 Chemical Reactivity: Thiol Supplier: Sigma-Aldrich		
5'-Hexachloro fluorescein (HEX)	λ_{abs} : 535 nm EM: 556 nm ϵ_{max} : 31.58 cm ⁻¹ M ⁻¹ CF ₂₆₀ : ND CF ₂₈₀ : ND Chemical Reactivity: Thiol Supplier: Gene Link		

Material

SYTO	λ_{abs} : 405 nm	not available
X blue	EM: 431 nm	
	ϵ_{max} : 59700 cm ⁻¹ M ⁻¹	
	CF ₂₆₀ : ND	
	CF ₂₈₀ : ND	
	Sub-Cellular Localization:	
	Nucleic Acids	
	Nucleus	
	Supplier: ThermoFisher Scientific	



Alexa Fluor 488 C5-maleimide, Alexa Fluor 594 C5-maleimide, Alexa Fluor 647 C5-maleimide, Atto 390 C2-maleimide CF₂₆₀ = $\epsilon_{260}/\epsilon_{\text{max}}$, CF₂₈₀ = $\epsilon_{280}/\epsilon_{\text{max}}$

5. Table for MutS/MutL/MutH Purification related Buffers

Categories	Concentration for Reagents	Final pH (25 °C)
1x STE Buffer	Tris/HCl	10 mM
	NaCl	100 mM
	EDTA	0.1 mM
Binding Buffer	Tris/HCl	20 mM
	NaCl	1 M
	Imidazole	5 mM
	Glycerol	10 %
Washing Buffer	Tris/HCl	20 mM
	NaCl	1 M
	Imidazole	20 mM
	Glycerol	10 %
Elution Buffer	Tris/HCl	20 mM
	NaCl	1 M
	Imidazole	200 mM
	Glycerol	10 %
HPLC Buffer for MutS and MutL	HEPES/KOH	10 mM
	EDTA	1 mM
	KCl	200 mM
	Glycerol	10 %
HPLC Buffer for MutH	HEPES/KOH	10 mM
	EDTA	1 mM
	KCl	500 mM
	Glycerol	10 %

Material

6. Table for MutS/MutL/MutH working Buffers

Categories	Concentration	for Reagents	Final pH (25 °C)
FB150T	HEPES/KOH	25 mM	7.5
	KCl	150 mM	
	MgCl ₂	5 mM	
	Tween 20	0.05 %	
FB125T	HEPES/KOH	25 mM	7.5
	KCl	125 mM	
	MgCl ₂	5 mM	
	Tween 20	0.5 %	
FB90T	HEPES/KOH	15 mM	7.5
	KCl	90 mM	
	MgCl ₂	5 mM	
	Tween 20	0.05 %	
FB80T	HEPES/KOH	25 mM	7.5
	KCl	80 mM	
	MgCl ₂	5 mM	
	Tween 20	0.5 %	
FB75T_2.5Mg ²⁺	HEPES/KOH	12.5 mM	7.5
	KCl	75 mM	
	MgCl ₂	2.5 mM	
	Tween 20	0.025 %	
FB75T_5Mg ²⁺	HEPES/KOH	12.5 mM	7.5
	KCl	75 mM	
	MgCl ₂	5 mM	
	Tween 20	0.05 %	
FB50T	HEPES/KOH	8.3 mM	7.5
	KCl	50 mM	
	MgCl ₂	5 mM	
	Tween 20	0.00167 %	
FB000	HEPES/KOH	25 mM	7.5
	MgCl ₂	5 mM	
	Tween 20	0.05 %	
Buffer M	KH ₂ PO ₄	40.5 mM	7.4
	K ₂ HPO ₄	9.5 mM	
	KCl	50 mM	
	MgCl ₂	5 mM	
	EDTA	0.1 mM	
Buffer M'	KH ₂ PO ₄	40.5 mM	7.4
	K ₂ HPO ₄	9.5 mM	
	KCl	32 mM	
	EDTA	0.1 mM	
	MgCl ₂	5 mM	

FB represent Fluorescence Buffer.

Material

7. Table for the other Buffers used in the experiments

Categories	Concentration	for Reagents	Final pH (25 °C)
TPE Buffer	Tris/H ₃ PO ₄	100 mM	8.2
	EDTA	2 mM	
SDS Electrophoresis Buffer	Tris	25 mM	8.3
	Glycin	190 mM	
	SDS	0.1 % (w/v)	
AAP (5x) Agarose Loading Buffer	Tris/C ₂ H ₄ O ₂	40 mM	8.0
	NaCl	20 mM	
	EDTA	1 mM	
SDS Loading Buffer (5x)	Tris/HCl	160 mM	6.8
	SDS	2 % (w/v)	
	Glycerol	40 % (w/v)	
	β-Mercaptoethanol	5 % (w/v)	
	Bromphenolblue	0.1 % (w/v)	
CutSmart Buffer (NEB)	Tris-acetate	20 mM	7.9
	Potassium acetate	50 mM	
	Magnesium acetate	10 mM	
	BSA	100 µg/ml	
Coomassie Staining Solution	Coomassie G250	0.1% (w/v)	
	Phosphoric acid	2 % (w/v)	
	Aluminium sulfate	5 % (w/v)	
	Ethanol	10 % (w/v)	
T4 DNA Ligase Buffer (NEB)	Tris/HCl	50 mM	7.5
	MgCl ₂	10 mM	
	DTT	10 mM	
	ATP	1 mM	
Exo I Buffer (NEB)	Tris-HCl	10 mM	7.5
	NaCl	100 mM	
	β-Mercaptoethanol	5 mM	
	EDTA	0.5 mM	
	BSA	100 µg/ml	
	Glycerol	50%	
Exo III buffer (NEB)	Bis Tris Propane-HCl	10 mM	7.0
	MgCl ₂	10 mM	
	DTT	1 mM	

Appendix

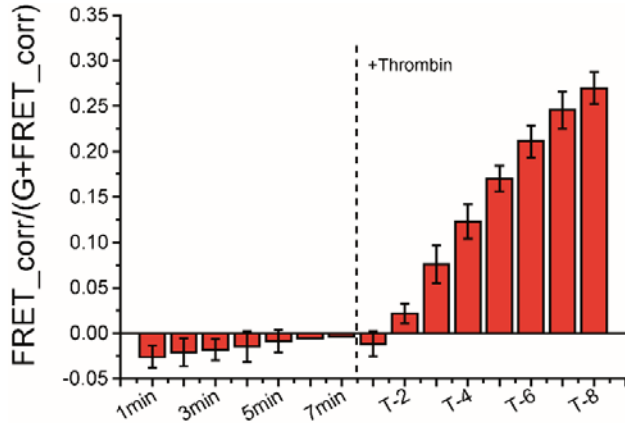
Chapter 1:

MutL CTD subunit exchange kinetics is affected by buffer conditions and MutL NTD. MutL exists as a dimer in solution (Guarne and Charbonnier 2015) but undergoes slow subunit exchange as described above. Due to low concentration of MutL existing aggregates phenomenon in FB125T (pH 7.5) buffer which not suitable to carry AUC and smFRET experiments (data not shown here), therefore all experiments were proceeded in buffer M (phosphate buffer, pH 7.4) except Figure 6 in FB150T (physiological ionic strength). However, when proceeding AF488 or AF594 labeled MutL452 CTD subunit exchange, the kinetics exists two phases (Appendix Figure 1.2 A, olive) while the full-length MutL452 subunit exchange was not affected (still with 0.12 min^{-1} apparent rate, Appendix Figure 1.2 A, magenta). However, the apparent rates of both the burst phase and slow phase of MutL452 CTD were slowed down when in the presence of the same amount of isolated NTD (Appendix 1.2 A, orange), and the burst phase entirely disappeared when increased the concentration of isolated NTD to 2 fold (Appendix Figure 1.2 A, blue). Otherwise, the subunit exchange of AF488 or AF594 labeled the isolated MutL297 NTD is complicated, and the kinetics cannot fit exponential fit at all both in the presence (Appendix Figure 1.2 B, red) or absence of CTD (Appendix Figure 1.2 B, dark green). Moreover, the presence of CTD seems accelerated the subunit exchange between the donor or acceptor labeled isolated MutL297 NTD (Appendix 1.2 B).

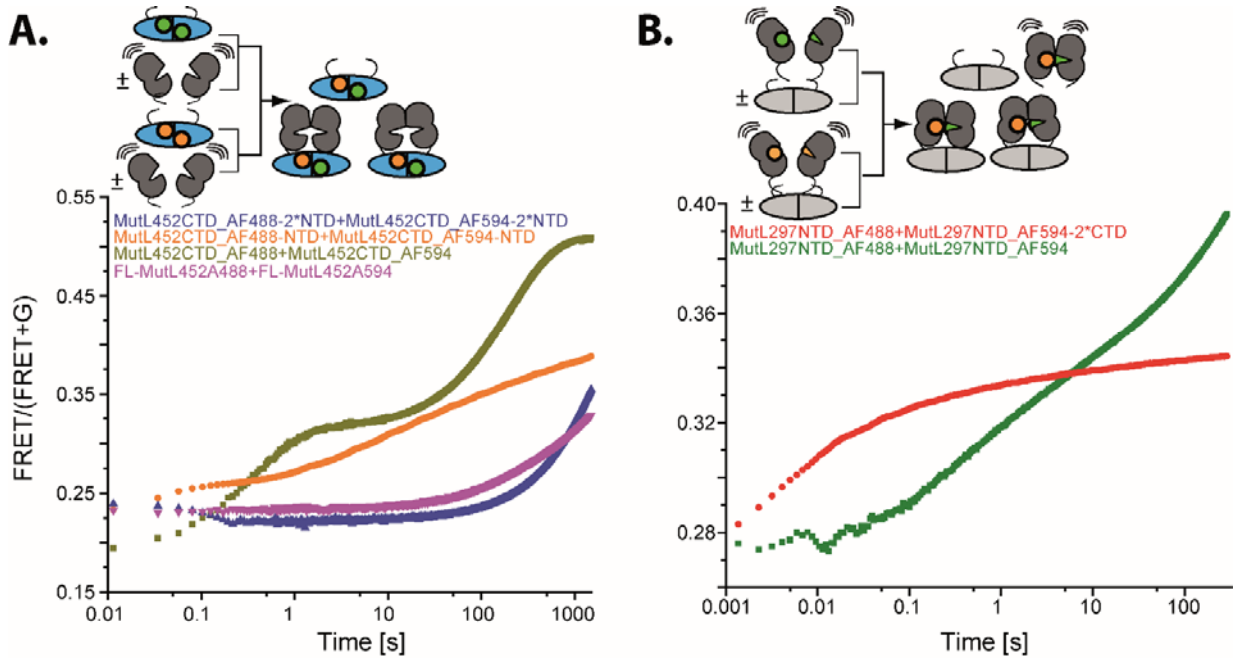
As we described above, MutL CTD subunit exchange behaves differently in buffer M and FB125T, hence we add 50mM KPi to FB125T or use 25 mM Tris-HCl substitute 25mM HEPES. Then we found that add 50mM KPi will not change the burst phase of MutL CTD subunit exchange while accelerate the slow phase (Appendix Figure 1.3 A, dark grey and dark green). Moreover, using Tris-HCl instead of HEPES makes the burst phase of MutL CTD subunit exchange vanish (Appendix Figure 1.3 A, dark purple). To convince that HEPES induced the burst phase of MutL CTD subunit exchange, we added a different concentration of Mg^{2+} and 25 mM HEPES to buffer M. The results indicated that Mg^{2+} does not affect MutL isolated CTD subunit exchange (Appendix Figure 1.3 B, red and blue). The burst phase appears in the presence of HEPES in buffer M, and with much higher amplitude for this burst phase (Appendix Figure 1.3 B, magenta). Owing to the difference in burst phase for MutL isolated CTD subunit exchange for adding 50mM KPi to FB125T buffer (Appendix Figure 1.3 A, grey) and adding HEPES to buffer M (Appendix Figure 1.3 B, magenta). Therefore, we try to add 50mM KPi to FB90T (HEPES/KOH 25 mM, KCl 90 mM, MgCl_2 5 mM, Tween 20 0.05 %) and FB125T

Appendix

(HEPES/KOH 25 mM, KCl 125 mM, MgCl₂ 5 mM, Tween 20 0.05 %) to test ionic strength effect. The result indicated that the burst phase takes



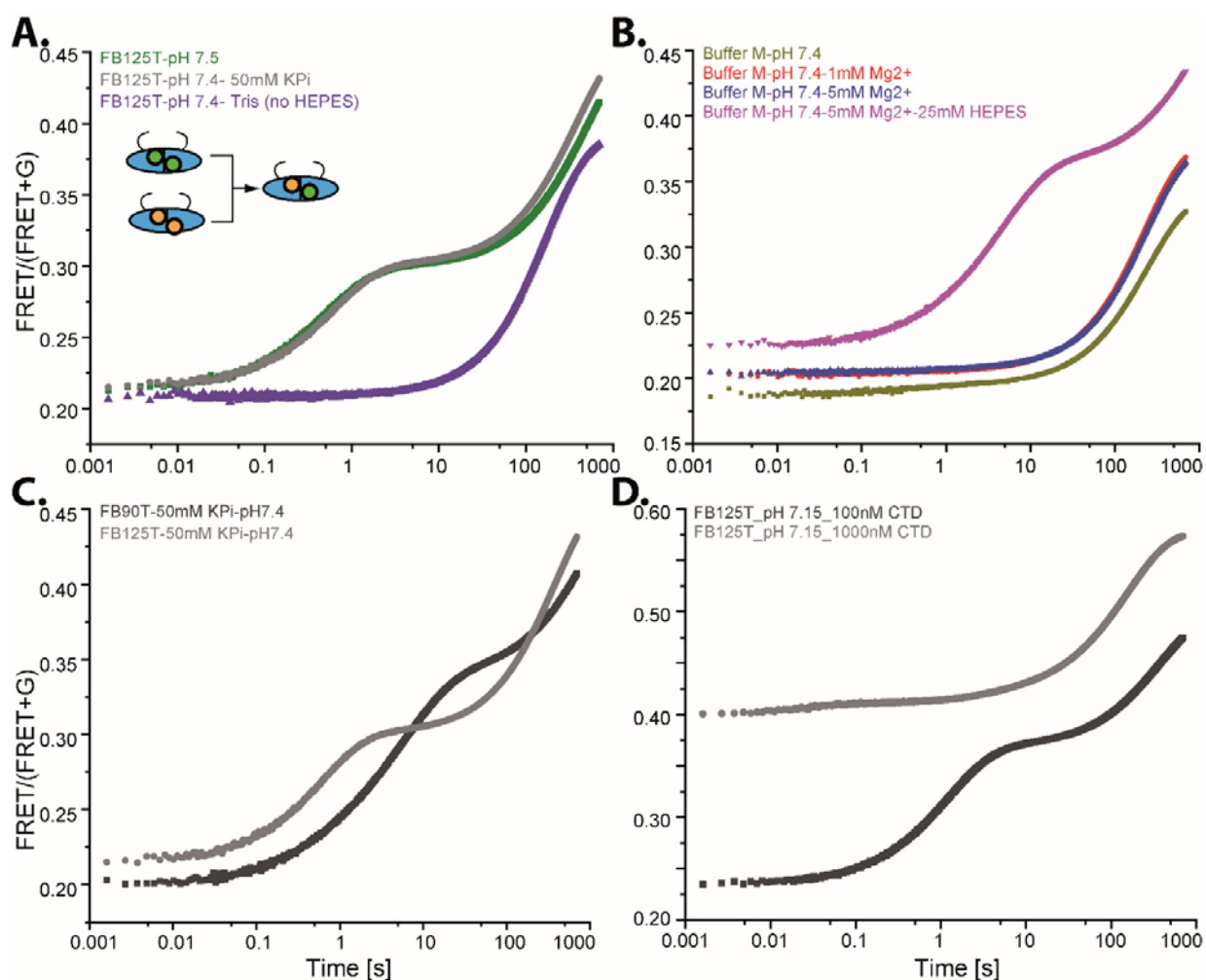
Appendix Figure 1.1 MutL452 CTD subunit exchange. The FRET efficiency calculated from thrombin cleavage 100 nM MutL452_AF594 -AMPPNP with 100 nM MutL452_AF488-AMPPNP after subunit exchanges.



Appendix Figure 1.2 The effect of NTD on CTD or CTD on NTD subunit exchange. (A) the subunit exchange of 50 nM MutL452-CTD_AF488 and 50 nM MutL452-CTD_AF594 in FB125 at 25 °C, in absence of NTD (olive), in the presence of 50 nM NTD (orange), in the presence of 100 nM NTD (blue) and full length of MutL (magenta) (ET525/50M_Voltage/637_Gain/1 and ET630/75M_Voltage/786_Gain/2); (B) the subunit exchange of 100nM MutL297-NTD_AF488 and 100 nM MutL297-NTD_AF594 in FB125 at 25 °C, in the absence of CTD (dark green), in the presence of 100 nM NTD (red) (ET525/50M_Voltage/600_Gain/1 and ET630/75M_Voltage/600_Gain/2).

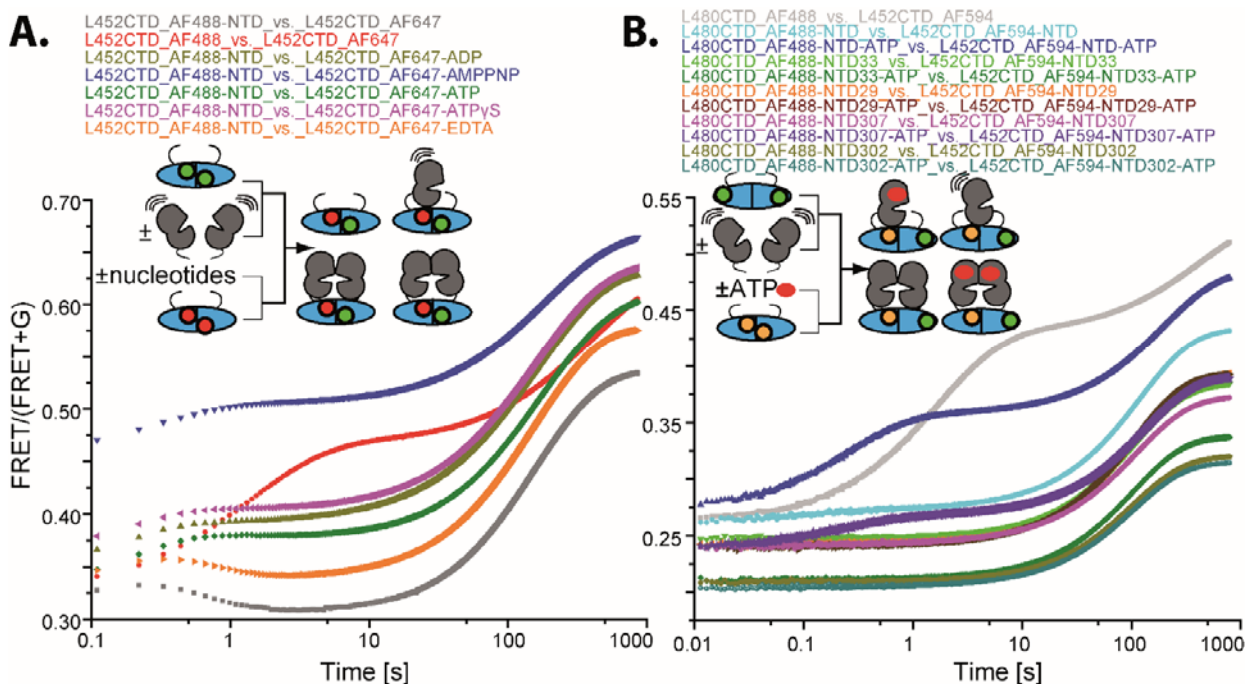
Appendix

more than 10 times longer and with 1.3 fold higher amplitude in lower ionic strength (FB90T-50 mM KPi, Appendix Figure 1.3 C, dark grey) than in higher ionic strength (FB125T-50 mM KPi, Appendix Figure 1.3 C, black grey). Otherwise, the burst phase accelerated when increasing the concentration of isolated MutL CTD. As we observed from Appendix Figure 1.3 D, the 10 fold higher concentration of CTD (1000 nM, dark grey) makes the burst phase of subunit exchange entirely unmeasurable than 100 nM isolated MutL CTD. As the starting point is the lower's (black-grey) end level of the burst phase, but they all finish in 10 s, after that the apparent subunit exchange rates are similar.



Appendix Figure 1.3 The effect of HEPES, Mg²⁺, pH, concentration of CTD and salt effect on MutL CTD subunit exchange. (A) the subunit exchange of 100 nM MutL452-CTD_AF488 and 100 nM MutL452-CTD_AF594 in buffer FB125T with 25 mM HEPES (dark green), in buffer FB125T with 25 mM HEPES and 50 mM KPi (dark grey), in buffer FB125T with 25 mM Tris-HCl instead of HEPES (dark purple); (B) the subunit exchange of 100 nM MutL452-CTD_AF488 and 100 nM MutL452-CTD_AF594 in buffer M without 25 mM HEPES or Tris-HCl (olive), buffer M with 1 mM Mg²⁺ (red), with 5 mM Mg²⁺ (blue), with 5 mM Mg²⁺ and 25 mM HEPES (magenta); (C) the subunit exchange of 100 nM MutL452-CTD_AF488 and 100 nM MutL452-CTD_AF594 in buffer FB90T (dark grey) or FB125T (light grey) with 50 mM KPi; (D) the subunit exchange of 100 (light grey) or 1000 nM (dark grey) MutL452-CTD_AF488 and 100 or 1000 nM MutL452-CTD_AF594 in buffer FB125T. Annotation: FB buffer always with 5 mM Mg²⁺ and 25 mM HEPES inside and the measured conditions are: ET525/50M_Voltage/657_Gain/1 and ET630/75M_Voltage/ 730_Gain/2.

To make sure the burst phase in AF488 and AF594 labeled the isolated MutL CTD subunit exchange in HEPES buffer independent of the dye and unique position, we substitute AF594 with AF647

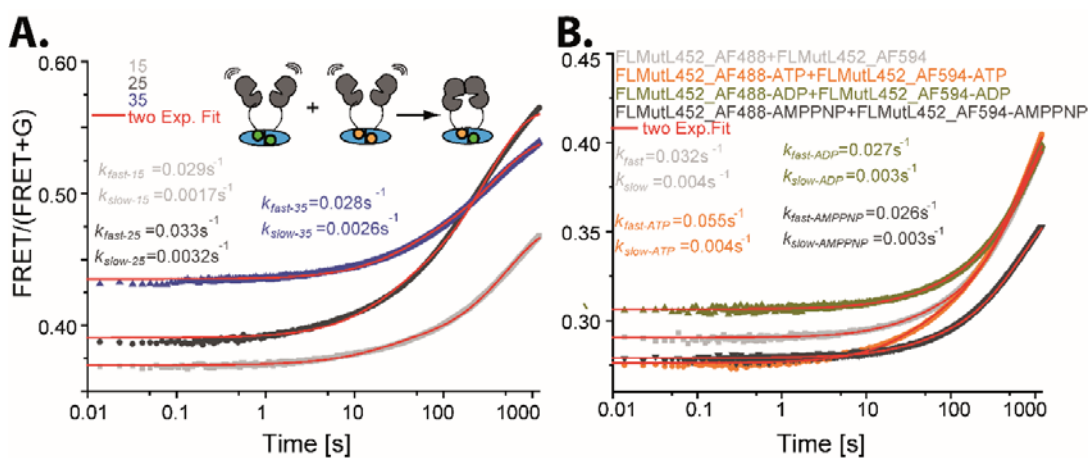


Appendix Figure 1.4 The effect of different type of nucleotides or NTD on MutL CTD subunit exchange. (A), subunit exchange of 50 nM AF488 labeled MutL452-CTD and 50 nM AF647 labeled MutL452-CTD (red); the grey is pre-incubate 50nM MutL452CTD_AF488 with 50 nM NTD (25 nM for final concentration); with 50 nM MutL452-CTD_AF488 pre-incubate with 50 nM NTD (25 nM for final concentration) and MutL452-CTD_AF647 pre-incubate with 2 mM nucleotide (1 mM for final concentration, ADP olive, AMPPNP blue, ATP dark green, ATPγS magenta), and orange is use 10 mM EDTA (5 mM for final concentration); (ET525/50M_Voltage/597_Gain/1 and ET670/50M_Voltage/800_Gain/1); (B), subunit exchange of 50 nM AF488 labeled MutL480-CTD and 50 nM AF594 labeled MutL452-CTD (grey), both MutL480-CTD_AF488 and MutL452-CTD_AF594 pre-incubate with 50 nM normal (with the same ability binding and hydrolysis ATP) NTD (light cyan) and together with 1 mM ATP (blue); both MutL480-CTD_AF488 and MutL452-CTD_AF594 pre-incubate with 50 nM MutLN33A NTD (deficient in hydrolyze ATP and always in open state) (light green) and together with 1 mM ATP (dark green); both MutL480-CTD_AF488 and MutL452-CTD_AF594 pre-incubate with 50 nM MutLE29A-NTD (deficient in hydrolysis ATP and always in closed state) (orange) and together with 1 mM ATP (dark red); both MutL480-CTD_AF488 and MutL452-CTD_AF594 pre- incubate with 50 nM MutL K307A (could binding and hydrolysis ATP, but mostly in open state) NTD (magenta) and together with 1 mM ATP (dark purple); both MutL480-CTD_AF488 and MutL452-CTD_AF594 pre-incubate with 50 nM MutL N302A-NTD (could binding and hydrolysis ATP, but mostly in closed state) (olive) and together with 1mM ATP (dark cyan); (ET525/ 50M_Voltage/657_Gain/1 and ET630/75M_Voltage/730_Gain/2).

together with AF488 labeled at MutL480-CTD as well in Appendix Figure 1.4. When compared Appendix Figure 1.4 A red (MutL452-CTD labeled with AF647 and AF488) and Appendix Figure 1.4. B. dark grey (MutL452-CTD labeled with AF594 and MutL480-CTD labeled with AF488) with Appendix Figure 1.3 A green, we could find that even though the FRET efficiency is not entirely consistent, the burst phase appeared in 1-10 s. While the amplitudes for MutL452-CTD labeled with AF647/AF488 and MutL452-CTD labeled with AF594/AF488 are the same while the amplitude for MutL452-CTD labeled with AF594/MutL480-CTD labeled with AF488 doubled (Appendix Figure

Appendix

1.4 B, dark grey) due to the distance between residue 452 to 480 is 45 nm which close to R0 of AF488 and AF594. Then we tested the isolated NTD effect on isolated MutL452-CTD subunit exchange in the presence of different nucleotides and EDTA. Compared without NTD (Appendix Figure 1.4 A, red), NTD seems to accelerate the later phase of MutL452-CTD subunit exchange (Appendix Figure 1.4 A, grey). The 2 mM ADP/ATP/ATP γ S facilitate MutL452-CTD subunit exchange (Appendix Figure 1.4 A, olive, dark green and magenta) compared to in the absence of nucleotide (Appendix Figure 1.4 A, grey) and the presence of EDTA (Appendix Figure 1.4 A, orange), while the non-hydrolysable analog AMPPNP seems to make MutL452-CTD subunit exchange faster (Appendix Figure 1.4 A, blue). From Appendix Figure 1.4 A, we could conclude that hydrolysable and non-hydrolysable nucleotide behaves differently in MutL452-CTD subunit exchange. Thus, the different types of MutL NTD mutants were used to investigate the effect on CTD subunit exchanges. Such as MutLN33A-NTD which deficient in hydrolyze ATP and always in open state; MutLE29A-NTD which deficient in hydrolysis ATP and always in closed state; MutL K307A-NTD which could bind and hydrolysis ATP, but mostly in open state; MutL N302A-NTD which could bind and hydrolysis ATP, but mostly in closed state (Appendix Figure 1.4 B). The burst phase vanished in the presence of the wtMutL NTD (Appendix Figure 1.4 B, cyan). However, it appears faster and finishes in 1s and lower amplitude (Appendix Figure 1.4 B, blue) in the presence of wtMutL NTD and ATP. That cannot be observed from AF488 and AF594 labeled MutL452-CTD subunit exchange (Appendix Figure 1.4 A).

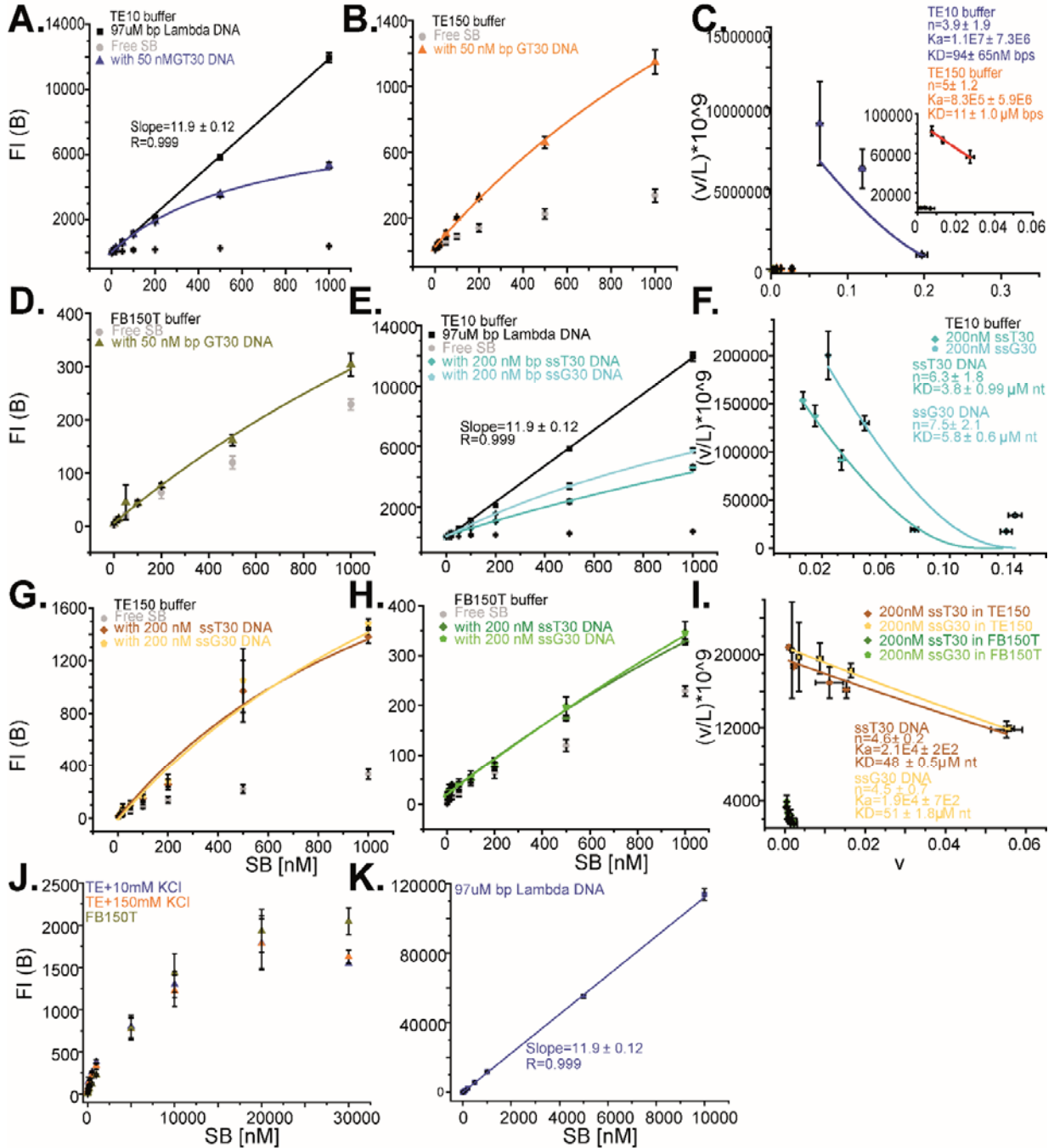


Appendix Figure 1.5. The temperature and nucleotides effect on FL MutL subunit exchange. (A) The subunit exchange of 100 nM FL MutL452_AF488 and MutL452_AF594 in FB125T buffer at different temperatures; (B) the subunit exchange of 100 nM FL MutL452_AF488 and MutL452_AF594 with 1 mM different nucleotides at 25 °C.

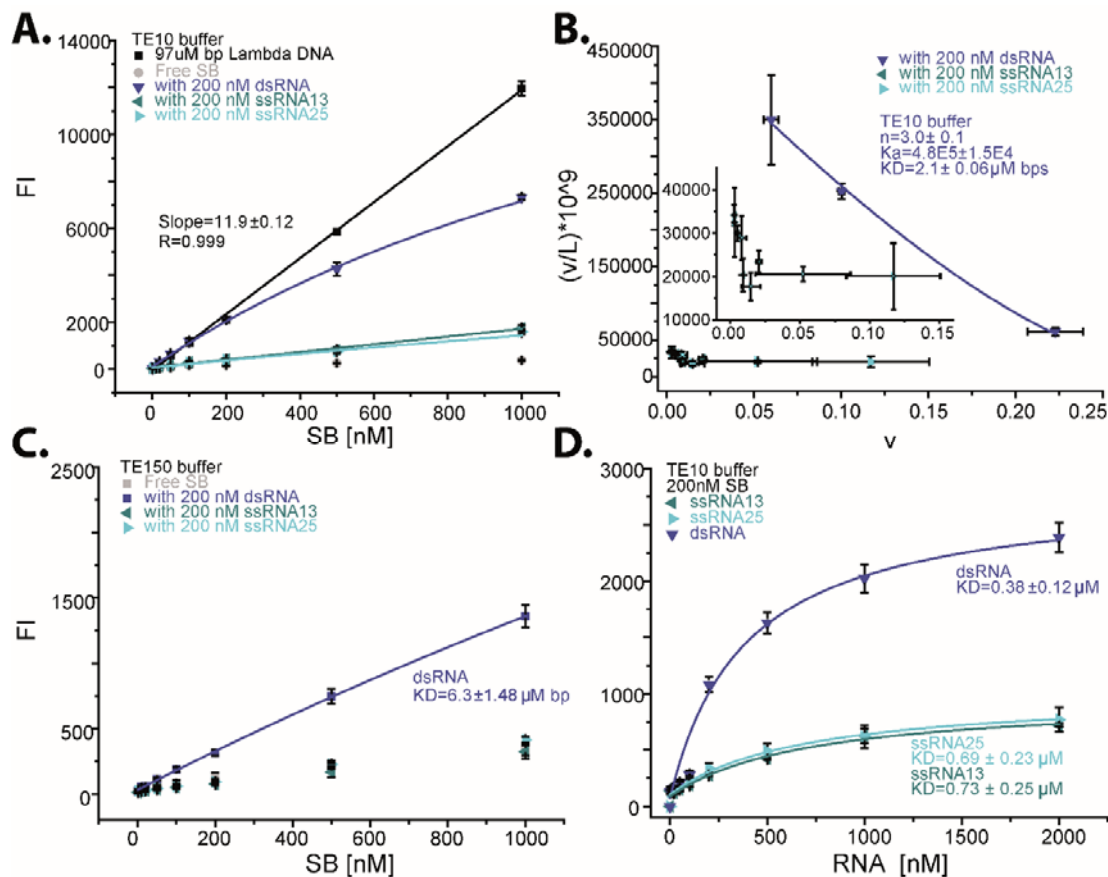
As indicated in the graph, the isolated NTD with the ability of binding and hydrolysis ATP and could exist in the monomer is essential for faster burst phase in isolated MutL452-CTD labeled with AF594 and MutL480-CTD labeled with AF488 subunit exchange (Appendix Figure 1.4 B).

Chapter 2:

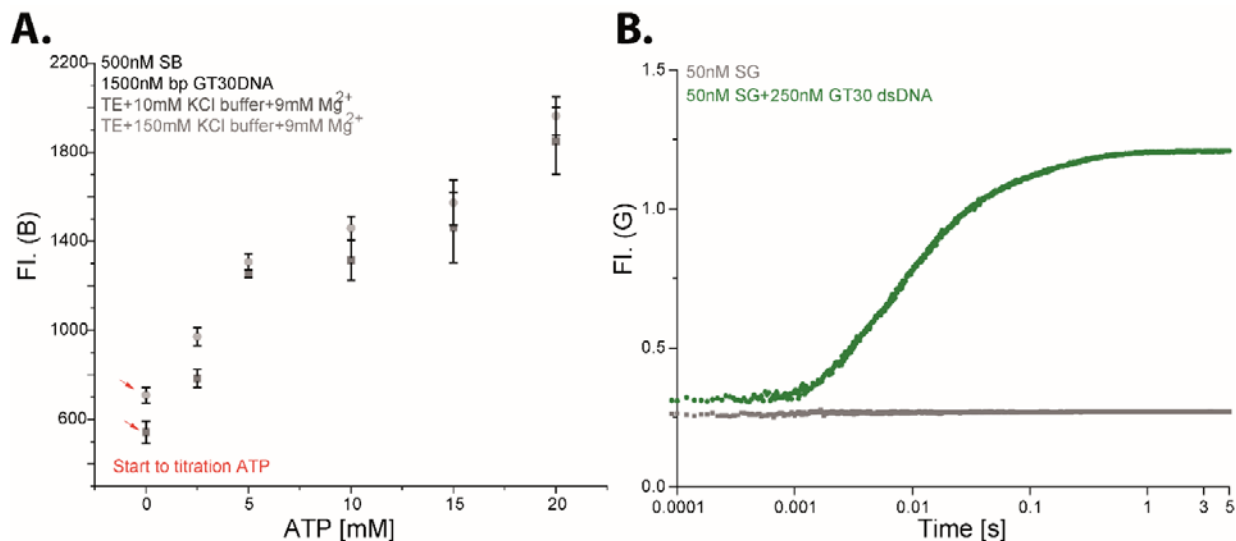
SYTOX blue stain dsGT30, ssG30, and ssT30 DNA with the similar binding site size ($n \sim 5$) in TE10, TE 150 and FB150T buffers (Appendix Figure 2.1). From Appendix Figure 2.1H, we could find that the fluorescence of SB-DNA (Lambda DNA) complexes increase linearly, compared to that the fluorescence intensity of free SB dye could be neglected (Appendix Figure 2.1, J). SB binding dsGT30 DNA with high affinity in TE10 buffer and 10 times lower when increase the salt concentration of KCl to 150 mM (TE150), and almost no binding in FB150T buffer observed (Appendix Figure 2.1, A-D). Similarly, SB staining ssDNA with much lower affinity even in TE10 buffer, and another 10 fold lower when increase the salt concentration of KCl to 150 mM (TE150), and almost no binding in FB150T buffer observed as well (Appendix Figure 2.1, E-I). However, only dsRNA-SB complexes formation observed when titration SB to 200 nM dsRNA and ssRNA in TE10 buffer (Appendix Figure 2.2, A-C). While the relative amplitudes of ssRNA only one fifth when titration RNA to 200 nM SB in TE10 buffer (Appendix Figure 2.2, D). Nevertheless, the titration of K^+ and Mg^{2+} induced the dissociation of SB from dsGT30 DNA (Chapter 2 Figure 5 B) could be rescued by titration ATP to the system (Appendix Figure 2.3 A). Appendix Figure 2.3 B is the process of the SYBR Green I (SG) staining dsGT30 DNA in FB150T buffer which need 1 s to reach the saturation while only 30 ms for SB staining dsGT30 DNA.



Appendix Figure 2.1 Titration SB to different types of DNA in TE10, TE150, or FB150T buffer. (A) Titration SB into 200 nM dsGT30 DNA in TE150 buffer (B) Titration SB into 200 nM dsGT30 DNA in TE150 buffer; (C) Analyzing SB binding dsGT30 DNA using the model for non-cooperative of McGhee and von Hippel (McGhee 1974) in TE10 and TE150; (D) Titration SB into 200 nM dsGT30 DNA in FB150T buffer; (E) Titration SB into 200 nM ssG30 DNA and ssT30 DNA in TE10; (F) Analysis of the SB binding ssG30 DNA and ssT30 DNA using the conditional probability model for non-cooperative of McGhee and von Hippel (McGhee 1974) in TE10 buffer; (G) Titration SB into 200 nM ssG30 DNA and ssT30 DNA in TE150; (H) Titration SB into 200 nM ssG30 DNA and ssT30 DNA in FB150T buffer; (I) Analysis of the SB binding ssG30 DNA and ssT30 DNA using the model for non-cooperative of McGhee and von Hippel (McGhee 1974) in TE150; (J) The fluorescence intensity of free SB in different buffers; (K) Titration SB to 97 μM bp Lambda DNA and 200 nM dsGT30 in TE10 buffer.



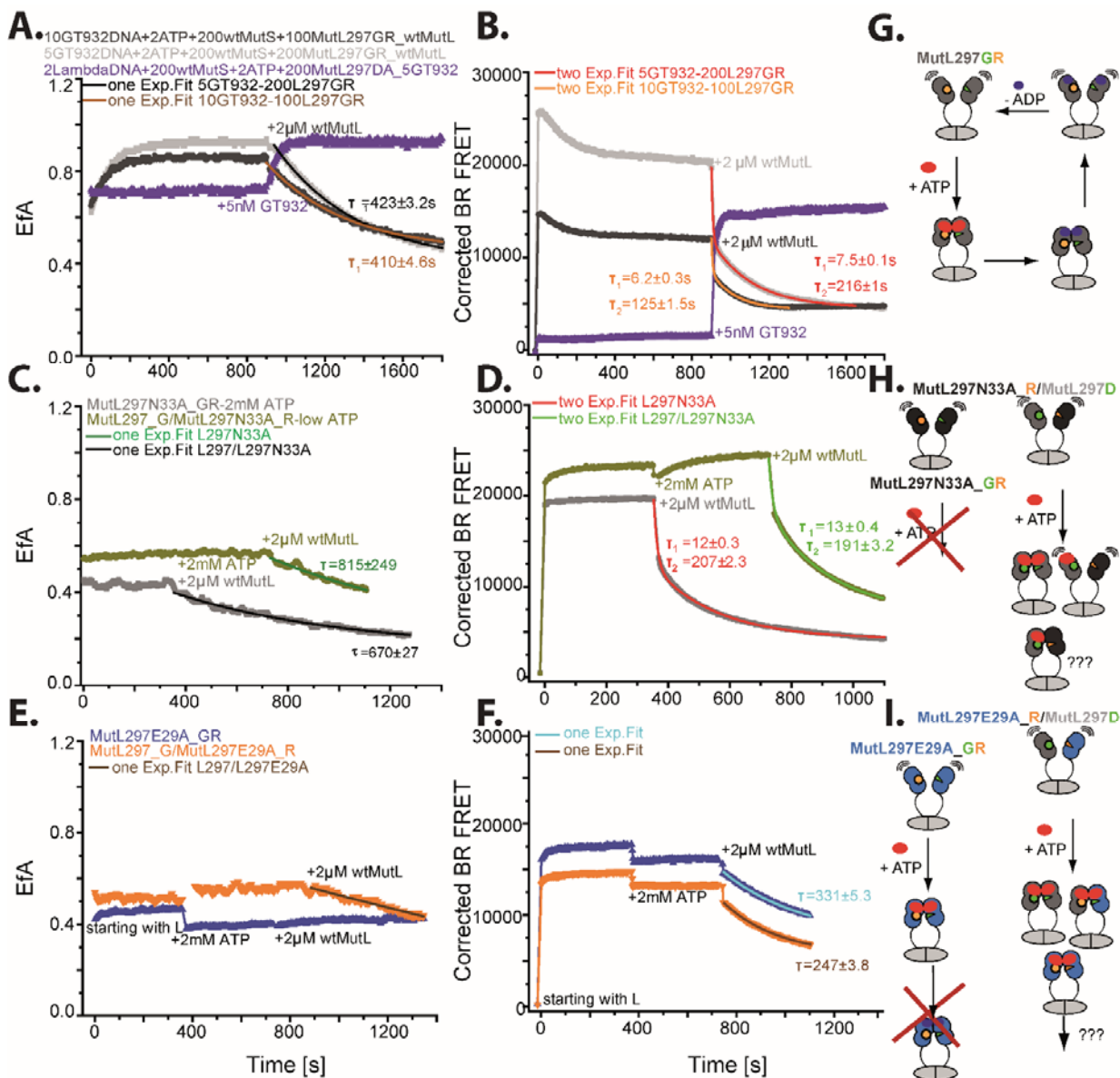
Appendix Figure 2.2 SB binding 200 nM different bp type of RNAs in TE10 buffer and TE150 buffer. (A) Titration SB into 200 nM ssRNA13, ssRNA25 and dsRNA25 in TE10 buffer; (B) Analysis of the SB binding ssRNA13, ssRNA25 and dsRNA25 using the conditional probability model for non-cooperative which derived by McGhee and von Hippel (McGhee 1974) in TE10 buffer; (C) Titration SB to the 200 nM different type of RNAs in TE150 buffer; (D) Titration ssRNA13, ssRNA25, and dsRNA25 to 200 nM SB free dye in TE150 buffer.



Appendix Figure 2.3 (A) Titration ATP to TE 10 buffer with 9 mM Mg²⁺, 0.5 μM SB, and 1.5 μM dsGT30 DNA (continue to titrate ATP to the system of Figure 5 B in chapter 2); (B) Kinetic of 50 nM staining 250 nM GT30 dsDNA (for final concentration) in buffer FB150T monitored with stopped-flow (436 nM ET525/50M).

Chapter 3:

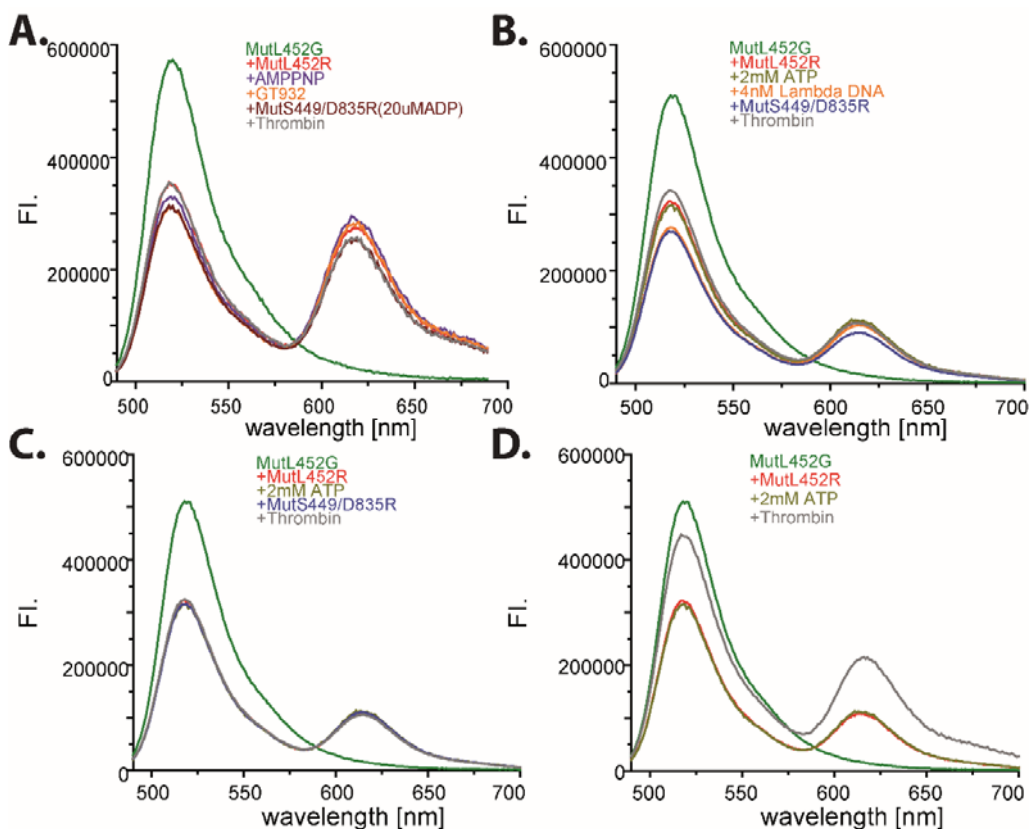
MutL cannot be loaded on DNA by MutS without mismatch as no observation of MutL binding lambda DNA in buffer M while the EfA and the corrected BR FRET strikingly increased after adding 5 nM GT932 circular (Appendix Figure 3.1 A and B, purple). With the mismatched GT932 circular DNA, both the EfA and the BR FRET of 200 nM MutL297_AF488AF594 hetero-dimers is higher when the concentration of DNA is lower (Appendix Figure 3.1 A and B, light and dark grey). Which indicated that, at lower concentration of DNA (5 nM) the density of MutL297_GR on the DNA is higher than the higher concentration of DNA (10 nM), hence generated more inter-dimer FRET. Both the EfA of the ATP binding deficient (MutL297N33A_GR) and ATP hydrolysis deficient (MutL297E29A_GR) variants stay no change with mismatched GT932 circular DNA, even though they are loaded on the DNA judged by the BR FRET (Appendix Figure 3.1, C-F, grey and purple). Adding MutL competitor, no completion observed for MutL297E29A_GR hetero- dimers (the EfA of MutL297E29A_GR state no change) while the BR FRET with monophasic decrease kinetic (Appendix Figure 3.1, C-F, grey and purple). Therefore, MutL297E29A_GR forms stable dimer on the GT932 circular DNA hooked by MutS, the DNA did not go through the MutL hetero-dimers. That is not observed for the MutL297_G/ MutL297E29A_R hetero-dimers (Appendix Figure 3.1, E-F, orange).



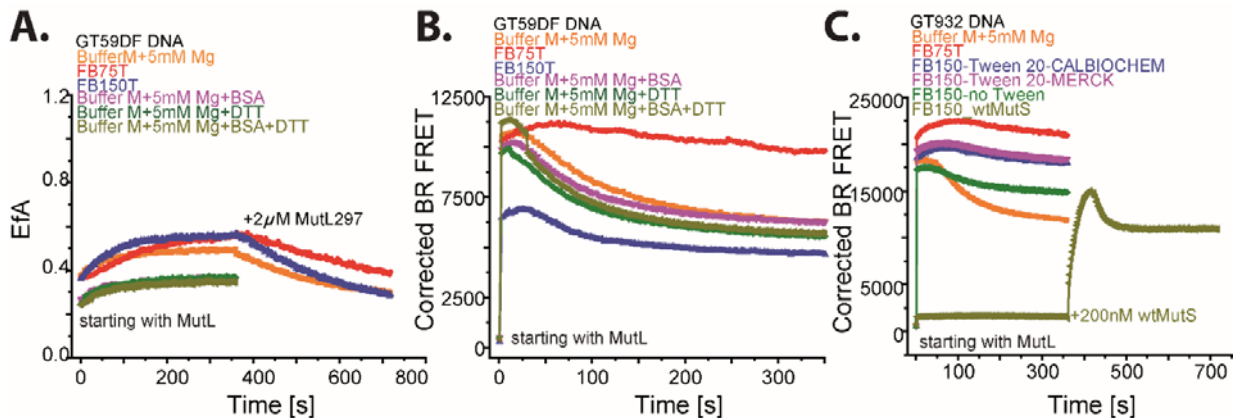
Appendix Figure 3.1 Extra Efa not observed from ATP binding or hydrolysis deficient mutants. (A-B) 100 /200 nM preformed MutL297_AF488AF594 hetero-dimer added to the 200 µl buffer M containing 2 mM ATP, 200 nM wtMutS and 5/10 nM GT932 DNA or 2 nM Lambda DNA to start the reaction, later added 2 µM wtMutL as competitor; (C-D) 200 nM preformed MutL297_AF488/MutL297N33A_AF594 or MutL297N33A_AF488AF594 hetero-dimer added to the 200 µl buffer M containing 10 µM/2 mM ATP, 200 nM wtMutS and 5 nM GT932 DNA to start the reaction, later added 2 mM ATP to the low ATP reaction, added 2 µM wtMutL as competitor at the end; (E-F) 200 nM preformed MutL297_AF488 /MutL297E29A_AF594 or MutL297E29A_AF488AF594 hetero-dimer was added to the 200 µl buffer M containing 10 µM/2 mM ATP, 200 nM wtMutS, and 5 nM GT932 DNA to start the reaction, later 2 mM ATP to the low ATP reaction, and added 2 µM wtMutL as competitor at the end.

MutLE29A could undergo slower subunit exchange ($0.05 \pm 0.002 \text{ min}^{-1}$) in the absence of ATP, MutS, and DNA (Appendix Figure 3.5 A). However, MutL297E29A_GR hetero-dimers' FRET efficiency (Efa) decreased upon loading on the GT59DF DNA (the BR FRET increased) by MutS at low ATP (10 µM) state (Appendix Figure 3.5 B and C). Addition 2 mM ATP to that system result the Efa goes

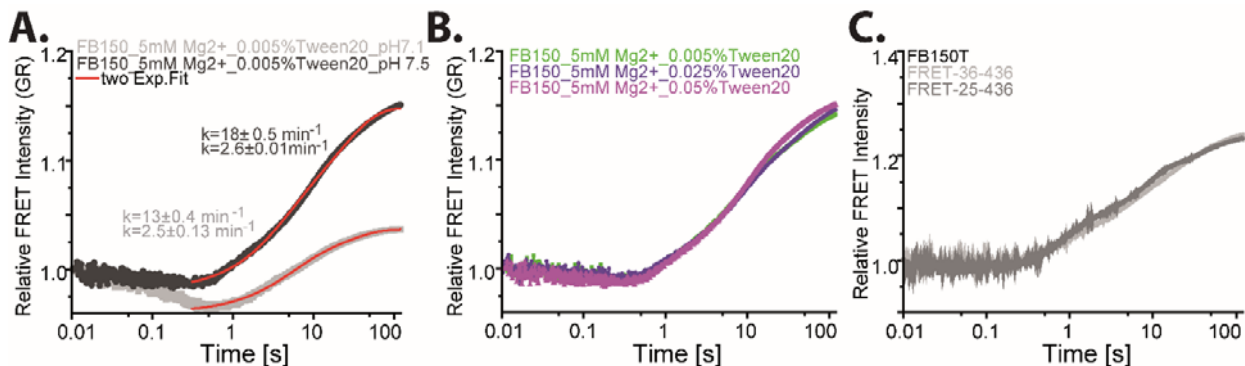
up to the starting value while the BR FRET slowly decreased (Appendix Figure 3.5 B and C) which did not observed with the GT932 circular DNA (only fast decrease at the beginning, Appendix Figure 3.1 F). The rate of the BR FRET decreased is $0.35 \pm 0.005 \text{ min}^{-1}$ which is only half as wild-type MutL297_GR conformational change on the GT59DF DNA (Figure 2.1, chapter 3) while the life time is similar as the slow phase of adding competitor (Appendix Figure 3.1 F, blue). Hence, it seems that the DNA did not go through the MutL structure and induced MutL297E29A conformational changes on the DNA. From the kinetics of spectra, we could observe that the high FRET state only appeared when all mismatched GT932 circular DNA, MutS and AMPPNP (or ATP) exist (Appendix Figure 3.2,



Appendix Figure 3.2 Effect of MutS, ATP/AMPPNP, GT932 DNA/GT59DF DNA affect MutL interaction. (A) Mixed 100 nM MutL452_AF488 with 100 nM MutL452_AF594 in 200 μl buffer M, later sequentially added 2 mM AMPPNP, 10 nM GT932 DNA, 400 nM MutS449/D835R and thrombin; (B) Mixed 100 nM MutL452_AF488 with 100 nM MutL452_AF594 in 200 μl buffer M, later sequentially added 2 mM ATP, 4 nM Lambda DNA, 400 nM MutS449/D835R and thrombin; (C) Mixed 100 nM MutL452_AF488 with 100 nM MutL452_AF594 in 200 μl buffer M and later sequentially added 2 mM ATP, 400 nM MutS449/D835R and thrombin; (D) Mixed 100 nM MutL452_AF488 with 100 nM MutL452_AF594 in buffer M and later sequentially added 2 mM ATP and thrombin. FI. Is fluorescence intensity.



Appendix Figure 3.3 MutL297 DNA interaction with GT mismatch-containing DNA in different buffers. (A and B) 200 nM preformed MutL297_AF488AF594 hetero-dimer added to pre-incubated 2 mM ATP, 200 nM wtMutS, and 100 nM GT59DF DNA to start the reaction in different buffers; (C) 200 nM MutL297_AF594 added to pre-incubated 2 mM ATP, and 100 nM GT59DF with/without 200 nM wtMutS and to start the reaction in different buffers (all buffers containing 5 mM Mg²⁺, blue Tween20 from CALBIOCHEMIE company while purple Tween20 from MERCK company), and added 200 nM wtMutS added to the non wtMutS reaction at the end; (D) Mixing pre-incubated 0.5 mM ATP-100 nM GT59DF DNA-200nM wtMutS, with 200 nM preformed MutL297_AF488AF594 hetero-dimer to observe MutL-MutL interaction on DNA in FB150T buffer (containing 5 mM Mg²⁺ and 0.005 % Tween 20) with varying the temperature.

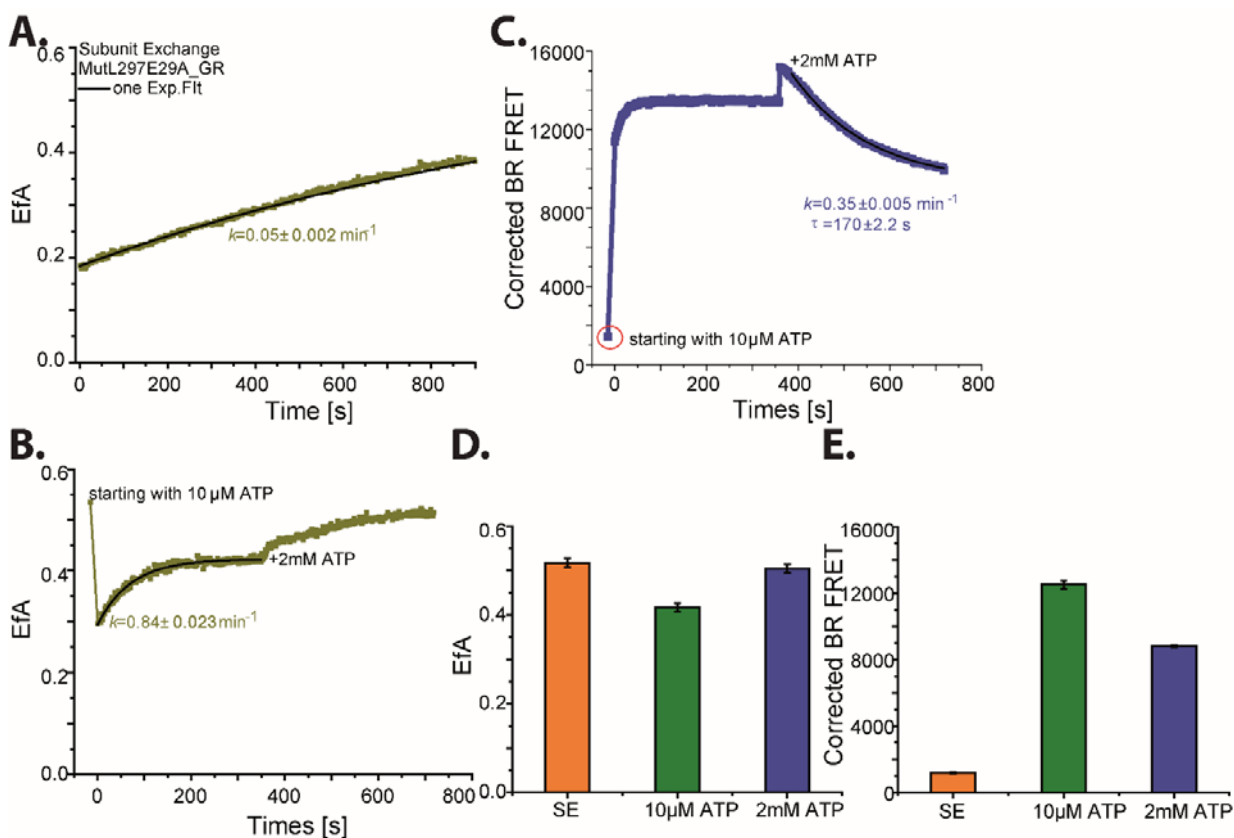


Appendix Figure 3.4 MutL297 DNA interaction with GT mismatch-containing DNA in different buffers (A) using Stopped-flow single mixing mode to mix pre-incubated 0.5 mM ATP-100 nM GT59DF DNA-200 nM wtMutS, with 200 nM preformed MutL297_AF488AF594 hetero-dimer to observe MutL-MutL interaction on DNA in FB150T buffer (containing 5 mM Mg²⁺ and 0.005 % Tween 20) with varying the pH; (B) using Stopped-flow single mixing mode to mix pre-incubated 0.5 mM ATP-100 nM GT59DF DNA-200 nM wtMutS, with 200 nM preformed MutL297_AF488AF594 hetero-dimers to observe MutL-MutL interaction on DNA in FB150T buffer (containing 5 mM Mg²⁺) with varying the percentage of Tween 20; all the mixing ratio are 1:1; (C) using Stopped-flow single mixing mode to mix pre-incubated 0.5 mM ATP-100 nM GT59DF DNA-200 nM wtMutS, with 200 nM preformed MutL297_AF488AF594 hetero-dimer to observe MutL-MutL interaction on DNA in FB150T buffer (containing 5 mM Mg²⁺ and 0.005 % Tween 20) with varying the temperature.

Figure 1.2 in chapter 3) and that is consistent with the Figure 1.1 kinetics in chapter 3. MutL cannot bind on mismatched DNA without MutS (Appendix 3.3, C, olive) and it stays more stable on the mismatched DNA in low ionic strength buffer (FB75T, Appendix 3.3). The interaction between MutL and mismatched DNA not affected by BSA, DTT and Tween 20 (Appendix 3.3 and Appendix 3.4 B). While the rate of the first phase of MutL297_AF488AF594 heterodimers conformational changes

Appendix

kinetics which related to the MutL loading on mismatched DNA and DNA bring two NTDs of MutL closer (depending on the Figure 2.4 and 2.5 in chapter 3) is faster at higher pH of FB150T buffer (7.5, $18 \pm 0.5 \text{ min}^{-1}$) than at lower pH (7.1, $13 \pm 0.5 \text{ min}^{-1}$) of FB150T buffer (Appendix 3.4 A). Even through the slow rate of MutL closure rate is similar (pH 7.1, $2.5 \pm 0.13 \text{ min}^{-1}$, and pH 7.5, $2.6 \pm 0.11 \text{ min}^{-1}$) which indicated that this phase is related to the MutL conformational changes on DNA (Appendix 3.4 A). This biphasic kinetics of MutL297_AF488AF594 heterodimers conformational changes more pronounced at RT (room temperature) than 37°C (Appendix 3.4 A).

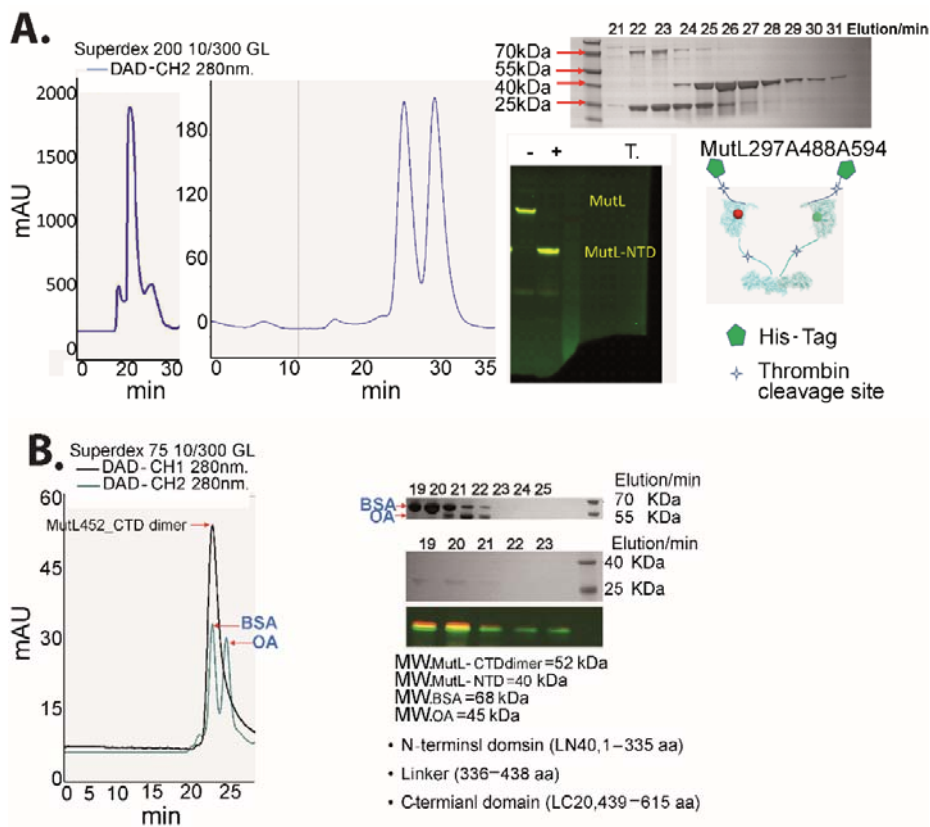


Appendix Figure 3.5 AF488 and AF594 labeled MutLE29A SE and loaded on GT59DF DNA (A) Kinetics of mixing 100 nM MutL297E29A_AF488 and 100 nM MutL297E29A_AF594 subunit exchange in FB75T; (B and C) After subunit exchange 200 nM MutL297E29A_AF488AF594 hetero-dimer incubated with 100 nM GT59DF DNA and 200 nM wtMutS, then starting the reaction with 10 μM ATP, later added 2 mM ATP; (D and E) The Bar graphs of the FRET efficiency (Efa, for MutL297E29A_AF488AF594 hetero-dimers, B) and the MutL/DNA FRET (BR FRET, C) averaged from 6 measurements.

Appendix Figure 3.6 is purification of full length MutL and MutL CTD and NTD fragments through size exclusion chromatography (SEC) with the flow rate of 0.5 min^{-1} . The full length MutL use Superdex 200 10/300 GL column and elution at 19-23 min (Appendix Figure 3.6 A left). Thrombin cleavage full length MutL NTD fragment eluted at 25-31 min with Superdex 200 10/300 GL column

Appendix

(Appendix Figure 3.6 A left and right top). And thrombin cleavage full length MutL CTD fragment eluted at 25-31 min with Superdex 75 10/300 GL column (Appendix Figure 3.6 B). The thrombin cleavage site showed as star in Appendix 3.6 A right bottom and inactivated with PMSF before loading on the column.



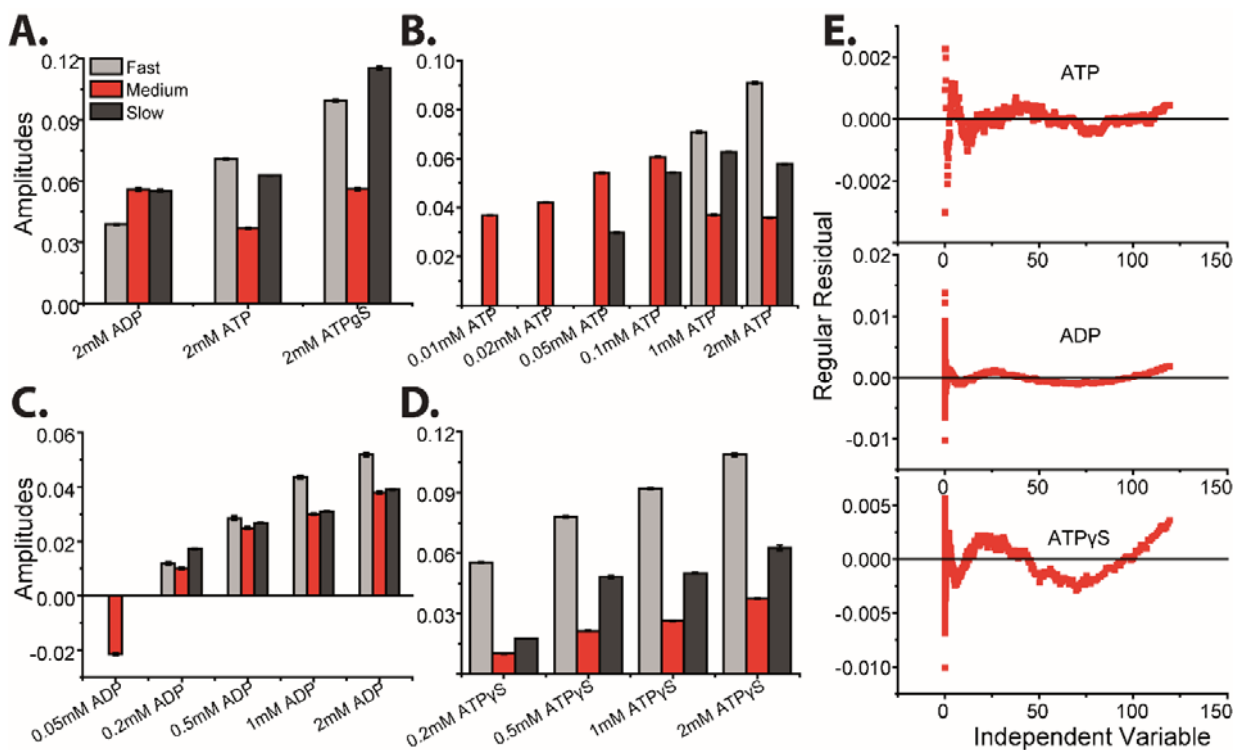
Appendix Figure 3.6 Size Exclusion Chromatography (SEC) purify full-length MutL, MutL CTD and NTD. (A) SEC purify full-length MutL297 and MutL297-NTD with Superdex 200 10/300 GL column with HPLC buffer 0.5 ml/min flow rates; (B) SEC purify full-length MutL452 and MutL452-CTD with Superdex 75 10/300 GL with HPLC buffer 0.5 ml/min flow rates. T. is stands for thrombin.

Chapter 4:

Appendix Figure 4.1 is the amplitudes of kinetics in Figure 5 (Chapter 4) and the variable of the three exponential fits of the kinetics. The slow hydrolysable ATP analogue ATP γ S mainly effect on the fast phase and the slow phase, but no effect on the medium phase (Appendix Figure 4.1, A). That is indicate that the medium phase is relate to the MutL NTD ATPase domain dimerization. The fast phase is relate to the ATP binding which proofed by the binding rate of ADP (without the γ phosphate group) is much faster than ATP due to the MutL R95 residue is in the ATP binding pocket and this do not affect the binding of ADP but ATP judged through the ternary structures of MutL with ADP and AMPPNP.

Appendix

Using ATP γ S results the accumulation of the slow state compared to ATP, while the rates of this state are similar for both ATP and ATP γ S. Therefore the last slow phase is relate to the ATP hydrolysis. Increase the concentration of ATP, ADP, and ATP γ S result the amplitudes for all three phases are increased (Appendix Figure 4.1, B-D), even though the rates of the medium and slow for all are similar (Figure 5, B, D and F, chapter 4).



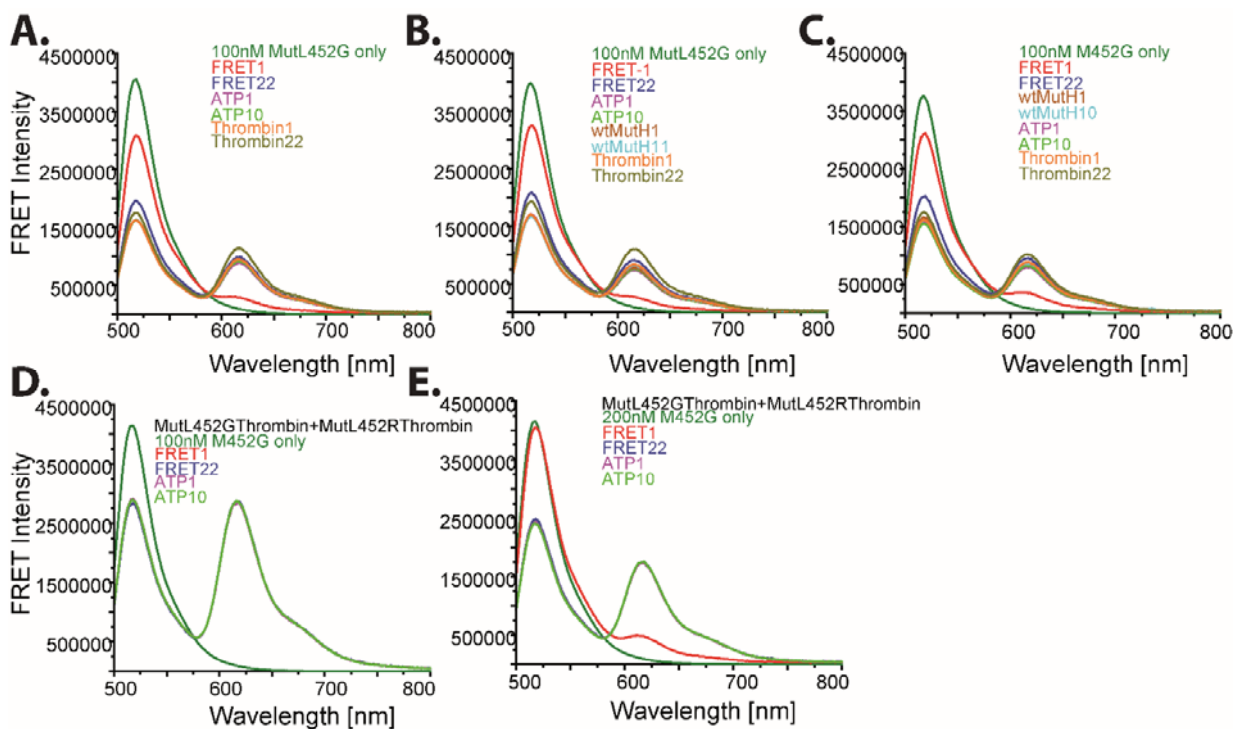
Appendix Figure 4.1 Amplitudes and regular residual (A) Amplitudes of derived from the three exponential fits of kinetics in Figure 5 A (Chapter 4); (B) Amplitudes of obtained from the one/two/three exponential fits of the kinetics of different concentration of ATP in Figure 5 C (Chapter 4); (C) Amplitudes of derived from the one and three exponential fits of different kinetics concentration of ADP in Figure 5 E; (D) Amplitudes of obtained from the three exponential fits of the kinetics of varying the concentrations of ADP in G; (E) the regular residual of three exponential fit kinetics of different nucleotides in Figure 5 A.

Chapter 5:

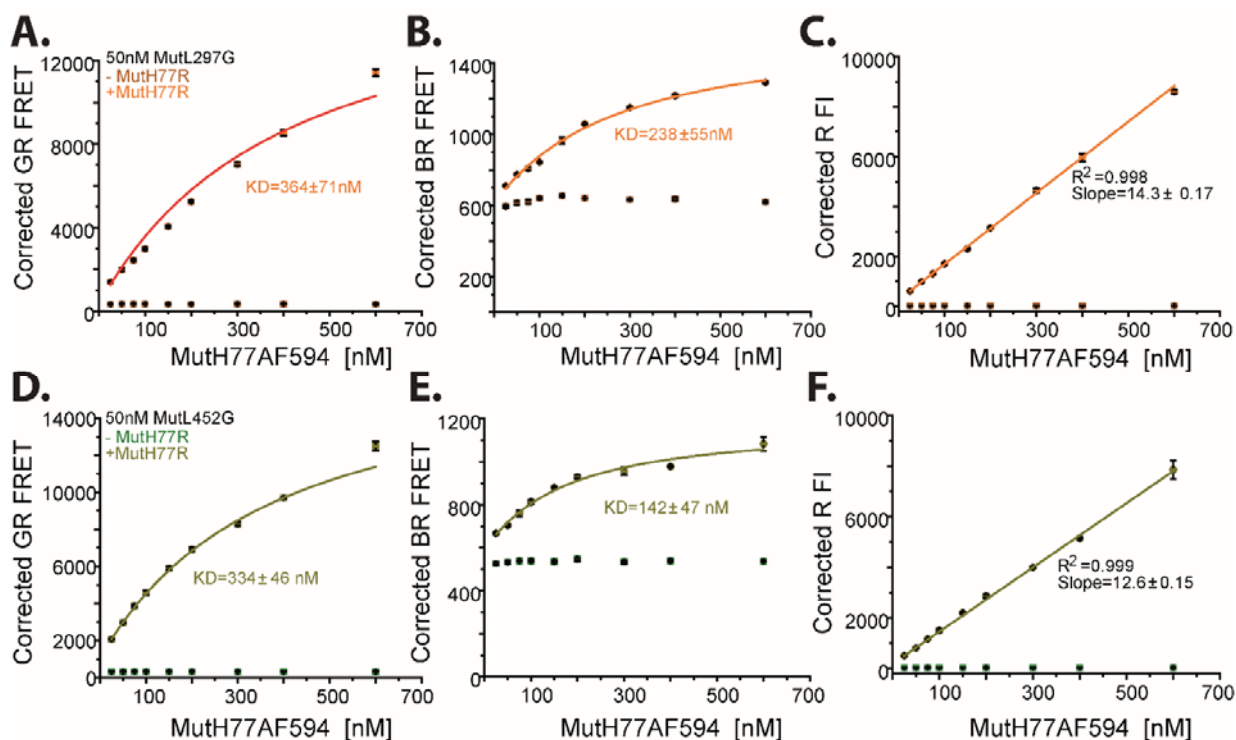
From Appendix Figure 5.1, we could observed that MutH have no effect on CTD labeled MutL452_AF488-MutL452_AF594 hetero-dimers formation, thrombin induced separate of the NTD and CTD fragments resulted the increase in FRET efficiency. The apparent affinity between MutL and MutH is ~ 200 nM through the nicking deficient mutant E77A which labeled at position 85 and assessed with TECAN which consistent with Figure 5 and Figure 6 in Chapter 5 (Appendix Figure 5.2). With HEX- Beacon we could observe that AF594 modified both Muth156 and Muth223 share the similar

Appendix

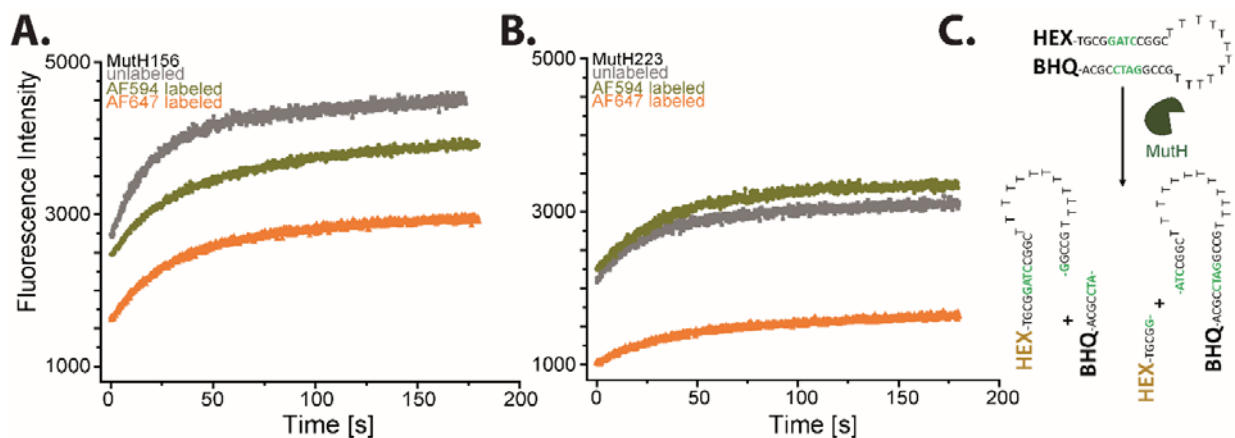
endonuclease activity as the unlabeled protein (Appendix Figure 5.3). MutH156 (MutH_E156C) share the similar endonuclease activity as the wild type, while MutH77 with very high mutation rate which similar as no MutH control through the complementation control in vivo (Toedt, Krishnan et al. 2003). MutH223 share the 81 % endonuclease activity as the wild type MutH through the endonuclease activity assay in vitro (Ahrends, Kosinski, et al. 2006).



Appendix Figure 5.1 The ATP and wtMutH effect to CTD labeled MutL FRET assessed with Spectra (A) Added 100 nM MutL452_AF594 to 100 nM MutL452_AF594 in 200 μ l Buffer M and measured FRET fluorescence intensity from 1-22 times in 10 min and later added 2 mM ATP (measured 1-10 times in 5 min) and Thrombin (measured 1-22 times in 10 min); (B) Added 100 nM MutL452_AF594 to 100 nM MutL452_AF594 in 200 μ l Buffer M and measured FRET fluorescence intensity from 1-22 times in 10 min and later added 2 mM ATP (measured 1-10 times in 5 min), 580 nM wtMutH (measured 1-11 times in 5 min) and Thrombin (measured 1-22 times in 10 min); (C) Added 100 nM MutL452_AF594 to 100 nM MutL452_AF594 in 200 μ l Buffer M and measured FRET fluorescence intensity from 1-22 times in 10 min and later added 580 nM wtMutH (measured 1-11 times in 5 min), 2 mM ATP (measured 1-10 times in 5 min) and Thrombin (measured 1-22 times in 10 min); (D) Added 100 nM MutL452_AF594 (pre-incubated with thrombin) to 100 nM MutL452_AF594 (pre-incubated with thrombin) in 200 μ l Buffer M and measured FRET fluorescence intensity from 1-22 times in 10 min and later added 2 mM ATP (measured 1-10 times in 5 min); (E) Added 100 nM MutL452_AF594 (pre-incubated with thrombin and 580 nM wtMutH) to 100 nM MutL452_AF594 (pre-incubated with thrombin and 580 nM wtMutH) in 200 μ l Buffer M and measured FRET fluorescence intensity from 1-22 times in 10 min and later added 2 mM ATP (measured 1-10 times in 5 min).



Appendix Figure 5.2 The KD value derived titration AF594 labeled MutHE77A/C96S to NTD/CTD labeled MutL assessed with TECAN (A-C) titration 25-600 nM MutH77_AF594 to 50 nM MutL297_AF488 in the presence of 25 nM GT59DF DNA, 50 nM wtMutS and 1 mM ATP in buffer FB75T; (D-F) titration 25-600 nM MutH77_AF594 to 50 nM MutL452_AF488 in the presence of 25 nM GT59DF DNA, 50 nM wtMutS and 1 mM ATP in buffer FB75T. The BR FRET is the FRET between MutH and SB stained DNA, while the GR FRET is the FRET between MutH, and R is the fluorescence intensity (FI.) of 20-600 nM MutH77_AF594.



Appendix Figure 5.3 Different labeled MutH activity test with HEX-Beacon (A) added 200 nM AF594 or AF647 labeled MutH156 and unlabeled MutH156 to 1 μ M HEX-Beacon in FB000 buffer containing 5 mM Mg^{2+} 1 mM $MnCl_2$, 10 % DMSO; (B) added 200 nM AF594 or AF647 labeled MutH156 and unlabeled MutH223 to 1 μ M HEX-Beacon in FB000 buffer containing 5 mM Mg^{2+} 1 mM $MnCl_2$, 10 % DMSO

References

Ahrends, R., J. Kosinski, D. Kirsch, L. Manelyte, L. Giron-Monzon, L. Hummerich, O. Schulz, B. Spengler and P. Friedhoff (2006). "Identifying an interaction site between MutH and the C-terminal domain of MutL by crosslinking, affinity purification, chemical coding and mass spectrometry." Nucleic Acids Res **34**(10): 3169-3180.

Guarne, A. and J. B. Charbonnier (2015). "Insights from a decade of biophysical studies on MutL: Roles in strand discrimination and mismatch removal." Prog Biophys Mol Biol **117**(2-3): 149-156.

Toedt, G. H., R. Krishnan and P. Friedhoff (2003). "Site-specific protein modification to identify the MutL interface of MutH." Nucleic Acids Res **31**(3): 819-825.